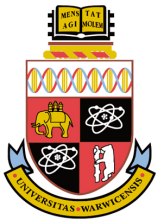

The role of Feronia in regulating growth and development in *Arabidopsis thaliana* roots

Jennifer Goodman

Thesis submitted to the University of Warwick

for the degree of

Doctor of Philosophy

Department of Life Sciences

September 2018

Contents

List of Tables

List of Figures

Acknowledgements

I would like to thank my supervisor Dr. Alex Jones for her support, guidance and patience throughout my PhD. My thanks to Dr. Cleidiane Zampronio and Dr. Juan Fernandez in Proteomics with an extra thanks to Juan for all his help with the phosphoproteomics. I would like to thank Jess Watts for her work on RALF1 activation while an undergraduate student in the lab and for all her help with using R for the ROTS analysis. My thanks to the whole of Lab C30 that have not only put up with me but have helped me every step of the way.

Last, but not least, thank you to my friends and family that have willingly put up with numerous conversations about troublesome proteins and have supported me throughout this project.

Declaration

This thesis is submitted to the University of Warwick in support of my application for the degree of Doctor of Philosophy. It has been composed by myself and has not been submitted in any previous application for any degree. The work presented (including data generated and data analysis) was carried out by the author.

Abstract

FERONIA (FER) is a receptor-like kinase (RLK) involved in a large number of processes in Arabidopsis. FER plays a role in cell elongation, mechanosensing, regulation of seed size, immunity and root hair development. A common theme in many of these processes is the involvement of FER as a regulator of location-specific growth (often called polar growth) and consistent with this observation FER is also known to interact with proteins that regulate the cytoskeleton (called Rho of plants, ROPs). The peptide, Rapid-Alkalinisation Factor 1 (RALF1), has been shown to elicit FER dependent signalling. Focusing within root tissue and using RALF1, we seek to explore early signalling events upon FER elicitation and clarify the interaction between FER and ROPs, using co-immunoprecipitation (CoIP) and mass spectrometry (MS). We have identified potential FER interactors, including Receptor for Activated C kinase 1B (RACK1B) and have identified two proteins, CAND1 and ILITYHIA, which are common between FER, ROP2 and ROP6. We also present data showing signalling events downstream of FER using a global phosphopeptide enrichment of Arabidopsis roots where we identified 684 phosphorylation sites dependent on RALF1 and/or FER.

Abbreviations

ABA	Abscisic Acid
AHA	H(+)-ATPASE 2
BAK1	BRI-associated kinase 1
BR	Brassinosteriods
CAA	2-Chloroacetamide
CAND1	Cullin-associated NEDD8-dissociated protein 1
CESA	Cellulose synthase
CID	Collision induced dissociation
CoIP	Co-immunoprecipitation
CPK	Calcium dependant Protein Kinase
CSI	Cellulose synthase interactive protein 1
DHB	2,5-dihydroxybenzoic acid
DTT	Dithiothreitol

ERF	ERECTA Family
ERU	ERULUS
ETD	Electron transfer dissociation
FDR	False Discovery Rate
FER	FERONIA
FLS2	FLAGELLIN SENSING 2
GEF	Guanine nucleotide Exchange Factors
GRF	General Regulatory Factor
HCD	Higher energy Collision induced Dissociation
HERK	HERCULES
HPLC	High Pressure Liquid Chromatography
IAA	Iodoacetamide
IPTG	Isopropyl β-D-1-thiogalactopyranoside
LC	Liquid chromatography
LFQ	Label Free Quantification
LLG1	LRE-like GPI-AP1
LRR	Leucine-rich repeat
m/z	mass-to-charge ratio

MAPK	Mitogen-activated protein kinases
MBP	Maltose Binding Protein
MQ	Max Quant
MS	Mass Spectrometry
NAA	1-Naphthaleneacetic acid (Auxin)
PBS	Phosphate-Buffered Saline
PC	Pavement Cells
PEP1	PROPEP protein 1
PMSF	Phenylmethylsulfonyl fluoride
PVDF	Polyvinylidene difluoride
RACK1B	Receptor for Activated C Kinase 1B
RALF	Rapid Alkalinisation Factor 1
RBOHD	RESPIRATORY BURST OXIDASE HOMOLOGUE D
RHD	Root Hair Defective
RHS	Root Hair Specific
RIC	ROP-interactive CRIB motif-containing protein
RIPK	RIP kinase 1
RLK	Receptor-Like Kinase

ROP	Rho-related GTPase from Plants
ROTS	Reproducibility-Optimized Test Statistic
SCN1	SUPER CENTIPEDE 1
TCEP	tris(2-carboxyethyl)phosphine
THE1	THESEUS1
TiO_2	Titanium dioxide

Chapter 1

Introduction

1.1 Root development and polar growth in *Arabidopsis thaliana*

Plants are sessile organisms and rely on their ability to maximise resources in their immediate environment to survive. Roots respond to different environmental stresses and stimuli by generating differential growth across the tissue. Root growth and development is fundamental to the health of plants and therefore of critical importance when considering crop yields. The need for higher crop yields is ever increasing and climate change is causing the environment to become more hostile, making it harder to achieve these higher yields. Understanding how roots develop enables us to aid plants to become better adapted to their environments. This is essential as two main constituents of the most commonly used fertilisers, nitrogen and phosphorus, are becoming limited (Dawson and Hilton, 2011).

The Arabidopsis root has 3 specific developmental zones that cells pass through before they become mature cells. The stem cells give rise to all cell types of the root; they surround a small group of mitotically less active cells, the quiescent centre. The quiescent centre promotes its neighbouring cells to continuously produce initial cells that give rise to cell files. In the meristematic zone, stem cells divide creating multiple cells that will lose the ability to divide and start to elongate in the elongation zone, which then become differentiated cells in the differentiation zone (DZ). Cells in the elongation zone undergo unidirectional growth which relies on cytoskeletal reorganisation and a vacuole is also developed at this stage (Verbelen et al. 2006). Once cells reach their desired size they enter the DZ and differentiate into cells with specific functions. It is in the DZ that root hair formation occurs from cells in a predetermined fashion.

The regulation of root development comes from hormone and peptide signals to generate coordinated growth of the tissue. The growth hormone auxin, the most biologically abundant of which is IAA (indol-3-ylacetic acid), but which also consists of several other forms including 1-NAA (naphth-1-ylacetic acid) and 2,4-D (2,4-dichlorophenoxyacetic acid), has a well documented involvement in regulation of root development through auxin gradients, summarised in Figure 1.1. Auxin is transported long distances from the shoot apex moving toward the base of the plant through the stele, finally reaching the root tip. At the root tip the root-ward transport of auxin through the central tissues allows a loop flow, and auxin is reversely transported in a shoot-ward direction through the lateral root cap and epidermis (Blilou et al. 2005). Just below the beginning of the elongation zone, the auxin flow is recycled into the stele (Grieneisen et al., 2007)(Doerner 2008)

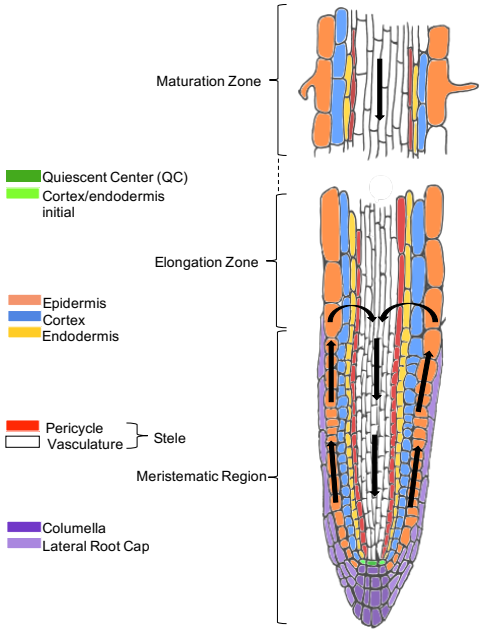

Figure 1.1: Root schematic showing different developmental zones. Arrows depict flow of auxin to generate an auxin gradient across a developing root.

The auxin gradients and coordination of cell polarity across tissues, which rely on extensive intercellular communication requiring a mechanism for localised cell–cell coordination of cell polarity on the basis of cytoskeleton dynamics/reorganisation and vesicular trafficking, are essential for development and pattern formation (reviewed by Yang, 2008). Leaf pavement cells (PCs), which develop multiple polarities across the cell to create interdigitated lobes and indentations, offer an ideal model for studying the regulation of these polarities. Several studies have identified a Rho GTPase-based signalling network underlying PC interdigitation, which includes intra- and intercellular interplays between two mutually exclusive Rho-related of plants (ROPs) pathways and a positive feedback loop, which are all activated by auxin (reviewed by Chen et al., 2015).

ROPs are small GTPases that act as molecular switches due to the change in conformation upon GTP binding (Berken and Wittinghofer, 2008). ROPs

are a family of 11 plant specific subfamily of Rho small GTP-binding proteins. ROPs are activated, switched to GTP bound form, via ROP guanidine exchange factors (ROPGEFs), of which there are 14 in Arabidopsis (Kanaoka and Torii 2010).

In PCs, the plasma membrane localised ROP2 localises to the lobe tips, where the ROP2 effector ROP-interacting CRIB-containing protein 4 (RIC4) induces the accumulation of cortical F-actin required for outgrowth (Fu et al., 2002, 2005). For the production of the indent, ROP6 regulates the parallel alignment of transversal cortical microtubules through its effector RIC1 (Fu et al., 2005, 2009), which exerts its function through the microtubule severing protein katanin (KTN1) to promote detachment of branched microtubules (Lin et al., 2013). In leaf PCs auxin was shown to activate ROP2-RIC4 and ROP6-RIC1 pathways (Xu et al. 2010). RIC are a family of ROP effector proteins that interact with activated ROPs through their CRIB motif (Fu et al 2005, Wu et al. 2001). RICs have been shown to help regulate the cytoskeleton, with ROP6 activated RIC1 being shown to promote microtubule organisation (Fu et al. 2009). Activated ROP2 inhibits the ROP6-RIC1 pathway and vice versa leading to lobe formation. Prior to 2015, the activation of ROPs by auxin was believed to due to auxin interacting with auxin binding protein (ABP1) and the signal transmitted through a receptor-like kinase (RLK), however a paper showing two null ABP1 mutants with no growth or developmental phenotypes caused questions to be asked of ABP1 function (Gao et al., 2015). The spatially regulated location of ROPs in pavement cells is summarised in Figure 1.2.

ROPs have been strongly linked to polar growth in both pollen tubes and root hairs, with many ROP associated proteins having root hair phenotypes.

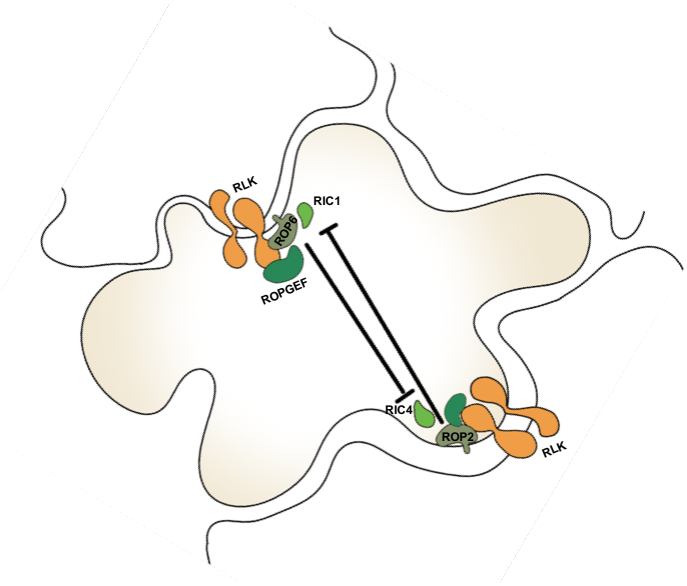

Figure 1.2: ROP2 and ROP6 are spatially regulated to control lobe formation in pavement cells. Schematic of ROP2 and ROP6 in pavement cells.

In order for the root hair to elongate multiple highly coordinated events must occur, including a large amount of vesicle trafficking to the tip and cytoskeleton remodelling to cope with a growing root hair. ROPs are known to regulate both the initiation of a root hair and also the elongation. The auxin gradient that forms at the site of root hair initiation prior to growth causes ROP2, ROP4 and ROP6 to accumulate at the initiation site (Molendijk et al., 2001; Jones et al., 2002; Fischer et al., 2006). Overexpression of ROP2 induced ectopic root hair initiation, leading to a higher root hair density, and overexpression of the constitutively active ROP2 ^{CA}increases the density of root hairs but not to the same extent as overexpressed ROP2. This indicates that the cycling of the activity of ROP2 is important in root hair initiation (Jones et al. 2002).

Root hairs are 1 mm or more long, thin tubular growths that form from trichoblasts in the epidermic cell layer (Grierson et al., 2014). The growth

of root hairs is commonly categorised into three stages: initiation of root hair growth, establishment of tip growth and finally arrest of the tip growth in mature root hairs (Dolan et al 1994). Initiation of the root hair occurs at the base of the trichoblast and involves the accumulation of specific proteins, remodelling of the cytoskeleton and the localised acidification of the cell wall. Tip growth is promoted by the establishment of a calcium gradient and highly polarised and dynamic actin skeleton. The internal Ca^{2+} concentration was found to increase after initiation of a root hair prior to tip growth, which leads to a Ca^{2+} gradient of 1 μM at the tip and 100 nM at the base of the root hair (Carol and Dolan 2002). The tip growth of root hairs makes an excellent model to study the regulation of polar growth.

There are several hormones, including auxin, that are heavily involved in the formation of root hairs and one such class of hormones is Brassinosteroids (BR). BRs are are essential for the regulation of WEREWOLF transcription factors that are responsible for epidermal cell fate (Kuppusamy et al., 2009). Auxin has multiple roles in root development and is crucial for the correct formation of root hairs (Grebe et al., 2002). Auxin gradients are essential for polar growth and auxin transporters AUX1 and PIN1 are believed to be involved in regulating the level of auxin that is required during tip growth. The plant hormone ethylene is also involved and promotes root hair morphogenesis using the same pathway as auxin (Masucci and Schiefelbein, 1996).

Tip growth requires extensive coordination of intracellular cargo through trafficking and also weakening of the apical cell wall to allow for the expansion. This coordination requires signalling events from both the cell wall and plasma membrane and also internally from the cytoplasm. The cytoskeleton plays a crucial role in tip growth by not only strengthening the internal cell

structure but by directing vesicles to specific locations. Actin bundles are present in growing root hairs along the shank of the root hair and highly dynamic fine actin filaments are present at the tip (Ketelaar et al., 2003). Microtubule organisation in root hairs depends on the stage of growth, with usually two types of microtubules present: cortical and endoplasmic. In a growing root hair, cortical microtubules extend outwards from the nucleus whereas mature root hairs have exclusively tipward polymerisation (Ambrose and Wasteneys, 2014).

Reactive oxygen species (ROS) are key signalling molecules that regulate many cell processes and are involved in root hair expansion. ROS are a by-product of aerobic metabolism that are highly reactive towards proteins, causing damage, but they also play a vital role in signalling and development (Schippers et al., 2012). Root hair development relies on the spatially distinct regulation of ROS production and has been shown to affect Ca^{2+} fluxes and cause pH fluxes, altering cell wall properties during polarised expansion (Takeda et al., 2008; Monshausen et al., 2007). ROS burst is produced by plasma membrane NADPH oxidases that are activated by several mechanisms including calcium signalling. Calcium is thought to result in stiffening of the cell wall and protons are believed to cause softening promoting cell wall plasticity (reviewed by Cosgrove et al., 2005). ROS levels are important for sustaining polar growth shown by an NADPH oxidase mutant known as RESPIRATORY BURST OXIDASE HOMOLOG C (RBOHC), which produces root hairs that burst after initiation as the root hairs enter the tip growth phase (Foreman et al., 2003). The localisation of ROS in the tip region also suggested a potential mechanism by which cell wall properties are regulated.

ROPs regulate ROS production most likely via NADPH oxidases. The role of ROP GTPases appears to be more than simple activation of RESPIRATORY BURST OXIDASE HOMOLOGUE D (RBOHD), but is involved in accurate spatial emulation of ROS. ROP activity is partly regulated by a group of proteins called Rho GDP Dissociation Inhibitors (RhoGDIs), like SUPER CENTIPEDE 1 (SCN1), which bind preferentially to GDP bound ROPs and remove them from the membrane and stabilise them in the cytoplasm (Boulter et al., 2010). The SCN1 and RHD2 dependent ROS accumulation at root hair initiation sites strongly suggest that ROP2/4 activates RHD2 (also known as RBOHC) during root hair formation and tip growth (Carol et al., 2005).

Cell wall remodelling is crucial for any cell expansion with about 10% of the genes in Arabidopsis predicted to be involved in some capacity of cell wall metabolism including polymer biosynthesis, transport, deposition, remodelling, turnover, and regulation of these processes (McCann and Carpita, 2008). Cellulose is a ubiquitous component of cell walls and is synthesised at the membrane by a large complex of proteins termed the cellulose synthase complex. The first genes identified as being involved in cellulose biosynthesis were termed cellulose synthase (CESA) proteins and have since been shown to be involved in the synthesis of various cell wall polysaccharides. 10 CESA family members have been identified through sequencing of the Arabidopsis genome (reviewed by Richmond, 2000). The cellulose synthase complex was found to be essential for cellulose synthesis through a temperature-sensitive mutant *radial swelling 1*, which had a defect in CESA1 (Arioli et al., 1998). The regulation of CESA proteins at the plasma membrane relies on not only transcription and translation but also on rates of endocytosis and exocytosis and has recently been identified as cargo for clathrin-mediated endocytosis

(Bashline L et al., 2013). The protein CELLULOSE SYNTHASE INTERACTING 1 (CSI) is involved in the highly regulated process of delivering the cellulose synthase complex to the plasma membrane by marking the docking site. This allows Cellulose Synthase Complexes - containing vesicles access to the plasma membrane through its interaction with microtubules. (Zhu et al., 2018).

The size and shape of plant cells is confined by the cell wall and therefore to achieve cell growth or expansion the cell wall must be altered. Cell walls consist of various polymers mixtures, including celluloses, pectins, lignins, and tip growing cells appear to have a different polymer make up, with pectin being considerably enriched at the tip growing cells (Bosch and Hepler, 2005). There is also increasing evidence that glycoproteins such as extensins and arabinogalactan proteins (AGPs) are involved in tip growth of pollen tubes, however there is little evidence connecting them to root hair growth.

1.2 Receptor-like kinases

1.2.1 Background and context to receptor-like kinases

The ability of plants to adapt to their environment is key to their survival and receptor-like kinases (RLKs) play a pivotal role in processing, signalling and transmitting extracellular signals into intracellular information. RLKs are essential in the coordinated growth of tissues as they allow cells to perceive external stimuli such as peptides, hormones and even mechanical stimuli. RLKs are a large protein family, over 600 in Arabidopsis, of putative transmembrane receptors that are divided into 44 sub-categories depending

on their N-terminal (extracellular) domains (Shiu et al., 2004). In general RLKs have an extracellular ligand binding domain, a transmembrane domain, a juxtamembrane domain and a serine/threonine kinase domain. Ser/Thr kinases predominantly have a conserved Arginine preceding a catalytic Aspartate in the catalytic loop, known as RD kinases, which are strong active kinases. RD Kinases contain an arginine and aspartic acid in the active site of the kinase domain. However, there are a large number of RLKs that are not RD kinases and have weaker kinase activity and often require other proteins to modulate their function. For example most RLKs involved in plant immunity are not RD kinases (Johnson et al., 1996; Dardick and Ronald, 2006).

One of the best characterised subfamilies of RLK is the leucine-rich repeat (LRR) - RLK, of which FLAGELLIN SENSING 2 (FLS2) is a member. FLS2 is a plasma membrane receptor that recognises the well-conserved protein flagellin from a broad class of bacterial plant pathogens (Gómez-Gómez and Boller, 2000). FLS2 forms heterodimers with BRI-associated kinase 1 (BAK1), a kinase that was originally identified due to its role in brassinosteriod signalling via the receptor BRI1 and has subsequently been identified as a common component of many RLK signalling complexes (Chinchilla et al., 2007)(Heese et al., 2007).

RLKs perceive an extracellular signal at the plasma membrane and transduce this into intracellular signalling events such as mitogen activated protein kinase (MAPK) signalling cascades (Figure 1.3). RLKs often exist in several different complexes, depending on whether they are elicited or not, as shown in Figure 1.3. For example, upon ligand binding of FLS2 and ERECTA Family (ERF) receptor, by flg22 and elf18 respectively, FLS2/EFR

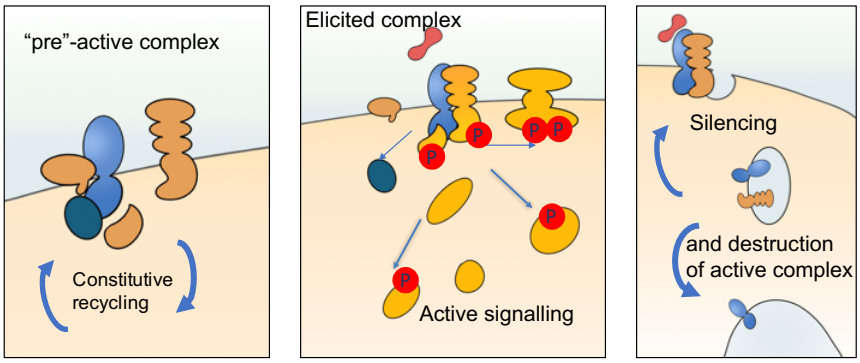

Figure 1.3: Schematic of Receptor-like kinase signalling. Pre-elicited complex. Elicited complex and downstream signalling through phosphorylation and regulation of the signalling by endocytosis.

physically associate with the LRR-RK coreceptor BAK1, mediating phosphorylation of the receptor-like cytoplasmic kinases (RLCKs) BIK1 and related PBL proteins, causing them to dissociate from the receptor complexes to regulate downstream signalling (Chinchilla et al, 2007)(Lin et al., 2014). BAK1 also associates with PEPR1/PEPR2 that bind PROPEP (PEP) peptides, which are danger-associated molecular patterns involved in the damage response.

RLK signalling is often regulated by endocytosis from the plasma membrane after elicitation (Figure 1.3). The protein kinase-associated protein phosphatase (KAPP) was identified as being important for the endocytosis of the receptor kinase SOMATIC EMBRYOGENESIS RECEPTOR-LIKE KINASE 1 (SERK1), and has been found to interact with the kinase domain of FLS2 (Gómez-Gómez and Boller, 2000; Shah et al., 2002). FLS2 is also known to interact with E3 ligases that polyubiquinate the receptor after elicitation, which leads to the receptor being degraded by the proteasome (Chuang and Ulevitch, 2004). As FLS2 signalling is so well documented, and BAK1 is known to interact with multiple receptors, FLS2-BAK1 signalling is often used as a model for RLK signalling.

1.2.2 *Catharanthus roseus* RLK1-Like signalling

The RLK family *Catharanthus roseus* RLK1-Like (CrRLK1L) is not as well documented as the LRR-RLKs exemplified by FLS2 signalling, but a number of both direct interactors of CrRLK1L receptors and downstream phosphorylated proteins have been identified. The CrRLK1L family is named after the first identified protein, CrRLK1L, which was identified from the plant *Catharanthus. roseus* (Schulze-Muth et al., 1996). Receptors of the CrRLK1L family have two extracellular malectin-like domains and although the primary sequence varies substantially, the predicted secondary structures are fairly well conserved which has lead to inference of a role in carbohydrate binding (reviewed by Boisson-Dernier et al., 2011). Subsequently 17 members of the family have been identified of which , FERONIA (FER), THESEUS (THE1), HERCULES1 (HERK1), HERK2 and ERULUS (ERU) have been implicated in cell wall function (Hematy and Höfte, 2008; Guo et al., 2009; Schoenaers et al., 2018).

The RLK, THE1, currently has the best known links to cell wall biosynthesis and cell growth compared to the rest of the CrRLK1L members, although the *fer* mutants exhibit a cell wall defect (Yeats et al., 2016). THE1 was first identified as a suppressor of the hypocotyl elongation defect of a loss-of-function mutation in the catalytic subunit of cellulose synthase 6 ($CESA6^{prc1}$). Subsequently *the1* mutant was found to suppress hypocotyl growth inhibition of cell wall function mutants including CESA3 ^{eli1} and $CESA^{rsw1}$, and to suppress the ectopic lignin accumulation observed in these cellulose-deficient mutants (Hematy et al., 2007). A single loss-of-function mutation in THE1 does not result in any growth and development phenotypes (Hematy et al., 2007). THE1 is genetically redundant with other

members of the CrRLK1L family as *the1-herk1/herk2* triple mutant shows strong effects on cell expansion causing reduced cell elongation, and decreased petiole length and shoot growth (Guo et al., 2009). THE1 functions as a sensor of cell wall integrity in situations where the cell wall is perturbed and cell elongation would be detrimental to the plant, but a ligand for THE1 is not known (Hematy et al., 2007).

Several members of the CrRLK1L family have also been linked more broadly to tip growth; FER, ANXUR1 (ANX1), ANX2, CVY1 and ERU, which was reviewed by Nibau and Cheung (2011). Although described in different tip growing tissues, FER, ANX1, ANX2 and CVY1 are all plasma membrane localised and all increase the production of ROS by a common mechanism (Duan et al., 2010; Gachomo et al., 2014). ERU acts slightly differently and is localised to the tonoplast of root hair cells where it responds to ammonium/nitrogen levels by activating nitrogen permease and facilitates accumulation of Ca^{2+} (Bai et al., 2014). FER also has links to Ca^{2+} signalling, particularly in relation to mechanosensing, however, the exact pathway in which FER and Ca^{2+} are involved in is unknown (Shih et al., 2014).

The extracellular malectin-like ligand binding domain of CrRLK1Ls was predicted to bind to carbohydrates and a recent paper showed that FER interacts with pectin (Feng et al., 2018). Despite the direct interaction between the extracellular domain of FER and pectin being detected *in vitro*, it still remains to be tested whether pectin fragments can directly activate FER signalling (Feng et al., 2018).

Surprisingly, a small secreted peptide known as Rapid Alkalinisation Factor 1 (RALF1) was determined to be a ligand for FER, leading to inhibition of the plasma membrane ATPase AHA2 (Haruta et al., 2014). The RALF family

of peptides consists of 34 members that have a conserved arginine-arginine (RR) motif first identified in tobacco RALF peptide, which was found to be a cleavage site for a proteolytic enzyme in plants (Pearce et al., 2001). The cleavage site is located at the junction between the propeptide and the active peptide. RALF1 is a small secreted peptide containing disulfide bonds that lacks N-glycosylation (Pearce et al., 2001) (Haruta et al., 2014).

An enzyme called SITE-1-PROTEASE (S1P) was later identified as the enzyme that cleaves the pro-peptide from the mature active RALF peptide in RALFs containing a dibasic amino acid motif RR (RRXL), which is present in 10 of the 34 RALF family peptides (Srivastava et al., 2009) (Liu et al., 2007). RALF1 and RALF23 are cleaved by S1P and can inhibit plant immunity but other RALF members, such as RALF32, have no S1P cleavage sites and have no effect on plant immunity (Stegmann et al., 2017). The *RALF* genes in Arabidopsis are involved in a variety of different processes such as inhibition of root development, nodule formation, tissue expansion and pollen development (Combier et al., 2008) (Covey et al., 2010).

Several coreceptors and chaperones of RALF1-FER signalling have been identified. The plant immunity receptor FLS2 has been shown to interact with RALF-FER signalling complex, which provides an interesting link between development and immunity (Stegmann et al., 2017). FER's link to immunity was strengthened as FER has been shown to interact with RPM1-induced protein kinase (RIPK), in a RALF1 dependant manner (Du et al., 2016). Two glycosylphosphatidylinositol-anchored proteins (GPI-APs), LORELEI (LRE) and LRE-like GPI-AP1 (LLG1), have been shown to bind to the extracellular juxtamembrane domain of FER and, in different developmental contexts, are essential for deposition and stability of FER as well

as effective RALF1-FER signalling (Li et al., 2015).

LLG1 interacts with the extracellular juxtamembrane region of FER, which interacts with ROPGEF1 to activate ROP2 to form a LLG1-FER-GEF–ROP complex. Auxin elicited ROS production through an NADPH oxidase-dependent route in root hairs occurs through ROP2 (Duan et al., 2010). RALF1 has been identified as upstream of ROP activation through RALF1 inhibition abscisic acid (ABA) responses. The RALF – FER – GEF1/4/10 – ROP11 pathway inhibits ABA response through activation of ABI2, with a feedback mechanism in which ABI2 interacts with and dephosphorylates FER to inhibit the RALF–FER signalling pathway (Chen et al., 2016). Another hormone with links to FER signalling is ethylene; FER physically interacts with two highly homologous S-adenosylmethionine (SAM) synthetases, SAM1 and SAM2, to participate in ethylene biosynthesis (Mao et al., 2015).

1.3 Proteomics techniques

1.3.1 Affinity enrichment

Three types of affinity enrichment are used throughout this research; Co-immunop-recipitation (CoIP) to identify protein-protein interactions, titanium dioxide (TiO_2) enrichment for phosphopeptide enrichment and affinity based enrichment using RIC-MBP (maltose binding protein) bound to amylose beads (Figure 1.4). The most common way to study proteins is to enrich for a subset of proteins of interest to reduce the complexity of the mixture.

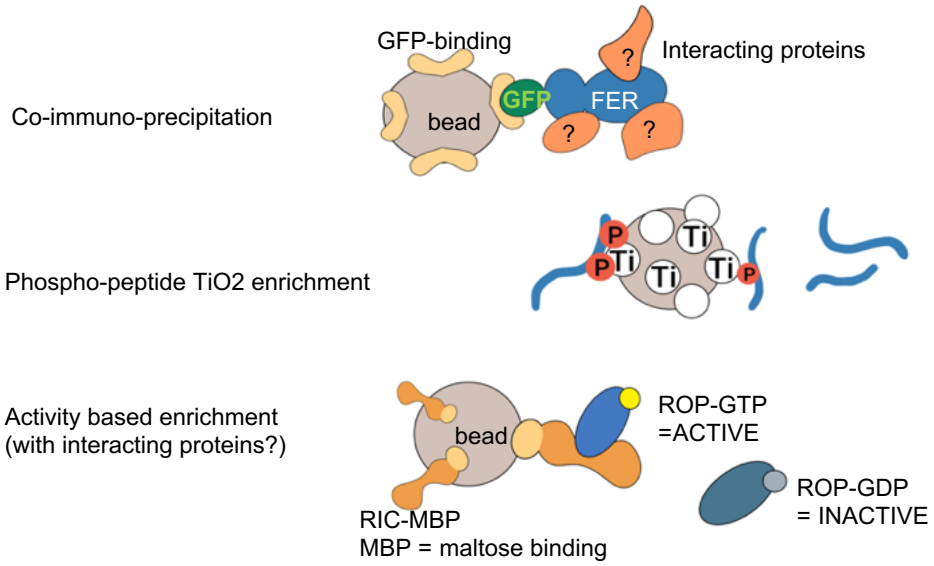

Figure 1.4: Affinity based tools for dissecting RLK pathway. Co-immunoprecipitation, phosphopeptide TiO_2 enrichment and activity based enrichment with interacting proteins.

A CoIP is an extension of an immunoprecipitation, with the aim of a CoIP enriching the protein of interest (antigen) and the proteins that interact with that protein. The CoIP antibody used for this research is GFP-TRAP (Chromotek) which is made from a specific binder for fluorescent proteins based on a 13-kDa GFP binding fragment, derived from a llama single chain antibody, bound to agarose beads (Rothbauer et al., 2008). The CoIP is based on the strong affinity of an antibody for its epitope. The strong binding allows the enrichment of the bait protein (antigen) by pulling down the protein bound to the antibody on the bead. The analysis of the CoIP is usually carried out with either a western blot, to detect specific proteins of the complex, or Mass Spectrometry (MS) to identify unknown components of the protein complex.

TiO_2 has a high affinity for phosphopeptides and therefore has been used to

enrich phosphopeptides. 2,5-dihydroxybenzoic acid (DHB) is used to reduce the high levels of non-specific binding when TiO_2 is used in a complex mixture and additional washes of the beads were added to optimise the enrichment (Larsen et al. 2005). The affinity enrichment using TiO_2 is based on TiO_2 being positively charged and the phosphate group being negatively charged. The enrichment is carried out under acidic conditions to aid the binding of TiO_2 to phosphopeptides.

The activity assay relies on the affinity of an active protein for its effector protein. MBP binds to amylose and therefore proteins fused to an MBP tag can be conjugated to amylose beads. Using RIC-MBP bound to amylose beads enables the enrichment of ROPs which are known to interact with RICs when activated. This affinity purification enables us to separate inactive (GDP bound) ROPs with active ROPs (GTP bound) and measure the activity of ROPs over time after different treatments.

1.3.2 Mass spectrometry (MS)

Mass spectrometry (MS) is widely used to analyse biological samples and has become an essential tool for the field of proteomics. The term proteomics, coined in the 1980s, aimed to identify the total proteome of an organism, including splice isoforms and post-translational modifications. One of the biggest complexities relating to determining an organism's proteome is that protein expression and abundance change between cell types and often exist in different post-translationally modified states. MS has enabled three areas of proteomics research; protein expression, protein-protein interactions and identifying sites of post-translational modifications such as phosphoryla-

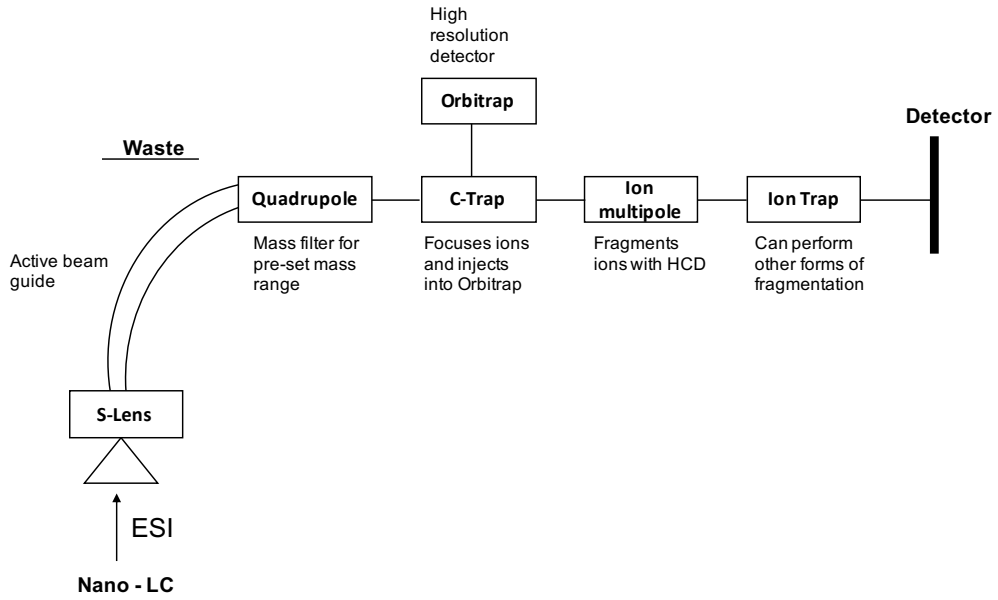

Figure 1.5: Schematic of Ion path in an Orbitrap. Schematic showing the ion path in an Orbitrap mass spectrometer, including the three mass analysers.

tion. Tandem mass spectrometry (MS/MS) is key to determining peptide sequences and therefore protein identification in complex mixtures as well as for the identification of post-translational modifications.

MS measures the mass-to-charge ratio (m/z) of gas-phase ions. There are many different types of mass spectrometers but they all contain variations of an ion source, a mass analyser and a detector that records the m/z value. The mass spectrometer used in this research was a Orbitrap Fusion (Thermo Scientific). The Orbitrap has three mass analysers, a Quadrupole, an Orbitrap Mass analyser and an Ion Trap as shown in Figure 1.5. In an Orbitrap Mass spectrometer the ions are trapped and orbit around a central spindle and oscillate along its axis depending upon their m/z values, which induces an image current that is Fourier transformed into the time domain producing spectra (Makarov A et al., 2006).

Prior to analysis by MS the protein is digested with an enzyme such as trypsin which cleaves the protein at Lysine (K) and Arginine (R) amino acids. These peptides are then separated by reverse phase C18 liquid chromatography (LC) followed by electrospray ionisation to generate positively charged peptide ions which are injected into the mass spectrometer. The LC conveniently separates peptides by hydrophobicity, giving the MS time to fragment a higher percentage of peptides when analysing a complex mixture. MS/MS involves two steps, firstly MS1 spectra is obtained from precursor ion masses of a specific m/z range, which are analysed in the orbitrap analyser, before being selected for subsequent peptide fragmentation, which is analysed in the c trap. The MS2 fragmentation is where peptide sequence information is obtained. The development of the Orbitrap-fusion has enabled better fragmentation methods to be used. Prior to the Orbitrap the fragmentation of peptides was done using collision induced dissociation (CID) (Hunt et al., 1986), which causes a third of ions to be lost due to using the ion trap. The orbitrap allows Higher energy Collision induced Dissociation (HCD), which produces better peptide identifications, due to ions being collected in the c trap, than both ion trap CID and electron transfer dissociation (ETD) (Frese et al., 2011). HCD was therefore used as the fragmentation energy for all experiments described here.

1.3.3 Data analysis

The method used for all MS in this research was: tryptic digest (cleaves at K and R residues), LC coupled to electrospray and MS/MS (Aebersold and Mann 2003). The MS/MS gives raw files that contain the MS2 spectra, these spectra are then pattern matched against a database to assign the

spectra to the peptide. Two types of database searches were carried out for this research.

Mascot (Matrix Science) program is a widely used commercially available peptide identification software. As is it a commercial software, the exact algorithm used to match MS2 to peptide sequences is not known but the basic concept of how such algorithms work are: A FASTA sequence database is used to predict the possible peptides, as trypsin cleaves at specific residues K and R, the algorithm then predicts the expected fragment b and y ion series for a particular peptide and then matches the observed spectrum to the predicted theoretical spectrum (Perkins et al., 1999).

Another software available to assign spectra to peptides is MaxQuant (MQ) which originally used Mascot search engine to assign peaks to peptides but has since been developed to use its own algorithm called Andromeda (Cox et al., 2011). This newer MQ approach relies on the same principle as the Mascot software, as it uses a probability based approach for which MQ assigns a score. The probability score (p-score) works by calculating the b and y ion masses, as described for Mascot, and then determines the number of matches, k. The probability (p) of obtaining k random matches between the predicted and the measured MS2 peaks can be obtained with a statistical test (the p-score) (Olsen and Mann 2004). This method is also employed for the localisation probability score when looking at post-translational modifications (Cox et al., 2011).

MQ allows for label free quantification (LFQ) of the proteins. This way of quantifying proteins from the MS is reviewed by Bantscheff et al. (2007). It works by taking the precursor ion chromatograms for every peptide from the LC-MS/MS run and the mass spectrometric peak areas are integrated

over the chromatographic time scale. The accuracy of LFQ data has been increased by mass spectrometers having a higher mass resolution, because accurate determination of the extracted ion currents is critical for comparison between samples. MQ LFQ was designed to combat two main issues with LFQ proteomics data; delayed normalisation that allows LFQ to be fully compatible with any up-front separation, and a novel approach that extracts the maximum ratio information from peptide signals in arbitrary numbers of samples to achieve the highest possible accuracy of quantification (Cox et al., 2014). There is also a match between run function that takes unidentified LC-MS features that did not trigger MS2 in one run but that are assigned to peptide identifications in other runs, and assigns them to the same peptide based on their accurate masses and aligned retention times (Cox et al., 2014). The combination of these two things means the match between run function works with a false discovery rate (FDR) in the range of 1% (Cox et al., 2014).

A bioinformatics tool named Perseus was designed by the Cox and Mann groups to enable researchers to better interpret protein quantification, interaction and post-translational modification data. The software, reviewed by Tyanova et al (2016), offers a variety of algorithmic activities that cover topics such as data normalisation through exploratory multivariate data analysis and integration with other omics. Perseus contains several computational and statistical tools allowing for a more standardised analysis. However currently the statistical tests available in Perseus are two variations of a *t*-test (one for normally distributed data and one aimed at data that is skewed), and ANOVA.

1.4 Project aims and objectives

There have been many advances to understanding the role of the receptor-like kinase FER over the last 10 years. However quite how FER manages to function in such a large number of roles remains unclear. The aim of this project was to identify proteins that interact with FER to form an active signalling complex in response to RALF1 and to look at proteins involved in signal propagation downstream of FER. Another aim was to identify whether RALF1 activates ROPs through FER, by developing a ROP activity assay and to identify ROP effector proteins.

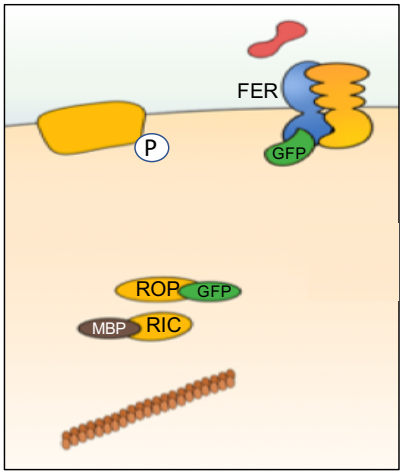

Figure 1.6: Schematic of the fusion protein baits used to decipher RALF1-FER signalling pathway. FER-GFP CoIP, ROP-GFP CoIP, RIC-MBP affinity purification and phosphopeptide enrichment.

In this project we used four affinity purification experiments to determine components of the RALF1-FER signalling pathway (Figure 1.6);

- FER-GFP CoIP,
- ROP-GFP CoIP,

- RIC-MBP affinity purification
- Phosphopeptide enrichment.

We identified candidates of the FER signalling complex with and without RALF1 elicitation and downstream targets of FER signalling and RALF1 dependent signalling through a phosphopeptide enrichment experiment. Despite different attempts to recreate a ROP activation assay published by Xu (2012) in our hands this assay did not show ROP activation. However we identified several potential interactors of ROP2, ROP6, RIC1 and RIC4.

Chapter 2

Material and Methods

2.1 Plant growth and treatments

2.1.1 Murashige and Skoog medium plates

Arabidopsis plants were grown on $\frac{1}{2}$ Murashige and Skoog medium (sigma), 0.5% sucrose, 1% phytoagar (Duchefa Biochemie) with 16 hours light at 22^{o}C for 7 days. Plants were then transferred to 10 mL liquid $\frac{1}{2}$ Murashige and Skoog media with 1% sucrose and allowed to equilibrate for 2 hours with gentle swirling. Plants were then treated with 1 μM RALF1 for 5 mins or 1 μM PEP1 for 15 mins (as a control). For RALF1 time course experiments, the plants were treated for 0, 2, 5, 10, 15, 20 and 30 minutes. Plants were then harvested and frozen in liquid N_2 and ground with a Dremel Drill.

2.1.2 Phytatrays

0.3g of Arabidopsis seeds were sown on suspended mesh in a phytatray (Sigma) with $\frac{1}{2}$ Murashige and Skoog (Sigma), 1% sucrose with 16 hours light at 22°C for 7 days. The volume of media was reduced to 80 mL and then the plants were left equilibrating while gently shaking for 3 hours. Roots were harvested separately to the leaf material and frozen in liquid N_2 and ground while frozen in a pestle and mortar.

2.1.3 Root phenotypes

Arabidopsis plants were grown on $\frac{1}{2}$ Murashige and Skoog medium (sigma), 0.5% sucrose, 1% phytoagar (Duchefa Biochemie) with 16 hours light at 22°C for 7 days. Images of the roots were taken 2 cm from the tip of the root using a bright-field microscope. At least 9 seedlings, and all root hairs in the frame, per line were characterised.

2.2 Cloning and protein expression

2.2.1 Cloning of synthetic constructs

A synthetic construct for RALF1-Active and RALF1-Null, containing a 6 his-tag at the 5' end, was produced by Integrated DNA Technologies (IDT). RALF1-Active is the bioactive form of the peptide, with a his-tag (HHHHHH) and linker (AIA) and the active peptide sequence (ATTKYISYQSLKRNSVPCSRRGASYYNCQNGAQANPYSRGCSKIARCRS).

Synthetic constructs were cloned into pET29a in DH5α and then the vector extracted using GeneJET Plasmid Miniprep Kit (Thermo Scientific) as per the manufacturer's protocol. The pET29a vectors were transformed into chemically competent BL21* cells.

A synthetic construct for RIC1/RIC4/ICR1 were ligated into pMAL-c2X and cloned into DH5α before being transformed into chemically competent BL21* cells for protein expression.

2.2.2 Protein expression

Expression of RALF1 was done by growing 750 mL of BL21* RALF1 *E. coli* to OD_{600} 0.6 at 28°C and then induced with 0.3 mM Isopropyl-β-D-thiogalactopyranoside (IPTG) (VWR) and incubated at 20°C over night and cells harvest, resuspended in 1 x Phosphate Buffered Saline (PBS) 0.3 M NaCl and stored at -20°C prior to lysis.

Expression of RICs was done by growing 750 mL of BL21* *E. coli* to OD_{600} 0.6 at 37°C and then induced with 0.3 mM IPGT (VWR) and incubated at 37°C for 2 hours before the cells were harvested, resuspended in 1 x PBS 0.3 M NaCl and stored at -20°C prior to lysis.

2.2.3 Native purification of RALF1

The expression of RALF1 was based on the methods used by Haruta et al (2014) and Morato do Canto (2014). RALF1 was extracted by sonication at 70% power 3 x 30 seconds with a native lysis buffer 50 mM NaH_2PO_4 and 300 mM NaCl, 10 mM imidazole and 1 mM phenylmethylsulfonyl fluoride

(PMSF) and centrifuged at max speed for 20 minutes at 4°C. Cell lysate was incubated with pre-equilibrated nickel (II) chloride beads (Thermo Scientific) for 2 hours mixing end-over-end. Beads were washed with 50 mM NaH_2PO_4 and 300 mM NaCl, 20 mM imidazole and 1 mM PMSF 3 x 1 mL and proteins eluted with 100 µL 50 mM NaH_2PO_4 and 300 mM NaCl, 250 mM imidazole and 1 mM PMSF.

2.2.4 Denatured purification of RALF1

RALF1 was expressed in BL21* and purified using batch method nickel (II) chloride beads (Thermo Scientific). Soluble proteins were extracted using native purification of RALF1 protocol in section 1.2.3. The pellet was washed twice with 50 mM NaH_2PO_4 and 300 mM NaCl, 10 mM imidazole, 1 mM PMSF and 0.5% triton x-100. The inclusion bodies were lysed by sonication at 70% power 3 x 30 seconds with a denaturing stock buffer 8M urea 100 mM NaH_2PO_4 10 mM Tris-HCl pH7.5 and 1 M NaCl, pH 8.0. Purification of RALF1 was done by incubating in nickel (II) chloride beads (Thermo Scientific) for 1 hour mixing end over end at 4°C. The beads were then washed with 3 x with stock buffer pH 6.3, then 3 x with pH 5.5.

The elutions were then dialysed using slide-A-lyzer (Thermo Scientific) in 3 steps in 0.1% formic acid (sigma). To concentrate the protein, RALF1 was lyophilised and resuspended in 0.1% formic acid to a concentration of 3.5 µg/µL.

2.2.5 Purification of Maltose Binding Protein tagged proteins

Cells were lysed using 5 mL lysis buffer [50 mM Hepes, 150 mM NaCl, 1 mM EDTA, 1 mM DTT and 1 mM PMSF] and sonication 3 x 30 seconds and centrifuged at max speed for 30 minutes at 4° C. Amylose beads (New England BioLabs) were pre-equilibrated with 4 washes with lysis buffer prior to incubating 0.03 mL of beads per 1 mg of protein lysate containing the MBP-tagged protein, for 2 hours mixing end-over-end at 4° C. Four washes with 2 mL lysis buffer were done and beads aliquoted into 20 µL.

2.2.6 HPLC purification of RALF1

Reverse-phase High Pressure Liquid Chromatography (HPLC) on a Beckman-Coulter Proteomelab PF2 machine was used with a C18 column. Undiluted 100-200 µg of cell lysate was injected onto the column in a volume of 200 µL. The solvent gradient was 2% Acetonitrile Nitrile (ACN):water up to 40% ACN:water over 15 minutes, then back to 2% ACN over 10 minutes. Fractions were collected and concentrated by lyophilising and resuspending in 0.1% formic acid.

2.3 Protein extraction

2.3.1 Microsome isolation

Seedlings were ground fresh in extraction buffer [100 mM Tris-HCl pH 8.8, 150 mM NaCl, 1 mM EDTA, 10% glycerol, 20 mM NaF, 1 mM PMSF, 1 x Protease Inhibitor Cocktail (PIC) (Sigma-Aldrich), and 1 mM Na_2MoO_4] and filtered through a Miracloth (Merck Millipore). The extract was centrifuged at 5,000 xg for 15 minutes at 4°C. Supernatant was transferred to ultracentrifuge compatible tubes and centrifuged at 130,000 xg for 30 minutes at 4°C . The microsome fraction was resolubilised using extraction buffer plus 1% NP-40 and sonicated in a water bath sonicator 3 x 30 seconds.

2.3.2 Protein extraction for phosphopeptide enrichment

Plants were grown in phytatrays for 10 days before being treated and harvested. Roots were ground in liquid nitrogen before adding 1 mL extraction buffer [50 mM Hepes, 150 mM NaCl, 1 mM EDTA, 20 mM NaF, 1 mM $Na_2MoO_4$and 1% Sodium dodecyl sulfate (SDS), 1 x PIC, 1 mM PMSF, 2 µM Calyculin A (Thermo Scientific), 1 mM Sodium orthovanadate and 1 mM Dithiothreitol (DTT)]. Samples were centrifuged at 3,000 xg for 15 minutes at 4°C. The supernatant was centrifuged again at 16,000 xg for 30 minutes at 4°C . A Bradford assay was done and a MAPK western blot was carried out with 30 µg of extract, and 20 µg was run on a SDS PAGE gel to check for protein degradation. The remaining protein was digested using FASP digest.

2.4 Nucleic acid

2.4.1 DNA extraction

Arabidopsis leaves were ground in liquid nitrogen and supplemented with 600 µL extraction buffer [100 mM Tris-HCl pH 8.0, 50 mM EDTA pH 8.0, 500 mM NaCl and 10 mM Beta Mercaptoethanol] and 40 µL of 20% SDS, before incubation at 65 ° C in a water bath for 20 minutes. The extract was then incubated on ice for 5 minutes and 200 µL potassium acetate added, prior to incubation on ice for a further 20 minutes. Samples were then centrifuged at max speed for 15 minutes and equal volumes of isopropanol added to the supernatant, and incubated over night at - 20 ° C. DNA was precipitated by centrifuging for 15 minutes at max speed and the supernatant removed and the pellet was washed by adding 1 mL of 70% ethanol and centrifuged for 5 mins. The ethanol was removed and the pellet allowed to dry before resuspending.

2.4.2 PCR

PCR for FER-ΔK-GFP genotyping was performed using forward primer: 5' CTGCTAGTGATGCAACATCAG 3' and reverse primer: 5' CATGGCG-GACTTGAAGAAG 3'. PCR programme: PCR mix was incubated at 95 ° C for 1.5 minutes prior to 30 cycles of 95° C 30 seconds, then 54 ° C for 30 seconds, and then 72 ° C for 1.75 minutes followed by a final 5 minutes at 72° C.

2.4.3 RNA extraction

Samples were ground using a tissue homogeniser with two glass beads, shaking for 2 x 5 seconds. 1 mL of Trizol (Thermo Fisher Scientific) was added to frozen material and vortexed thoroughly, followed by 200 µL of chloroform and vortexed for a further 15 seconds. Samples were then incubated on ice for 2 minutes and centrifuged at 4° C for 30 minutes at 13,500 rpm. The top layer of the supernatant was transferred to a new tube and 500 µL of isopropanol was added and left to precipitate overnight at -20° C. The samples were then centrifuged for 50 minutes at 4° C at 13,500 rpm. The supernatant was then discarded and the pellet washed with 75% EtOH/DEPC. The EtOH was left to evaporate and the pellet resuspended in 20 µL of DEPC/H_2O.

2.4.4 RT-qPCR

RNA samples were treated with TURBO DNA-free (Qiagen) to remove DNA contamination. cDNA synthesis was performed using RevertAid First Strand cDNA Synthesis Kit (Thermo Fisher Scientific) with 750 ng - 1000 ng of RNA along with the oligo $(dT)_{18}$ primer. 10 ng of cDNA with 0.4 µM concentration of primers and SYBR GREEN master mix (Thermo Fisher Scientific) was used for RT-qPCR with three technical replicas for each reaction. The PCR cycle was: 95° C for 5 minutes prior to 48 cycles of the following 95° C for 15 seconds 60° C for 30 seconds and 72° C for 30 seconds. A dissociation curve step was also used which consisted of 95 ° C for 1 minute, 55° C for 10 seconds and 95° C for 10 seconds.

Table 2.1: List of RT-qPCR primers

Gene	Primer (5' - 3')	Tm	GC%
PRP1 FP	ACACTCCACCCACCAAACCAT	61.89	52.38
PRP1 RP	TTGCTTTCGCTCCTTGAATAGGGT	62.63	45.83
TCH4 FP	TCACTGCTTCTTACCGTGGCT	61.71	52.38
TCH4 RP	CGAGCCAGTAGTAGTCCCCTGT	62.92	59.09
BR6OX2 FP	TCACTCGAGCTGTGATCTTTGAGAC	62.55	48
BR6OX2 RP	AACCGTTGAGTTCTAAGTCGTGAG	60.79	45.83
UBQ5 FP	GTAAACGTAGGTGAGTCCA	52.4	37
UBQ5 RP	GACGCTTCATCTCGTCC	54.7	58.8

2.5 Assays

2.5.1 pH change

Arabidopsis cell cultures derived from leaf material were diluted 1 in 7 in cell culture media and allowed to grow for 4 days under constant light, 22°C and 175 rpm shaking. The cell culture was then aliquoted into 10 mL fractions and allowed to equilibrate for 2 hours on a shaker prior to treatment. 1 μM RALF1 was added and the pH measured at 0, 0.5, 2, 5, 10, 15, 20, 25 and 30 minutes. Control treatments of equal volume of 0.1% Formic acid and 1 μM PEP1 were performed and the pH measured over the same time points.

2.6 Protein detection via western blot

2.6.1 MAPK western blot

20-30 μg of total protein extract was loaded onto a 12% acrylamide SDS gel. The gel was transferred to a PVDF blotting membrane (GE Healthcare) using wet transfer at 30 volts over night at 4°C. The membrane was then

rinsed in 1 x TBS- 0.1% Tween (T). All subsequent procedures were carried out on a rocking platform at room temperature. Blocking was performed with 5% (w/v) milk in TBS-0.1%T for 1 hour. Then rinsed in TBS-0.1%T and incubated in 1:2000 α-phopho MAPK (Cell Signalling technology) antibody diluted in TBS-0.1%T 3% BSA, for 2 hours. The membrane was washed for 3 x 10 minutes in TBS-0.1%T and then incubated in secondary antibody, α-Rabbit – HRP (Abcam), for 1 hour. The membrane was then washed as before and incubated in ECL (GE healthcare) and detected using Image Quant (GE healthcare).

2.6.2 Anti-GFP western blot

A 12% acrylamide SDS gel was run and transferred to a PVDF blotting membrane (GE Healthcare) using wet transfer at 30 volts over night at 4°C. The membrane was then rinsed in 1 x TBS- 0.1%T and all subsequent procedures were carried out on a rocking platform at room temperature. Blocking was performed with 5% (w/v) milk in TBS-0.1%T for 1 hour. The membrane was rinsed in TBS-0.1%T and incubated with 1:10000 α-GFP (Santa Cruz Biotechnology) antibody diluted in TBS-0.1%T 3% BSA for 2 hours and then washed 3 x 10 minutes with TBS-0.1%T and incubated in ECL (GE healthcare) and detected using Image Quant (GE healthcare).

2.7 Affinity purification

2.7.1 GFP Co-immunoprecipitation (Chromotek)

Protein was extracted from ground Arabidopsis material by supplementing with extraction buffer [10 mM Tris HCl pH 7.5, 150 mM NaCl, 0.5 mM EDTA, 1 x PIC, 1 mM PMSF and 0.5% NP-40] in a 2:1 volume to weight ratio. The samples were centrifuged at 16,000 xg at 4°C for 15 minutes. The supernatant was then transferred to a new tube and centrifuged again at 16,000 xg for 30 minutes at 4°C. The protein extract was added to 5 µL of equilibrated GFP trap (Chromtek) beads and incubated for 2 hours mixing end over end at 4°C. The beads were washed with 5 x 1 mL of stock extraction buffer and stored in 50 µL at -20°C.

2.7.2 ROP activation assay

Plants were grown on phytatrays as described in section 1.1.2 and a protein extraction was performed using the same procedure as previously described in 1.7.1, but with an extraction buffer [25 mM Hepes pH 7.4, 10 mM MgCl2, 100 mM KCl, 5 mM DTT, 5 mM NaF, 1 mM PMSF, 0.5% NP-40 and 1x PIC]. The ground Arabidopsis material was supplemented with extraction buffer in a 2.5 : 1 volume to weight ratio. The samples were then centrifuged at max speed at 4°C for 20 minutes to remove large debris and then centrifuged at max speed at 4°C for 30 minutes. The protein extract was incubated in pre-equilibrated amylose beads (New England BioLabs) for 15 minutes at 4° C and incubated with 20 µL RIC-MBP bound amylose beads for 2 hours at 4°C. The beads were washed with stock extraction buffer plus

5 mM DTT for 3 x 5 minutes.

2.7.3 Phosphopeptide Enrichment

After Filter Aided Sample Preparation (FASP) digestion of proteins, the peptide concentration was determined using Qubit (Thermo Fisher Scientific) and phosphopeptides were enriched using TiO_2 beads. First the proteins were diluted to a final concentration of 80% acetonitrile, 5% Trifluoroacetic acid (TFA) and incubated for 20 minutes before centrifuging at 5,000 xg for 15 minutes. TiO_2 beads were diluted to 1 mg of beads in 10 µL of DBH at 20 mg/mL and mixed for 10 minutes at 600 rpm. The TiO_2 beads were added to the peptides at a concentration of 1 mg of peptide, 2 mg of beads, mixed gently end-over-end for 20 minutes. This was repeated 3 times, keeping the three fractions separate throughout. A wash step was added to aid percentage enrichment with 10% acetonitrile, 5% TFA and the beads were centrifuged at 4,500 rpm for 2 minutes and supernatant removed. A C8 membrane was made in house using a pipette tip (200 µL tips), by placing a circular piece of C8 membrane inside a tip, making a column. The beads were added to the column before being washed with 40% acetonitrile and 5% TFA and centrifuging at 3000 rpm for 2 minutes. A final wash step using 60% acetonitrile and 5% TFA, and centrifuged as before, was then performed. The peptides were eluted from the TiO_2 beads using 20 µL of 5% ammonium hydroxide solution and centrifuging as before, followed by 20% ammonium hydroxide, 25% acetonitrile and centrifuging again. The ammonium hydroxide was then removed by speed vac for 20 minutes and the phosphopeptides were then cleaned up using C18 stage tip protocol.

2.8 Mass Spectrometry

2.8.1 In Solution Tryptic Digest

Equal sample volumes of ammonium bicarbonate (ABC) were added to the sample. 1 mM tris(2-carboxyethyl)phosphine (TCEP) was added and incubated for 60 minutes to reduce disulfide bonds. Cysteine alkylation was performed in 5.5 mM iodoacetamide (IAA) and incubating for 45 minutes in the dark. If the sample was in 8 M urea then a further dilution to 2 M urea was done by diluting with ABC. 1 µg of trypsin (Thermo Fisher Scientific) per 50 µg of protein was added and incubated at 37°C overnight. To cease the reaction, Trifluoroacetic Acid (TFA) was added to a final concentration of 0.1%. If samples had contained detergent or strong salt, a further clean up was done using C18-Stage tip prior to loading onto the MS.

2.8.2 On Bead Digest

Beads were centrifuged at max speed, supernatant removed and 50 µL of Ammonium Bicarbonate (ABC) was added to the sample. 1 mM DTT was added to the sample and then incubated for 60 minutes to reduce disulfide bonds. Cysteine alkylation was performed in 5.5 mM iodoacetamide (IAA) and incubating for 45 minutes in the dark. 1 µg of trypsin per 50 µg of protein was added and incubated at 37°C overnight. To cease the reaction TFA was added to a final concentration of 0.1%. If samples had contained detergent or strong salt, a further clean up was performed using C18-Stage tip prior to loading onto the MS.

2.8.3 In Gel Tryptic Digest

Gel slices were cut into cubes of 2-4 mm and transferred to a 1.5 mL tube. Coomassie stain was removed with 3 x destain washes using 50% EtOH, 50 mM ABC and incubating for 20 minutes while shaking at 650 rpm. The gel pieces were then dehydrated using 100% EtOH for 5 minutes at 650 rpm before proteins were reduced using 10 mM DTT (in 50 mM ABC) for 30 minutes at 56°C and shaken at 650 rpm. 55 mM IAA (in 50 mM ABC) was added to alkylate cysteine residues for 20 minutes in the dark. The band pieces were washed twice with 50% EtOH, 50 mM ABC for 20 minutes with shaking at 650 rpm, before dehydrating the gel pieces as before with 100% EtOH. 1 μg trypsin was added and gel pieces rehydrated at 4°C for 20 minutes and excess liquid removed and digested overnight at 37°C while shaking at 650 rpm. Peptides were extracted from the gel with 25% acetonitrile and sonicated in a water bath sonicator for 10 minutes. This was repeated three times. The peptides were concentrated in a Speed-vac until all acetonitrile was removed and then a C18-Stage tip clean-up was performed prior to MS.

2.8.4 FASP Digest

A 2 mL 3 kDa cut off filter column (Milipore) was used throughout the FASP digest. The column was washed using 2 mL of buffer (Phospho) and centrifuged at 4,500 rpm for 30 minutes. 1 mL of sample was the loaded and diluted with 1 mL 8 M urea and centrifuged for 15 minutes (or until 1 mL of buffer was passed through the column). Another 1 mL of 8 M urea buffer was added and centrifuged as before. Once the volume was at 1 mL, 10

mM TCEP and 40 mM chloroacetamide (CAA) were added and incubated for 20 minutes, then 1 mL of 25 mM Hepes was added and the sample was centrifuged as before. The urea was then washed out using 5 washes of 1 mL 25 mM Hepes and reducing the volume to no less than 1 mL. Next, 0.03 µg of LysC per 1 mg of protein and 1 µg of trypsin per 100 µg of protein was added and the sample left to digest overnight at 37°C. The peptides were then centrifuged through the column for 30 minutes. Finally 400 µL 20% acetonitrile was added to wash any residual peptides through the column and centrifuged for 10 minutes.

2.8.5 C18-Stage Tip

Samples were cleaned prior to MS using two C18 membranes layered in a 200 µL pipette tip. All centrifugations were performed at 2000 rpm. The membranes were washed prior to sample loading with 50 µL 100% MeOH and centrifuged for 2 minutes, followed by the addition of 50 µL of 100% acetonitrile and then centrifuging for 2 minutes. The membranes were equilibrated using 50 µL 2% acetonitrile and 0.1% TFA and centrifuged for 4 minutes. The sample was diluted, if needed, to 10 µg of peptides in a maximum total volume of 150 µL before being added to the column and centrifuged for 10 minutes. The bound peptides were then washed with 50 µL ethylacetate to remove detergents and centrifuged for 4 minutes. A final wash step of 50 µL of 2% acetonitrile 0.1% TFA was added and centrifuged for 4 minutes. The peptides were eluted with 20 µL of 80% acetonitrile and then centrifuged for 2 minutes. The samples were then concentrated in a Speed-Vac to remove the acetonitrile and then resuspended in 40 µL 2% acetonitrile and 0.1% TFA before being loaded onto the MS.

2.8.6 Protein identification from CoIP

Samples were generated by on-bead tryptic digests (section 1.8.2). Sample loading was optimised and 2 μL of sample loaded. the sample were separated with an UltiMate® 3000 HPLC series in Nano SeriesTM Standard Columns. The samples were analysed by means of nanoLC-ESI-MS/MS using the ultimate 3000/Orbitrap Fusion instrumentation (Thermo Scientific), with HCD fragmentation, in data dependent mode using a 90 or 120 minute separation on a 50 cm column.

2.8.7 Phosphopeptide detection

Samples were generated by phosphopeptide enrichment following the FASP tryptic digests in section 1.8.4. 20μL of sample was loaded, keeping all incubations as separate fractions. Samples were separated with an UltiMate® 3000 HPLC series in Nano SeriesTM Standard Columns and analysed by means of nanoLC-ESI-MS/MS using the ultimate 3000/Orbitrap Fusion instrumentation (Thermo Scientific), with HCD fragmentation, in data dependent mode using a 90 minute separation on a 50 cm column.

2.9 Data Analysis

2.9.1 Mascot

MS2 spectra peak lists in Mascot Generic Format (mgf) files were generated using the Xcalibur raw files, which are used for the subsequent mascot search:

Table 2.2: Mascot search parameters used.

Enzyme	Trypsin
Max number of missed cleavages	2
Fixed modifications	Carbamidomethylation
Variable modifications	Methionine oxidation, Phosphorylation on Serine, Threonine, Tyrosine
Peptide Tolerance (+/-)	10 ppm
MS/MS tolerance (+/-)	0.6 Da
Peak type	Monoisotopic
Peptide charge	2^+, 3^+ and 4^+

2.9.2 Max Quant

Table 2.3: Max Quant parameters used.

Enzyme	Trypsin
Max number of missed cleavages	2
Fixed modifications	Carbamidomethylation
Variable modifications	Methionine oxidation, Phosphorylation on Serine, Threonine, Tyrosine
Peptide Tolerance (+/-)	4.5 ppm
Label free quantification	Including match between runs
Peak type	Monoisotopic
Peptide charge	2^+, 3^+ and 4^+

2.9.3 StavroX

Table 2.4: StavroX search parameters used.

Enzyme	Trypsin
Max number of missed cleavages	3
Variable modification	Oxidised methionine
Cross linker	disulfide bond c-c, loss of H2
Precursor precision	10 ppm
Fragment ion precision	0.6 Da

2.9.4 Reproducibility-Optimized Test Statistic (ROTS)

Reproducibility-Optimized Test Statistic (ROTS) was used as an 'R' package as described by Pursiheimo et al., (2015). The number of bootstraps was set to 100 and the top list was set to $\frac{1}{4}$ of the input size.

Chapter 3

Expression and Purification of Rapid Alkalinisation Factor1 (RALF1)

3.1 Introduction

3.1.0.1 Rapid Alkalinisation Factor

Cell to cell messages are fundamental to many processes within the plant. The signalling peptide Rapid Alkalinisation Factor (RALF) was identified by Pearce et al. (2001) and is believed to be involved in growth and development. RALF was named after its ability to rapidly raise the pH of the media when applied to a cell culture (Pearce et al., 2001). The RALF family consists of 34 proteins in Arabidopsis, with high levels of homology with a hydrophobic region at the C-terminal end of the protein (Pearce et al., 2001). A review paper by Murphy and De Smet (2014) shows ten of the

RALF family proteins (including RALF1) share a conserved signal peptide, a propeptide with a dibasic Arg-Arg cleavage site just before the mature peptide. RALF23, one of the RALF family proteins that is highly homologous with RALF1, has been shown to be cleaved by site-1 protease just before the junction between the propeptide and mature RALF1, leaving the mature RALF peptide containing four cysteines (Srivastava et al., 2009). Pearce et al mapped two disulfide bonds in the mature RALF1 peptide using Mass Spectrometry (MS) and showed a bridge between cys-18 and cys-28 and a bridge between cys-41 and cys-47 (Pearce et al., 2001). By reducing and alkylating the disulfide bonds, Pearce et al., (2001) showed the activity of RALF1 was lost, meaning that the structure of RALF1 is crucial for its function. A hydrophobic conserved motif (YISY) at the N-terminal of RALF1 was also identified as being crucial for RALF function (Pearce et al., 2010).

A landmark paper identified the peptide RALF1 as a ligand for the receptor-like kinase FERONIA (FER). RALF1 interacts with the extracellular domain of the plasma membrane localised FER and the 'YISY' motif at the N-terminal of the RALF1 peptide is essential for interaction with FER (Haruta et al., 2014). Exogenous RALF1 lead to the inhibition of the plasma membrane ATPase, AHA2, leading to the alkalinisation of the apoplast, which is known to cause cell elongation inhibition (Haruta et al., 2014). When RALF1 is applied exogenously to sugar cane, inhibition of primary root growth and the number of lateral roots was reduced, indicating a strong link with RALF1 inhibiting cell elongation in Arabidopsis (Mingossi et al., 2010). RALF1 was also shown to reduce hypocotyl length as well as root length but did not have any effect on pollen grain germination (Mingossi et al., 2010). In relation to FER signalling in roots, mutants of FER have a root hair phenotype (Duan et al., 2010). The peptide RALF1 is highly

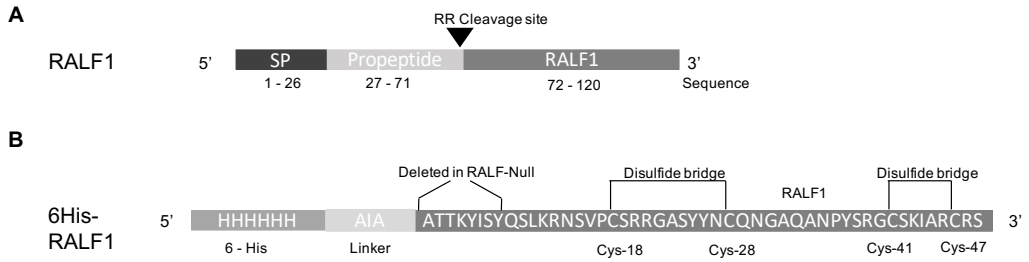

Figure 3.1: Schematic of RALF1

expressed within the developing root, considerably higher than in any other tissue (Klepikova et al., 2016).

Many defence related peptides lead to mitogen activated protein kinase (MAPK) activation when applied to plants. The peptide PEP1 was shown to induce MAPK activation after 15 minutes (Bartels et al., 2013). RALF causes a peak MAPK activation after five minutes, which almost completely reduced by 30 minutes (Pearce et al. 2001). This is much quicker than a large number of known defence related peptides including systemins, which activate MAPKs after 15 minutes (Pearce et al., 2001).

To study the downstream signalling events of RALF1, two synthetic RALF1 (RALF1-Active and RALF1-Null) constructs were produced by IDT (Figure 3.1). RALF1-Active is the bioactive form of the peptide, with a N-terminal his-tag (HHHHHH) and linker (AIA) followed by the active peptide (ATTKYISYQSLKRNSVPCSRRGASYYNCQNGAQANPYSRGCSKIARCRS) as used by Haruta et al (2014). The Null version was also used by Haruta et al. (2014) and contains the same his-tag and linker but with an eight amino acid deletion (ATTKYISY) from the beginning of the peptide sequence, which prevents RALF1 from interacting with FER.

RALF1 has been linked with a variety of other responses including links to

brassinosteroid signalling. Plants over-expressing RALF1 were found to be less affected by exogenous brassinolide (a brassinosteroid (BR) involved in promoting plant growth) and exogenous RALF1 induced two negatively regulated brassinosteroid-related genes, CONSTITUTIVE PHOTOMORPHOGENIC DWARF (CPD) and DWARF 4 (Bergonci et al., 2014), suggesting that RALF1 may act antagonistically with brassinosteroid signalling. A review by Murphy and De Smet (2014) proposed that RALF1 and brassinolide may act through shared signalling components because the addition of RALF1 led to the upregulation of some cell wall-remodelling enzymes such as PROLINE RICH PEPTIDE 1 (PRP1) and TOUCH 4 (TCH4), which was greatly reduced when treated with RALF1 and Brassinolide simultaneously (Bergonci et al., 2014). Furthermore, Haruta et al also showed that RALF1 caused the down regulation of some key genes involved in cell expansion including brassinosteroid-6-oxidase 2 (BR6OX2) and that this down regulation was lost in the *fer-4* mutant (Haruta et al., 2014).

3.1.0.2 Identifying X-linked peptides

Studying the structure and topology of proteins and complexes with mass spectrometry (MS) is becoming increasingly popular. StavroX is a leading software for the analysis of cross-linked peptides (Gotze et al., 2012). The software works by predicting tryptic digests from a protein FASTA sequence and calculates all possible theoretical cross-linked peptide candidates and then calculates all possible b and y ion series for a given cross-link site. The spectra are assigned by pattern matching and StavroX then scores how well the expected and observed fragmentation ions match up, while taking into account the intensity of the ions and signal to noise ratio of the spectra

(Gotze et al., 2012).

3.1.0.3 Aims

The aim of this chapter was to purify large quantities of RALF1 to enable our research into the RALF1-FER signalling pathway by looking at root growth inhibition. Once RALF1 was purified the aim was to test the activity of the purified RALF1 and to test which RALF1 responses depend on FERONIA in our system.

3.2 Results

3.2.1 Cloning and expression of His-RALF1 from *E. coli*

The expression and purification of RALF1 was based on the methods used by Haruta et al (Haruta, Sabat et al. 2014) and Do Canto (Morato do Canto, et al. (2014). A synthetic construct for RALF1-Active and RALF1-Null, containing a 6 his-tag at the 5' end, was produced by IDT, shown in Figure 3.1. The gene blocks were cloned into the expression vector pET29a and transformed into BL21* *E. coli* strain. BL21 strain of *E.coli* was also used but BL21* showed marginally better levels of protein expression, therefore BL21* was used for all future expression. Expression was induced by 0.03 mM IPTG and expression was optimised; leaving the induced culture overnight showed good levels of protein expression, as seen in Figure 3.2.

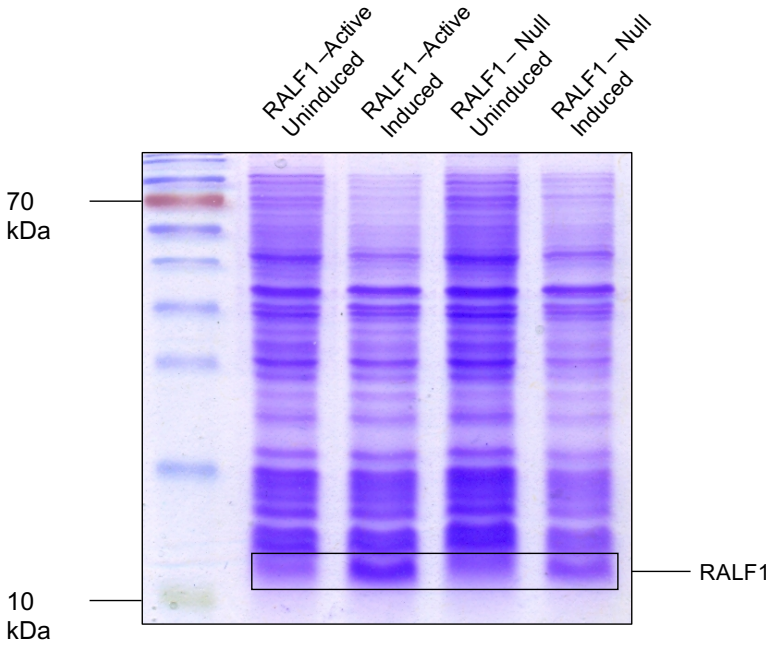

Figure 3.2: Expression of His-RALF1 after induction with IPTG. Coomassie stained SDS PAGE gel of total cell lysate from BL21* strain of E.coli before and after induction with 0.03 mM IPTG. RALF1-Active and RALF1-Null expected to be ~6 kDa, the bands that differ between the induced and uninduced are 12 kDa.

3.2.2 Purification of His-RALF1 from *E. coli* using nickel (II) chloride

To purify His-RALF1 from the soluble fraction of *E.coli* we used the AKTA system with an imidazole buffer which failed due to the protein forming inclusion bodies when expressed in *E.coli*. Purification using nickel (II) chloride beads with a batch method from inclusion bodies, using 8 M urea buffers to solubilise the protein aggregates, resulted in the purification of His-RALF1. The side chain of histidine binds to nickel (II) chloride immobilised on beads (Thermo Fisher Scientific), which can be added to the lysate to purify his-tagged proteins. Good purified protein yields were achieved using nickel (II) chloride to purify His-RALF1, as shown in Figure 3.3. By decreasing the pH to 6.3 the beads were washed and to aid the cleanup a further wash step using pH 5.5 was used. RALF1 was then eluted using a pH of 3.3, therefore the purified protein was denatured. On a SDS PAGE gel, RALF1 appears to run at 12 kDa rather than 6 kDa and also appears in double bands (Figure 3.3). To determine whether the protein at 12 kDa was RALF1, the band was cut out and the proteins identified by LC-MS/MS (Table 3.1). The 12 kDa band did contain RALF1 and several *E. coli* proteins, which may cause problems for downstream assays as they may trigger an immune response. In order to check that RALF1 responses were true and not a result of contaminating *E. coli* proteins from the purification, we planned to use RALF1-Null. RALF1-Null was a lot more variable and gave very poor yields when purified so RALF1-Null was not used.

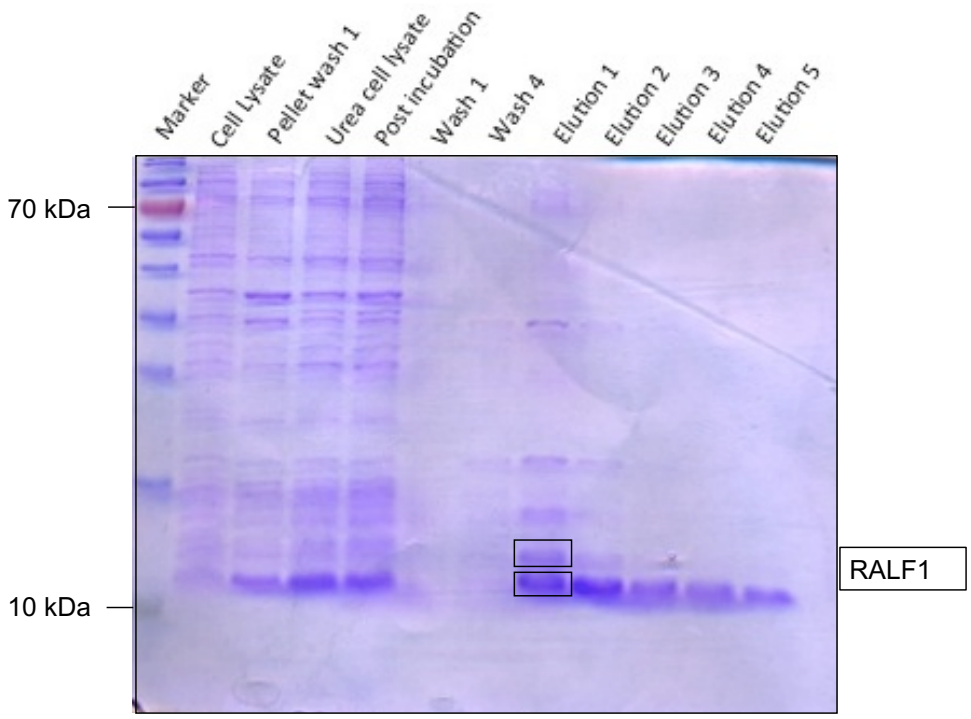

Figure 3.3: Purification of His-RALF1 from *E. coli* using nickel chloride beads. Coomassie stained SDS PAGE gel of each step of the purification of RALF1 using 8M urea. The highlighted bands were cut out and analysed by MS and confirmed that these bands contained RALF1.

Table 3.1: Proteins identified with His-RALF1 from SDS PAGE gel slice. The gel slices shown in Figure 3.3 were run on LC-MS/MS. The table shows the unique peptide count of all proteins identified from the two gel slices.

Accession number	Protein ID	Unique Peptide Count	
		Upper Band	Lower Band
AT1G02900.1	Rapid alkalinisation factor 1	4	4
Tryp_PIG	Trypsin	4	4
VanSb_Deletion	VanSb_Deletion	5	3
C5WBM0_ECOBB	50S ribosomal protein	4	4
AT1G07660.1	Histone superfamily protein	2	2
C5W4E3_ECOBB	Murein lipoprotein OS, E. coli	2	2
C5WBL9_ECOBB	50S ribosomal protein L10, E. coli	2	2
ALBU_BOVINE	Serum albumin	1	2

3.2.3 Activity of His-RALF1

To determine if our purified His-RALF1 was active, we looked at a variety of different known downstream targets of RALF1 elicitation. Firstly we looked at pH change of the media when a cell culture from *A. thaliana* leaves were treated with His-RALF1. As seen in Figure 3.4, His-RALF1 causes an increase in the pH of the media steadily over time, as does the control, PEP1. A concern was that the buffer that His-RALF1 is stored in was pH 2.5, due to the solubility issues. We found that raising the pH of the buffer to around pH 7 caused precipitation over time of His-RALF1. The precipitation was probably due to the higher pH being favourable for disulfide bond formation and in the absence of correct folding, this creates

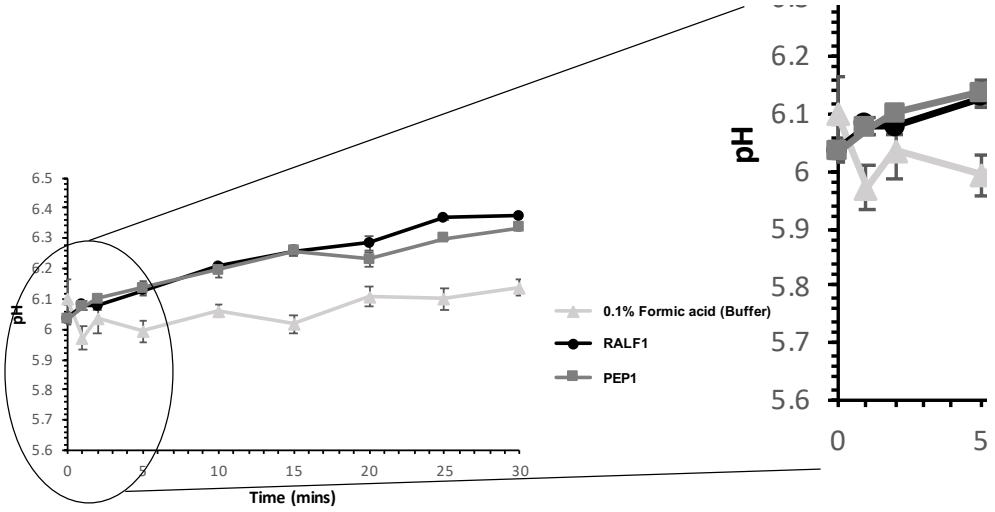

Figure 3.4: His-RALF1 induces alkalinisation of extracellular media in *A. thaliana* cell culture. pH measured over 30 minutes with His-RALF1 and PEP1 causing alkalinisation of the media when compared to the buffer only control.

aggregates (Trivedi et al., 2012). The effect of the low pH of the buffer can be seen in Figure 3.4 with the sudden drop of pH in the buffer only sample visible at 1 minute. Despite being in the same buffer, the drop in the His-RALF1 treated culture was not observed, suggesting that the increase in pH in the media is an incredibly quick response, occurring within 30 seconds, after His-RALF1 treatment. This suggests His-RALF1 is active.

To test that His-RALF1 responses depend on FER, we used MAPK activation in Col-0 and *fer-4* after RALF1 treatment, which occurs at 5 minutes (Pearce et al., 2001). *fer-4* is a null mutant and was used to determine if the activation of MAPKs by RALF1 was FER dependent. *A. thaliana* seedlings were transferred to a liquid media and left to equilibrate for 3 hours prior to being treated with either 1 μM His-RALF1 for 5 minutes or 1 μM PEP1 for 15 minutes as a control. An α-pMAPK western blot was performed to observe activated MAPKs after treatment. MAPK activation was observed weakly in Col-0 with His-RALF1 treatment along with a strong MAPK ac-

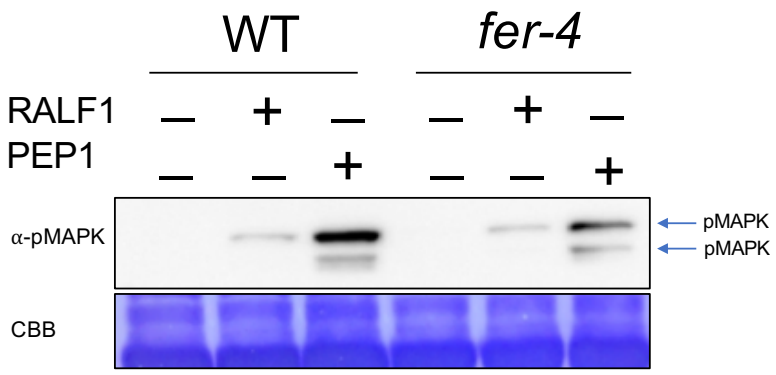

Figure 3.5: MAPK activation in *A. thaliana* seedlings after treatment with His-RALF1 or PEP1. Seedlings were treated with 1 μM His-RALF1 for 5 minutes or 1 μM PEP1 for 15 minutes as a positive control for MAPK activation. Anti- phosphorylated MAPK western blot showing weak RALF1 activation of MAPKs and strong MAPK activation by PEP1. Coomassie stained membrane showing equal loading of protein extracts.

tivation from PEP1 (Figure 3.5). We expected that no MAPK activation would be observed with RALF1 elicitation in *fer-4* as RALF1 is only known to interact with FER. However, there is a slightly weaker but still an increased level of phosphorylated MAPKs in *fer-4* when compared to Col-0 after His-RALF1 treatment (Figure 3.5). This could be due to a few contaminating *E. coli* proteins still present after Ni purification. The *E. coli* proteins could be causing an immune response or another form of stress and therefore triggering the MAPK response. To further purify His-RALF1 from the remaining *E. coli* proteins we used high pressure liquid chromatography (HPLC).

3.2.4 HPLC purification and characterisation of His-RALF1

To separate His-RALF1 from any remaining *E.coli* proteins, HPLC was performed. The HPLC purification of His-RALF1 was optimised to 100-200

Table 3.2: Proteins identified in HPLC purified His-RALF1. In solution tryptic digest done from HPLC purified His-RALF1 and analysed by LC-MS/MS. The table shows the top 10 proteins identified from 25 in total based on total spectrum count with a minimum of 2 peptides observed.

Accession Number	Name	Species	Total spectrum count
K2C1_HUMAN	Keratin, type II cytoskeletal 1	Human	39
AT1G02900	Rapid Alkalinisation Factor 1	Arabidopsis	34
K22E_HUMAN	Keratin, type II cytoskeletal 2 epidermal	Human	22
K1C9_HUMAN	Keratin, type I cytoskeletal 9	Human	17
K1C10_HUMAN	Keratin, type I cytoskeletal 10	Human	16
Tryp_PIG	trypsin	Pig	14
P60422_ECOLI	50S ribosomal protein L2	*E. coli*	11
K1C15_SHEEP	Keratin, type I cytoskeletal 15	Sheep	7
AT3G46520	Actin-12	Arabidopsis	7
ALBU_BOVINE	Serum albumin	Bovine	4

μg of RALF1 being loaded onto the column and a gradient of 2% ACN:water up to 40% ACN:water over 15 minutes, then back to 2% ACN over 10 minutes. HPLC purification of His-RALF1 showed one main peak of eluted protein at 5.5 minutes and continued eluting for approximately 1 minute. The peak was collected over 1 minute into two fractions of 500 μL each and these were run on a SDS PAGE gel in order to determine if the peak corresponded to His-RALF1, Figure 3.6. The strongest band at 12 kDa is exactly the same size as RALF1 previously confirmed via MS, however, the other two bands remained unidentified.

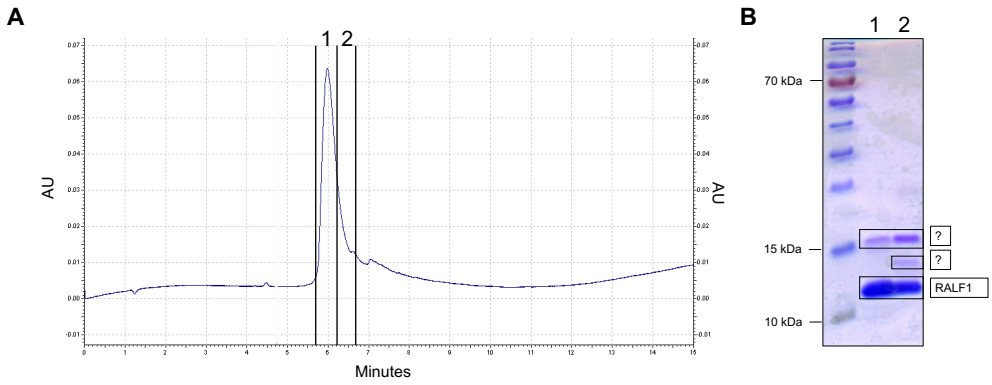

Figure 3.6: HPLC purified RALF1 contained within eluted protein at 5.5 minutes. A) HPLC of 150 µg His-RALF1 using a Reverse-phase c18 10 cm x 4.6 mL x 5 µm column with a flow rate of 1.2 mL/minute, 0.1% formic acid (FA) (solvent A) and Acetonitrile and 0.1% FA (solvent B) with a gradient of 2-50% solvent B over 7 minutes. 50-2% solvent B over 5 minutes. Wavelength at 280 nm to identify proteins. B) Coomassie stained SDS PAGE gel of two fractions collected from the peak in fraction 1. The 12 kDa band predicted to be His-RALF1 and the other two bands remained unidentified.

The activity of the HPLC purified RALF1 was analysed by an α-MAPK western blot, the previously observed weak activation of MAPKs by RALF1 was lost. Given the loss of activation of MAPKs and the unidentified bands seen in Figure 3.6 and the shoulder on the peak from the chromatogram, the eluted His-RALF1 fraction was analysed further. The purified His-RALF1 underwent an in solution tryptic digested and was analysed via LC-MS/MS to identify proteins, Table 3.2. The MS data was analysed against the *A. thaliana, E. coli* and common contaminants database using a commercially available programme (Mascot) to assign the spectra to peptides. 25 proteins were identified from the purified RALF1 sample, with nine proteins being identified from the common contaminants database, with five out of the top 10 proteins being identified as human. 10 proteins were identified from the *E. coli* database, but all with relatively low abundance by looking at

total spectrum counts. There were five proteins identified from *A. thaliana* database, which would not be expected due to RALF1 being expressed in *E. coli* and were possibly false positives and/or misassigned. A decoy database was used to try limit the number of misassigned peptides, however, by using the entire *A. thaliana* database to search for RALF1 the pattern matching nature of the software will often result in noisy spectra being incorrectly assigned.

3.2.5 Analysis of His-RALF1 folding

To investigate whether HPLC purified His-RALF1 was properly folded, different tryptic digests of RALF1 were analysed by LC-MS/MS. A tryptic digest was performed in which RALF1 was neither reduced with Dithiothreitol (DTT) or alkylated with Iodoacetamide (IAA), allowing for the disulfide bonds to remain intact when injected into the Mass Spectrometer. Using a cross-linking software, StavroX, the disulfide bonds could be assigned. As previously published by Pearce et al, (2001), RALF1 should contain 2 disulfide bonds.

RALF1 was observed predominately in two states, with some RALF1 showing the correct disulfide bonds formation with a bond between Cys-18 and Cys-28 (Figure 3.7). However, a large proportion of the HPLC purified RALF1 was dimerised, with a bond between Cys-28 of one RALF1 peptide and Cys-28 of another RALF1 peptide (Figure 3.8). This dimerisation could have been caused during expression in *E. coli*, as the cytoplasm of *E.coli* does not possess protein folding systems like those found in eukaryotes. However, given the faint MAPK activation that was previously detected prior to HPLC

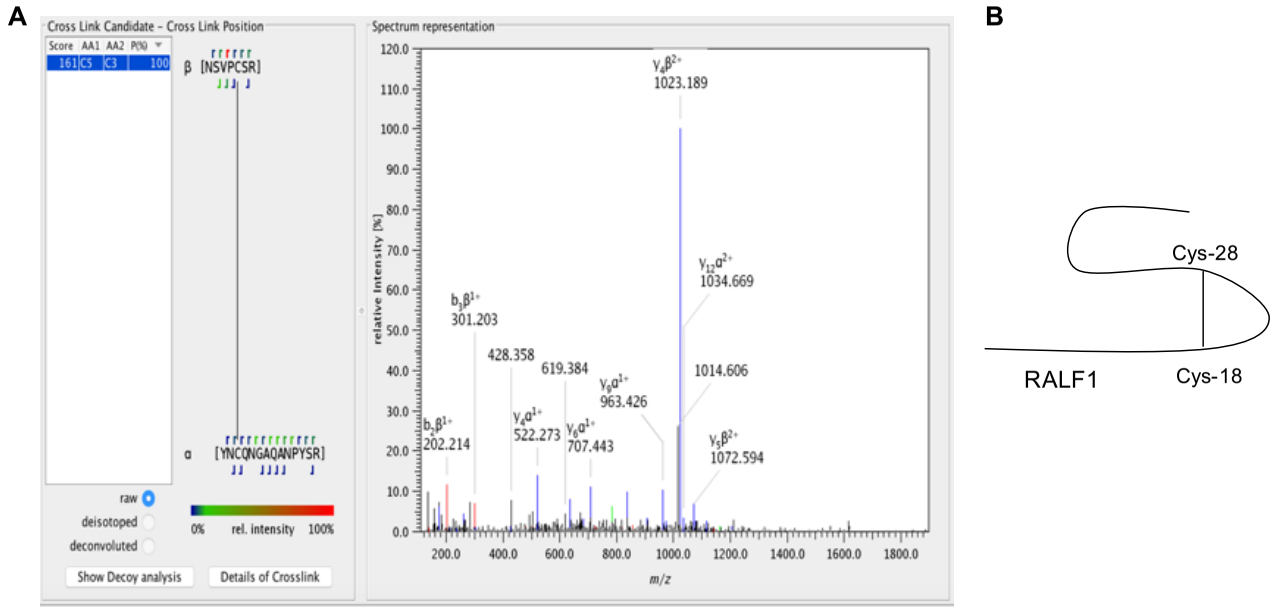

Figure 3.7: HPLC Purified His-RALF1 exists correctly folded. MS2 spectra of disulfide bonds visualised using StavroX of correctly folded RALF, with disulfide bond formation between Cys-18 and Cys-28.

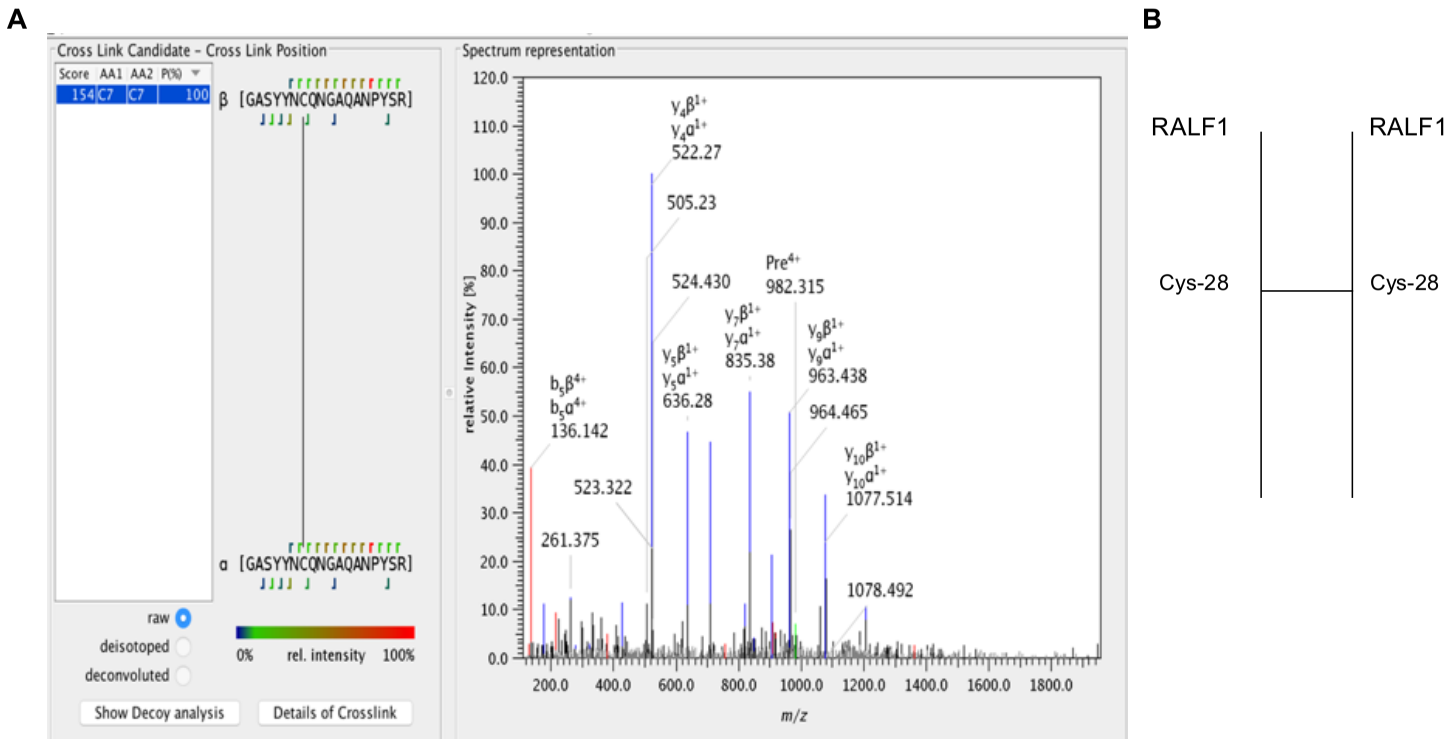

Figure 3.8: HPLC purified His-RALF1 exists as a dimer. MS2 spectra of disulfide bonds visualised using StavroX RALF1 existing as a dimer at Cys-28

purification was no longer observed, the handling of the protein could have caused further dimerisation to occur. The decision was made to order a synthetic RALF1 protein and not try and refold RALF1, as Morato do Canto et al., (2014) showed synRALF1 worked similarly to His-RALF1 at a 500 nM concentration.

3.2.6 Synthetic RALF1

Synthetic RALF1 (synRALF1) was made by Peptide Synthetics and underwent a Glutathione oxidisation / reduction reaction to aid disulfide bond formation. To test whether synRALF1 was active, a time course was performed looking at activated MAPKs. Using seedlings in swirling liquid media, 1 μM synRALF1 was added and the plants were harvested at specific time points from 0 minutes to 30 minutes. An α-MAPK western blot was performed to examine activated MAPKs. MAPK activation peaked at 5 minutes and then gradually reduced from 10 - 30 minutes (Figure 3.9). This indicates that synRALF1 is active as Pearce et al., (2001) showed the same RALF1 effect on MAPK activation.

To test whether MAPK activation depends on FER, we performed an α-MAPK western blot, using *fer-4* as a control. The seedlings were treated for 5 minutes with 1 μM synRALF1 in both Col-0 and *fer-4* lines and the peptide PEP1 was included as a control for MAPK activation. synRALF1 activation of MAPKs was only observed in Col-0 and no increase in MAPK activation in *fer-4* was observed, showing that RALF1 activation of MAPKs is dependent on FER signalling (Figure 3.10). Importantly, *fer-4* is still capable of producing a MAPK response, activated MAPKs are present after

treatment of 1 μM PEP1 after 15 minutes, but synRALF1 does not cause activation of MAPKs in *fer-4*.

In order to confirm synRALF1 activates responses downstream of MAPKs, the expression of three genes that are known to change in response to RALF1 treatment was measured by RT-qPCR. Seedlings were grown on plates and treated with 1 μM synRALF1 and harvested after 30 minutes. A Welch's *t*-test was performed on the ΔΔct values to determine gene expression that changed significantly with RALF1 treatment. *PRP1* and *TCH4* have been shown to be upregulated downstream of RALF1 and *BR6OX2* has been shown to be downregulated (Bergonci et al., 2014) (Haruta et al 2014).

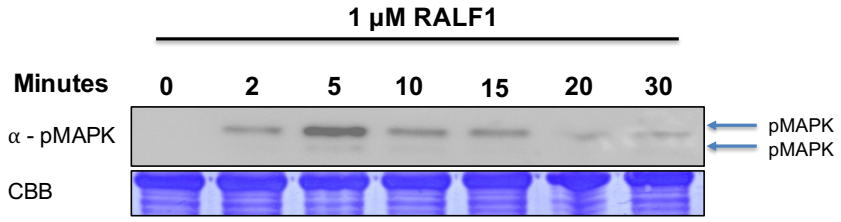

Figure 3.9: MAPK activation peaks at 5 minutes after RALF1 treatment of *A. thaliana* seedlings. Seedlings were treated with 1 μM RALF1 over 8 time points from 0 minutes to 30 minutes. An α-phosphorylated MAPK western blot shows peak activation at 5 minutes. Coomassie stained membrane to show equal loading of protein extract.

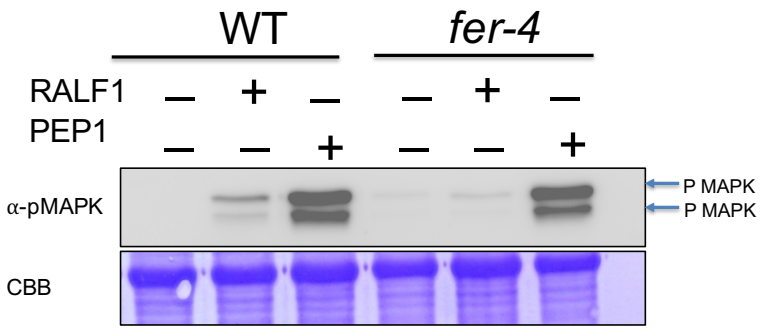

Figure 3.10: RALF1 activation of MAPK depends on FERONIA in *A. thaliana* seedlings. Col-0 and *fer-4* seedlings were treated with 1 μM RALF1 for 5 minutes and 1 μM PEP1 for 15 minutes. Coomassie stained membrane to show equal loading of protein extract.

However, our RT-qPCR data does not show such a clear cut result for all the genes (Figure 3.11). Transcript levels of *TCH4* are upregulated by a fold change of 13.8 in Col-0, which is significantly reduced in the *fer-4* RALF1 treated samples. Neither *PRP1* nor *BR6OX2* appear to change in response to RALF1 in Col-0 under our experimental conditions (Figure 3.11). *PRP1* expression was very variable over the three replicas and therefore if the increase in expression is small this would not have been seen. The ct value (the cycle at which is was detected) for BR6OX2 was very high under these PCR conditions which could be the reason why no downregulation was observed. An interesting result, is the downregulation of PRP1 by more than double (fold change of 0.4) in *fer-4* RALF1 treated plants. Why this occurs was not investigated further due to time restraints.

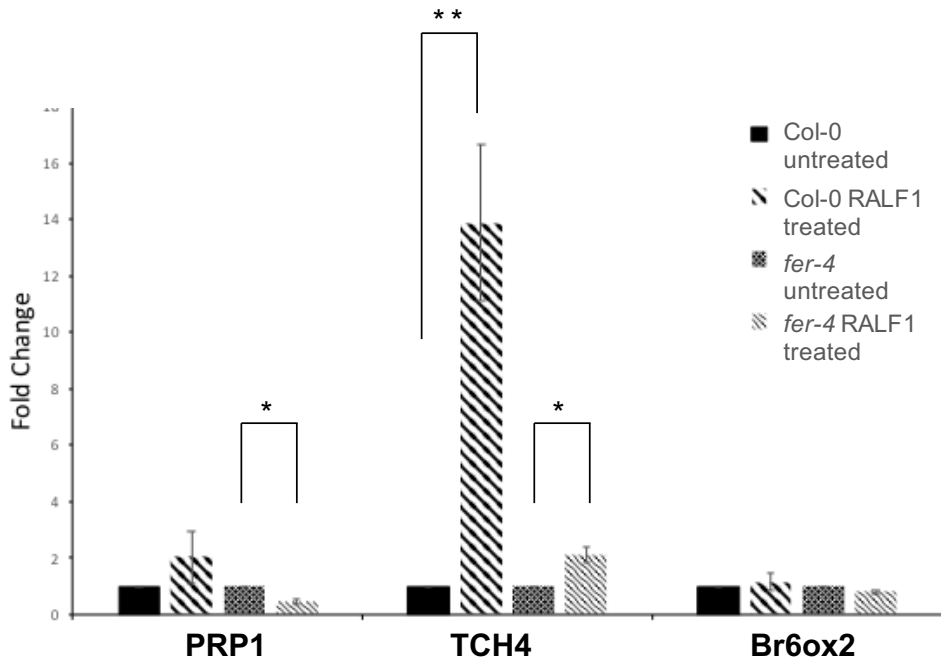

Figure 3.11: RALF1 induced changes to expression of TCH4. Fold change of expression after RALF1 treatment in Col-0 and *fer-4* seedlings. Expression was normalised to untreated sample for each genotype. Error bars show standard error over 4 biological replicas. Welch's t-test was performed for statistical significance with * = $P \leq 0.05$ and ** = $P \leq 0.005$.

3.3 Discussion

The aim of this chapter was to purify RALF1 and to determine if it induces FERONIA dependent responses. The purification of RALF1 proved challenging despite publications from Haruta et al., (2014) and Do canto et al., (2014). At first we attempted to follow the protocol described by Haruta et al., (2014), which used a native purification step. However, without the additional maltose binding protein (MBP) tag that they had included along with a tobacco etch virus (TEV) cleavage site to remove the tags, making their protein sequence His-MBP-TEV-RALF1), RALF1 was insoluble. We

then moved to purifying RALF1 under denaturing conditions as described by Do Canto et al., (2014). Despite having successfully optimised an expression and purification method for RALF1, the activity of RALF1 was lost. The purification of RALF1 could have been optimised further with the addition of reducing agents to the extraction buffers to break the disulfide bonds and keep them reduced throughout purification with DTT added to 8 M urea. However, there was no guarantee that when the protein underwent dialysis to remove the 8 M urea that the correct disulfide bonds would form. As Do Canto et al showed that synRALF1 worked as efficiently as purified RALF1, in the interest of time we decided to purchase synRALF1.

Having purchased RALF1, the activity of synthetic RALF1 was assessed. Synthetic RALF1 was successfully shown to be active and yielding biological responses expected from the literature (Morato do Canto et al., 2014). The MAPK western blots demonstrated that synRALF1 activates MAPKs at 5 minutes after treatment, and that MAPK activation is lost in the *fer-4* line, indicating RALF1 induced MAPK responses require FER. The wound response peptide PEP1 activates MAPKs at 15 minutes (Bartels et al., 2013), and Pearce et al., (2001) showed that RALF1 activates MAPKs at 5 minutes, and Haruta et al., (2014) identified FER as a RALF1 receptor, however the loss of MAPK activation by RALF1 in the *fer-4* mutant has not been shown before.

We examined the changes further downstream, such as gene expression changes with the RT-qPCR. Although these were not quite as conclusive as the MAPK western blots, the response of *TCH4* showed promising signs that RALF1 was active. It would have been interesting to follow up why *PRP1* was significantly downregulated with RALF1 treatment in *fer-4*. The

downregulation of *PRP1* with RALF1 treatment in the *fer-4* is unexpected and could be due to RALF1 interacting with another receptor in the absence of FER, causing differing downstream gene changes. To date there is no other known receptor of RALF1. *TCH4* was significantly upregulated in the *fer-4* mutant with RALF1 treatment, although greatly reduced when compared to the upregulation observed in wild type. This strengthens the idea that RALF1 could be acting through another receptor. Another explanation could be that the upregulation of *PRP1* with RALF1 treatment is part of an intricate feedback loop and when FER is removed it leads to the downregulation of *PRP1*. As the data for these genes is published and the aim of the experiment was to look for RALF1 activity, these questions were not pursued further.

Chapter 4

Feronia signalling components

4.1 Introduction

Feronia was first identified for its role in fertilisation (Escobar-Restrepo et al., 2007) but has been shown to be constitutively expressed across all tissues except pollen tubules (Escobar-Restrepo et al., 2007)(Guo et al., 2009; Duan et al., 2010). FER has been linked to a variety of different processes across the plant, including pathogen resistance (Keinath et al., 2010; Kessler et al., 2010), vegetative growth, root hair elongation and seed development as reviewed by Li and Zhang (2014). The expression of FER is induced by auxin, ethylene and brassinosteroid (BR), but is repressed by abscisic acid, which supports the theory that it has a critical role in developmental processes (Guo et al., 2009; Deslauriers and Larsen, 2010; Yu et al., 2012). FER has also been shown to influence the production of ROS, alter apoplast pH and be implicated in Ca^{2+} signalling (Duan et al., 2014; Haruta et al., 2014). Recently Shih et al determined that FER is a key regulator of mechanical

Ca^{2+} signalling, and that this FER-dependent signalling pathway regulates growth in response to external or intrinsic mechanical stimuli (Shih et al., 2014).

Several interactors of FER have been identified, summary of known FER interactors is shown in Figure 4.1. A ligand for FER has been identified as Rapid-Alkalinisation Factor 1 (RALF1), which specifically interacts with the extracellular domain of FER, leading to downstream phosphorylation changes (Haruta et al., 2014). RALF1 induces phosphorylation of FER kinase domain at S-871, S-874 and S-858, with phosphorylation at S-858 being increased ∼20 fold with RALF1 treatment (Haruta et al., 2014). RALF1 interaction with FER leads to the phosphorylation of plasma membrane H(+)-ATPASE 2 (AHA2) resulting in the inhibition of proton transport (Haruta et al. 2014). Phosphorylation studies show this to be due to the increase in phosphorylation of S-899 of the AHA2, as seen with flg22 and FLS2 (Nühse et al., 2007)(Haruta et al., 2014). In addition to the three phosphosites found by Haruta et al., (2004), a large scale phosphoproteomics experiment identified five phosphorylation sites in FER kinase and C-terminal domains; S-695, T-696, S-701, S-861 and S-866 (Nühse et al., 2004).

Other proteins known to interact with FER are the female gametophyte-expressed glycosylphosphatidylinositol (GPI) anchored protein LORELEI and the GPI anchored protein LLG1, which is expressed in seedlings (Li et al., 2015). LLG1 forms a complex with FER by interacting with the extracellular juxtamembrane region of FER in *A. thaliana* protoplasts (Li et al., 2015). This complex of RALF1–LLG1/FER triggers activation of the guanine nucleotide exchange factor (GEF) – Rho-related GTPase from plants

(ROP) pathway that mediates auxin-dependent root hair development (Li et al., 2015). Duan et al. (2010) showed that ROP-GEF1 interacts with FER and ROP2 independently of RALF1, in mesophyll and root protoplasts made from plants grown on high auxin.

FER also uses the GEF1/4/10–ROP11 pathway to activate ABI2 phosphatases, inhibiting the ABA response (Yu et al., 2012). These interactions were shown using yeast-2-hybrid, Bimolecular Fluorescence Complementation (BiFC) in protoplasts and in seedlings with a FLAG tagged FER line, and was shown to inhibit FER phosphorylation (Chen J et al., 2016). FER link to hormone perception is further strengthened with FER phosphorylation shown to increase in plants treated with ABA, as is the same when plants are treated with RALF1 (Chen J et al., 2016). Duan et al. (2010) showed a link between FER signalling and auxin with plants grown in high auxin showing FER interaction with ROPs. RALF1 has been shown to inhibit brassinosteroid signalling with overexpressing RALF1 plants being less sensitive to exogenous brassinosteriods and the gene *BR6OX2* (a brassinosteriod regulated gene involved in cell expansion) (Bergonci et al., 2014)(Haruta et al., 2014).

FER's link to immunity has been demonstrated in addition to the developmental processes described above. RALF1 has been shown to cause the recruitment of an immunity associated cytoplasmic kinase (RIPK) to the RALF1-FER complex and lead to phosphorylation of both FER and RIPK (Du et al., 2016). RALF1 is part of large family of signalling peptides and two closely related family members, RALF23 and RALF33, have been found to interact with the extracellular domain of FER (Stegmann et al., 2017). A well known receptor complex involved in immunity, FLS2-EFR/BAK1, is

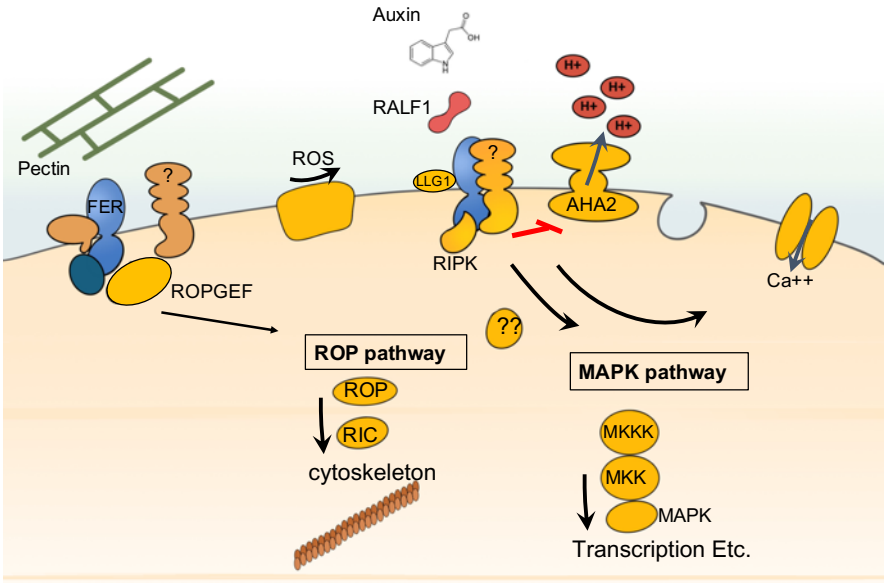

Figure 4.1: Schematic showing FERONIA signalling pathways.

reduced in the *fer-4* mutant, strengthening the theory that FER is involved in immunity (Stegmann et al., 2017). FER is said to promote the complex formation between FLS2/EFR and their co-receptor BAK1 and RALF23 inhibits this formation (Stegmann et al., 2017).

All the plant lines used in this research are already published characterised lines. The phenotypes of two FER mutants have been characterised and published (Duan et al., 2010), *fer-4* and *fer-5*. Using RT-PCR Duan et al. (2010) determined *fer-4* has a T-DNA insertion in the extracellular domain-coding region, making it a null mutant (Duan et al., 2010). *fer-5* is described as having truncated transcripts, consistent with its T-DNA insert being close to the end of its kinase domain-coding region (Duan et al., 2010). *fer-4* and *fer-5* are in Columbia (Col-0) background. Two further FER lines were characterised by Shih et al., (2014); FER-KR-GFP and FER-ΔK-GFP. The mutants, *pFER::FER-KR-GFP* and *pFER::FER-ΔK-GFP*, are in *fer-4 (*Col-0*)* background and are the result of chimeric genes being

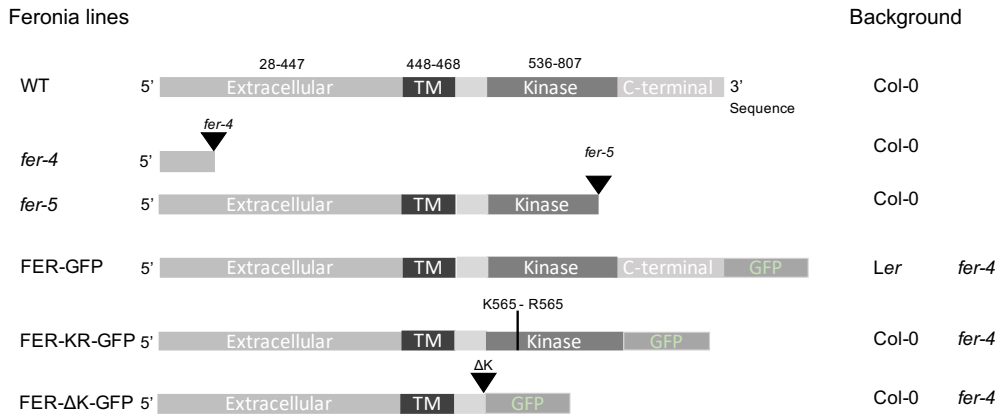

Figure 4.2: Domain map of the FERONIA lines and their plant background used in this research. *fer-4* has a T-DNA insertion in the extracellular domain-coding region, making it a null mutant. *fer-5* is described as having truncated transcripts with a T-DNA insertion close to the end of the kinase domain. KER-KR is a mutation K565 to R565 and FER-ΔK is a truncated transcript without the kinase and C-terminal domain.

introduced into *fer-4* (Shih et al., 2014). FER-KR-GFP has a mutation at K565 which was changed to R565 making the kinase domain inactive and the FER-ΔK-GFP is a truncated form with a deleted kinase domain (Shih et al., 2014). Figure 4.2 shows the location of the FER mutants. The FER-GFP line used in this project is the full length transcript under the native FER promoter in Landsberg (L*er*) background that complements the *fer-4* loss of function mutation (*pFER::FER- GFP*). We also attempted to work with a *pFER::FER- GFP* complementation of the *fer-4* mutant in Col-0.

The aim of this chapter was to identify FER-GFP interacting proteins with RALF1 elicitation in a native root system and use FER-KR-GFP and FER-ΔK-GFP mutants to assess the contribution of FER kinase activity.

4.2 Results

4.2.1 Root hair phenotypes of mutants used and FER kinase activity.

The root hair phenotypes of FER mutants, *fer-4* and *fer-5*, were characterised by Duan et al., (2010). In order to check the recovery of the *fer-4* phenotypes in mutants expressing FER-KR-GFP or FER-ΔK-GFP, the root hairs were characterised, illustrated in Figure 4.3.

By characterising the root hairs of the different lines a more rounded view of the phenotypes is observed. Col-0 has 100% of root hairs classified as normal and the introduction of FER-GFP in the Landsberg (*fer-4* /L*er)* line caused almost full recovery of wild type root hair phenotype (Figure 4.4). Therefore we concluded that FER-GFP was comparable to wild type as the phenotype was rescued. The four mutants shown in Figure 4.4 are in Col-0 background. 48% of root hairs in FER-ΔK-GFP were classified as defective, which is similar to *fer-4*, the complete knockout mutant, where 60% of all root hairs were classified as defective (Figure 4.4). FER-KR-GFP had a very similar phenotype to the truncated FER mutant *fer-5*, with 80% normal root hairs in FER-KR-GFP and 86% normal root hairs in *fer-5*. This shows that the kinase domain and the kinase activity are important for FER function.

For the three GFP lines, pFER::FER-GFP (L*er*), pFER::FER-KR-GFP (*fer-4* /Col-0) and pFER::FER-ΔK-GFP (*fer-4* /Col-0), the localisation of the FER-GFP was observed using confocal microcopy to determine if the mutations altered localisation. Seedlings were grown on plates for seven days and then imaged on a laser scanning microscope 710 (Zeiss). All three of the

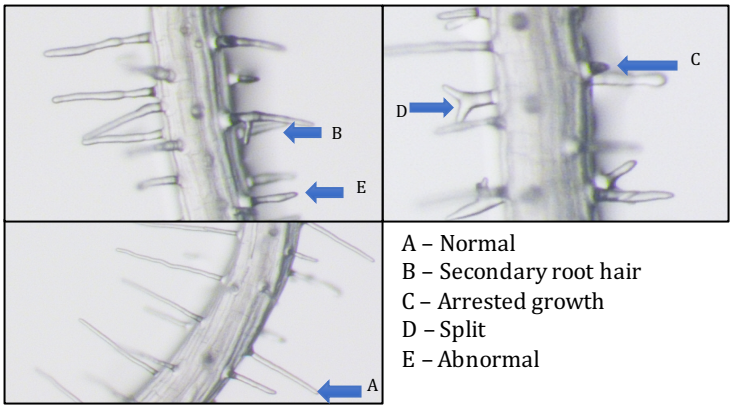

Figure 4.3: Characterisation of root hair phenotypes induced by mutations in FERONIA in *A. thaliana*. Seedlings were grown on plates and imaged at 7 days old. Root hair phenotypes were classified into 5 categories: Normal, secondary root hair, arrested growth, spilt and abnormal (short or bulging).

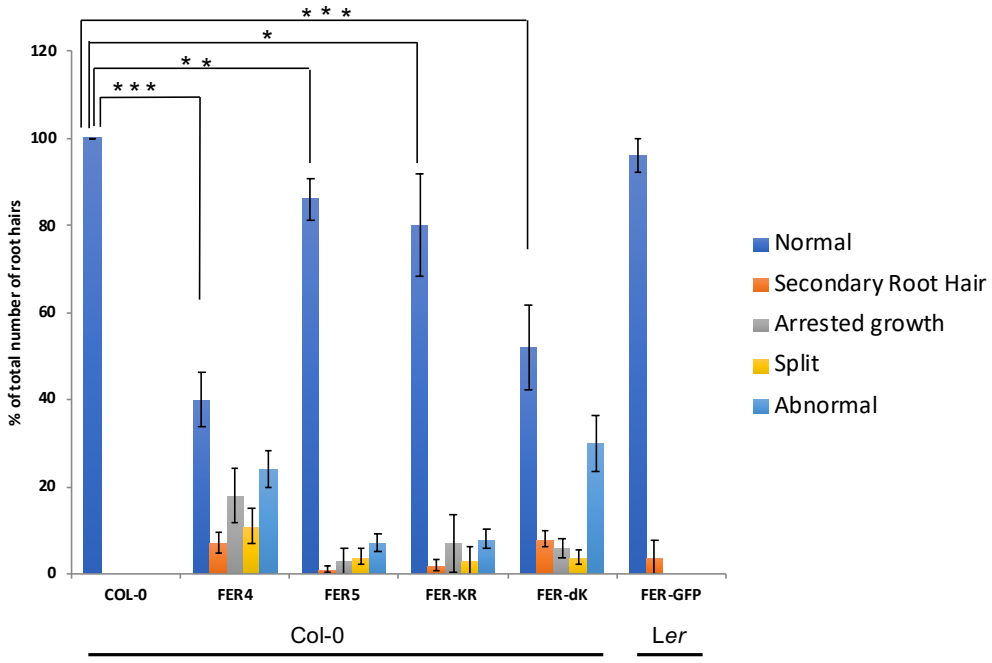

Figure 4.4: FERONIA mutants induce root hair phenotypes in *A. thaliana* . Seedlings from 4 different FER mutants were grown on plates, imaged at 7 days old and characterised as per Figure 4.3. pFER::FER-ΔK-GFP shows no recovery of the phenotype and pFER::FER-KR-GFP shows partial recovery of the root hair phenotype, whereas pFER::FER-GFP shows a full recovery of the *fer-4* mutant root hair phenotype. The error bars denote standard error from at least 9 seedlings. * = $p < 0.05$, ** = $p < 0.005$ and *** = $p < 0.0005$

GFP expressing FER lines are under the FER natural promoter which enabled a more accurate look at the how the FER mutants altered localisation. FER-GFP is expressed in all cells including root hairs and the introduction of the FER mutations did not change FER-GFP localisation to the PM, which was also seen in the FER-KR-GFP (Figure 4.5). The FER-ΔK-GFP also shows expression of FER in all cell types and at the PM, however more aggregates of GFP signal (localised to specific dots) were observed compared to the wild type line FER-GFP. The GFP signal of FER-ΔK-GFP was much weaker than that observed from both FER-GFP and FER-KR-GFP.

4.2.2 Identification of FER interacting proteins from hydroponically grown roots

An attempt to work with FER-GFP in *fer-4* Col-0 background proved complicated, as despite showing a normal root phenotype with full recovery of the *fer-4* phenotype, there was no GFP expression observed. An anti-GFP western blot on the total protein extract was performed, and in case the expression was low, an anti-GFP CoIP was done to enrich for GFP followed by a western blot, however anti-GFP signal could not be detected on either of the western blots. Confocal microscopy was also used to identify GFP expression and again none was observed. In the interest of time FER-GFP (L*er*) was used for proteomic experiments.

To investigate which proteins interact with FER upon synRALF1 elicitation within roots, FER-GFP CoIPs were performed with 1 μM synRALF1 elicitation for 5 minutes using the 35S::GFP (Col-0) overexpressing line as a control. Seedlings were grown in phytatrays and the roots were harvested.

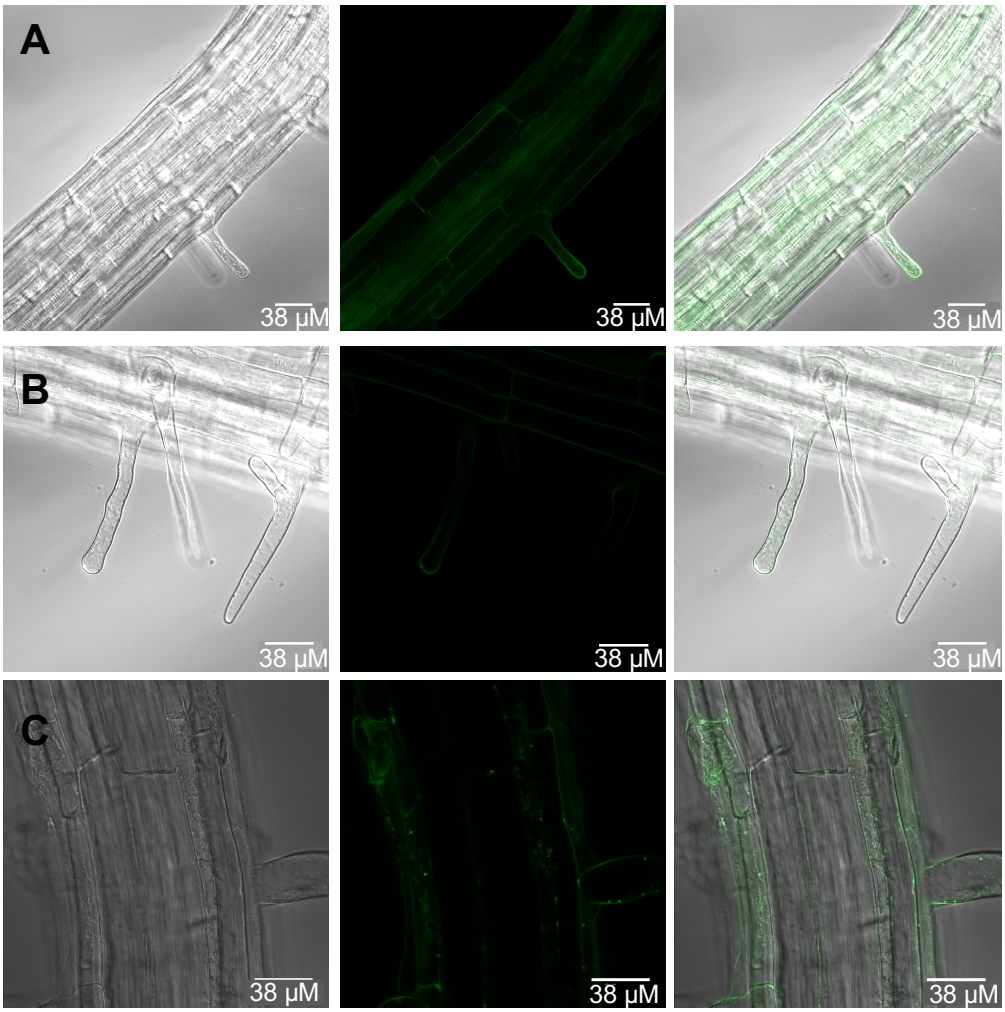

Figure 4.5: FER-GFP localisation is not altered in FER-KR-GFP, however FER-ΔK-GFP showed aggregated FER-GFP signal in *A. thaliana* roots. Seedlings were grown on plates and imaged using a confocal (laser scanning) microscope 710. A) pFER::FER-GFP localisation in a root using a x10 lens. B) pFER::FER-KR-GFP localisation in a root using a x20 lens and C) pFER::FER-ΔK-GFP localisation in a root using a x20 lens.

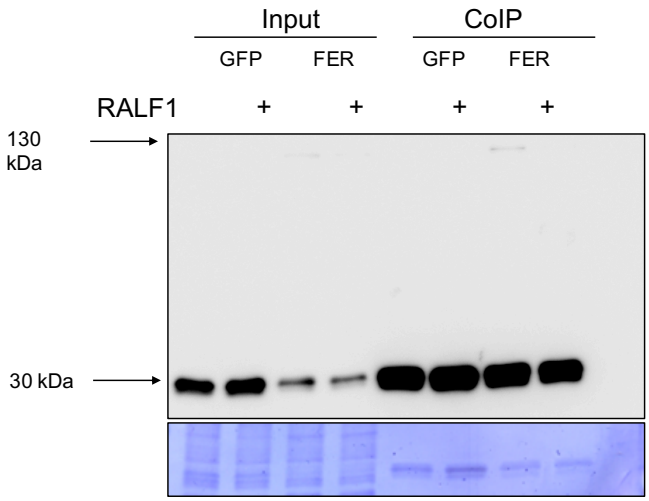

Figure 4.6: FER-GFP was unreliably detected in FER-GFP CoIP samples. A representative anti-GFP western blot of FER-GFP CoIP (Batch 1), showing amounts of free GFP present in FER-GFP line and FER-GFP unreliably detected in FER-GFP sample.

Phytatrays enable 1,500 seedlings to be grown hydroponically in liquid media within one tray, keeping the environment of a large number of roots the same. A protein extraction was done from the root material and was used for the CoIP using Chromotek GFP-TRAP beads. The experimental set-up is shown in Figure 4.7 A. 10% of the CoIP was tested by an anti-GFP western blot. As FER-GFP is under its natural promoter we were unable to detect FER-GFP reliably using a small percentage of material on the western blot, but could detect a free GFP band in the GFP only control (Figure 4.6), we continued to MS analysis for all four replicas of the FER-GFP CoIPs.

The CoIP samples were digested on the beads with trypsin and analysed with LC-MS/MS on a Oribtrap Fusion (Thermo Scientific). Each sample was run on the LC with 90 minutes for separation of the peptides before the mass spectrometer. The peptide identification was performed using Max Quant (MQ), which works by pattern matching the observed spectra with that of a theoretical spectra for each peptide and then gives a score of the probability

that the spectrum was assigned correctly. Label free quantification (LFQ) and match between runs was carried out in order to improve the accuracy of the quantification. Match between runs does not require a peptide to be selected for MS2 for it to be quantified, as long as an MS2 was observed for that precursor peak in another run. The average intensity of GFP was calculated across all samples and then all proteins within each sample were corrected by a normalisation factor (the difference between the average and the observed value of GFP).

To evaluate the differences between the CoIPs we used euclidean clustering to check the quantity of identified proteins in the CoIPs, as we would expect all four replicas from each of the four samples to cluster similarly. There was no distinction between GFP untreated and GFP RALF1 treated samples, which is shown in the heatmap (Figure 4.7B). The clustering showed that three samples (FER-GFP untreated (un) B4, FER-GFP RALF1 treated (RALF1) B4 and GFP RALF1 treated (RALF1) B2) were distinctly different compared to the other replicas (Figure 4.7). We therefore, have removed FER-GFP un B4, FER-GFP RALF1 B4 and GFP RALF1 B2 from all further analyses. Proteins of interest were filtered in PERSEUS by the following rule: a protein must be seen in at least three replicas of each condition. However, to add to the stringency of the analysis, both GFP samples were combined (treated and untreated) and the above rule remained. The intensities were log2 transformed and missing values were replaced with 0 as CoIP data is presence or absence data, therefore any value that was not observed was believed to be truly absent from the CoIP.

When comparing FER-GFP untreated and FER-GFP RALF1 treated samples against the GFP controls, a volcano plot was done to visualise how our

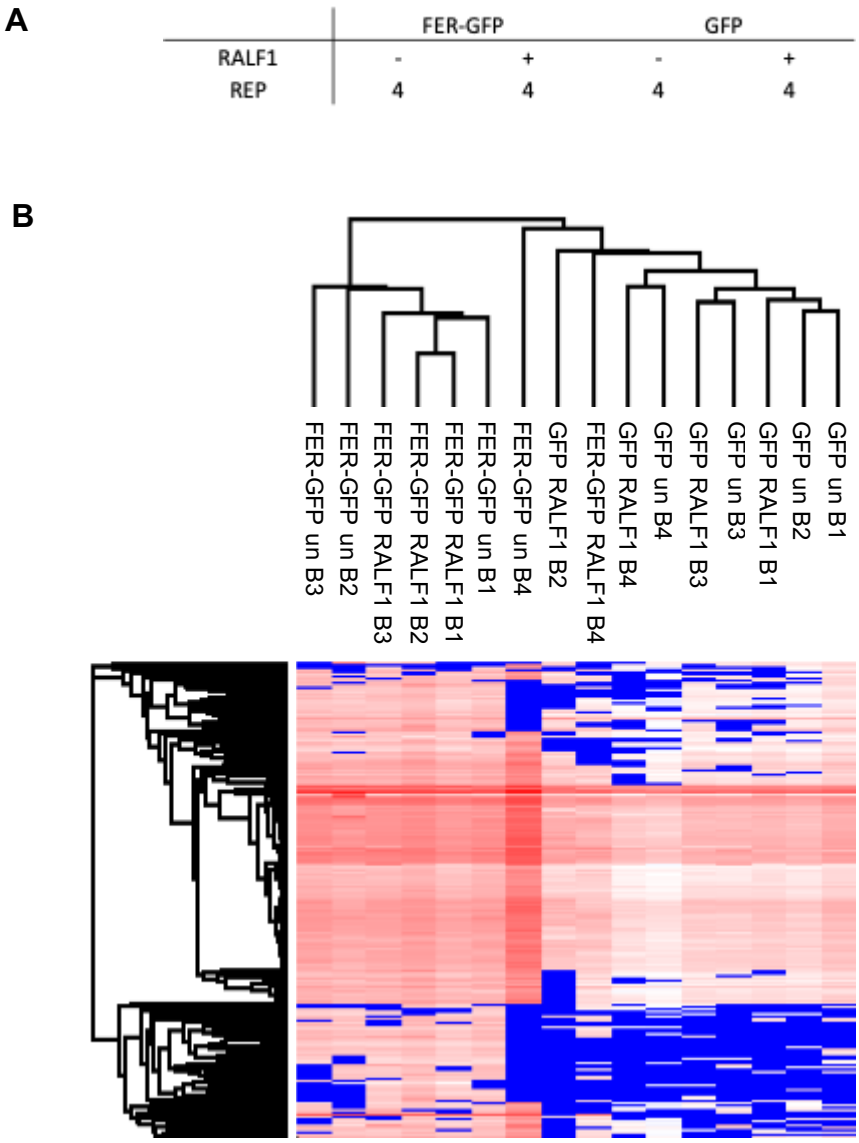

Figure 4.7: FER-GFP untreated B4, FER-GFP RALF1 treated B4 and GFP RALF1 treated B2 do not cluster with their replicas. A) Experimental set-up. B) CoIP data was run on LC-MS/MS and spectra assigned using Max quant. The samples were normalised to GFP and then euclidean clustering was done to determine the difference in replicas. Un = untreated, B = batch.

samples behaved and whether we see proteins that are unique to the FER-GFP CoIPs. A *t*-test was done with FDR set to 0.05 and s0 set to 0.1 and volcano plots drawn. The s0 is in essence a minimal fold change, which means even if a protein gives a p-value less than 0.05 if the fold change is below that value it won't be significant. With s0 set 0.1 we aimed to identify almost all protein with a low p-value. The volcano plot shows the difference plotted against the -Log of the p-value, showing the difference between the sample (FER-GFP untreated or FER-GFP RALF1 treated) and the control (all GFP samples, treated and untreated). The volcano plot shows proteins that are significantly different between the sample and the control, for both untreated and RALF1 treated (Figure 4.8). The bait protein (FER-GFP) is highlighted in red and shows the biggest difference when compared with the GFP controls for both FER-GFP untreated and FER-GFP RALF1 treated, which would be expected.

To analyse the enriched proteins, a list of significantly different proteins for both FER-GFP untreated and FER-GFP RALF1 treated were obtained by carrying out the Reproducibility-Optimized Test Statistic (ROTS) analysis in R. The ROTS analysis takes into account the differences in variance between samples and also has bootstrapping built into the package which aids the reliability of the data when a low number of replicas are done. ROTS was shown by Pursiheimo et al (2014) to be the best performing statistical test for large scale proteomic data sets. Previous analysis was performed using a student's *t*-test within the programme PERSEUS, which identified a much higher number of proteins classified as significant. This could be a result of CoIP data often not being equal in variance due to the nature of MS data.

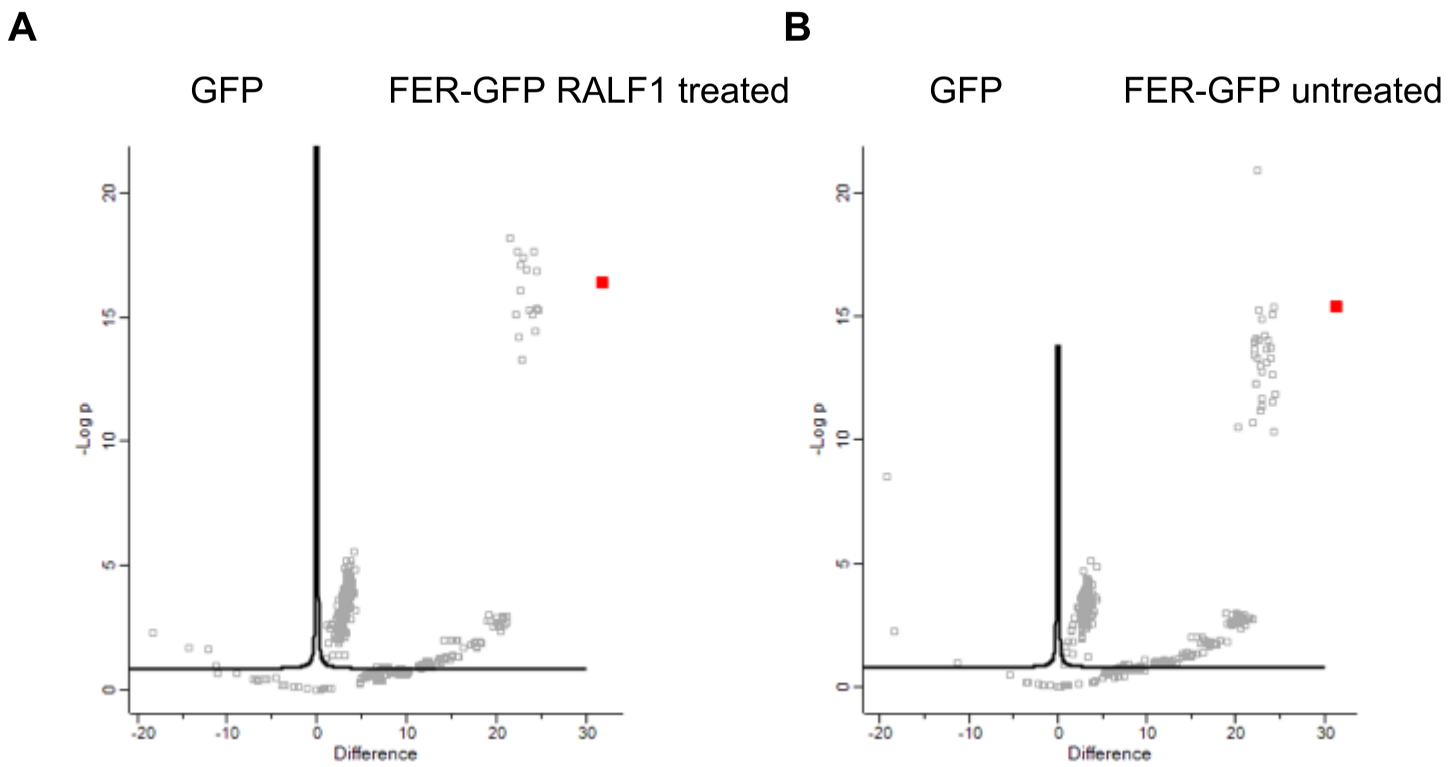

Figure 4.8: FERONIA is the most significantly enriched protein in FER-GFP CoIPs. A students t-test (FDR set 0.05 and s0 set to 0.1) was done on filtered protein lists for FER-GFP CoIP RALF1 treated against GFP controls and FER-GFP untreated against GFP controls. Graphs show difference plotted against the -Log of the p-value. A) FER-GFP RALF1 treated, B) FER-GFP untreated. FERONIA is highlighted in red.

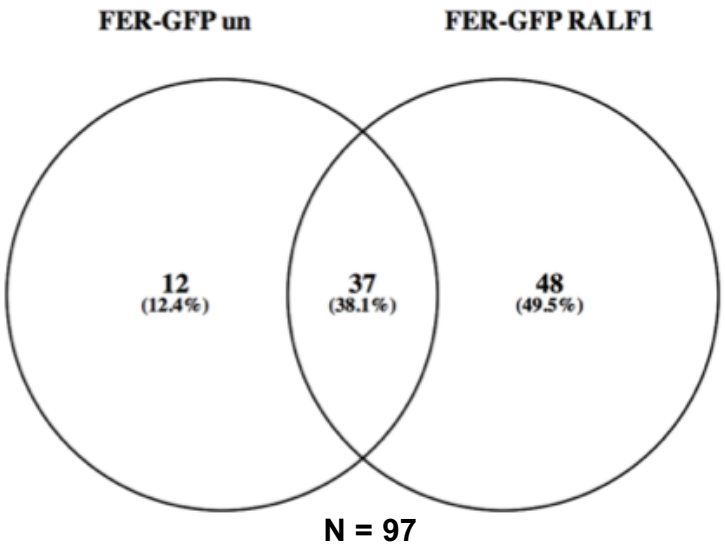

Figure 4.9: 48 proteins are unique to RALF1 elicited FER-GFP complex. Venn diagram was plotted from significantly enriched proteins from ROTS analysis of FER-GFP untreated and FER-GFP RALF1 treated. N=97.

Proteins significantly enriched in the FER-GFP CoIP were identified by ROTS. The ROTS analysis for both FER-GFP untreated and FER-GFP RALF1 treated against the combined GFP control gave a list of 97 significantly enriched proteins. To determine proteins that may form part of the unelicited, core or RALF1 induced FER-GFP complex, a Venn diagram was plotted, shown in Figure 4.9. From Figure 4.9 we can see that 12 proteins were found to be unique to the unelicited FER-GFP, 37 proteins were found to be present in both and potentially involved in a core complex and 48 proteins were identified to be unique to the RALF1 elicited CoIPs (Supp. Table 1).

The list of putative FER interacting proteins was refined by looking at the biological significance. The sub-cellular localisation was used to filter these proteins further. Proteins were classified as potential contaminants and

not true interactors if they were localised solely in the nucleus, chloroplast, mitochondria or if they were ribosomal proteins, leaving 64 proteins. Using UNIPROT and GO terms these 64 proteins were categorised by their function into the following categories: cell wall, cytoskeleton, degradation, hormone, immunity, kinase, metabolism, proteasome, Transcription Factor (TF) and trafficking. The 64 proteins are summarised in Table 4.1.

There were 26 proteins identified as core complex components, including an auxin transporter, several proteasome associated proteins and five proteins related to the cell wall including Cullin-associated NEDD8-dissociated protein 1 (CAND1). There were 29 proteins that were enriched in the RALF1 elicited complex, including calcium-dependent protein kinase 3 (CPK3) and there were nine proteins that were unique to the unelicited complex.

We searched our protein lists against known interactors of FER, and although we did identify H(+)-ATPASE 2 (AHA2) in our CoIPS, it was not significantly enriched in the FER-GFP CoIP. We also searched for predicted FER interactions in STRING database (Szklarczyk et al., 2017), but none were found. STRING is a database that uses both experimental and homology prediction over a large range of species to predict protein-protein interactions.

Table 4.1: Potential FERONIA interactors in *A. thaliana* roots. Proteins identified from ROTS statistical analysis of FER-GFP CoIP data. Function identified from UNIPROT and Tair.

Accession	**Name**	**Function**	**Proposed complex**
AT3G51550	FERONIA	Kinase	Core

Accession	Name	Function	Proposed complex
AT1G01800	NAD(P)-binding Rossmann-fold superfamily protein	Cell wall	Core
AT2G02560	CAND1	Cell wall	Core
AT4G20360	RabE1b	Cell wall	Core
AT5G19820	ARM repeat superfamily protein	Cell wall	Core
AT5G65270	RABA4a	Cell wall	Core
AT4G29350	PROFILIN 2	Cytoskeleton	Core
AT3G02260	BIG	Hormone	Core
AT1G64790	ILITYHIA	Immunity	Core
AT1G70730	PHOSPHOGLUCOMUTASE 2	Metabolism	Core
AT2G40890	CYTOCHROME P450	Metabolism	Core
AT2G42790	CSY3	Metabolism	Core
AT3G16400	NSP1	Metabolism	Core
AT3G29410	TPS25	Metabolism	Core
AT3G53110	LOS4	Metabolism	Core
AT4G35830	ACONITASE 1	Metabolism	Core
AT5G43010	RPT4A	Proteasome	Core
AT3G02200	Proteasome component	Proteasome	Core
AT5G45620	26S proteasome non-ATPase regulatory subunit 13 homolog A	Proteasome	Core
AT5G23540	Mov34/MPN/PAD-1 family protein	Proteasome	Core
AT5G16070	TCP-1/cpn60 chaperonin family protein	Trafficking	Core
AT1G52760	CAFFEOYL SHIKIMATE ESTERASE	Trafficking	Core
AT2G46520	Exportin-2 (Exp2)	Trafficking	Core

Accession	Name	Function	Proposed complex
AT3G56190	ALPHA-SNAP2	Trafficking	Core
AT4G04910	N-ETHYLMALEIMIDE SENSITIVE FACTOR	Trafficking	Core
AT5G63190	MRF1	Trafficking	Core
AT1G03220	Aspartyl protease family protein	Cell wall	RALF1 Elicited
AT1G21750	PDI-LIKE 1-1	Cell wall	RALF1 Elicited
AT4G16260	Probable glucan endo-1,3-beta-glucosidase	Cell wall	RALF1 Elicited
AT5G64100	Peroxidase 69	Cell wall	RALF1 Elicited
AT5G65430	GRF8	Cell wall	RALF1 Elicited
AT2G30870	GSTF10	Cell wall	RALF1 Elicited
AT3G51460	RHD4	Cell wall	RALF1 Elicited
AT1G20450	ERD10	Cytoskeleton	RALF1 Elicited
AT5G59880	ADF3	Cytoskeleton	RALF1 Elicited
AT5G15970	KIN2	Hormone	RALF1 Elicited
AT1G70850	MLP-like protein 34	Immunity	RALF1 Elicited
AT1G78380	GSTU19	Immunity	RALF1 Elicited
AT2G01530	MLP-LIKE PROTEIN 329	Immunity	RALF1 Elicited
AT5G12140	CYS-1	Immunity	RALF1 Elicited
AT5G67500	VOLTAGE DEPENDENT ANION CHANNEL 2	Immunity	RALF1 Elicited
AT4G23650	CPK 3	Kinase	RALF1 Elicited
AT5G63400	ADENYLATE KINASE 1	Kinase	RALF1 Elicited
AT5G63680	Pyruvate kinase	Kinase	RALF1 Elicited

Accession	Name	Function	Proposed complex
AT2G29560	ENOLASE 3	Metabolism	RALF1 Elicited
AT3G12290	MTHFD1	Metabolism	RALF1 Elicited
AT3G16450	JACALIN-RELATED LECTIN 33	Metabolism	RALF1 Elicited
AT3G32980	Peroxidase	Metabolism	RALF1 Elicited
AT2G46140	LEA27	Metabolism	RALF1 Elicited
AT5G11670	NADP-ME2	Metabolism	RALF1 Elicited
AT1G16890	UBIQUITIN-CONJUGATING ENZYME 36	degradation	RALF1 Elicited
AT1G17880	BASIC TRANSCRIPTION FACTOR 3	TF	RALF1 Elicited
AT2G16950	TRANSPORTIN-1	Trafficking	RALF1 Elicited
AT4G13770	REDUCED EPIDERMAL FLUORESCENCE 2	Trafficking	RALF1 Elicited
AT5G42890	STEROL CARRIER PROTEIN 2	Trafficking	RALF1 Elicited
AT1G28290	ARABINOGALACTAN PROTEIN 31	Cell wall	Unelicited
AT1G48630	RACK1B	Kinase	Unelicited
AT4G09000	GRF1	Metabolism	Unelicited
AT4G15093	LIGB	Metabolism	Unelicited
AT1G29150	REGULATORY PARTICLE NON-ATPASE 6	Proteasome	Unelicited
AT3G42170	DAYSLEEPER	TF	Unelicited
AT3G63460	SEC31B	Trafficking	Unelicited
AT2G36290	Alpha/beta-Hydrolases superfamily protein	Trafficking	Unelicited
AT4G11420	eIF3a	Trafficking	Unelicited

4.2.3 FERONIA phosphorylation

FER is known to be phosphorylated upon RALF1 treatment, (Haruta et al., 2014), so we looked for phosphorylation on FER in the FER-GFP CoIPs. We used a MQ LFQ search and added phosphorylation at serine, threonine and tyrosine as a variable modification parameter. MQ uses a probability based approach of matching the observed spectrum to a theoretical spectrum of a fragmented peptide, which is used for both the peptide identification and the localisation probability. Phosphorylation modification causes a mass change of 79.96633 on the precursor ion mass and how the peptide fragments allows the exact location of the phosphorylation to be determined.

MQ identified six phosphorylation sites on FER, summarised in Table 4.2. Three sites were identified as Class I sites; a site that has a localisation score of greater than 0.75 and a score difference of greater than 5. The localisation score is a probability score, determined through a statistical test, that the modification is assigned to the correct site. Class I sites are sites that have a high degree of certainty about the exact location of the modification. Only one site identified was seen reproducibly (at least three times) within our CoIP data set, site 692, and it was observed in three FER-GFP untreated samples and two RALF1 treated FER-GFP samples.

The peptide 'SSDVYEGNVTDSR' was only observed in one sample and had poor localisation score, therefore we have discounted this peptide. As there were three sites identified on the peptide 'TGPTLDHTHVSTVVK' we tried to determine the site specificity using Scaffold, with the easy visualisation of annotated MS2 spectra to match the spectrum to a sequence, to determine if all three sites existed. Using Scaffold we analysed the MS2 spectra for the

Table 4.2: All FERONIA phosphorylation sites observed in the FER-GFP CoIPs. Table shows all, Class I, Class II and Class III, identified phosphorylation sites on FER. The peptide score and localisation score show the confidence in the correct identification of the modification.

Peptide	Site	Peptide score	Localisation score	Score difference	Seen in	Class
TNTTGSYASSLPSNLCR	508	88.992	0.72	6.29	1	2
	509	137.84	0.98	16.56	2	1
TGPTLDHTHVSTVVK	692	139.64	0.99	22.76	5	1
	695	102.63	0.92	12.15	1	1
	696	83.792	0.76	4.94	2	2
SSDVYEGNVTDSR	856	92.039	0.64	2.53	1	2

peptide 'TGPTLDHTHVSTVVK', with the best spectrum shown in Figure 4.10A. There is very poor coverage of the peptide with both the b and y ion series and all intensities are very low and almost indistinguishable from the noise. For this reason we have chosen to discount the sites on this peptide despite the good scores seen in MQ.

The peptide 'TNTTGSYASSLPSNLCR' contains two phosphorylation sites according to MQ with 509 being classified as a Class I. As MQ identified site 508 and 509, which is incredibly difficult to assign correctly as it relies on almost perfect fragmentation of the peptide to distinguish which amino acid carries the extra mass, we cross referenced to the observed spectra for this peptide. Using Scaffold to visualise the best spectra obtained for these two sites, we conclude that it is not possible to tell if both sites exist, spectra shown in Figure 4.10, however we are confident that this peptide does carry a phosphorylation modification.

As FER shares a high degree of homology with the members of the CrRLK family, we carried out a sequence alignment, using MUSCLE alignment, which confirmed that the peptide 'TNTTGSYASSLPSNLCR' was unique

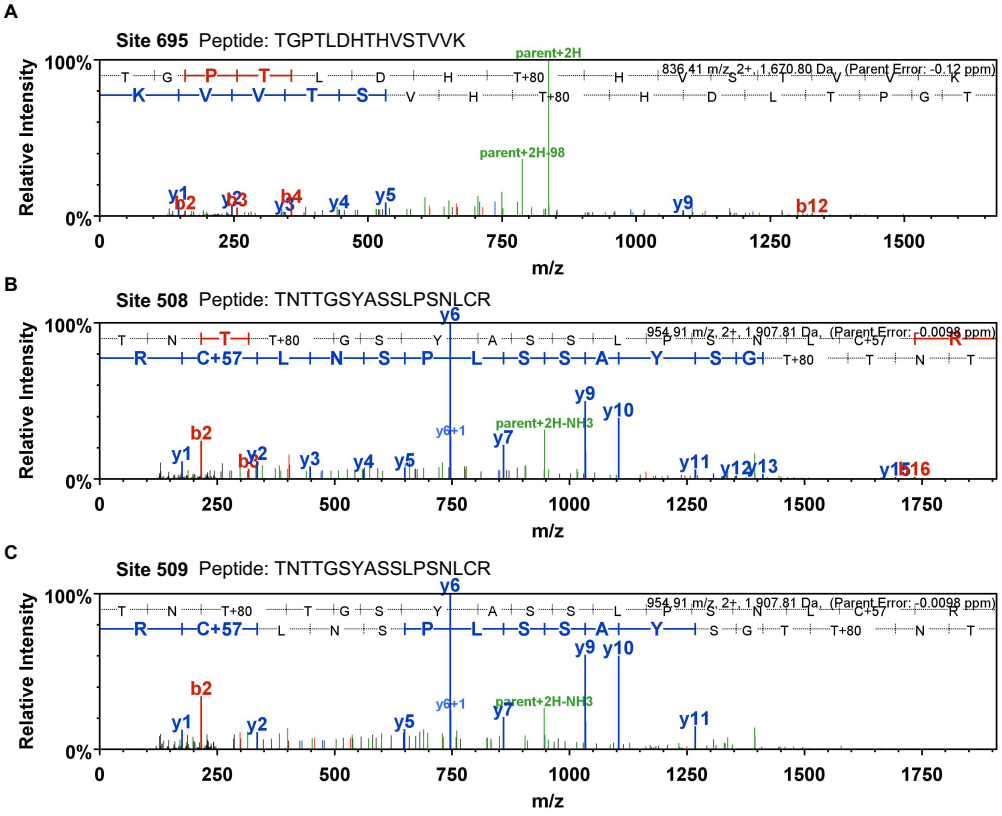

Figure 4.10: Phosphorylation modification is located in 'TNTTGS' region of 'TNTTGSYASSLPSNLCR' peptide. CoIP data was analysed using LC-MS/MS and MS2 spectrum of a FER peptide carrying a phosphosite was assigned by Mascot in FER-GFP RALF1 treated CoIP. A) Best spectrum for 'TGPTLDHTHVSTVVK'. B) Best spectrum for 'TNTTGSYASSLPSNLCR', site 508. C) Best spectrum for 'TNTTGSYASSLPSNLCR', site 509.

to FER, (Figure 4.11). We conclude from the FER-GFP CoIP that one FER phosphopeptide was observed 'TNTTGSYASSLPSNLCR' that carries a RALF1 dependent phosphorylation modification within 'TNTTGS' region.

4.2.4 Identification of proteins interacting with FER-ΔK-GFP and FER-KR-GFP using Co - immunoprecipitation

A preliminary experiment to identify proteins that require a functioning FER kinase domain to interact with FER was performed using anti-GFP Co-immunoprecipitation (CoIP) with the FER-ΔK-GFP and FER-KR-GFP lines. Plants were grown on soil for 4 weeks and then the leaves harvested and protein extracted: as this was a test we used 1 replicate per line. An anti-GFP CoIP was then performed and an anti GFP western blot was used to visualise whether the bait protein had been pulled down. An on bead tryptic digest was performed and the samples analysed by LC-MS/MS. Peptide identification was performed using a commercially available programme Mascot.

Nine FER peptides were identified in the FER-ΔK-GFP CoIP (Table 4.3). The sequence of FER was reduced to the first 501 amino acids in the FER-ΔK-GFP line (Shih et al., 2014), removing the kinase domain. Eight peptides were identified from the kinase domain of FER that should have been deleted in the FER-ΔK-GFP line. There is a large amount of homology between FER and other 17 CrRLKs family receptors so a sequence alignment using MUSCLE, was carried out for the peptides to confirm that these peptides are from FER and not other CrRLKs. Of the eight peptides, only one

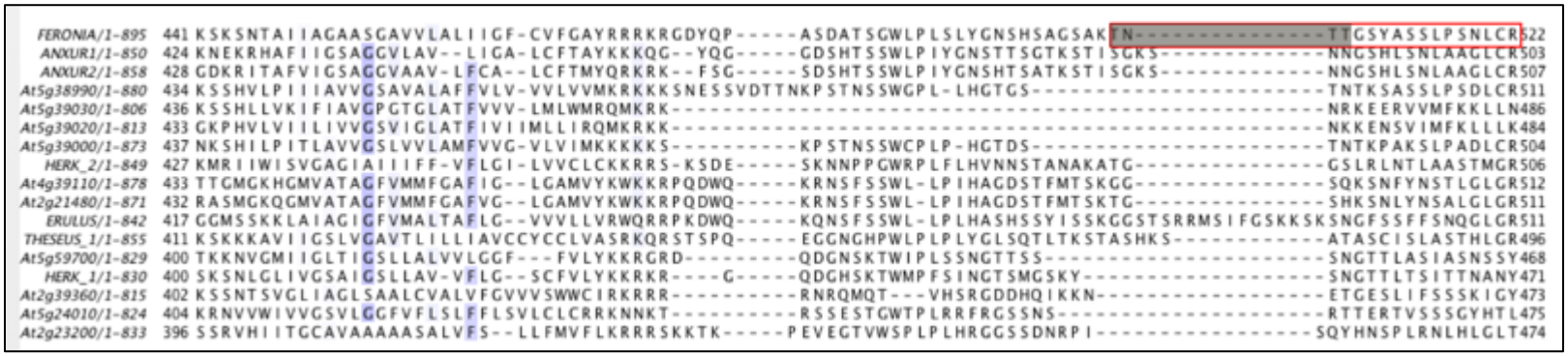

Figure 4.11: FERONIA phosphopeptide is unique to FER. The phosphopeptide assigned in Figure 4.10B and C, was aligned with the 17 members of CrRLK family using MUSCLE alignment.

peptide was conserved between family members '(K)GSFGYLDPEYFR(R)'; this peptide was observed twice and once with a very poor Mascot ion score. The spectra of the remaining peptides were assessed to determine if the kinase of FER was truly seen in the FER-ΔK-GFP line.

The peptide '(K)GMLDQIVDPYLK(G)' is from within the kinase domain of FER at position 760-771. The spectrum was assessed to determine whether it had been correctly assigned and the spectra looks good with a good signal to noise ratio and good fragmentation especially of the y ions (Figure 4.12). Using a MUSCLE alignment the peptide '(K)GMLDQIVDPYLK(G)' was identified as unique to FER (Figure 4.12). From the alignment there were four other peptides that were unique to FER kinase domain with only '(K)GSFGYLDPEYFR(R)' being conserved with 10 other members of the CrRLKs family. It is therefore believed that the kinase domain of FER was present in this line.

Genotyping was performed to determine whether the seeds were FER-ΔK-GFP. Genotyping proved more complicated than expected but it appeared that some plants were FER-GFP rather than FER-ΔK-GFP (Figure 4.12). The expected band size of the FER-GFP fragment was ∼1800 bp and the primers spanned the deleted region with the reverse primer in the eGFP sequence to avoid the genomic gene sequence. The expected band size in FER-ΔK-GFP was 360 bp. Figure 4.12 shows that two FER-ΔK-GFP plants gave the same size product as FER-GFP indicating that these plants are FER-GFP. The smaller band size that was expected in FER-ΔK-GFP was never observed but in the interest of time this was not followed up. Given FER has a fertility phenotype, seeds were harvested from six FER-ΔK-GFP plants and these showed significant differences in yield (Figure 4.12). From the gen-

Table 4.3: FER-ΔK-GFP peptides from the FER kinase domain. CoIP sample was run on LC-MS/MS and the spectra assigned using Mascot. Table shows FER peptides identified from FER-ΔK-GFP CoIP.

Sequence	Start	MUSCLE alignment of 17 CrRLK family	Mascot Ion score	Charge	Observed Mass	Actual Mass	Delta PPM	Modifications
(K)FLSSSSEDSK(T)	63	Unique	70.43	2	543.7458	1,085.48	-9.797	
(K)TSPALTQDPSVPEVPYMTAR(V)	73	Unique	42.4	2	1,080.53	2,159.04	-8.066	
(K)TSPALTQDPSVPEVPYmTAR(V)	73	Unique	34.38	2	1,088.52	2,175.03	-10.05	Oxidation
(R)SPFTYTFPVASGR(K)	96	Unique	49.15	2	715.353	1,428.69	-8.666	
(R)SPFTYTFPVASGR(K)	96	Unique	49.11	2	715.353	1,428.69	-8.666	
(R)LNVGGNDISPSADTGLYR(S)	229	Unique	61.37	2	924.9493	1,847.88	-9.499	
(R)LNVGGNDISPSADTGLYR(S)	229	Unique	66.77	2	924.9503	1,847.89	-8.377	
(K)YPTGTPTYVAPVDVYSTAR(S)	274	Unique	84.88	2	1,029.50	2,056.99	-9.883	
(K)RGDYQPASDATSGWLPLSLYG NSHSAGSAK(T)	476	Unique	63.3	2	774.1158	3,092.43	-8.062	
(K)TNTTGSYASSLPSNLcR(H)	506	Unique	80.95	2	914.9203	1,827.83	-8.743	Carbamidomethyl
(R)HFSFAEIK(A)	523	Unique	39.43	2	489.7512	977.4878	-9.506	
(R)VLGVGGFGK(V)	541	Unique	44.58	2	417.2436	832.4726	-9.886	
(K)TQNPSLPWK(Q)	625	Unique	35.09	2	535.7803	1,069.55	-9.132	
(R)LEIcIGAAR(G)	636	Conserved in 7	45.02	2	501.7693	1,001.52	-8.865	Carbamidomethyl
(R)LEIcIGAAR(G)	636	Conserved in 7	39.56	2	501.7696	1,001.52	-8.22	Carbamidomethyl
(R)GLHYLHTGAK(H)	645	Conserved in 3	43.05	2	548.7933	1,095.57	-9.734	
(K)TGPTLDHTHVSTVVK(G)	685	Unique	43.55	2	796.418	1,590.82	-9.664	
(K)GSFGYLDPEYFR(R)	700	Conserved in 11	31.39	2	725.8288	1,449.64	-9.327	
(K)EQVSLAEWAPYcYK(K)	745	Unique	47.52	2	872.3983	1,742.78	-8.807	Carbamidomethyl
(R)SSGIDMSIGGR(S)	860	Unique	70.36	2	540.256	1,078.50	-9.69	

otyping and the seed harvest it was concluded that these seeds were mixed and although we couldn't identify FER-ΔK-GFP from the genotyping we could determine that there were multiple plant lines and therefore in the interest of time FER-ΔK-GFP was no longer used.

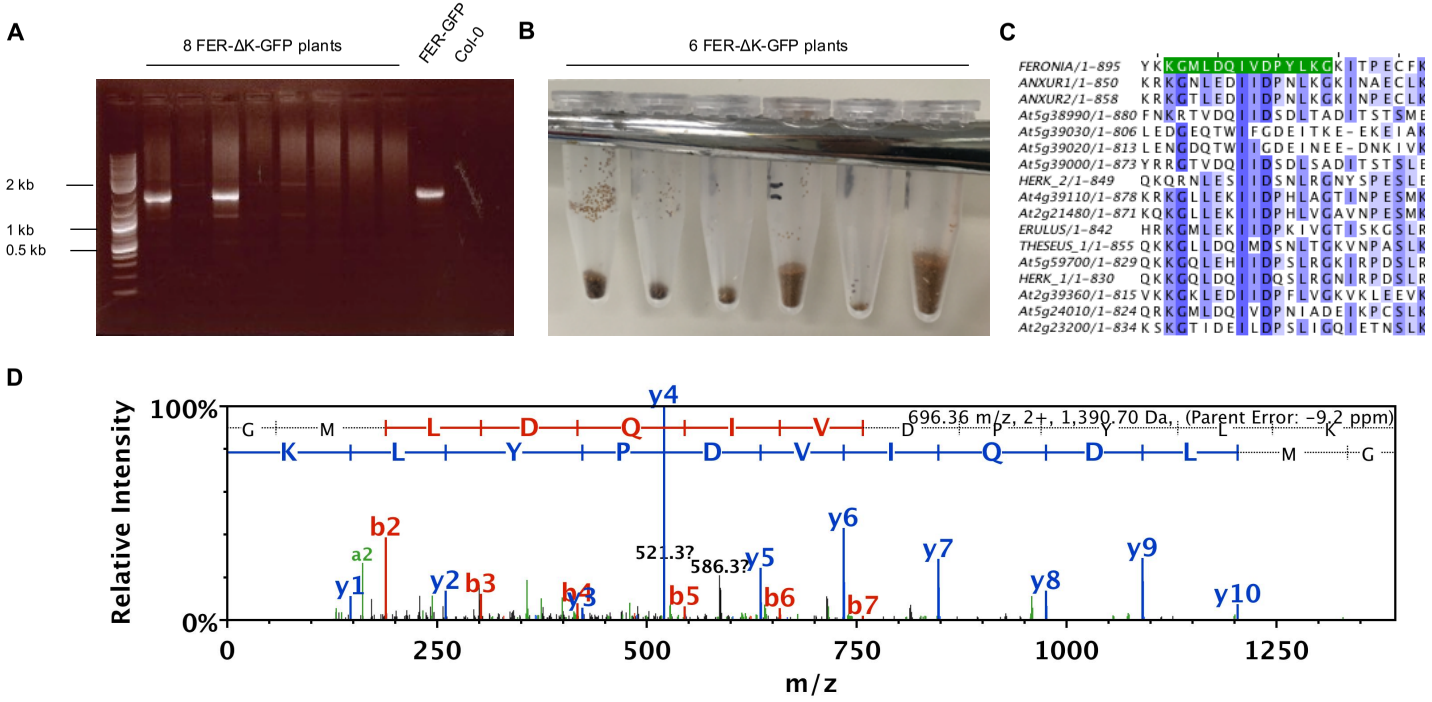

Figure 4.12: FER-ΔK-GFP seeds are mixed with FER-GFP seeds. A) 1.5% agarose gel showing same PCR product (~1800 bps) in FER-GFP in two FER-ΔK-GFP plants. B) Volume of seeds collected from 6 FER-ΔK-GFP plants with 3 plants producing large amounts of seeds not expected from a fertility phenotype mutant. C) FER-ΔK-GFP kinase domain peptide is unique to FERONIA. A muscle sequence alignment of all 17 members of CrRLKs was done. Sequence highlight was a peptide identified from FER-ΔK-GFP CoIP. D)FERONIA kinase domain peptide '(K)GMLDQIVDPYLK(G)' is assigned correctly. Peptide assigned from FER-ΔK-GFP using Mascot was analysed by LC-MS/MS. MS2 spectrum showing fragmentation of FER kinase domain peptide

4.3 Discussion

The addition of FER-GFP into the mutant *fer-4* L*er* background showed an almost total recovery of the phenotype seen in the *fer-4* (Col-0), as first described by Escobar-Restrepo et al. (2007). Therefore we conclude that FER-GFP (L*er*) is comparable to wild type. FER-GFP in a Col-0 (*fer-4*) background would have been preferable as all other lines used in the root hair phenotypes, and the proteomics, are in the Col-0 background. The FER-GFP (Col-0) line did not express GFP and so in the interest of time the FER-GPF (L*er*) line was used for analysis. Unfortunately we did not have *fer-4* in the L*er* background and as we planned to obtain a FER-GFP in a Col-0 background we did not pursue this line. The L*er* proteome has only recently been available and therefore is not as well annotated. We did analyse the FER-GFP CoIPs against the L*er* proteome but due to it being poorly annotated, we concluded that, although not ideal, using Col-0 proteome was better for this analysis of possible interactors.

The FER-KR-GFP mutant showed a much greater recovery of the *fer-4* phenotype compared to FER-ΔK-GFP, however FER-KR-GFP still showed a root hair defect suggesting that the activity of the kinase domain is important for FER signalling. Shih et al., (2014) showed that the mutants with reduced kinase activity (FER-KR-GFP and FER-ΔK-GFP) had reduced ion signalling in response to mechanical stimulation. The partial recovery shown by these two lines indicates the importance of the kinase domain of FER and although the kinase activity is not essential to all functions, as shown by the partial recovery of the phenotype in FER-KR-GFP, the kinase activity is crucial for normal FER signalling. Originally the aim had been to identify proteins that interacted with FER complex within these different

mutants with the goal of identifying proteins that relied on the activity of the kinase domain. However the seed mix up meant that this aim could not be achieved and instead we focused on looking for root specific FER interactors and downstream signalling events.

Previous interactors of FER have been identified using a variety of different techniques often using protoplasts (Duan et al., 2010)(Yu et al., 2012). The aim of the root FER-GFP CoIP was to identify proteins that interact specifically with FER in roots, in a native system, with the aim of getting a better understanding of the root hair phenotype observed in the FER mutants. The differences in the experimental methods could be a reason as to why we do not find any previously identified FER interactors in the CoIP. The protein AHA2, which was shown to be involved in FER signalling (Haruta et al. 2014), was identified in the CoIP. AHA2 was pulled down by both the FER-GFP CoIP and the GFP only control, therefore we are unable to say whether the interaction with FER-GFP is due to AHA2 interacting with FER not the GFP tag. This could have been altered with different buffers but also differing statistical analysis altered whether it was statistically significant in the FER-GFP samples.

We identified 64 proteins as potential FER interactors from our FER-GFP CoIPs in *A. thaliana* roots, and the proteins interacting with FER in three different complexes, unelicited, core and RALF1 elicited, are summarised in Figure 4.12. There were 26 proteins identified as part of a core complex, with four proteasome related proteins; 26S proteasome regulatory subunit 10B homolog A, Proteasome component, 26S proteasome non-ATPase regulatory subunit 13 homolog A and 26S proteasome non-ATPase regulatory subunit 14 homolog. The identification of these proteasome regulatory pro-

teins provides an interesting insight to the degradation of FER, which is a method commonly used to regulate RLKs (Antolín-Llovera et al., 2014).

From the core complex we identified five proteins that are associated with cell wall growth, which included a Ras-related protein (RABA4a), RAB GTPASE HOMOLOG E1B and Cullin-associated NEDD8-dissociated protein 1 (CAND1). CAND1 has been shown to act positively to regulate multiple ubiquitin E3 ligases and their associated developmental processes in plants (Feng et al., 2004). CAND1 mutants show overlapping phenotypes with *fer-4* plants with low fertility and altered responses to hormones (Feng et al., 2004), suggesting that this interaction would be worth investigating with reciprocal IPs.

Another protein identified in the core complex that exhibits an interesting phenotype in the loss of function mutant is ILITHYIA. ILITHYIA is associated with immunity and stress responses and has been shown to be essential for proper root development, as the loss of function mutants exhibit reduced root length (Faus et al., 2018).

A protein that was unique to the unelicited complex was Receptor for activated C kinase 1B (RACK1B). RACKIB has been identified as a MAPK scaffold protein in FLS2 signalling (Cheng et al., 2015). From Chapter 3 we showed that RALF1 activation of MAPKs is dependent on FER and therefore we propose that RACK1B could act as a scaffold for the MAPKs involved in FER signalling. RACK1B could act to anchor the MAPKs close to FER to enable rapid phosphorylation of MAPKs after RALF1 elicitation. It is known that RALF1 acts on MAPKs especially quickly, 5 minutes, when compared to flg22 and PEP, 15 minutes, and therefore it would be logical to think that MAPK cascade would be anchored nearby and rapidly disso-

ciate from the FER complex upon elicitation to enable this rapid signalling cascade.

We identified 31 proteins that were unique to the RALF1 elicited FER complex, including root hair defective 4 (RHD4). RHD4 is a phosphatidylinositol-4-phosphate phosphatase required for normal root hair development, with a mutation in RHD4 causing root hairs to become short and bulged (Thole et al., 2008)(Schiefelbein and Somerville, 1990). RHD4 has been shown to be involved in coordinating delivery of cell wall materials and is selectively recruited to RABA4b labelled membranes (Thole et al., 2008). We identified RABA4a as part of the core FER complex, which leads to interesting thoughts as to whether FER is recruited to RABA4a labelled membranes too and whether RHD4 is recruited to RABA4a membranes as RABAs are closely related proteins.

FER regulates calcium signalling in response to mechanical stimulation and salt stress (Shih et al., 2014)(Feng et al., 2018), however a mechanism of how this occurs is not known. We identified Calcium-dependent protein kinase 3 (CPK3), as enriched in RALF1 elicited FER complex. Calcium-dependent protein kinases are a large group of kinases that have links to regulation of ROS bursts in immunity signalling, with flg22 induced phosphorylation of RBOHD being dependent on Calcium-dependent protein kinase 5. A quadruple mutant of *cpk3/4/6/11* was identified as disrupting ABA-induced trafficking and degradation of RopGEF1 and CPK4 binds to and phosphorylates RopGEF1 and promotes the degradation of RopGEF1 (Li et al., 2018). It would be interesting to obtain a CPK3 mutant to further evaluate the link between FER and CPK3, and determine if CPK3 can alter ROPGEF signalling, as FER is known to activate ROPGEF1 which leads to the activation

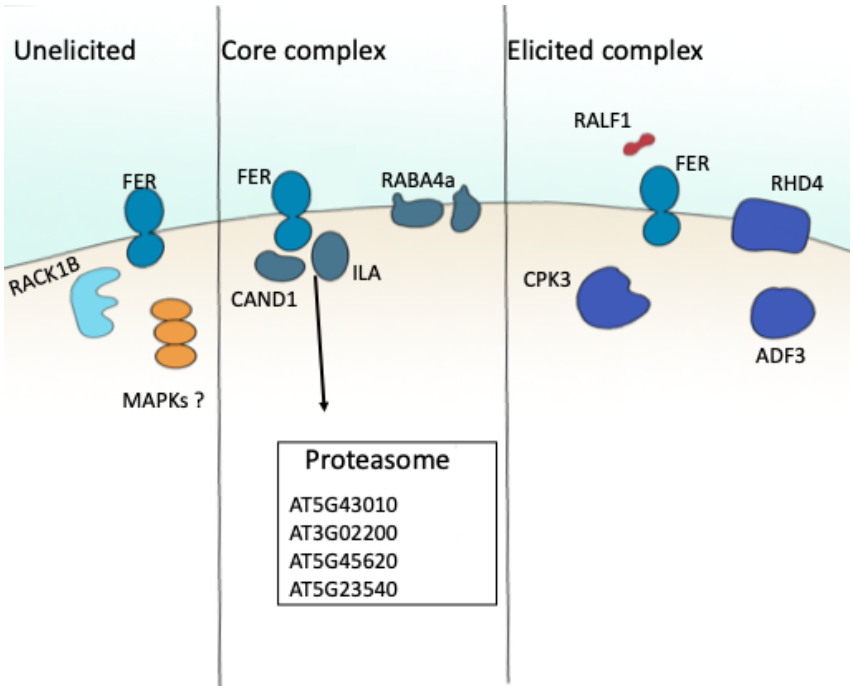

Figure 4.13: Schematic of FER signalling pathways from proteins identified in FER-GFP CoIP.

of ROP2 (Duan et al., 2010).

ROPs are known to regulate the cytoskeleton and although we did not identify either ROPGEFs or ROPs in our FER-GFP CoIP we identified several proteins related to the cytoskeleton including Actin depolymerising factor 3. Actin depolymerising factor 3 is a member of the Class I subfamily that have strong F-actin-severing/depolymerising activity (Nan et al., 2017). ROP2 which is known to interact with FER (Duan et al., 2010) interacts with RIC4 to promote F-actin assembly and ROP6 interacts with RIC4 to inhibit this assembly (Fu et al., 2005)(Lin et al., 2012). It would be interesting to see whether RIC1 or RIC4 interact with Actin depolymerising factor 3 making Actin depolymerising factor 3 a mechanism for how RIC1 and RIC4 regulate the cytoskeleton. A schematic of the potential FER signalling complexes is shown in Figure 4.13.

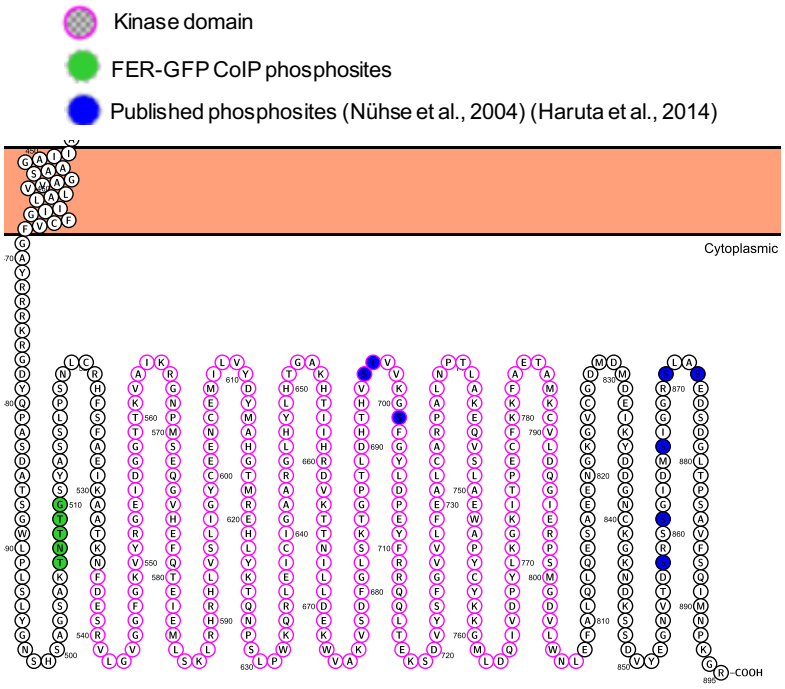

Figure 4.14: Schematic of FER phosphosites. Schematic showing the sites of published FER phosphosites and the region that contains the modification identified in the FER-GFP CoIP. (Nühse et al., 2004)(Haruta et al., 2014) (Protter)

The indication that the kinase domain of FER is essential for complete function made us investigate the phosphorylation sites on FER. We identified eight phosphopeptides on FER with eight different phosphosites assigned. A large scale phosphoproteomics study identified five phosphosites on FER S-695, T-696, S-701, S-861 and S-866 (Nühse et al., 2004) and Haruta et al., (2014) identified three RALF1 induced phosphorylation sites at S-871, S-874 and S-858, with S-858 being increased ∼20 fold with RALF1 treatment. From our CoIP data we have identified a new region, 506-510, that has phosphorylation on FER, shown in Figure 4.14. These residues are in the juxtamembrane domain of FER, which has been identified as a highly phosphorylated region on RLKs associated with regulation (Nühse et al., 2004).

Chapter 5

Identification of phosphorylation events downstream of FERONIA and RALF1

5.1 Introduction

Protein phosphorylation is a common and intensively studied Post-Translational Modification (PTM) that plays a key role in signal transduction from receptors at the plasma membrane, causing intracellular changes to protein activity and gene expression. Phosphorylation is a reversible modification catalysed by kinases transferring a phosphoryl group from ATP, specifically to the hydroxyl group of specific serine, threonine, or tyrosine residues (Champion et al., 2004). The addition and removal of phosphorylation, by kinases and phosphatases respectively, plays an important role in the regulation of protein activity.

There have been several large scale phosphoproteomic studies and a study by Nühse et al., (2004) identified more than 300 phosphosites from Arabidopsis plasma membrane proteins. Nühse et al., (2004) identified 51 Receptor-like kinase (RLK) phosphoproteins, with three quarters of the sites identified being in the juxtamembrane region or the domain C-terminal of the kinase core. Their work highlights specific domains within RLKs that provide large regulatory importance.

RALF1 elicitation leads to phosphorylation of FER at S-871, S-874 and S-856, with phosphorylation at S-858 being increased ∼20 fold with RALF1 treatment (Haruta et al., (2014). Activation of FER by RALF1 leads to the phosphorylation of plasma membrane H+-adenosine triphosphotase 2 (AHA2) at site S899, probably causing the inhibition of proton transport (Haruta et al., 2014). A plasma membrane enriched phosphoproteomic study identified five phosphorylation sites on FER; S-695, T-696, S-701, S-861 and S-866 (Nühse et al., 2004)

Another protein known to be phosphorylated downstream of RALF1 is RIPK. The phosphorylation of RIPK is an early event of RALF1 signalling, and FER–RIPK may form a protein kinase complex to perceive RALF1 signal through phosphorylating each other (Du et al. 2016). FER-RIPK trans-phosphorylate each other in a dependent manner as RIPK phosphorylation was reduced in *fer-4* mutant regardless of the addition of RALF1 and FER phosphorylation level in the *ripk*-col-0 mutant compared with that in col-0 (Du et al. 2016). These phosphorylation changes were shown with band shifts on a western blot.

The use of TiO_2 for phosphopeptide enrichment has been used to study early elicitor signalling by enriching for phosphopeptides in Arabidopsis (Benschop

et al. 2007). The affinity enrichment using TiO_2 is based on TiO_2 being positively charged and the phosphate group being negatively charged. The enrichment is carried out under acidic conditions to aid the binding of TiO_2 to phosphopeptides. Quantitative analysis of phosphopeptides can then be achieved using MS/MS and MQ to assign the spectra to proteins. MQ has a match between runs function which aids the accuracy of quantification as it does not require an MS2 to have been trigged for a peptide to be quantified. Match between runs, uses the retention time of peptides from the LC to match peptides that have triggered an MS2 in one run with the LC peak from another even if no MS2 was triggered.

MQ uses a probability based approach to match an observed spectrum to theoretical peptide fragments from which MQ assigns a score. The probability score (p-score) works by calculating the b and y ion masses and then determines the number of matches, k. The probability (p) of obtaining k random matches between the predicted and the measured MS2 peaks can be obtained with a statistical test (Olsen and Mann 2004). This method is also employed for the localisation probability score when looking at post-translational modifications (Cox et al., 2011). It is this localisation score that provides the classification for Class I, Class II and Class III phosphorylation sites when combined with the score difference (Olsen et al., 2006). The score difference is calculated by the difference in localisation score for phosphorylation sites that could be on multiple residues. Class I phosphosites have a localisation probability for the modification of at least 0.75, meaning the added probability of all other potential sites is less than 0.25. For Class II phosphosites, the localisation probability is between 0.75 and 0.25 and match to a known motifs and Class III sites have the same localisation score but do not match to known motifs.

The aim of this chapter was to identify phosphorylation events downstream of FER and RALF1.

5.2 Results

5.2.1 Overview of phosphorylation sites

To identify phosphorylation changes related to the receptor-like kinase FER, we performed a phosphopeptide enrichment on roots of Col-0 and *fer-4* with and without RALF1 elicitation. Using Col-0 and *fer-4* plants gives an indication of proteins that are phosphorylated downstream of FER as Col-0 has native RALF1 and FER. Treating the roots with 1 µM synRALF1 enables us to identify phosphorylation that is RALF1 (and FER) dependent. The experimental setup is summarised in Table 5.1

Table 5.1: Summary of phosphoproteomics experimental setup.

	Col-0 untreated	Col-0 RALF1 treated	*fer-4* untreated	*fer-4* RALF1 treated
Replicas	7	7	7	7
Replicas in final analysis	4	4	3	4

To achieve good recovery of phosphopeptides we first optimised the enrichment methods for protein extracted from Arabidopsis roots. After tryptic digest, phosphopeptide enrichment used three TiO_2 incubations for each sample. The enrichment protocol was optimised to include the Filter Aided Sample Preparation (FASP) digest protocol as protein precipitation was causing problems. The FASP digest uses an urea buffer to help keep the pro-

teins soluble prior to digestion. The earlier protocols used MeOH/chloroform precipitation, but resolubilising the proteins or even the peptides after tryptic digest proved very challenging. Different protein precipitation methods were tested and different amounts of trypsin was added but resolubilisation was still not efficient. The remaining precipitate was separated on a SDS PAGE gel and it was determined that the precipitate probably contained digested peptides. Given this, protein precipitation methods were avoided as too much protein was lost during precipitation, therefore we performed FASP digests. The FASP digest was done using a 3 kDa cut off, so proteins less than 3 kDa were lost through the membrane. Not only was the resolubilisation of precipitated proteins an issue, the proteins also precipitated when centrifuged through the C-8 membrane. An additional incubation step of 30 minutes was added after the addition of acetonitrile and TFA prior to incubation with the TiO_2 beads, to allow proteins that may precipitate in the newly acidic condition time to precipitate. The peptide solution was then centrifuged at max speed to remove all precipitated proteins.

Once the enrichment method was optimised and peptides analysed by LC-MS/MS, the data was analysed using MQ and match between runs used. The main analytical experiment required three independent biological replicas of each of the four treatments. To achieve good phosphopeptide recovery and reproducibility, seven full batches of the enrichment were done and the reproducibility evaluated using Scaffold. For each batch, to determine the quality of the protein extraction, 20 µg was run on a SDS PAGE gel to check for protein degradation and to check whether RALF1 elicitation was successful an anti-MAPK western blot was performed (Figure 5.1). The enrichment success was assessed by checking the percentage of proteins that were phosphopeptides, with 50% enrichment being the threshold for inclu-

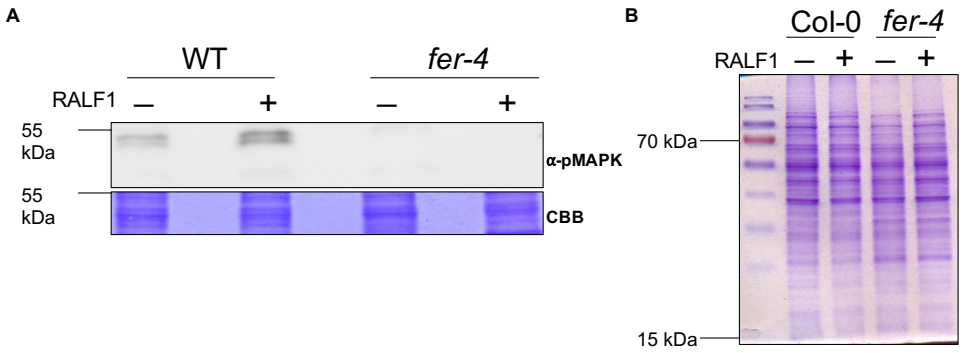

Figure 5.1: MAPK activation in Arabidopsis roots after treatment with RALF1. Roots were treated with 1 μM RALF1 for 5 minutes. A) Anti- phosphorylated MAPK Western Blot showing RALF1 activation of MAPKs. B) Coomassie stained SDS PAGE gel of protein extract to check for protein degradation.

sion. The sample was removed even if in a single fraction one of the TiO_2 incubations failed to meet the enrichment threshold.

Having removed the samples with poor enrichment, there were three replicas of *fer-4* untreated and four replicas of the other three groups; *fer4* RALF1 treated, Col-0 untreated and Col-0 RALF1 treated. The phosphosites were filtered for Class I sites, a site that has a localisation score of > 0.75 and a score difference of >5, removing peptides that contain ambiguity over the exact location of the modification. The total number of Class I phosphorylation sites across all samples was assessed, they ranged from 3254 sites in a *fer4* untreated sample to 5310 in a RALF1 treated sample. We were able to quantify phosphopeptide sites that were observed at least three times in group, in the range of 81% - 87% of the spectra identified (Figure 5.2).

A principal component analysis (PCA) was plotted for the quantified phosphopeptide sites to determine how closely the replicas matched. There is an obvious difference between the Col-0 plants and the *fer-4* regardless of RALF1 treatment as seen by the distinct separation of the plots in Figure

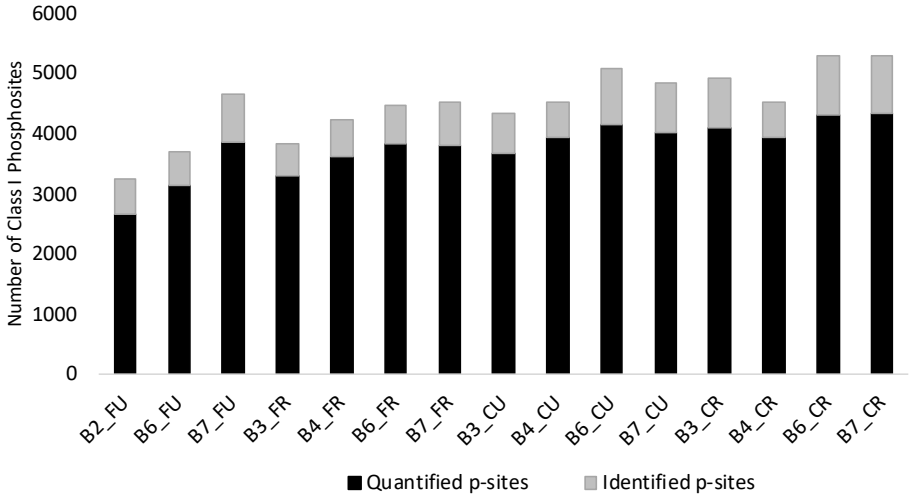

Figure 5.2: Large number of Class I phosphosites with 81% - 87% quantified. Number of identified phosphosites, with the percentage of which were quantified. FU - *fer-4* untreated, FR - *fer-4* RALF1 treated, CU - Col-0 untreated and CR- Col-0 RALF1 treated. B = batch.

5.3. There is a high degree of overlap between RALF1 treated and untreated *fer-4* plants, which is not the case when comparing RALF1 treated Col-0 against untreated Col-0. There is a distinct difference with no overlap between Col-0 RALF1 treated and untreated samples in Figure 5.3.

To determine phosphopeptides that were significantly different, either between genotype or with RALF1 treatment, a two way ANOVA was performed on the quantifiable phosphosites. Using an ANOVA statistical test, 684 significant phosphosites were identified as significantly different. A Venn diagram was used to compare phosphosites that change in response to RALF1 and genotype and were therefore dependent on RALF1 and FER, and phosphosites that just change with genotype (Figure 5.4). From the 684 phosphosites there were 667 unique phosphosites, as some would have been observed on peptides with multiple phosphorylation modifications. There were 54 phosphosites that changed solely with the addition of RALF1 and are unchanged when comparing genotype, suggesting that these sites are independent of

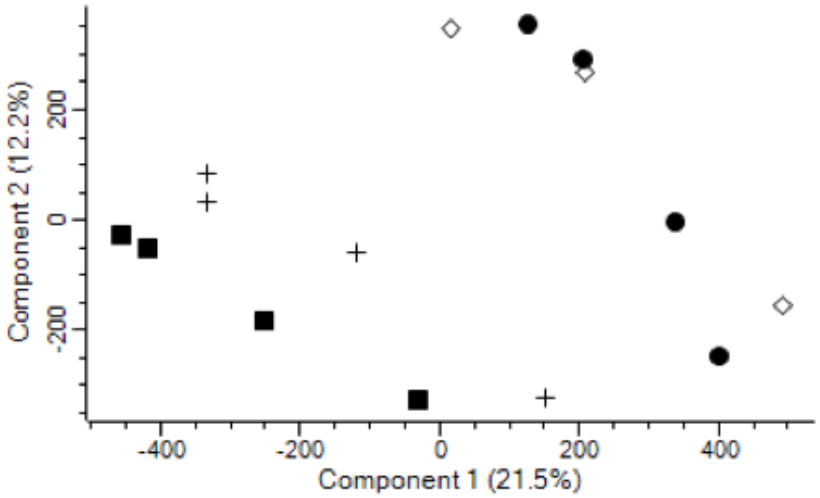

Figure 5.3: Col-0 and *fer-4* show distinct phosphosites, with similarity between *fer-4* untreated and *fer-4* RALF1 treated. PCA plot of quantified phosphosite showing the difference between the samples. Four replicates of Col-0 untreated (+), four replicates of Col-0 RALF1 treated (Square), four replicates of *fer-4* RALF1 treated (circle) and three replicas *fer-4* untreated (Diamond).

FER. 385 sites changed when comparing genotype, Col-0 to *fer-4*, but did not change with RALF1 elicitation, suggesting that these sites are FER dependent but RALF1 independent. Finally, 255 phosphosites changed with both RALF1 elicitation and genotype, therefore dependent on both RALF1 and FER.

To determine how the phosphosites change in relation to RALF1 elicitation and genotype a *post-hoc* *t*-test was performed on the quantified phosphopeptide sites with an FDR of 0.05 and a S0 (measure of fold change) set to 2. As the data is Log2 this equals a four fold change. To determine RALF1 dependent changes a *t*-test was performed between Col-0 RALF1 treated and *fer-4* RALF1 treated samples, and to determine changes related to genotype, a *t*-test of Col-0 verses *fer-4* was done. The results of the *t*-test were plotted using a volcano plot, plotting the -Log of the p-value against

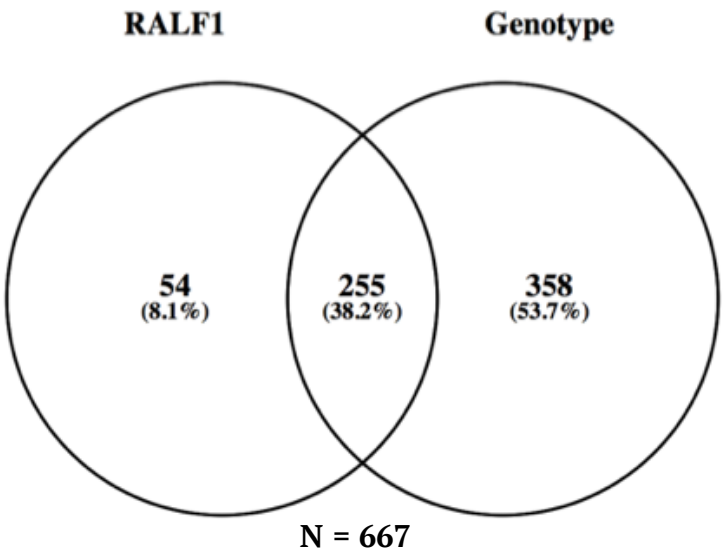

Figure 5.4: 255 phosphosites are dependent on RALF1 and FER. A Venn diagram plotted from two way ANOVA results, highlight phosphosites that are dependent on RALF1, FER and both RALF1 and FER.

the difference between samples (Figure 5.5).

The volcano plots show that for the RALF1 dependent comparison and the genotype comparison there were phosphorylation sites that increase and decrease. The volcano plots allowed us to visualise the phosphosites that change most dramatically between the samples, however, to look at which proteins are unique to RALF1 dependence, and or genotype, a Venn diagram was plotted (Figure 5.6). There were 341 phosphosites that were unique to the genotype comparison, and therefore dependent on FER but not RALF1, with 256 sites showing increases in phosphorylation and 85 sites that showed decreased phosphorylation. 76 phosphopeptides were unique to RALF1 treatment and independent of FER, which is interesting as RALF1 is not known to interact with any other receptors, with 64 phosphosites showing increased phosphorylation and 12 sites with decreased phosphorylation. There were 158 phosphosites that were common and therefore dependent of

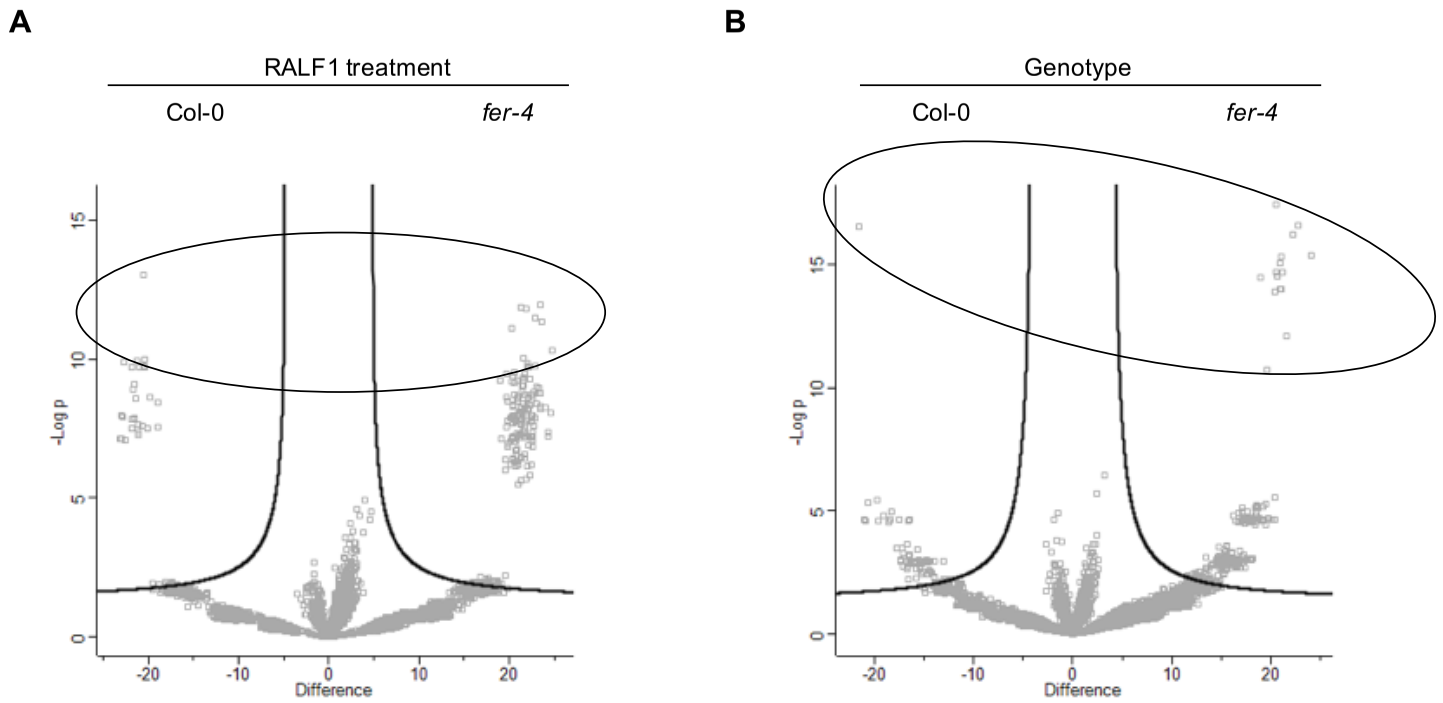

Figure 5.5: Distinct set of phosphorylation sites that change with RALF1 treatment and genotype. A post-hoc students t-test (FDR set 0.05 and s0 set to 2) was done on ANOVA results. A) Col-0 RALF1 treated against *fer-4* RALF1 treated. B) Col-0 against *fer-4*. Proteins circled are defined in Table 5.1

both RALF1 and FER, given the aim was to identify downstream signalling events of RALF1-FER, we focused on these sites.

Using the *t*-test with FDR set to 0.05 and a minimum fold change of four, to increase stringency, and the volcano plots, the 18 phosphosites that showed the lowest p-value and the biggest difference for both the RALF1 and genotype comparison were identified. The top 18 phosphosites from both the RALF1 treated and the genotype comparison was chosen due to time restraints, we focused on the phosphosites that changed the most significantly and therefore sites that we are most confident of. These phosphosites were analysed to determine if they were dependent on RALF1 or genotype, or whether the change relied on both FER and RALF1. The phosphopeptides was then compared with Figure 5.7 to look at the function of the proteins the phosphosites were identified on. Table 5.2 shows the 36 phosphosites that showed the biggest change according to the *t*-test.

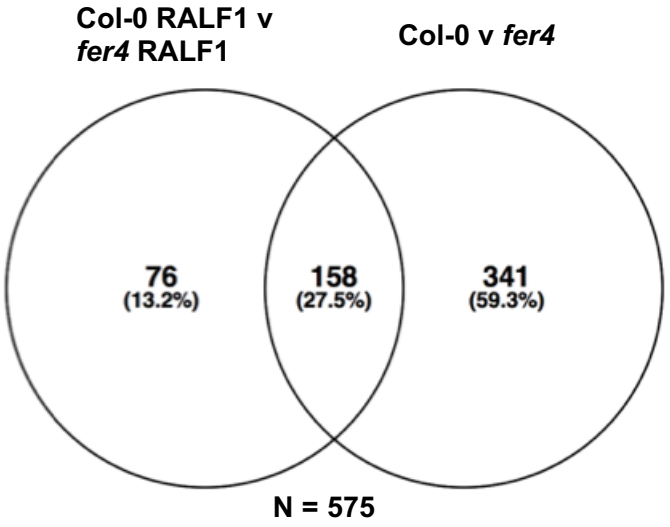

Figure 5.6: 499 phosphosites are dependent on FER with 158 of those also being dependent on RALF1. A post-hoc students t-test (FDR set at 0.05 and s0 set at 2) and the significant proteins were plotted in a Venn diagram.

Table 5.2: Top 18 proteins from genotype and the top 18 from RALF1 treatment comparison. The top 18 proteins from the post-hoc t-test (FDR set at 0.05 and s0 2). Highlighted in volcano plots in Figure 5.5

Accession	Name	p-Site	Significant in	Increase or Decrease	Function
AT2G18960	H(+)-ATPase 1	904	RALF1 and genotype	↑	Cell growth
AT4G30190	H(+)-ATPase 2;	904	RALF1 and genotype	↑	Cell growth
AT3G13530	mitogen-activated protein kinase kinase kinase 7	503	RALF1 and genotype	↑	Kinase
AT2G40270	Protein kinase family protein	169	RALF1 and genotype	↑	Kinase
AT5G59010	Protein kinase protein with tetratricopeptide repeat domain	329	RALF1 and genotype	↑	Kinase
AT4G24100	Protein kinase superfamily protein	516	RALF1 and genotype	↑	Kinase
AT1G70460	root hair specific 10 (PERK)	312	RALF1 and genotype	↑	Kinase
AT5G56180	actin-related protein 8	16	RALF1 and genotype	↑	Cytoskeleton
AT1G20450	Dehydrin family protein	14	RALF1 and genotype	↑	Cytoskeleton

Accession	Name	p-Site	Significant in	Increase or Decrease	Function
AT1G72410	COP1-interacting protein-related	624	RALF1 and genotype	↑	Trafficking
AT1G14380	IQ-domain 28	570	RALF1 and genotype	↑	Trafficking
AT2G26410	IQ-domain 4	349	RALF1 and genotype	↑	Trafficking
AT1G74830	Protein of unknown function, myosin binding	226	RALF1 and genotype	↑	trafficking
AT2G19710	IST1-LIKE 3	898	RALF1 and genotype	↑	Trafficking
AT2G19710	IST1-LIKE 3	903	RALF1 and genotype	↑	Trafficking
AT5G47480	RGPR-related	1290	RALF1 and genotype	↓	Trafficking
AT1G71940	SNARE associated Golgi protein family	22	RALF1	↑	Trafficking
AT2G26190	calmodulin-binding family protein	505	RALF1 and genotype	↑	Calcium
AT2G26190	calmodulin-binding family protein	509	RALF1 and genotype	↑	Calcium
AT2G26100	Galactosyltransferase family protein	18	RALF1 and genotype	↑	Cell growth

Accession	Name	p-Site	Significant in	Increase or Decrease	Function
AT1G22300	general regulatory factor 10	234	RALF1 and genotype	↓	Cell growth
AT1G11310	Seven transmembrane MLO family protein	510	RALF1 and genotype	↓	Defense
AT3G49590	Autophagy-related protein 13	337	RALF1	↓	Degradation
AT5G65200	plant U-box 38	553	RALF1 and genotype	↓	Degradation
AT4G15900	pleiotropic regulatory locus 1	145	RALF1 and genotype	↑	Hormone
AT3G60240	eukaryotic translation initiation factor 4G	1365	RALF1 and genotype	↑	Metabolism
AT1G01580	ferric reduction oxidase 2	639	RALF1 and genotype	↑	Metabolism
AT2G02010	glutamate decarboxylase 4	8	RALF1 and genotype	↓	Metabolism
AT3G57340	Heat shock protein DnaJ, N-terminal with domain of unknown function	233	RALF1 and genotype	↓	Metabolism
AT2G26570	Plant protein of unknown function, light	778	RALF1 and genotype	↑	Metabolism

Accession	Name	p-Site	Significant in	Increase or Decrease	Function
AT2G46860	pyrophosphorylase 3	28	RALF1 and genotype	↑	Metabolism
AT5G59960	sodium pump	6	RALF1 and genotype	↑	Metabolism
AT1G13940	Plant protein of unknown function , TF	716	RALF1 and genotype	↓	Transcription Factor
AT5G43830	Aluminium induced protein with YGL and LRDR motifs	12	RALF1 and genotype	↓	Unknown
AT3G47210	Plant protein of unknown function	29	RALF1 and genotype	↑	Unknown
AT5G46780	VQ motif-containing protein	147	RALF1 and genotype	↑	Unknown

5.2.2 Functional analysis of quantified RALF1 and FER dependent phosphosites

All 684 detected phosphosites were categorised by protein function to determine if downstream FER signalling influences particular cellular processes. The groups used to categorise the proteins were: calcium related, cell growth, cytoskeleton, defence, degradation, hormone related, kinase, transcription factors (TF), transport (including chaperones and ion transporters), metabolism and unknown. The proteins were categorised using

Uniprot and Tair multi-list uploads to obtain GO terms to look at known biological functions. Figure 5.7 shows the spread of the different functions that proteins have that are differentially phosphorylated in relation to FER and RALF1. This offers crucial evidence for future experiments that can look at targeted pathways downstream of FER.

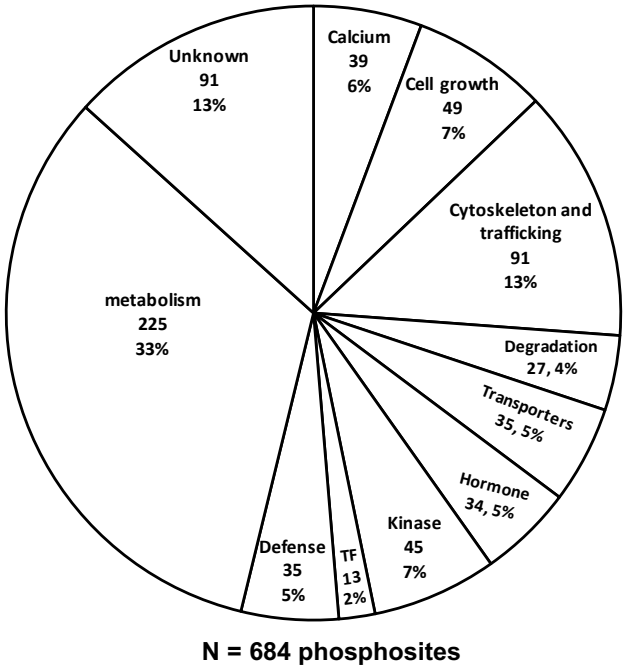

Figure 5.7: RALF1-FER downstream phosphorylation events cover a large number of biological processes. Phosphosites were categorised by GO terms using Tair and Uniprot.

To interpret the functional significance of significantly changing phosphosites we first examined FER phosphosites, summarised in Table 5.3. Haruta et al (2014) showed that there are three RALF1 dependent phosphorylation sites on FER; pS871, pS874 and pS858, with pS858 increasing by ∼20 fold in RALF1 treated tissue. Given this, we examined FER phosphopeptides in detail. We observed three Class I phosphorylation sites, which were the same as identified by Haruta et al; pS871, pS874 and pS858. Phosphorylation sites

pS871 and pS874 are on the peptide "(pS)LA(pS)EDSDGLTPSAVFSQIMNPK" (depicted by (p)), and pS585 in the peptide "SSDVYEGNVTD(pS)R". However, the reproducibility of these were poor with pS858 only being seen in one replicate of RALF1 treated col-0, and therefore it has been seen too irregularly to draw any conclusions. pS871 was identified in five replicas including in one *fer-4* sample. There was no MS2 spectrum for the occurrence of this peptide in the *fer-4* sample and therefore it is a result of the match between runs function. Therefore, we discounted this peptide as its highly likely to be a result of noise on the LC that had the same retention time as this peptide in another sample, as *fer-4* is a complete knock out. The phosphorylation sites of pS874 on FER kinase domain are not RALF1 dependent in our data, however, pS871 does appear to increase in abundance reproducibly with RALF1 elicitation.

Unexpectedly, we identified RALF1 as being phosphorylated at two sites in our phosphopeptide enrichment, pS78 and pS81, in both *fer-4* and Col-0 RALF1 treated samples. No phosphorylated RALF1 was detected in Col-0 untreated samples, which could be due to the low abundance and therefore it not being detectable or an artefact from the elicitation. To confirm whether RALF1 phosphorylation was an artefact of the synthetic RALF1, we digested an aliquot of synthetic RALF1 and analysed this using the MS and Mascot to identify the spectra. No phosphorylation modifications were observed so we conclude that RALF1 is not phosphorylated prior to treatment. The phosphosite pS78 was observed in one *fer-4* RALF1 treated sample and one Col-0 RALF1 treated sample. The phosphosite pS81 was observed with high abundance in all eight RALF1 treated samples, with a very good probability score of 166.07 and a small mass error of -0.011 ppm (how much the observed mass differs from the predicted mass), seen in Fig-

Table 5.3: S871 is a RALF1 dependent phosphorylation site on FERONIA. Table of all the FER phosphosites identified from global phosphoproteomics.

Phosphopeptide	Site	Localisation	Score difference	Seen in Col-0 untreated	Seen in Col-0 RALF1	Conclusion
(pS)LASEDSDGLT PSAVFSQIMNPK	pS871	0.95	15.2	1	3	Seen with a 2-4 fold increase in RALF1
SLA(pS)EDSDGLT PSAVFSQIMNPK	pS874	0.76	7.6	3	1	Not RALF1 dependent
SLASED(pS)DGLT PSAVFSQIMNPK	pS877	0.74	5.6	1	1	seen too unreliably
SLASEDSDGLT P(pS)AVFSQIMNPK	pS883	0.54	5.7	0	2	seen too unreliably
SLASEDSDGL(pT) PSAVFSQIMNPK	pT881	0.76	5.0	0	2	seen too unreliably
SSDVYEGNVTD(pS)R	pS858	0.85	10.8	0	1	seen too unreliably

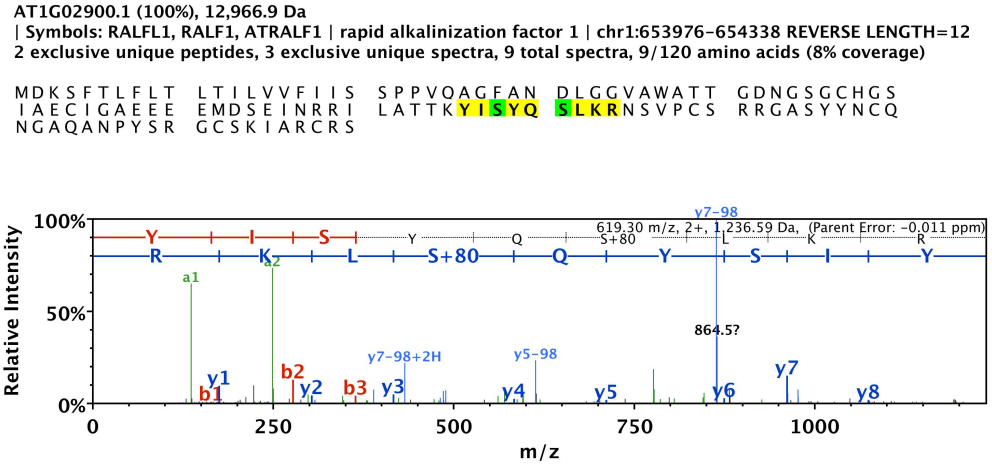

Figure 5.8: RALF1 peptide is phosphorylated at pS78 and pS81. Sequence coverage from Scaffold of RALF1 phosphopeptides. Spectrum showing identified phosphosite with mass error of -0.011 ppm.

ure 5.8. The MQ probability score is a measure of how well the observed spectra matches the predicted theoretical spectra, given the reproducibility combined with the high probability score and low mass error we believe RALF1 was phosphorylated at pS81.

In Chapter 4 we identified probable components of the FER complex and we compared these with the significant phosphosites identified by ANOVA. Only one protein was identified in both, FER-GFP CoIP and this global phosphoproteomics analysis. Dehydrin family protein, ERD10, (AT1G20450) is linked to cold stress, dehydration and abscisic acid (ABA) signalling that has known interactions with acidic phospholipid vesicles and actin binding. Three phosphorylation sites were quantified in the enrichment, T218 was significant with RALF1 treatment only and when looking at abundances it is only seen in Col-0 RALF1 treated samples where it has a high abundance. Another site on the same protein is T220, which significantly changes with genotype, suggesting that this site depends on FER. The third site quantified is T14, which was completely absent in the *fer-4* line and also increased in

abundance in the RALF1 treated sample. These two sites linked to RALF1 are interesting as ERD10 was enriched in the RALF1 elicited FER complex, and further experiments to determine the interaction should be performed.

Looking at the functional categories defined in Figure 5.7, we observed two proteins with proton pump function, AHA1 and/or AHA2. AHA2 is known to interact with FER and although it was not a significantly enriched protein within the FER-GFP CoIP it was seen in all samples. The ANOVA results from the phosphopeptide enrichment identified both phosphorylation of AHA1 (p904) and AHA2 (p904) to be RALF1 and and FER dependent.

There were 91 phosphosites categorised into cytoskeleton and trafficking identified from 59 proteins. Nine of these proteins were identified as the highest significantly changing sites shown in Table 5.2, the largest category identified from the top 18 list of the *post-hoc* *t*-test, with IST1-LIKE 3 having two sites, p899 and p903 increasing in phosphorylation in a RALF1 and FER dependent manner.

FER has strong links to calcium signalling and 39 phosphosites were identified within this category, with sites on calmodulin-binding family protein (AT2G26190) being identified as increasing in a RALF1 and FER dependent manner.

There were 45 phosphosites identified in the kinase category, with nine phosphosites on Leucine-rich repeat kinases and four phosphosites on four MAPK related proteins. A proline-rich receptor-like kinase (PERK) named root hair specific 10 was identified from the post-hoc t-test as have increased levels of phosphorylation in a RALF1 and FER dependent way.

There are 43 phosphosites that were related to cell growth, which included

cellulose synthases for cell wall biosynthesis, from 34 proteins. A phosphopeptide identified as highly significant in both the genotype comparison and RALF1 elicitation was cellulose synthase family protein (AT5G05170). There were 10 cellulose synthase related phosphopeptides that were identified as significantly different with a two-way ANOVA. Another phosphosite that was identified from the ANOVA related to cell growth was RHO guanyl-nucleotide exchange factor 4 (AT2G45890) at site 27 which has family members that are known to be downstream of FER.

5.3 Discussion

The aim of the phosphopeptide enrichment was to identify downstream signalling events of FER and RALF1. The optimisation of the widely used TiO_2 enrichment, and the seven replicates performed, enabled us to achieve very good numbers of identified phosphopeptides with a high percentage (over 80%) of those phosphopeptides being quantified. A review of phosphoproteomic studies by Wijk et al. (2014) showed 28 published studies that ranged between 16 phosphopeptides being identified to 5472, with the only root specific tissue identifying 239 phosphopeptides, which highlights the high numbers of Class I phosphopeptides, 7607, we achieved.

RALF1 has been shown to lead to phosphorylation of FER at S-871, S-874 and S-858, with S-858 being increased $\sim$20 fold with RALF1 treatment (Haruta et al., 2014) and Nühse et al., (2004) identified five other phosphorylation sites, S-695, T-696, S-701, S-861 and S-866, from a large scale phosphoproteomics study of plasma membrane proteins. From our phosphopeptide enrichment we identified six FER phosphosites, however only two

were seen reliably with phosphorylation enough to quantify, S871 and S874, S871 being RALF1 dependent. In contradiction to Haruta et al., (2014) we identified the phosphorylation site S874 in Col-0 untreated samples rather than RALF1 treatment and therefore we conclude that this phosphorylation is not RALF1 dependent. Haruta et al., (2014) identified the phosphorylation site from a single replicate and therefore we would argue that our data shows a more robust view of the phosphosite S874, as we see it in three of our untreated replicas and only once in our RALF1 treated. The Col-0 untreated samples contain native RALF1 and FER so it is possible that some RALF1 dependent FER phosphorylation sites would be detected in the untreated sample, however, we would expect this to be less reproducible and with a lower abundance when compared to the RALF1 treated sample. Our data also does not identify phosphorylation at S858 as being greatly increased after RALF1 elicitation; we identified this site in only one replicate of our RALF1 treated Col-0 samples, suggesting that the abundance of this peptide is low.

From our global phosphoproteomics study of roots we identified four AHA phosphosites, with three sites showing increased levels of phosphorylation in a RALF1 and FER dependent way. Haruta et al. (2014) identified phosphorylation of S899 of AHA2 as downstream of RALF1 and FER. Along with this site we identified three more RALF1 and FER dependent phosphorylation sites which showed higher levels of phosphorylation with RALF1 elicitation and in Col-0 plants; AHA1 904, AHA2 904 and AHA5 913.

FER regulates calcium signalling in response to mechanical stimulation and salt stress (Shih et al., 2014)(Feng et al., 2018). We identified a large number of calcium signalling related proteins, 24 proteins with 39 phosphosites that

significantly changed with RALF1 elicitation, genotype or both including CALCIUM DEPENDENT PROTEIN KINASE 1 (CPK1). A paper by Gao et al. (2013) identified that CPK1 phosphorylated RBOHD and RBOHF for ROS production, therefore CPK1 is likely to play a role in immunity. We also identified RBOHD as differentially phosphorylated at site 347 in Col-0 compared to wild type, independent of RALF1 elicitation, suggesting the phosphorylation is FER dependent. Phosphorylation at site 347 on RBOHD has been identified as being downstream of flg22 and elf18 treatment (Kadota et al., 2014). This provides an interesting link as Stegmann et al., (2017) showed FER interacts with FLS2, the receptor for flg22.

CPK1 is thought to have a predominant role in ETI signalling mediated by RPM1 and RPS2 in Arabidopsis (Gao et al., 2013). RPM1 is a nucleotide-binding domain leucine-rich repeat protein, that form complexes to sense infections and trigger robust immune responses in plants (Staskawicz et al., 1995). A protein called RPM1-induced protein kinase (RIPK) is downstream of RPM1 activation and was shown to interact with FER causing transphosphorylation of FER and RIPK1 in a RALF1 dependent manner (Du et al., 2016). In our global phosphorylation study we identified a protein that is known to be phosphorylated by RIPK1, RPM1-INTERACTING PROTEIN4 (RIN4) (Liu et al., 2012). We observed RIN4 phosphorylation increased in a RALF1 and FER dependent manner. RIN4 can directly interact with the C-terminal regulatory domain of AHA1 and AHA2, and acts as a positive regulator of the proton pump (Liu et al., 2009), which provides an interesting link between the plants decision of growth or immunity and poses the question of whether FER plays a key role in this switch.

RALF1 activates MAPKs and we showed in Chapter 3 that this was FER

dependent. The anti-pERK antibody western blot used to observe MAPK activation corresponds to a TEY motif in MAPK6 as the top band, MAPK3 middle band and MAPK4 the bottom band (Nühse et al., 2000)(Zhang et al., 2018). We identified 44 phosphosites on MAPKs including MAPK6. Although Y223 on MAPK6 was not one of the significant phosphosites, we did identify phosphorylation at Y223, which is part of the TE(pY) motif. We identified two MAPK proteins, MAP3K7 and MAPKK1, that had significantly higher phosphorylation in a RALF1 and FER dependent manner, which means that potentially MAP3K7 and MAPKK1 could form part of the same cascade after FER elicitation by RALF1.

41 of the 684 significantly identified phosphosites were kinases and we identified two RLKs that were quantified (and not significant) one of which was aCrRLK, HERCULES RECEPTOR KINASE 1 (HERK1). There has been functional redundancy noted within the CrRLK with THE1 and HERK1. Interestingly THE1, HERK1 and FER are all transcriptionally induced by brassinosteroids (BRs) (Guo et al., 2009). We identified two proteins that are regulators of BR signalling, Brassinosteroid signalling positive regulator (BZR1) family protein (AT1G19350) and BRI1 suppressor 1 (BSU1)-like 2 (AT1G08420). Phosphorylation on both BZR1 and (BSU1)-like 2 increased in a RALF1 and FER dependent manner.

FER has been shown to interact with ROPGEF1 which interacts with ROP2 (Duan et al., 2010). In this global phosphoproteomics study we identified ROPGEF4 to be phosphorylated in a RALF1 and FER dependent manner. This provides a potential mechanism to the link that ROPGEF4 is required for FERONIA-mediated developmental root hair elongation, but not in response to environmental factors (Huang et al., 2012).

Future work will focus on using a motif analysis tool to help identify phosphosites and help to assign biological function. We will also look at Class II and Class III phosphosites of specific proteins of interest to increase our knowledge of how the protein is phosphorylated even if the specific residue cannot be assigned.

Chapter 6

ROP signalling

6.1 Introduction

6.1.1 Rho-Related Proteins From Plants (ROPs)

Rho-Related Proteins from Plants (ROPs) are a plant specific family of 11 Rho small GTP-binding proteins, which act as molecular switches due to the change in conformation upon GTP binding (reviewed by Berken and Wittinghofer, 2008). ROPs are activated by ROP guanidine exchange factors (ROPGEFs), of which there are 14 in *A. thaliana*, that switch ROPs to a GTP bound form (Kanaoka and Torii 2010)(Reviewed by Moon and Zheng, 2003). ROPs are then inactivated by ROP-GTPase activating proteins (ROPGAPs) that aid GTP cleavage to switch ROPs back to the inactive GDP-state (Kanaoka and Torii 2010)(Reviewed by Moon and Zheng, 2003). Activated ROPs are removed from the membrane and stabilised in the cytoplasm by a group of proteins called Rho GDP Dissociation Inhib-

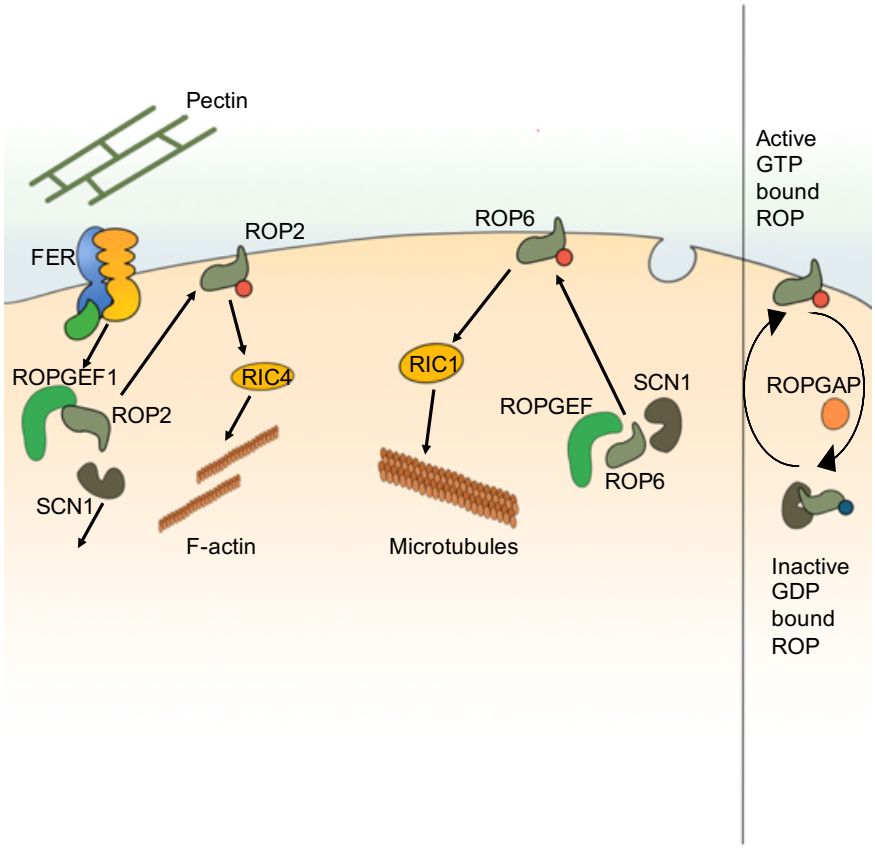

Figure 6.1: Schematic showing ROP2 and ROP6 interactors and the ROP activation cycle.

itors (RhoGDIs), which bind preferentially to GDP bound ROPs (Boulter and Garcia-Mata, 2010). The ROP activation cycle is summarised in Figure 6.1.

In *A. thaliana,* ROPs have been linked to a variety of processes with some degree of redundancy between the ROPs. ROPs 1-6 are involved in spatially controlling a variety of cellular processes by regulation of the cytoskeleton and vesicular trafficking. ROPs have been linked to the regulation of cell growth and are often studied in relation to pollen tube or root hair cell growth. ROP1, ROP3 and ROP5 may act redundantly in the modulation of tip growth in pollen tubes (Li et al., 1999)(Gu et al., 2003).

ROPs are also linked to polar cell growth and polarity in relation to root hairs, where ROP2 and ROP4 modulate tip growth in root hairs. ROP6 shares very high levels of sequence homology with ROP2 but they function differently and work antagonistically with *rop2* mutants leading to disruption of F-actin at the tips of root hairs (Jones, et al. 2002). Whereas, *rop6* loss of function mutants have mild changes to microtubule organisation (Fu et al., 2009).

Jones et al (2002) looked at four different ROPs; ROP2, ROP7, ROP8 and ROP11 in relation to root hairs. Loss of function mutants of *rop8* and *rop11* have no effect on root hair development, whereas *rop7* and *rop2* do show root hair phenotypes. Overexpression of *rop7* caused a significant proportion of root hairs to fail to elongate at the tip, resulting in thick short hairs. ROP2 is expressed in root hair cells and overexpression led to multiple hairs forming on individual cells and hairs with multiple tips. *rop2* mutants have also been shown to have fewer lateral roots (Wu et al. 2011). ROP1 is involved in the control of cell polarity development in pollen tubules (Gu et al. 2003).

The different ROP functions are due to interactions with different effectors post activation via a ROPGEF. One such effector is ROP-interactive CRIB motif-containing protein 1 (RIC1). Activated ROP2 causes inhibition of RIC1, suppressing microtubule formation and stimulating F-actin assembly via activation of RIC4 (Fu et al., 2002, 2005). Activated ROP6 activates RIC1 and hence promotes microtubule assembly. These interactions are known to occur in pavement cells and further studies have shown that RIC1 has a multitude of roles in differing tissues (Fu et al., 2002, 2005). RIC1 signalling plays a large role in root development and localises to punctate structures in the cytoplasm of root cells (Choi et al., 2013). A ROP-GEF

named SPIKE1 activates ROP6 in the ROP6-RIC1 pathway in roots (Lin et al., 2012). Another ROP effector protein with a root phenotype is INTERACTOR OF CONSTITUTIVE ACTIVE ROPs 1 (ICR1), which showed cell deformation and loss of root stem-cell population in a knockdown or silencing *icr1* mutant (Lavy et al., 2007). A summary schematic of ROP2 and ROP6 is shown in Figure 6.1.

Multiple studies have shown ROPGEFs are activated by membrane bound receptor-like kinases (reviewed by Miyawaki and Yang, 2014). FER interacts with and activates ROP2 through ROPGEF1 in plants grown on high auxin media (Duan et al., 2010). A ROPGEF and FER association has also been shown in relation to seed size, where the signalling network inhibits cell elongation in seed development (Yu et al. 2014). ROP signalling cascades are well documented to be involved in auxin signalling. Duan et al showed that FER acts upstream of ROP signalling pathway involving the production of ROS in root hair development, and that FER mutants were unresponsive to auxin (Duan et al. 2014). This interaction indicates the importance of FER in polar cell growth due to the interaction with ROP, which has a connection with polar growth.

6.1.2 ROP activation assay

Auxin has been implicated in ROP activation (Tao et al., 2002; Wu et al., 2011; Miyawaki and Yang, 2014) and an assay developed by Xu (2012), enabled the activation of ROPs to be studied by using RIC1 as bait in a pull down in leaf protoplasts. As ROPs only interact with RIC1 in their GTP bound, active, form it provides a novel way of looking at ROP activation.

The ROP activation assay uses protein affinity purification to enrich for activated ROPs and then a western blot to visualise the amount of activated ROPs bound to RIC1. ROP2-GFP and ROP6-GFP were studied over a time course with NAA, which showed that both ROP2 and ROP6 were activated 0.5 minutes after treatment with 100 nM NAA in protoplasts (Xu 2012).

6.1.3 Aims

There were two main aims for this chapter, firstly identify ROP interactors using ROP2-GFP and ROP6-GFP CoIP and the RIC1 and RIC4 affinity purification, with the aim of identifying FER and using ROPs and RICs to isolate different parts of FER signalling pathway. Secondly the aim was to build upon the ROP activation assay developed by Xu (2012) and use it as a measure of ROP activation after RALF1 treatment in various mutants. By analysing the ROP assay by mass spectrometry rather than western blot it enables us to not only gain more information about the which ROPs are interacting with the RICs but as it does not rely on using a protein (GFP) tagged line it is not limited by plant lines.

6.2 Results

6.2.1 ROP-GFP interactors in *A. thaliana* seedlings

To investigate proteins involved in ROP signalling we used anti-GFP Chromotek GFP-TRAP beads from whole seedlings grown in liquid swirling cultures, as described in the methods. To identify components of ROP sig-

nalling pathways two ROPs that work antagonistically with each other were used. A *35S::ROP2-GFP* line and a *35S::ROP6-GFP* were used with a *35S::GFP* line as a control. All samples were untreated and four replicates of ROP2-GFP CoIPs, three ROP6-GFP CoIPs and five GFP only control CoIPs were done. The CoIPs were digested with trypsin and analysed using LC-MS/MS with a two hour separation time on the LC prior to being analysed by the MS. The spectra were assigned using MQ and quantification of the identified peptide was analysed with LFQ. Match between runs was carried out in order to improve the accuracy of the quantification, as match between runs does not require the peptide to have been selected for MS2. The intensities of each protein in all samples were then normalised to the amount of GFP: the average intensity of GFP was calculated across all samples and then all proteins within each sample were corrected by a normalisation factor (the difference between the average and the observed value).

To evaluate the reproducibility of the replicas in the CoIP, euclidean clustering was done to observe the differences between replicas. Samples that did not cluster with replicas were removed from all future analysis and the remaining replicas were analysed using principle components analysis to determine the difference. 3/5 GFP samples 3/4 ROP2-GFP samples were used and 3/3 ROP6-GFP were used. The 3 remaining replicas of ROP2-GFP and GFP CoIPs were highly reproducible however ROP6-GFP CoIPs was slightly more variable (Figure 6.2). Proteins of interest were filtered in Perseus by the following rule: a protein must be in seen in at least 3 replicas of each sample. The intensities were log2 transformed and NA values were replaced with 0.

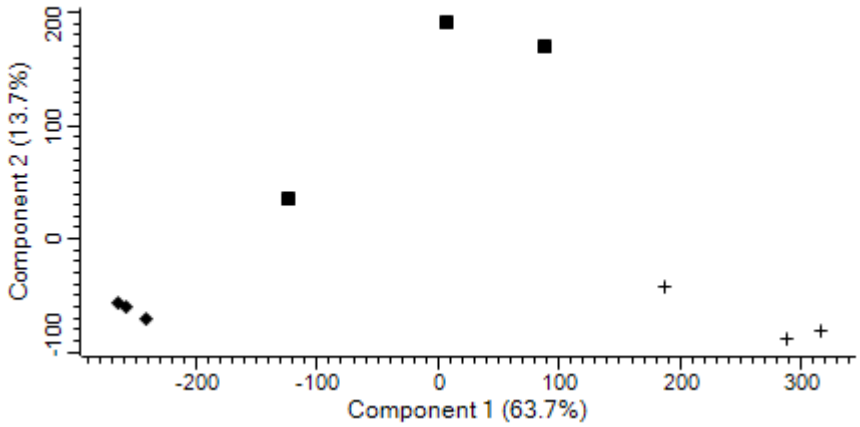

Figure 6.2: ROP2-GFP and GFP CoIPs show good reproducibility whereas ROP6-GFP is more variable. PCA plot of all ROP-GFP CoIP replicates. Cross is GFP, Diamond is ROP2-GFP and square is ROP6-GFP.

A volcano plot was constructed to show the significant differences between ROP2-GFP or ROP6-GFP when compared to GFP (Figure 6.3). A t-test was performed with FDR set 0.05 and s0 set to 0.1, which was then used to plot the volcano plot. The s0 is in essence a minimal fold change, which means even if a protein has a p-value less than 0.05, if the fold change is below that value it won't be significant. Using a S0 set at 0.1 we aimed to identify almost all protein with a p-value less than 0.05. The volcano plot shows the difference plotted against the -Log of the p-value, showing the difference between the ROP2-GFP and ROP6-GFP and the GFP control. ROP2 and ROP6 were observed in both ROP2-GFP and ROP6-GFP CoIPs, which could be a result of the high homology between ROPs, as highlighted in Figure 6.3 (Circle is ROP2, Square is ROP6). The *t*-test identified 622 significantly enriched proteins in ROP2 when compared to GFP and 120 significant proteins in ROP6 compared to GFP.

To analyse the significantly enriched proteins in the ROP2-GFP CoIP and ROP6-GFP CoIP compared to the GFP control, a Reproducibility Optim-

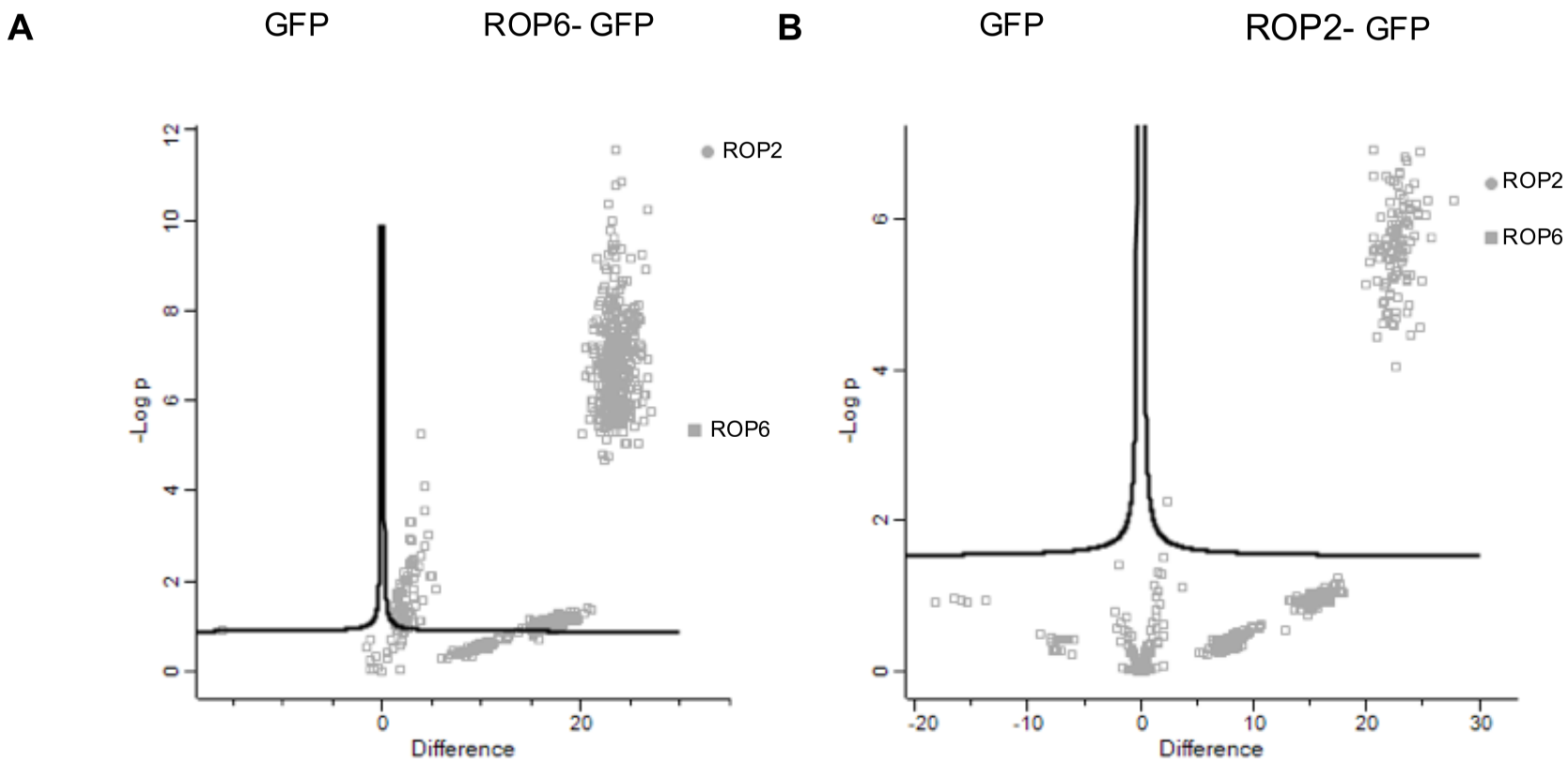

Figure 6.3: ROP2 and ROP6 are identified in both ROP2-GFP and ROP6-GPF CoIP. A students t-test (FDR set 0.05 and s0 set to 0.1) was performed on ROP-GFP CoIPs. A) ROP6-GFP compared with GFP. B) ROP2-GFP compared to GFP. Circle depicts ROP2 and square ROP6.

ised Test Statistic (ROTS) statistical test was performed using the R package, which handles unequal variance better than a standard t-test. ROTS identified 550 significantly enriched proteins in ROP2-GFP, which fits what we expected to see from both the PCA plot and the volcano plot as ROP2-GFP is hugely different from the GFP controls. The ROP6-GFP ROTS analysis displayed 130 significantly enriched proteins in the CoIP. The list of potential ROP interacting proteins was refined by looking at the biological significance. The sub-cellular localisation was used to filter these proteins further. Proteins were classified as potential contaminants and not true interactors if they were localised solely in the nucleus, chloroplast or mitochondria. The list was further narrowed down by looking at GO terms for function and biological significance and ribosomal proteins were removed as were uncharacterised proteins. There were 267 proteins remaining in ROP2-GFP CoIP and 62 proteins in ROP6-GFP. This shows that over half the proteins identified (283) in the ROP2-GFP CoIP were potential contaminants based on GO terms and, if these were to be repeated, extra wash steps would have to be added prior to MS analysis. Table 6.1 shows a summary of the function of the proteins identified from the CoIPs.

The list of significantly enriched proteins were categorised into 15 categories as shown in Table 6.1 using UNIPROT and TAIR. To look for known interactors of ROPs the database IntAct was used; this is a database that contains protein-protein interactions in Arabidopsis that have been manually curated. None of the known and verified interactors of ROP2 and ROP6 were identified. STRING was used to look for potential candidates of ROP2 and ROP6 interactors, a program that shows interactions both experimentally proven and from text mining homology similarity. STRING identified 13 possible candidates for ROP2 interactions including tubulin proteins, GEN-

Table 6.1: Summary of the functions of proteins identified in ROP2-GFP and ROP6-GFP CoIPs.

Category	ROP2-GFP	ROP6-GFP
Calcium	6	1
Cell growth	10	4
Chaperones	11	2
Cytoskeleton	8	4
Hormone	9	2
Immunity	9	3
Kinase	8	1
Metabolism	74	8
Proteasome	14	3
Proton transport	5	3
Root development	7	1
ROP associated	5	3
Transmembrane proteins	19	4
Trafficking	69	21
Translation	13	2

ERAL REGULATORY FACTOR 8 (GRF8) and SUPERCENTIPEDE 1 (SCN1), which had the highest probability of the interaction. GRF8 was also identified in the FER-GFP CoIP. STRING identified 10 possible ROP interacting proteins for ROP6 including SCN1, which again had the highest confidence, and some tubulin family proteins identified in the ROP2-GFP CoIP with three also being seen in ROP6-GFP; TUBULIN BETA-6 CHAIN (AT5G12250), TUBULIN ALPHA-5 CHAIN (AT5G19780) and TUBULIN BETA-4 CHAIN (AT5G44340). Some interesting proteins related to root growth were identified in the ROP2-GFP CoIP including two root hair defective proteins; Protein ROOT HAIR DEFECTIVE 3 and Phosphoinositide phosphatase (Protein ROOT HAIR DEFECTIVE 4), which was also observed in the FER-GFP CoIP.

The five ROP associated proteins identified in the ROP-GFP CoIPs consisted of SCN1, ROP2, ROP6, ROP7 and ROP8, with three being common

to both ROP2 and ROP6; ROP2, ROP6 and SCN1. There is a high degree of homology between the 11 ROP family members and sequence alignment was done to determine whether ROP7 and ROP8 were truly observed. There were no unique peptides found for ROP8, however the peptide 'GADVFLLAFSLISK' is unique to ROP7 and was observed once with a high degree of confidence in a ROP2-GFP CoIP. There were multiple fully conserved peptides observed, however with only one unique ROP7 peptide that was observed once there is insufficient evidence to determine whether ROP7 was interacting with ROP2.

6.2.2 ROP interacting proteins in *A. thaliana* roots

Anti-GFP CoIPs were performed using GFP-TRAP (Chromotek) beads from roots grown hydroponically in phytatrays in order to identify proteins that interact with ROPs within *A. thaliana* roots . The anti-GFP CoIP was performed as before in section 6.2.1, and prior to analysis with LC-MS/MS, 10% of the CoIP material was run on a western blot to check the CoIPs had worked. Figure 6.4 shows that all three replicas for ROP2, ROP6 and GFP contained detectable levels of bait protein. The 30 kDa band relates to free GFP, which can be seen in all samples including the ROP line. These lines have high levels of free GFP however they do still contain ROP-GFP tagged protein, shown in Figure 6.4, with the 50kDa band. With the remaining 90% of the CoIP sample, an on bead tryptic digest was performed and analysed by LC-MS/MS. The MS data were analysed using MQ and LQF performed with match between runs. The intensities of each protein in all samples were normalised to the amount of GFP: the average intensity of GFP was calculated across all samples and then all proteins within each sample were

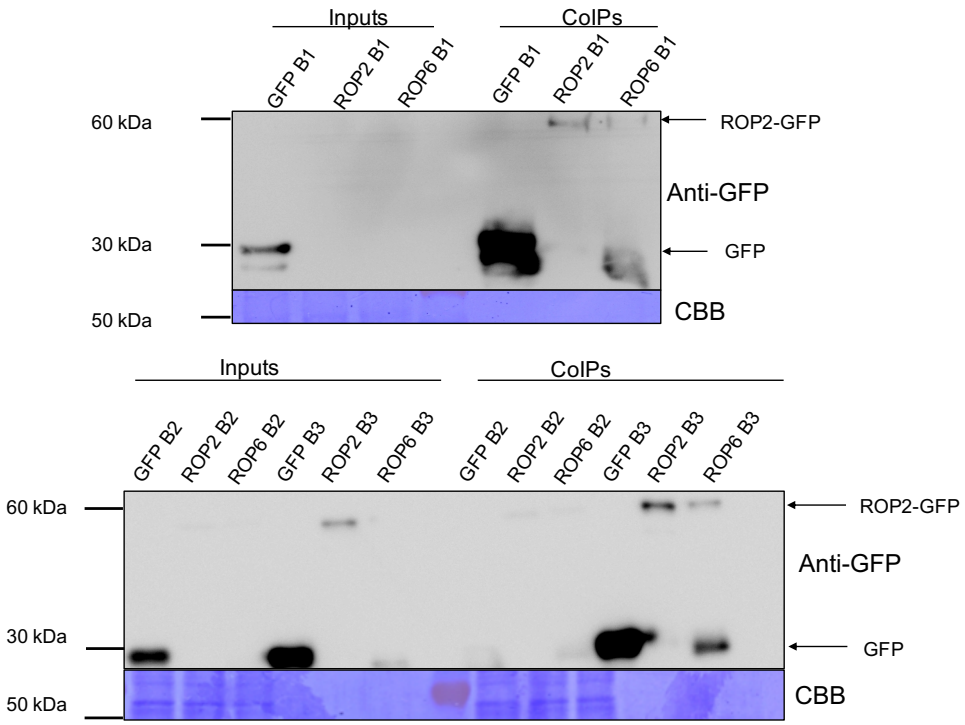

Figure 6.4: The bait protein was enriched in all three samples. Anti-GFP western blot using 10% of the CoIP material to test for bait enrichment. 30 kDa band corresponds to free GFP and the bands at approximate 55 kDa corresponds to ROP-GFP. B = batch.

corrected by a normalisation factor (the difference between the average and the observed value).

The western blot showed that all CoIPs contained the GFP tagged bait protein prior to MS, however, there were three samples that contained very low numbers of proteins as shown in Figure 6.5. ROP2 B2, ROP6 B1 and GFP B1, all contained the bait protein with good intensity seen on the Western Blot (Figure 6.4) and confirmed on the MS, but with less than 40 other highly abundant proteins this seemed too random compared to the other replicas and therefore they were not comparable with the other samples that contained several hundred proteins. These samples were removed from the analysis.

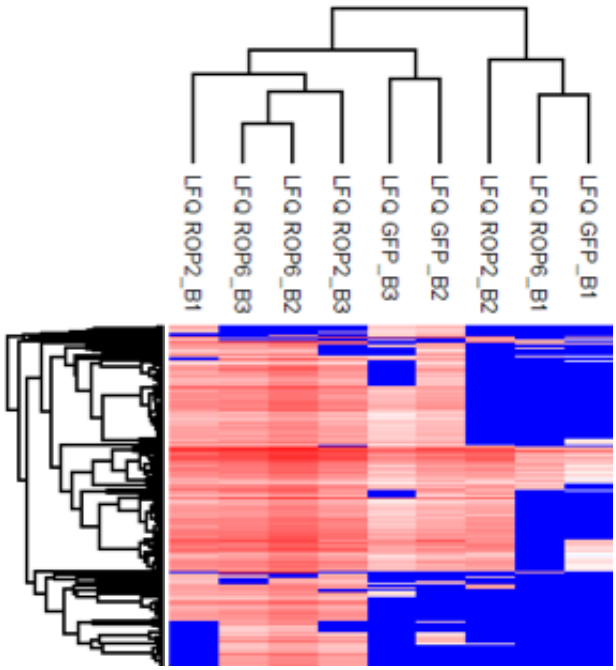

Figure 6.5: ROP2 B2 and ROP6 B1 and GFP B1 all contain very few number of proteins. Euclidean clustering showing the reproducibility of the CoIP replicas. B = batch.

Having removed the failed CoIPs from the analysis there were not enough reps to perform reliable statistical tests as each sample only has two replicates. Despite this, we wanted to cross reference the root specific CoIPs with the ROP-GFP CoIPs from whole seedlings, making any interactor seen in both root and seedling CoIPs more reliable. The proteins were filtered by the following rule: a protein must be in seen in at least two replicas of each condition. A fold change was then calculated for each protein by taking the average of the intensity for each protein in the ROP2-GFP and ROP6-GPF CoIP and dividing by the average intensity in the control. Only fold changes that were tending to infinity (absent in the GFP controls and present in the ROP-GFP CoIPs) were used to generate a list of 56 proteins that were identical between ROP2-GFP and ROP6-GFP CoIPs. These were then filtered by protein function to remove probable contaminants leaving 41 proteins.

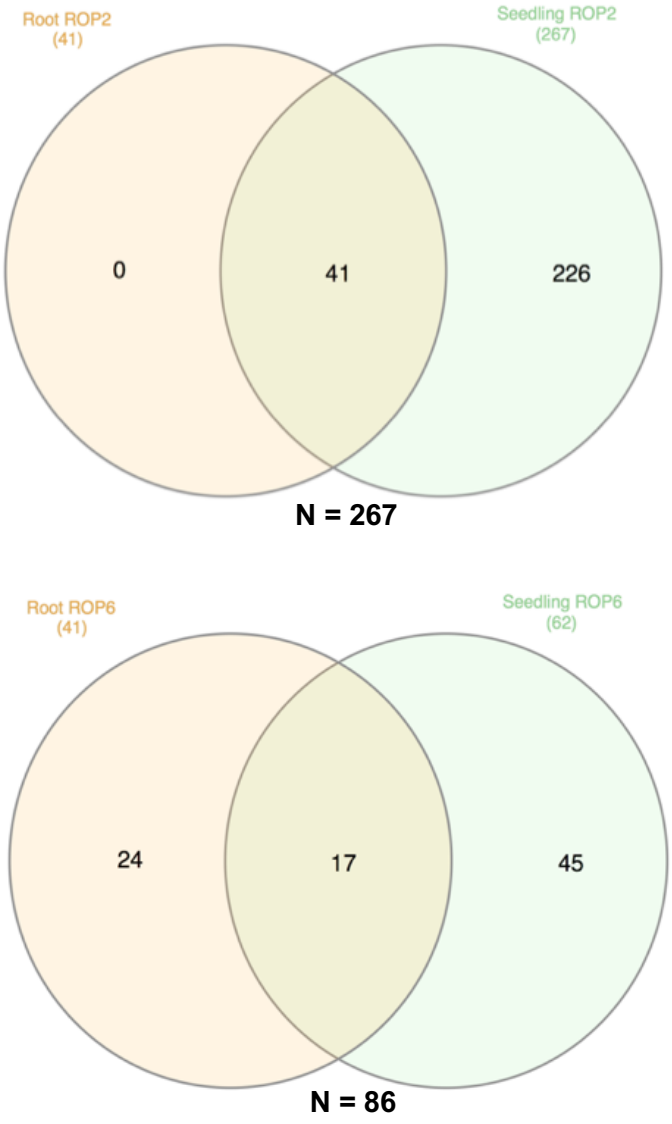

Figure 6.6: Comparison between proteins identified in the root and seedling ROP-GFP CoIPs. Venn diagram of ROP2-GFP and ROP6-GFP CoIP proteins identified in roots and seedlings.

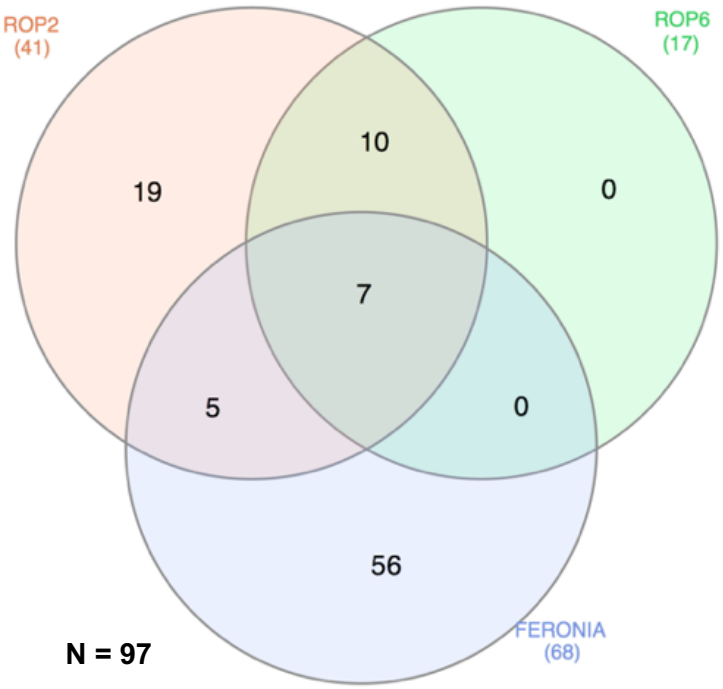

Figure 6.7: 13 proteins identified from FER-GFP were also identified in both ROP-GFP CoIPs. A summary Venn diagram of all three anti-GFP CoIPs: ROP2-GFP and ROP6-GFP CoIP proteins identified in both root and seedlings, from Figure 6.6, compared with proteins identified in FER-GFP CoIP.

Table 6.2: Proteins identified from ROP2-GFP and ROP6-GFP CoIPs. Proteins identified from Venn diagram in Figure 6.7.

Accession	Name	Function
AT1G12840	V-type proton ATPase subunit C	Proton transport
AT1G20090	ROP2	ROP
AT1G70320	E3 ubiquitin-protein ligase UPL2	Proteasome
AT2G22125	CELLULOSE SYNTHASE INTERACTIVE 1	Cell growth
AT2G31660	Importin beta-like SAD2 (Protein UNARMED 9)	Trafficking
AT3G07880	SCN1	ROP
AT3G18820	Ras-related protein RABG3f (AtRABG3f)	Trafficking
AT3G59020	ARM repeat superfamily protein	Trafficking
AT4G35020	ROP6	ROP
AT4G35790	Phospholipase D (EC 3.1.4.4)	Calcium

The list of 41 proteins from the root CoIPs was compared with the enriched proteins from whole seedlings in section 6.2.1, where all 41 of the root CoIP proteins were in common with ROP2-GFP seedling CoIP and 17 were in common between root and seedling ROP6-GFP CoIPs (Figure 6.6). These proteins that were in common between the two tissue CoIPs were used for further analysis and compared with the list of significant proteins from the FER-GFP CoIP to try and identify common components (Figure 6.7). From the Venn diagram, 10 proteins

were found to be common between ROP2-GFP and ROP6-GFP CoIPs, summarised in Table 6.2, with SCN1 a known ROP interactor being identified. There were seven proteins that were identified in all three CoIPs and these included an immunity related protein, ILITHYIA and CAND1 (Table 6.3). The function of these proteins was determined by using GO terms from UNIPROT and TAIR.

Table 6.3: Proteins identified ROP2-GFP, ROP6-GFP and FER-GFP. Proteins identified from Venn diagram in Figure 6.7.

Accession	Name	CoIP	Function
AT1G64790	ILITHYIA	All 3	Immunity
AT2G02560	CAND1	All 3	Cell growth
AT2G16950	TRN1	All 3	Trafficking
AT2G46520	Putative cellular apoptosis susceptibility protein	All 3	Trafficking
AT3G56190	Alpha-soluble NSF attachment protein 2	All 3	Trafficking
AT5G19820	ARM repeat superfamily protein	All 3	Cell growth
AT5G36230	ARM repeat superfamily protein	All 3	Translation
AT3G53110	DEAD-box ATP-dependent RNA helicase 38	ROP2 and FER	Metabolism
AT3G57290	Eukaryotic translation initiation factor 3 subunit E	ROP2 and FER	Translation
AT5G23540	Mov34/MPN/PAD-1 family protein	ROP2 and FER	Proteasome
AT4G11420	Eukaryotic translation initiation factor 3 subunit A	ROP2 and FER	Translation
AT3G56150	Eukaryotic translation initiation factor 3 subunit C	ROP2 and FER	Translation

6.2.3 Developing an affinity purification tool to extend activated ROP assay

ROPs are known to interact with RIC1 and RIC4 when activated, which enables a more focused study of activated ROPs. Xu (2012) developed an assay that measured the activation of ROPs by using affinity purification with RIC1-MBP immobilised to amylose beads, and observing the amount of ROP2-GFP and ROP6-GFP protein that was enriched after treatment. The aim was to use this as a method of testing RALF1-FER activation, given that Duan et al. (2010) showed that FER interacts with ROPGEFs which are known to activate ROPs.

To develop the affinity purification tool to measure activated ROPs three known ROP interactors, RIC1, RIC4 and ICR1, were cloned into an IPTG

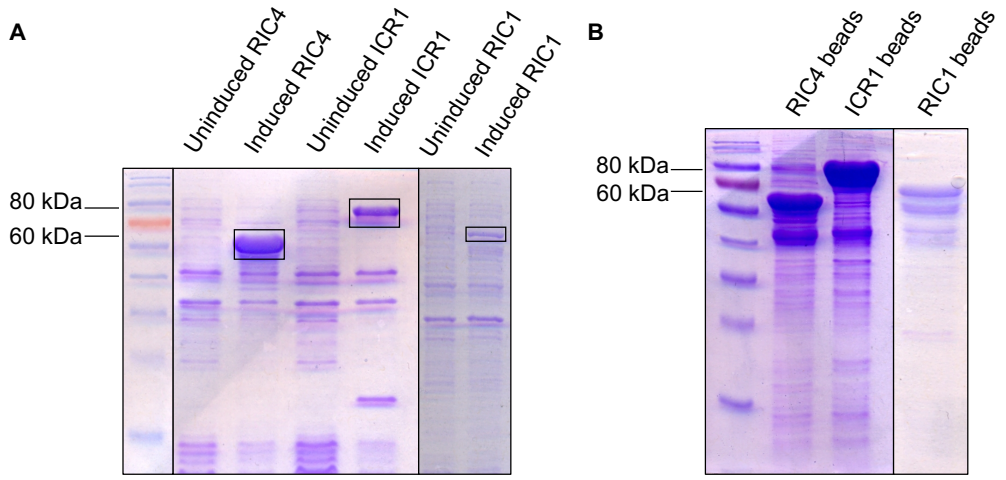

Figure 6.8: Expression and purification of MBP tagged proteins. Coomassise stained SDS PAGE gels. A) Expression after induction with 0.03 mM IPTG. B) Amylose bead purification of MBP tagged proteins.

inducible expression vector, pMAL21, which contains a C-terminal MBP tag. The RIC1 construct was shared with us (Li et al., 2008) and RIC4 and ICR1 were produced by Integrated DNA Technologies (IDT). Using the BL21* strain of *E.coli* protein expression was induced and expression was checked using coomassie staining of an SDS PAGE gel as shown in Figure 6.8.

The MBP tagged RIC1, RIC4 and ICR1 protein was then purified using amylose beads, based on the methods used in Xu (2012). The purification was optimised as our aim was to use the affinity purification in conjunction with MS analysis, which meant that the buffers used throughout the protein purification have to be MS compatible. Early attempts included 1 % Triton X-100 used during the purification of the affinity purification beads, which helped remove some unspecific bound proteins, however Triton X-100 interfered with the MS as molar excesses of detergents ionise strongly and bind to the C18 reverse phase column on the LC. The concentration of deter-

gent was reduced to 0.5% and switched to NP-40 and another wash step was added to remove unspecific bound proteins. The purification of the proteins using the amylose beads was checked by boiling the beads in SDS loading dye and using coomassie staining to identify the purified proteins. Figure 6.8 shows the successful binding of RIC1-MBP, RIC4-MBP and ICR1-MPB to the amylose beads. However, these samples show a lot a nonspecific bound proteins too and so another wash step was added prior to use as affinity purification beads.

6.2.4 Activation of ROP2-GFP

Xu (2012) developed an assay to measure the activation of ROPs by observing the amount of ROP2-GFP and ROP6-GFP binding to a known interactor RIC1. Using the RIC1-MBP affinity purification of activated ROPS in ROP2-GFP line, the activation of ROPs can be visualised using an anti-GFP western blot. Xu (2012) showed, using RIC1-MBP affinity purification and an anti-GFP western blot, that activation of ROP2-GFP and ROP6-GFP increases quickly at 30 seconds and continues to increase through to 8 minutes after NAA (auxin) treatment in protoplasts.

To determine whether RALF1 activates ROPs through FER we sought to establish the Xu assay in native system using whole seedlings, as FER is likely to be involved in cell wall perception and therefore we wanted to avoid protoplasts. *35S::ROP2-GFP* plants were grown on plates for seven days and transferred to swirling liquid media and left to equilibrate for three hours prior to treatment. They were then treated with 25 μM NAA (as a control) or 1 μM RALF1 and the plants harvested at 8 time points from

0 minutes to 120 minutes to determine the activation of ROPs after auxin treatment in whole plants.

Enrichment of activated ROPs was done using RIC1 affinity purification assay on the protein extracts taken at each time point and visualised with an anti-GFP western blot. Great care was taken to equalise the protein and bead concentrations between samples and this was always checked by western blot. The same volume of RIC1 beads was used and again the membrane from the western was always stained using coomassie to check that there was an equal amount of RIC1 on the membranes.

Despite the multiple controls the RIC1-MBP affinity enrichments proved to be very variable and had very little reproducibility between samples after NAA and RALF1 treatment, with many western blots showing fluctuating levels of ROP2-GFP enriched over the time course. Often the untreated control samples showed some of the highest levels of ROP activation. However several ROP activation assays showed promising results with increasing levels of activated ROP2-GFP after NAA treatment, with the best shown in Figure 6.9. The inputs show a fairly level amount of ROP2-GFP in each of the time points apart from 120 minutes which appears to be a lot less. This could be a western blot artefact or a genuine observation that less ROP2-GFP is present in the 120 minute sample. The activation of ROP2-GFP starts at 0.5 minutes and continues through to 120 minutes as seen in Figure 6.9. There is a slight dip in activation at 30 minutes, which could be genuine as both the input and the coomassie stained membrane for the CoIP look to have similar levels of protein compared to the others.

When looking at RALF1 activation of ROP2-GFP with the ROP activation assay, the most reproducible results showed activation of ROP2-GFP after

RALF1 treatment as shown in Figure 6.9. Great care was taken to make sure equal concentrations of the protein input and the amount of RIC1-MBP beads were used. The inputs show an even amount of ROP2-GFP across the time points and the activated ROP2-GFP appears to increase at 0.5 minutes and stay activated to 90 minutes. There is a dip in activation at 15 minutes but there appears to be slightly less RIC1 on the coomassie stained membrane as shown in Figure 6.9. Activation of ROP2-GFP also appears to reduce at 120 minutes, which could be genuine as the controls appear to show the same amount of RIC1 on the membrane.

The high variability observed between western blots for the ROP activation assay meant we wanted to confirm the observed ROP2-GFP activation in Figures 6.9 quantitatively by MS. The MS data was analysed using MQ and match between runs was applied to enable better quantification. The intensities for LFQ were then analysed using Excel and the intensity of ROP2 in the sample was normalised to the amount of RIC1 present at each time point. This was done by calculating the average RIC1 intensity for each of the two treatments across the time points. The levels of RIC1 were then adjusted to the average intensity value by a normalisation factor, which was calculated by dividing the intensity of RIC1 by the average intensity. To normalise ROP2 the intensity of ROP2 was divided by the normalisation factor. Once the intensity of ROP2 was normalised it was plotted for both NAA and RALF1, Figure 6.10, showing that there is no increased binding of ROP2 with either NAA or RALF1 once the data was normalised. From this we conclude that the ROP2-GFP activation assay using RIC1-MBP pull downs and western blots was not a reliable way of measuring ROP2 activation in a native system.

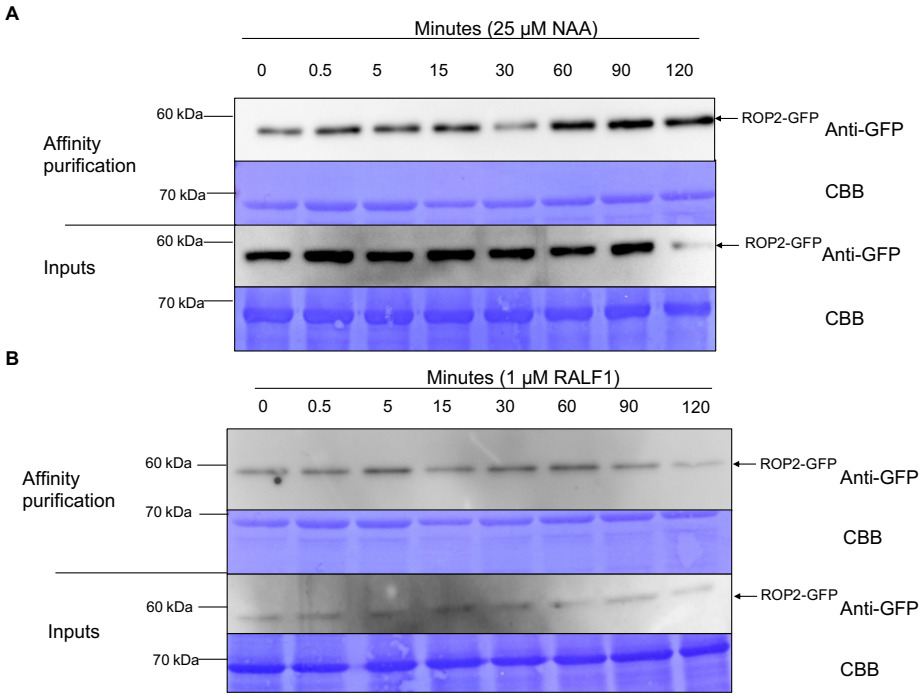

Figure 6.9: Time course of binding of ROP2-GFP to RIC1. Affinity purification of ROP2-GFP by RIC1-MBP over time after treatment with 25 µM NAA (A) or 1 µM RALF1 (B). Anti-GFP western blot of affinity purification and inputs as a control. Coomassie stained membrane to show equal loading.

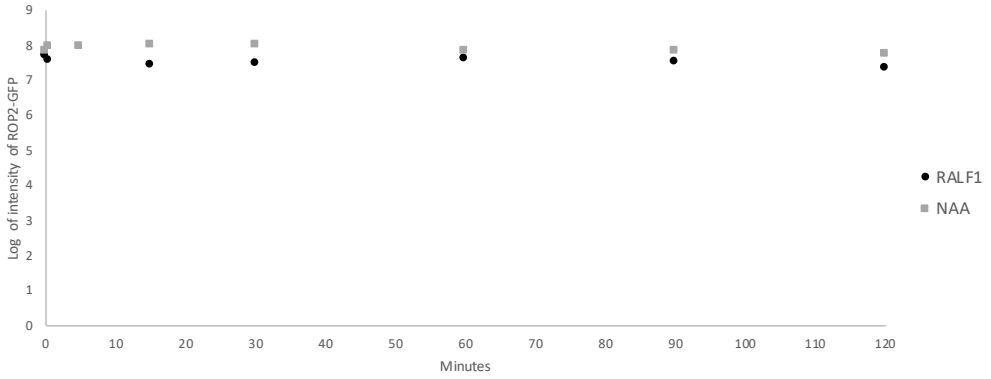

Figure 6.10: No increases in ROP2 binding to RIC1 after treatment of NAA and RALF1 after data normalised to RIC1 Label free quantification by MS of affinity purification shown in Figure 6.9. Normalisation to amount of RIC1 in each MS run and then the amount of ROP2. Only one replicate as from same experiment, 20% of affinity purification used for western blot in Figure 6.9 and 80% analysed by LC-MS/MS.

ROPs are cycled from their inactive form localised in the cytosol to their activated (GTP bound) form that is localised at the plasma membrane, which is then recycled back to the inactive cytocsolic form (reviewed by Bloch and Yalovsky, 2013). We hypothesised that isolating the microsomal fraction of a protein extraction may enable a way of measuring activated ROPs, therefore we isolated the microsomal fraction and soluble fractions from seedlings. ROP-GFP Seedlings were grown in swirling cultures for 7 days and then treated with 1 μM RALF1 or 25 μM NAA over a time course from 0 minutes to 120 minutes. The protein extraction was separated into three parts, the total protein, soluble protein and microsomal fraction. An anti-GFP western blot was performed for each of the different protein fractions over the time course. The hypothesis was that the amount of ROP2-GFP in the soluble fraction should decrease as ROP2-GFP is activated and trafficked to the plasma membrane, meaning if there is activation there should be more ROP2-GFP in the microsomal fraction. The total protein extract was used as a control for the amount of ROPs at each time point. To examine the activation of ROP2-GFP an anti-GFP western blot was used to visualise the amount of ROP2-GFP present in each of the fractions.

The western blots, Figure 6.11, show the amount of ROP2-GFP over the NAA time course of 0 minutes to 120 minutes in each of the three protein fractions. Xu et al (2012) showed that ROPs are activated after NAA treatment in protoplasts, however, when looking at Figure 6.11 we observed no change in the amount of ROPs in the different fractions. Free GFP was not observed in the microsomal fraction, suggesting that the microsomal fraction was successfully separated from the soluble fraction. The amount of ROP2-GFP in the total fraction remains constant throughout as does the ROP2-GFP signal in the soluble fraction, which we would expect to de-

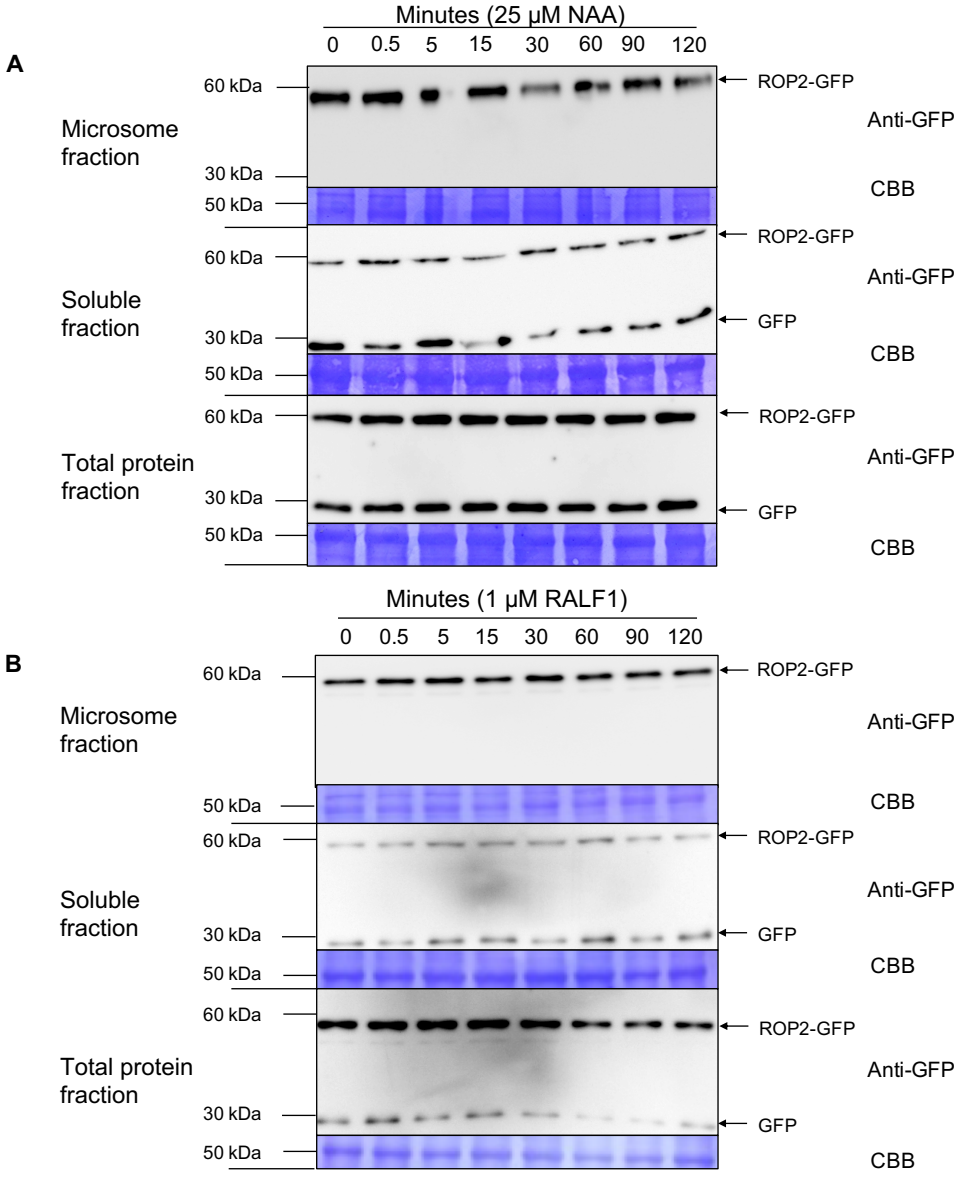

Figure 6.11: ROP2-GFP localisation after treatment. Anti-GFP western blots observing ROP2-GFP localisation in membrane fraction, soluble protein fraction and the total protein fraction. Coomassie stained membranes for controls. A) Time course of 25 µM NAA treatment of seedlings. B) Time course of 1 µM RALF1 treatment of seedlings.

crease as proteins are trafficked to the membrane. From this western blot we cannot conclude that NAA activates ROP2-GFP.

The western blots for RALF1 activation of ROP2-GFP over 2 hours do indicate that there is activation of ROP2-GFP from 0.5 minutes through to 90 minutes after which it seems to drop off slightly at 120 minutes, Figure 6.11. No substantial change is observed over the time course. The amount of ROP2-GFP in the total protein does not change over the time course. More repeats would needed to say with any certainty that RALF1 does activate ROP2-GFP at 0.5 minute to 90 minutes.

The ROP activation assay using RIC1-MBP affinity purification was attempted on the membrane fraction of both the NAA and RALF1 time courses, however no ROP2-GFP signal was detected on an anti-GFP western blot and time restraints meant this could not be continued.

6.2.5 ROP interactors - using RIC1 / RIC4

To determine whether there are any differences in ROP interactors in the FERONIA mutant, *fer-4,* affinity purification using RIC1-MBP and RIC4-MBP beads was performed in Col-0 and *fer-4*. Initially the aim was to use RALF1 elicitation, however given that no reliable increased RIC1 binding was observed when using the ROP activation assay, only untreated samples were analysed. The controls used for this experiment were pre-clear blank amylose beads that were incubated in the protein extraction for 15 minutes to pre-clear the extract prior to RIC1-MBP and RIC4-MBP beads being added. Using amylose beads as a pre-clear physically removes proteins that bind to amylose before incubating the protein extract with RIC1-MBP.

The plants were grown in phytatrays and the roots harvested and a protein extraction done. Affinity purification of RIC1 and RIC4 interactors were performed with three replicas of Col-0 RIC1 and three replicas RIC4 with the same in the *fer-4* line. All samples were pre-cleared to remove proteins that bind to amylose with only three pre-clear replicas for Col-0 and three replicas for *fer-4* being analysed by MS. The affinity purifications were performed with the protein extracts and the enriched proteins digested using an on bead tryptic digest and analysed by LC-MS/MS. The data was analysed using MQ and LFQ calculated with match between runs.

The proteins were filtered based on whether they had been seen three times in at least one group (a group being the replicas for that sample) and analysed by ROTS. The ROTS analysis showed almost no significant proteins for any of the four groups when compared against the pre-clear (Col-0 RIC1, *fer-4* RIC1, Col-0 RIC4 and *fer-4* RIC4). This is likely to be due to the pre-clear being significantly different to the affinity purified samples. A students *t*-test was performed and visualised with volcano plots (Figure 6.12). Figure 6.12 shows the number of proteins enriched in the pre-clear (all proteins with a difference less than 0) compared to the RIC-MBP affinity purification. The volcano plots show a large number of enriched proteins in all samples in the pre-clear, which is likely to be proteins that interact with MBP and the amylose beads.

The pre-clear was intended to remove proteins that bind to the amylose beads before incubation with the RIC-MBP beads, therefore, they are subtractive. As expected, there was very little difference between the proteins identified interacting with the amylose pre-clear beads between Col-0 and *fer-4* so the pre-clear beads were grouped for the following analysis. The

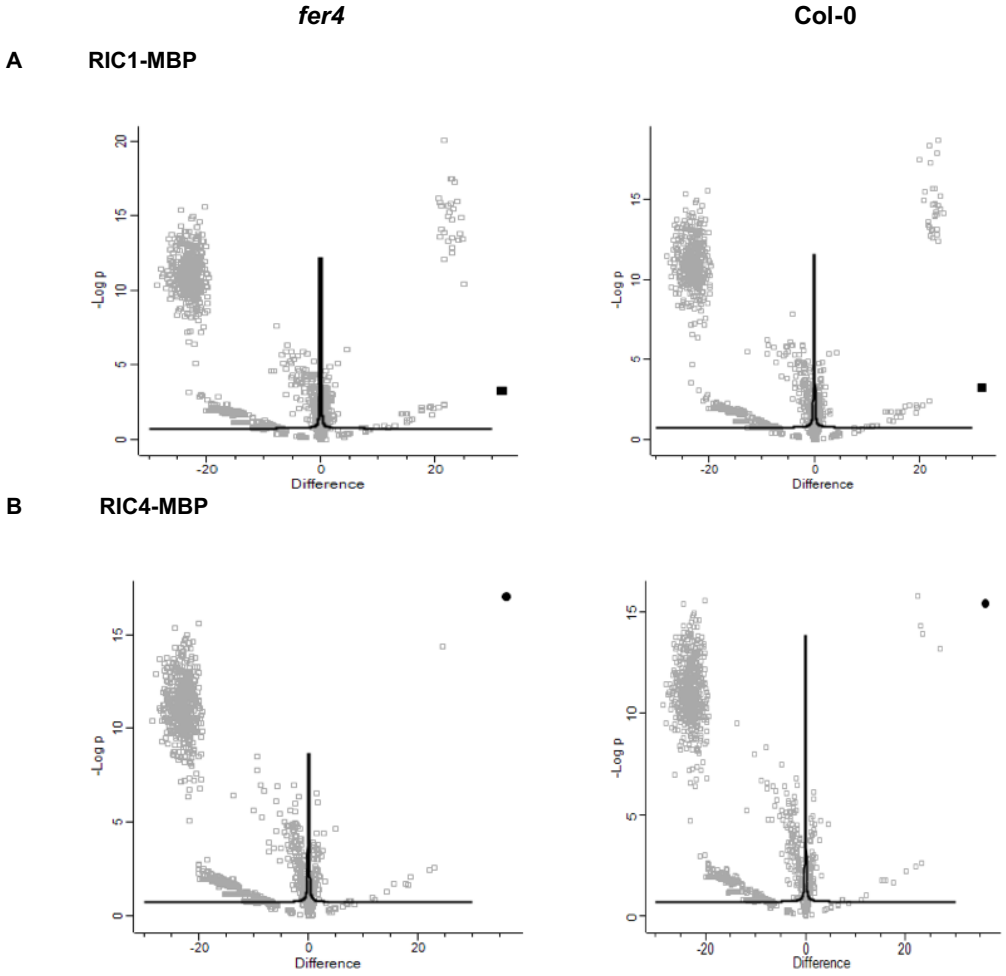

Figure 6.12: Pre-clear successfully removed a large number of proteins that bind to amylose beads. A students t-test was performed with FDR = 0.05 and S0 = 0.1. A) RIC1-MBP affinity purification with square depicting RIC1. B) RIC4-MBP affinity purification with a circle depicting RIC4.

proteins were filtered by removing all proteins that were seen three or more times in the six pre-clear bead controls. From the remaining proteins they were filtered on whether they were seen two or more times in each RIC group. A further filter was applied to improve stringency, which stated that if a protein was seen in the pre-clear control group it would have to be seen more reproducibly in the pull down group to remain.

With this filtered dataset there were 52 proteins identified in the RIC1 pull downs in both Col-0 and *fer-4*, with 42 of them being found in both Col-0 and *fer-4* as shown in Figure 6.13 A. For RIC4 there were 14 proteins that passed the filters and nine of which are shared between Col-0 and *fer-4* as shown in Figure 6.13 B. The RIC4 pull downs seemed to have more variability than the RIC1 pull downs which probably accounts for the lower number of proteins in the filtered table.

The proteins identified in the RIC-MBP affinity purifications were compared using a Venn diagram. Figure 6.13 shows proteins that differ between RIC and also between genotype. There were six proteins that are unique to Col-0 RIC1 and two proteins that were unique to Col-0 but shared between RIC1 and RIC4, these are summarised in Table 6.4. There are no unique proteins to Col-0 RIC4 and eight proteins that were shared between RIC1 and RIC4 in Col-0. There are four proteins that are unique to RIC1 and one protein unique to RIC4 in the *fer-4* background.

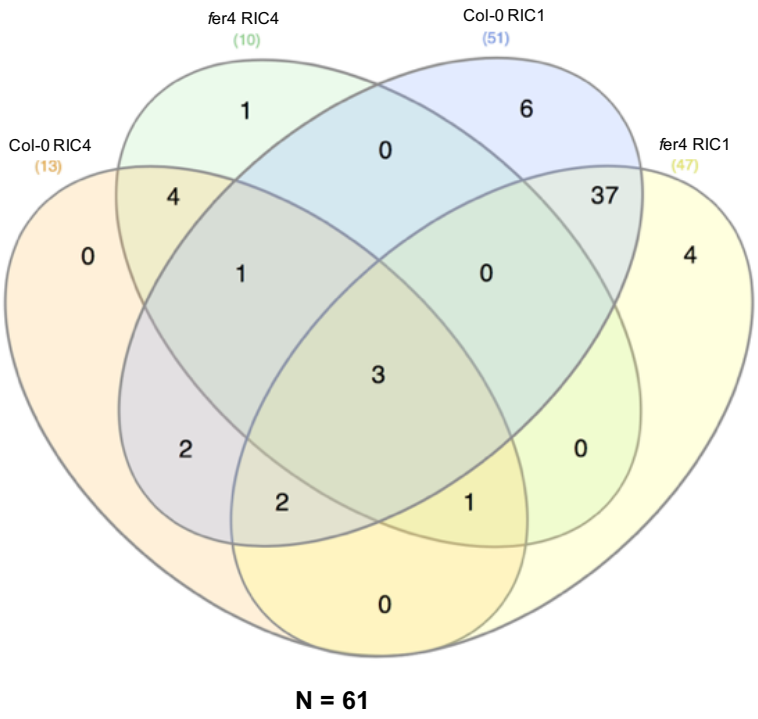

Figure 6.13: Comparison between RIC-MBP affinity purifications shown in a Venn diagram.

Table 6.4: ROP2 and Calcium-dependent phosphotriesterase superfamily protein RIC interactions were lost in *fer-4* plants. Table summarising interacting proteins that are lost in ***fer-4*** plants

Acession	Name	Unique to
AT2G45220	Plant invertase/pectin methylesterase inhibitor superfamily	Col-0 RIC1
AT3G10710	RHS12	Col-0 RIC1
AT4G01700	Chitinase family protein	Col-0 RIC1
AT1G07830	ribosomal protein L29 family protein	Col-0 RIC1
ATCG00380	chloroplast ribosomal protein S4	Col-0 RIC1
ATCG00780	ribosomal protein L14	Col-0 RIC1
AT1G20090	ROP2	Col-0
AT3G57020	Calcium-dependent phosphotriesterase superfamily protein	Col-0

The aims of this affinity purification were to identify RIC1/4 interactors and to identify if any of these interactors were dependent on FER with no

exogenous treatment. Crucially there were two proteins unique to Col-0 interaction with RIC1 and RIC4 which were ROP2 and calcium-dependent phosphotriesterase superfamily protein (AT3G57020), suggesting that these two proteins are interacting with both RICs and are dependent on FER (Table 6.4).

There were six proteins unique to Col-0 RIC1 with three being identified as contaminants due to their localisation (chloroplast and mitochondria) and three proteins associated with cell growth; plant invertase/pectin methylesterase inhibitor superfamily (AT2G45220), root hair specific 12 (AT3G10710) and Chitinase family protein (AT4G01700).

6.3 Discussion

The aims of this chapter were to identify components of the FER-ROP signalling pathway using ROP2-GFP and ROP6-GFP CoIP to identify protein interactors. We intended to follow this up using the ROP activation study to measure ROP activation downstream of RALF1 treatment in various mutants and to repeat the ROP2-GFP and ROP6-GFP CoIPs with RALF1 elicitation. However, these aims changed somewhat as we observed no increase in ROP2 binding to RIC1 and therefore no detectable increase in ROP activation. We used the ROP activation assay and focused more on proteins interacting with RIC1/4 and ROP2/6 which are downstream of FER.

Originally we aimed to treat the ROP2-GFP and ROP6-GFP CoIPs with RALF1 and look for proteins that changed upon RALF1-FER elicitation. Our first aim was to show a clear link between RALF1 and ROP activation

using the ROP activation assay designed by Xu (2012) using protoplasts. In whole seedlings the ROP activation assay showed no increase in ROP activation with either NAA or RALF1. The activation assay had been used to look at ROP activation in protoplasts. Our MS analysis showed that despite the western blot showing ROP2-GFP activation, once the level of ROP2 had been normalised to the amount of RIC1 in the sample there was no change in the amount of ROP2 interacting with RIC1 after NAA or RALF1 treatment.

The MS data of RIC-MBP affinity purifications showed multiple ROPs, ROP2 and ROP6 interacting with RIC1, which casts doubt on the validity of the Xu assay if using a single ROP-GFP tagged line. We would argue that due to the redundancy between ROPs, measuring the activity of a single GFP tagged ROP does not give an accurate representation of ROP activity. Another reason that may have caused the variability we observed is, the ROP lines we used were under an *35S::* promoter. This could have altered the localisation of the ROPs and also how the ROP cycle functions. Xu (2012) also used overexpression lines of ROP2 and ROP6, which again casts some doubt on the accuracy of the original experiment.

Upon activation, ROPs are relocated to the plasma membrane and interact with membrane lipids (Bloch and Yalovsky, 2013). We hypothesised that when looking at the total protein fraction we might not observe activated ROPs due to some being in the insoluble membrane fraction meaning that the changes in activation would be missed. Using ROP2-GFP the soluble and membrane protein fractions were isolated and the amount of ROP2-GFP present in the membrane fraction, as a measure of activated ROPs, was analysed by western blot, without the ROP activation assay. The RIC1

binding was another variable and therefore a first test was performed by measuring the amount of ROP2-GFP in the membrane fraction. The NAA time course did not show any clear relocalisation to the membrane fraction whereas the RALF1 time course showed a slight increase in ROP2-GFP in the membrane. A ROP activation assay was performed, as ROP2 is known to recruit RIC1 to the plasma membrane (Fu et al., 2005), on these membrane extracts to determine if the assay confirmed the results seen in the membrane extract but these failed, possibly due to the membrane solubilisation buffer being incompatible. Unfortunately time restraints meant this couldn't be continued.

We chose to work with ROP2-GFP and ROP6-GFP because they have proven links to root hairs and work antagonistically with distinct functions. This is also true of RIC1 and RIC4. This poses an interesting question as to how do ROP2 and ROP6 gain their specificity given the high sequence homology and how is their closely regulated localisation controlled.

ROP2 is known to interact with FER through ROPGEF1 (Duan et al., 2010). A recent paper published in 2018 in a non peer-reviewed journal shows FER interacts with pectin and this Pectin-FER complex is what activates ROP6 (Lin et al., 2018). Lin et al. (2018) used the ROP activation assay developed by Xu (2012) to show the ROP activation after treatment with demethylesterified pectin in protoplasts, they do not comment on RALF1. Given FER and other receptors in the CrRLKs family are known to perceive the cell wall, we opted to not work in protoplast as we felt this could give results that were due to protoplast and not because they would be observed under a native system. Had more time been available we would have performed the ROP activation in protoplasts to see if we could

replicate the Xu system.

The paper by Lin et al (2018) was the first paper to link FER-ROP6, as previously Duan (2010) linked FER-ROPGEF1-ROP2. The fact that the same receptor activates these two antagonistic pathways suggests that spatial regulation of ROPs could be key to their function in regulating cell growth through organisation of the cytoskeleton amongst other things.

The seedling CoIPs identified a known interactor of ROPs, the RhoGDI SCN1. *scn1* mutants have been shown to have a root hair phenotype where multiple root hair initiations are seen in a trichoblast, and ROP2-GFP and ROS production is mislocalised (Carol et al., 2005). STRING highlighted 13 proteins from the ROP2-GFP CoIP and 10 proteins from the ROP6-GFP CoIP which are potential interactors based on text mining, homologues in different species and experimental evidence. There were six tubulin proteins identified in the ROP2-GFP CoIP with three also identified in the ROP6-GFP CoIP: TUBULIN BETA-6 CHAIN (AT5G12250), tUBULIN ALPHA-5 CHAIN (AT5G19780) and TUBULIN BETA-4 CHAIN (AT5G44340). Microtubule organisation is widely reported to change in ROP6 mutants and RIC1 has been shown to interact with the P60 subunit of the MT-severing protein katanin (KTN1) (Lin et al., 2013), making tubulin a highly plausible candidate for ROP6 and ROP2 interaction, with a ROP-RIC1-KTN1-Tubulin complex being involved in the regulation of microtubules a possibility. Future work would need a secondary method of testing the interaction by reciprocal IP or BiFC.

From the ROP2-GFP CoIPs we identified 10 proteins that were interactors of both ROP2-GFP and ROP6-GFP, including SCN1. We also identified CSI1, which is involved in the highly regulated process of cellulose synthase

complex being delivered to the plasma membrane (Zhu et al., 2018). In a cellulose synthase mutant, *procuste1*, accumulation of ROPs at future root hair formation sites has been shown to be altered, linking the cellulose synthase complex to ROPs. CSI1 is a microtubule-associated protein that bridges CESA complexes and cortical microtubules (Li et al., 2012). Given ROPs association with the regulation of microtubules through RIC1, CSI1 would be a candidate to look into reverse IPs and mutant studies.

There were 12 proteins that were found in common between ROP2-GFP, ROP6-GFP and FER-GFP CoIPs, and although we did not detect FER or ROPs pulled down by the bait protein in the any of the three CoIPs, these proteins offer an insight into proteins in the pathway. Two proteins of particular interest are ILITHYIA and CAND1. Both of these proteins have been identified as having growth phenotypes with ILITHYIA mutants producing much shorter roots (Faus et al., 2018). CAND1 has been shown to positively regulate multiple ubiquitin E3 ligases and their associated developmental processes in plants (Feng et al., 2004). As these two proteins were identified in the Core FER complex it poses an interesting question as to whether ROP2/6, CAND1, ILITHYIA and FER form a complex to regulate developmental processes within the plant, summarised in Figure 6.14.

The RIC affinity purification experiment was designed to determine any FER dependent interactions with RIC1 or RIC4. There were three proteins identified that were unique to Col-0 RIC1 all with links to cell growth; Plant invertase/pectin methylesterase inhibitor superfamily, RHS12, chitinase family protein. Plant invertase/pectin methylesterase inhibitor superfamily and chitinase family protein are both extracellular proteins and therefore are unlikely to be true RIC interactors. RHS12 is an exciting protein as it is an

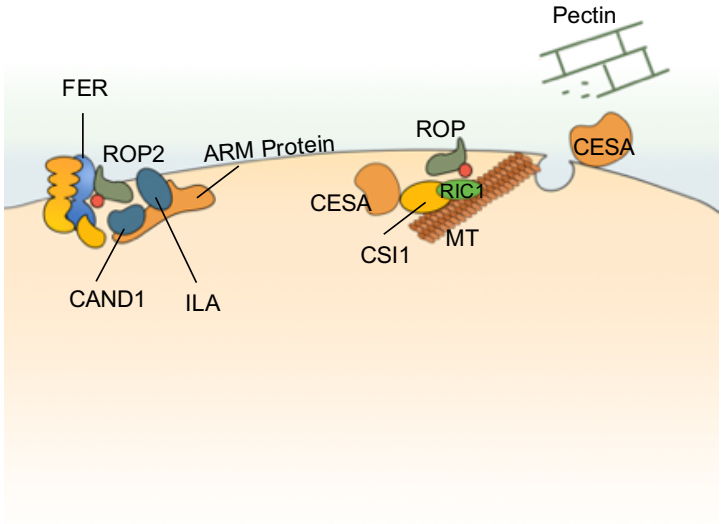

Figure 6.14: Schematic of ROP interactors.

RLK and therefore it would be an exciting protein to continue researching the link between RIC and RHS12. There were two proteins that were unique to Col-0 but seen in both RIC1 and RIC4; a Calcium-dependent phosphotriesterase superfamily protein (AT3G57020) and ROP2 (AT1G20090). The absence of ROP2 in the *fer-4* samples is really interesting, as it suggests that FER is essential for ROP2 activation and interaction with its effectors. We had hoped that the ROP activation assay would allow us to test whether FER is required for ROP2 activation but due to the limitations of the ROP activation assay this was not possible. In the future, to test this we would cross the ROP2-GFP line with the *fer-4* mutant line and repeat the affinity purification with RIC1-MBP and RIC4-MBP.

Chapter 7

Discussion

The overall aims of this research were to identify components of the Rapid Alkalinisation Factor 1 (RALF1) and FERONIA (FER) signalling pathway with particular focus on roots and the regulation of polar growth. We used three affinity purification techniques targeting different aspects of the pathway to decipher how FER plays such a pivotal role in development and immunity.

The purification of biologically active RALF1 was not achieved but synthetic RALF1 was shown to trigger MAPK activity as describe by Pearce et al., (2001). Without purified RALF1 we did not have the quantities to do root growth assays in various mutants, which had been our original plan. We decided to instead focus on the biochemistry of RALF1-FER signalling and attempted to identify mechanisms by which FER transmits the extracellular RALF1 signal to intracellular cell changes.

RALF1 treatment was shown to lead to MAPK activation and we demonstrated that this activity is lost in *fer-4*, indicating that FER is essential for

MAPK activation by RALF1. The FER CoIP identified a possible scaffold protein, RACK1B, for MAPKs (Cheng et al., 2015). RALF1 activation of MAPKs is very quick, 5 minutes compared to 15 minutes for PEP1 and flg22, and gene expression changes are observed at 30 minutes after treatment. RACK1B was only observed as part of the unelicited FER complex and we propose that RACK1B could act as scaffold for MAPKs, anchoring them in close proximity to FER prior to elicitation. Upon elicitation of FER, the RACK1B-MAPK scaffold dissociates from the RALF1-FER complex allowing the MAPK cascade to relocate.

The anti-pMAPK western blots from RALF1 elicitation showed activation of MAPK6 and MAPK3 but did not show activation of MAPK4. The anti-pERK antibody western blot used to observe MAPK activation corresponds to a TEY motif in MAPK6 as the top band, MAPK3 middle band and MAPK4 the bottom band (Nühse et al., 2000)(Zhang et al., 2018). This is interesting as MAPK4 is often associated with flg22, and therefore immune activated MAPK signalling (Berriri et al., 2012). MEKK1, MKK4/5, and MPK3/6 are the Arabidopsis MAPK kinase kinase (MAPKKK), MAPK kinases (MAPKKs), and MAPKs, respectively, that were proposed to constitute a MAPK-signalling cascade in the flg22/ FLS2 signalling pathway (Asai et al., 2002). We identified 44 phosphosites on MAPKs in our global phosphorylation study, including MAPK6. Although Y223 on MAPK6 was not one of the significant phosphosites, we did identify phosphorylation at Y223, which is part of the TE(pY) motif.

We observed multiple MAPKs phosphorylated in our global phosphorylation study, with MAPKKK7 and MAPKK1 showing increased phosphorylation in a RALF1 and FER dependent manner. We also identified MAPK6 in our

phosphopeptide enrichment but it did not show significant increases, possibly due to the Class I filtered phosphopeptide restriction: we do, however, observe a strong increase in MAPK6 on our western blots downstream of RALF1 treatment. From these findings we hypothesise that RACK1B acts as a scaffold for MAPKKK7, MAPKK1 and MAPK6/3, anchoring them in close proximity of FER to allow rapid activation of the MAPK cascade.

The root phenotype study of FER mutants with inactive or absent kinase domains, showed that the activity of kinase domain of FER is essential for correct root hair growth, suggesting that FER phosphorylates proteins that regulate root hair tip growth. From our proteomic experiments we identified several potential mechanisms of how FER links to cell growth. ROPs have been well documented in their spatially regulated localisation leading to polar growth in root hair initiation sites and pavement cells. Although we did not find a direct link between FER and ROPs in our FER-GFP CoIP, ROP-GFP CoIP or RIC-MBP affinity purification we did identify some common proteins. The ROP-GFP CoIPs contained large amounts of background and in retrospect we should have optimised the wash steps of the CoIP to enable a clearer idea of proteins that could have biological significance. The RIC-MBP affinity purifications could have been improved by having MBP bound to amylose beads and then comparing that to the RIC1-MBP bound beads, allowing for better statistical analysis of the results. An exciting point to highlight from the RIC-MBP affinity purification is that ROP2 interaction with RICs was lost in *fer-4,* suggesting that ROP2 activation is dependent on FER.

A paper by Huang et al., (2013) showed that ROPGEF4 is important in FER mediated developmental regulation of root hair growth. Here we provide an

insight into the mechanism of the regulation as we identified ROPGEF4 from our phosphoproteomics data, which showed increase phosphorylation in a RALF1 and FER dependent manner at site 27, strengthening the FER-ROP link as ROPGEF4 was shown to interact with ROP2 and ROP6 (Huang et al., 2013).

Another link to FER and root hair growth came from the identification of a proline-rich extensin-like receptor kinase, root hair specific 10 (RHS10). RHS10 is a cell wall-associated receptor-like kinase, which is a negative regulator of root hair growth that modulates the duration of root hair growth rather than the growth rate (Hwang et al., 2016). Our phosphopeptide data shows that RHS10 exhibits increased levels of phosphorylation at site 312 in a RALF1 and FER dependent manner.

The regulation of the cell wall plays a crucial role in cell growth and expansion, and our data suggests that FER plays an intrinsic role in the regulation of cell wall integrity. From the RIC-MBP affinity purification we identified another root hair specific protein, root hair specific 12 (RHS12), which is a pectin methyl-esterase (PME). PMEs are enzymes that demethylesterify a highly abundant type of pectin homogalacturonan, with a high spatiotemporal resolution (Wolf et al., 2009). RHS12 is a type-1 PME, which are cleaved by S1P as a prerequisite for their secretion to the apoplast (Wolf et al., 2009). S1P also cleaves RALF1 from its pre-propeptide (Stegmann et al., 2017). This suggests the presence of complex networks involving CrRLK1L/RALF signalling for the regulation of cell wall maintenance.

Strengthening the link with RALF1-FER and the cell wall further, we identified two cellulose synthase proteins that were differentially phosphorylated in our phosphoproteomics study. They showed different responses at specific

sites that had a different dependence of FER and RALF1. Six different phosphorylation sites were observed on CELLULOSE SYNTHASE 3, CESA3, with two being RALF1 and FER dependent and four being FER dependent but independent of RALF1. This is interesting as in our ROP-GFP CoIPs we identified Protein CELLULOSE SYNTHASE INTERACTIVE 1 (CSI1), which is known to be involved in trafficking cellulose synthase complexes to the plasma membrane along microtubules (Zhu et al., 2018). We also observed multiple phosphorylation sites on cellulose synthase-like D3, also known as ROOT HAIR DEFECTIVE 7 (RHD7). RHD7 mutants exhibit root hairs that burst at the tip (Favery et al., 2001).

We also identified root hair defective 4 (RHD4), a phosphatidylinositol-4-phosphate phosphatase, in the RALF1 elicited FER complex, which is required for normal root hair development. A mutation in *rhd4* causes root hairs to become short and bulged (Thole et al., 2008), which is a similar phenotype to root hairs seen in *fer-4*. RHD4 has been shown to be involved in coordinating delivery of cell wall materials and is selectively recruited to RABA4b labelled membranes (Thole et al., 2008). These findings, linking FER to proteins involved in cell wall synthesis and the trafficking of materials, could mean that FER plays a crucial role in the regulation of the cell wall structure.

We also identified several immune related proteins downstream of RALF1 and FER, including phosphorylation of RIN4 that is known to be downstream of RIPK, a known RALF1-FER interactor (Du et al., 2016). We also identified FER dependent phosphorylation of RBOHD at a site characterised to be downstream of flg22 and elf18 elicitation, along with 35 phosphosites related to defence proteins. Our FER-GFP CoIPs identified a

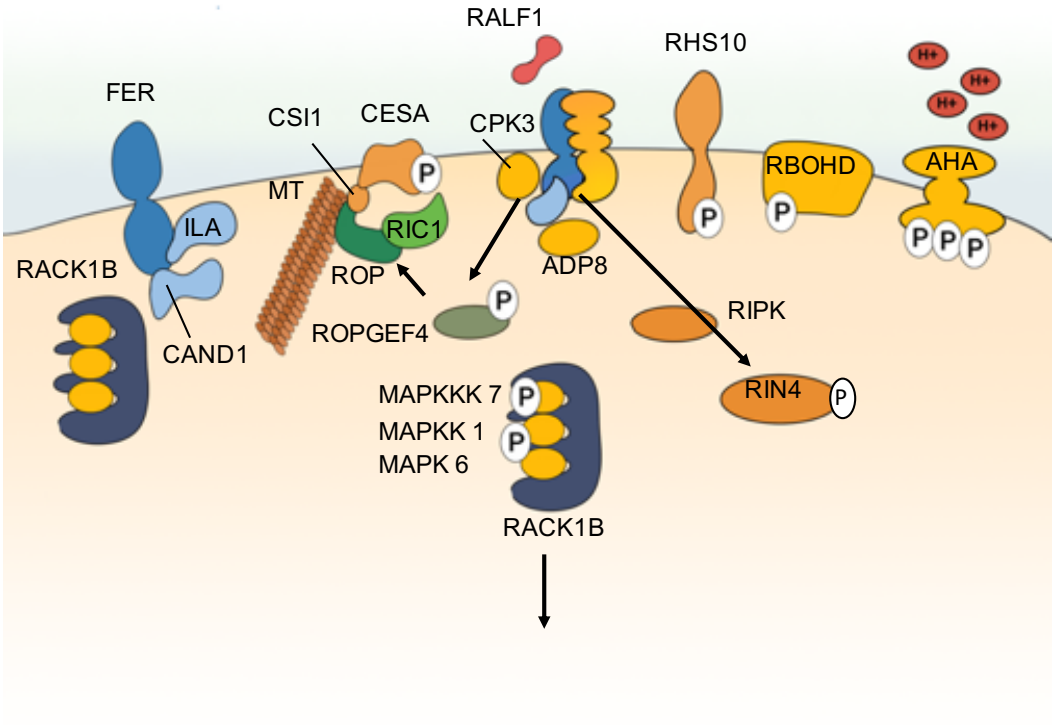

Figure 7.1: Schematic proposing a mechanism for new FER interactors and downstream targets.

possible FER interactor as IILITYHIA, a protein that functions in bacterial immunity (Monaghan and Li, 2010).

The links we have identified between immunity and development strengthen the hypothesis that FER acts as a key regulator of both immunity and growth. The key proteins of interest identified in our research are summarised into FER signalling pathways in Figure 7.1.

7.0.1 Conclusions and future work

During this research, we have identified several novel downstream phosphorylation target of RALF1-FER signalling from the global phosphoproteomic targets. To further decipher the phosphorylation sites on proteins of interest Class II and Class III phosphosites should be examined. We have also identified several potential candidates for FER interactors including the MAPK scaffold protein RACK1B. This interaction should be validated further by reciprocal IPs and/or BiFC studies in order to really show these proteins interact. It would also be beneficial to include MAPKKK7, MAPKK1 and MAPK6/3 in the reciprocal IPs to see whether they interact with RACK1B to test our hypothesis of RACK1B anchoring them in close proximity to FER. To determine whether FER is essential for the activation of ROP2, ROP2 should be crossed into *fer-4* to determine if ROP2 activation still occurs.

Chapter 8

Bibliography

Aebersold, R. and M. Mann (2003). "Mass spectrometry-based proteomics." Nature 422(6928): 198-207.

Ambrose, J. C. and G. O. Wasteneys (2008). "CLASP modulates microtubule-cortex interaction during self-organization of acentrosomal microtubules." Mol Biol Cell 19(11): 4730-4737.

Antolin-Llovera, M., M. K. Ried and M. Parniske (2014). "Cleavage of the SYMBIOSIS RECEPTOR-LIKE KINASE ectodomain promotes complex formation with Nod factor receptor 5." Curr Biol 24(4): 422-427.

Arioli, T., L. Peng, A. S. Betzner, J. Burn, W. Wittke, W. Herth, C. Camilleri, H. Hofte, J. Plazinski, R. Birch, A. Cork, J. Glover, J. Redmond and R. E. Williamson (1998). "Molecular analysis of cellulose biosynthesis in Arabidopsis." Science 279(5351): 717-720.

Asai, T., G. Tena, J. Plotnikova, M. R. Willmann, W. L. Chiu, L. Gomez-Gomez, T. Boller, F. M. Ausubel and J. Sheen (2002). "MAP kinase signalling cascade in Arabidopsis innate immunity." Nature 415(6875): 977-983.

Bai, L., X. Ma, G. Zhang, S. Song, Y. Zhou, L. Gao, Y. Miao and C. P. Song (2014). "A Receptor-Like Kinase Mediates Ammonium Homeostasis and Is Important for the Polar Growth of Root Hairs in Arabidopsis." Plant Cell 26(4): 1497-1511.

Bantscheff, M., S. Lemeer, M. M. Savitski and B. Kuster (2012). "Quantitative mass spectrometry in proteomics: critical review update from 2007 to the present." Anal Bioanal Chem 404(4): 939-965.

Bartels, S. and T. Boller (2015). "Quo vadis, Pep? Plant elicitor peptides at the crossroads of immunity, stress, and development." J Exp Bot 66(17): 5183-5193.

Bashline, L., S. Li, C. T. Anderson, L. Lei and Y. Gu (2013). "The endocytosis of cellulose synthase in Arabidopsis is dependent on mu2, a clathrin-mediated endocytosis adaptin." Plant Physiol 163(1): 150-160.

Benschop, J. J., S. Mohammed, M. O'Flaherty, A. J. Heck, M. Slijper and F. L. Menke (2007). "Quantitative phosphoproteomics of early elicitor signaling in Arabidopsis." Mol Cell Proteomics 6(7): 1198-1214.

Bergonci, T., B. Ribeiro, P. H. Ceciliato, J. C. Guerrero-Abad, M. C. Silva-Filho and D. S. Moura (2014). "Arabidopsis thaliana RALF1 opposes brassinosteroid effects on root cell elongation and lateral root formation." J Exp Bot 65(8): 2219-2230.

Berken, A. and A. Wittinghofer (2008). "Structure and function of Rho-type molecular switches in plants." Plant Physiol Biochem 46(3): 380-393.

Berriri, S., A. V. Garcia, N. Frei dit Frey, W. Rozhon, S. Pateyron, N. Leonhardt, J. L. Montillet, J. Leung, H. Hirt and J. Colcombet (2012). "Constitutively active mitogen-activated protein kinase versions reveal functions of Arabidopsis MPK4 in pathogen defense signaling." Plant Cell 24(10): 4281-4293.

Blilou, I., J. Xu, M. Wildwater, V. Willemsen, I. Paponov, J. Friml, R. Heidstra, M. Aida, K. Palme and B. Scheres (2005). "The PIN auxin efflux facilitator network controls growth and patterning in Arabidopsis roots." Nature 433(7021): 39-44.

Bloch, D. and S. Yalovsky (2013). "Cell polarity signaling." Curr Opin Plant Biol 16(6): 734-742.

Boisson-Dernier, A., S. A. Kessler and U. Grossniklaus (2011). "The walls have ears: the role of plant CrRLK1Ls in sensing and transducing extracellular signals." J Exp Bot 62(5): 1581-1591.

Bosch, M. and P. K. Hepler (2005). "Pectin methylesterases and pectin dynamics in pollen tubes." Plant Cell 17(12): 3219-3226.

Boulter, E., R. Garcia-Mata, C. Guilluy, A. Dubash, G. Rossi, P. J. Brennwald and K. Burridge (2010). "Regulation of Rho GTPase crosstalk, degradation and activity by RhoGDI1." Nat Cell Biol 12(5): 477-483.

Carol, R. J. and L. Dolan (2002). "Building a hair: tip growth in Arabidopsis thaliana root hairs." Philos Trans R Soc Lond B Biol Sci 357(1422): 815-821.

Carol, R. J., S. Takeda, P. Linstead, M. C. Durrant, H. Kakesova, P. Derbyshire, S. Drea, V. Zarsky and L. Dolan (2005). "A RhoGDP dissociation inhibitor spatially regulates growth in root hair cells." Nature 438(7070): 1013-1016.

Champion, A., M. Kreis, K. Mockaitis, A. Picaud and Y. Henry (2004). "Arabidopsis kinome: after the casting." Funct Integr Genomics 4(3): 163-187.

Chen, J., F. Wang, S. Zheng, T. Xu and Z. Yang (2015). "Pavement cells: a model system for non-transcriptional auxin signalling and crosstalks." J Exp Bot 66(16): 4957-4970.

Chen, J., F. Yu, Y. Liu, C. Du, X. Li, S. Zhu, X. Wang, W. Lan, P. L.

Rodriguez, X. Liu, D. Li, L. Chen and S. Luan (2016). "FERONIA interacts with ABI2-type phosphatases to facilitate signaling cross-talk between abscisic acid and RALF peptide in Arabidopsis." Proc Natl Acad Sci U S A 113(37): E5519-5527.

Cheng, Z., J. F. Li, Y. Niu, X. C. Zhang, O. Z. Woody, Y. Xiong, S. Djonovic, Y. Millet, J. Bush, B. J. McConkey, J. Sheen and F. M. Ausubel (2015). "Pathogen-secreted proteases activate a novel plant immune pathway." Nature 521(7551): 213-216.

Chinchilla, D., C. Zipfel, S. Robatzek, B. Kemmerling, T. Nurnberger, J. D. Jones, G. Felix and T. Boller (2007). "A flagellin-induced complex of the receptor FLS2 and BAK1 initiates plant defence." Nature 448(7152): 497-500.

Choi, Y., Y. Lee, S. Y. Kim, Y. Lee and J. U. Hwang (2013). "Arabidopsis ROP-interactive CRIB motif-containing protein 1 (RIC1) positively regulates auxin signalling and negatively regulates abscisic acid (ABA) signalling during root development." Plant Cell Environ 36(5): 945-955.

Chuang, T. H. and R. J. Ulevitch (2004). "Triad3A, an E3 ubiquitin-protein ligase regulating Toll-like receptors." Nat Immunol 5(5): 495-502.

Combier, J. P., H. Kuster, E. P. Journet, N. Hohnjec, P. Gamas and A. Niebel (2008). "Evidence for the involvement in nodulation of the two small putative regulatory peptide-encoding genes MtRALFL1 and MtDVL1." Mol Plant Microbe Interact 21(8): 1118-1127.

Cosgrove, D. J. (2005). "Growth of the plant cell wall." Nat Rev Mol Cell Biol 6(11): 850-861.

Covey, P. A., C. C. Subbaiah, R. L. Parsons, G. Pearce, F. T. Lay, M. A. Anderson, C. A. Ryan and P. A. Bedinger (2010). "A pollen-specific RALF from tomato that regulates pollen tube elongation." Plant Physiol 153(2):

703-715.

Cox, J., M. Y. Hein, C. A. Luber, I. Paron, N. Nagaraj and M. Mann (2014). "Accurate proteome-wide label-free quantification by delayed normalization and maximal peptide ratio extraction, termed MaxLFQ." Mol Cell Proteomics 13(9): 2513-2526.

Cox, J., N. Neuhauser, A. Michalski, R. A. Scheltema, J. V. Olsen and M. Mann (2011). "Andromeda: a peptide search engine integrated into the MaxQuant environment." J Proteome Res 10(4): 1794-1805.

Dardick, C. and P. Ronald (2006). "Plant and animal pathogen recognition receptors signal through non-RD kinases." PLoS Pathog 2(1): e2.

Dawson, C. J. and J. Hilton (2011). "Fertiliser availability in a resource-limited world: Production and recycling of nitrogen and phosphorus." Food Policy 36: S14-S22.

Deslauriers, S. D. and P. B. Larsen (2010). "FERONIA is a key modulator of brassinosteroid and ethylene responsiveness in Arabidopsis hypocotyls." Mol Plant 3(3): 626-640.

Doerner, P. (2008). "Plant roots: recycled auxin energizes patterning and growth." Curr Biol 18(2): R72-74.

Dolan, L., C. M. Duckett, C. Grierson, P. Linstead, K. Schneider, E. Lawson, C. Dean, S. Poethig and K. Roberts (1994

). "Clonal relationships and cell patterning in the root epidermis of Arabidopsis."

Du, C., X. Li, J. Chen, W. Chen, B. Li, C. Li, L. Wang, J. Li, X. Zhao, J. Lin, X. Liu, S. Luan and F. Yu (2016). "Receptor kinase complex transmits RALF peptide signal to inhibit root growth in Arabidopsis." Proc Natl Acad Sci U S A 113(51): E8326-E8334.

Duan, Q., D. Kita, E. A. Johnson, M. Aggarwal, L. Gates, H. M. Wu and

A. Y. Cheung (2014). "Reactive oxygen species mediate pollen tube rupture to release sperm for fertilization in Arabidopsis." Nat Commun 5: 3129.

Duan, Q., D. Kita, C. Li, A. Y. Cheung and H. M. Wu (2010). "FERONIA receptor-like kinase regulates RHO GTPase signaling of root hair development." Proc Natl Acad Sci U S A 107(41): 17821-17826.

Escobar-Restrepo, J. M., N. Huck, S. Kessler, V. Gagliardini, J. Gheyselinck, W. C. Yang and U. Grossniklaus (2007). "The FERONIA receptor-like kinase mediates male-female interactions during pollen tube reception." Science 317(5838): 656-660.

Faus, I., R. Ninoles, V. Kesari, P. Llabata, E. Tam, S. G. Nebauer, J. Santiago, M. T. Hauser and J. Gadea (2018). "Arabidopsis ILITHYIA protein is necessary for proper chloroplast biogenesis and root development independent of eIF2alpha phosphorylation." J Plant Physiol 224-225: 173-182.

Favery, B., E. Ryan, J. Foreman, P. Linstead, K. Boudonck, M. Steer, P. Shaw and L. Dolan (2001). "KOJAK encodes a cellulose synthase-like protein required for root hair cell morphogenesis in Arabidopsis." Genes Dev 15(1): 79-89.

Feng, S., Y. Shen, J. A. Sullivan, V. Rubio, Y. Xiong, T. P. Sun and X. W. Deng (2004). "Arabidopsis CAND1, an unmodified CUL1-interacting protein, is involved in multiple developmental pathways controlled by ubiquitin/proteasome-mediated protein Degradation." Plant Cell 16(7): 1870-1882.

Feng, W., D. Kita, A. Peaucelle, H. N. Cartwright, V. Doan, Q. Duan, M. C. Liu, J. Maman, L. Steinhorst, I. Schmitz-Thom, R. Yvon, J. Kudla, H. M. Wu, A. Y. Cheung and J. R. Dinneny (2018). "The FERONIA Receptor Kinase Maintains Cell-Wall Integrity during Salt Stress through Ca(2+) Signaling." Curr Biol 28(5): 666-675 e665.

Fischer, U., Y. Ikeda, K. Ljung, O. Serralbo, M. Singh, R. Heidstra, K.

Palme, B. Scheres and M. Grebe (2006). "Vectorial information for Arabidopsis planar polarity is mediated by combined AUX1, EIN2, and GNOM activity." Curr Biol 16(21): 2143-2149.

Foreman, J., V. Demidchik, J. H. Bothwell, P. Mylona, H. Miedema, M. A. Torres, P. Linstead, S. Costa, C. Brownlee, J. D. Jones, J. M. Davies and L. Dolan (2003). "Reactive oxygen species produced by NADPH oxidase regulate plant cell growth." Nature 422(6930): 442-446.

Frese, C. K., A. F. Altelaar, M. L. Hennrich, D. Nolting, M. Zeller, J. Griep-Raming, A. J. Heck and S. Mohammed (2011). "Improved peptide identification by targeted fragmentation using CID, HCD and ETD on an LTQ-Orbitrap Velos." J Proteome Res 10(5): 2377-2388.

Fritzsche, R., C. H. Ihling, M. Gotze and A. Sinz (2012). "Optimizing the enrichment of cross-linked products for mass spectrometric protein analysis." Rapid Commun Mass Spectrom 26(6): 653-658.

Fu, Y., Y. Gu, Z. Zheng, G. Wasteneys and Z. Yang (2005). "Arabidopsis interdigitating cell growth requires two antagonistic pathways with opposing action on cell morphogenesis." Cell 120(5): 687-700.

Fu, Y., H. Li and Z. Yang (2002). "The ROP2 GTPase controls the formation of cortical fine F-actin and the early phase of directional cell expansion during Arabidopsis organogenesis." Plant Cell 14(4): 777-794.

Fu, Y., T. Xu, L. Zhu, M. Wen and Z. Yang (2009). "A ROP GTPase signaling pathway controls cortical microtubule ordering and cell expansion in Arabidopsis." Curr Biol 19(21): 1827-1832.

Gachomo, E. W., L. Jno Baptiste, T. Kefela, W. M. Saidel and S. O. Kotchoni (2014). "The Arabidopsis CURVY1 (CVY1) gene encoding a novel receptor-like protein kinase regulates cell morphogenesis, flowering time and seed production." BMC Plant Biol 14: 221.

Gao, X. and P. He (2013). "Nuclear dynamics of Arabidopsis calcium-dependent protein kinases in effector-triggered immunity." Plant Signal Behav 8(4): e23868.

Gao, Y., Y. Zhang, D. Zhang, X. Dai, M. Estelle and Y. Zhao (2015). "Auxin binding protein 1 (ABP1) is not required for either auxin signaling or Arabidopsis development." Proc Natl Acad Sci U S A 112(7): 2275-2280.

Gomez-Gomez, L. and T. Boller (2000). "FLS2: an LRR receptor-like kinase involved in the perception of the bacterial elicitor flagellin in Arabidopsis." Mol Cell 5(6): 1003-1011.

Grebe, M., J. Friml, R. Swarup, K. Ljung, G. Sandberg, M. Terlou, K. Palme, M. J. Bennett and B. Scheres (2002). "Cell polarity signaling in Arabidopsis involves a BFA-sensitive auxin influx pathway." Curr Biol 12(4): 329-334.

Grieneisen, V. A., J. Xu, A. F. Maree, P. Hogeweg and B. Scheres (2007). "Auxin transport is sufficient to generate a maximum and gradient guiding root growth." Nature 449(7165): 1008-1013.

Grierson, C., E. Nielsen, T. Ketelaarc and J. Schiefelbein (2014). "Root hairs." Arabidopsis Book 12: e0172.

Gu, Y., V. Vernoud, Y. Fu and Z. Yang (2003). "ROP GTPase regulation of pollen tube growth through the dynamics of tip-localized F-actin." J Exp Bot 54(380): 93-101.

Guo, H., L. Li, H. Ye, X. Yu, A. Algreen and Y. Yin (2009). "Three related receptor-like kinases are required for optimal cell elongation in Arabidopsis thaliana." Proc Natl Acad Sci U S A 106(18): 7648-7653.

Haruta, M., G. Sabat, K. Stecker, B. B. Minkoff and M. R. Sussman (2014). "A peptide hormone and its receptor protein kinase regulate plant cell expansion." Science 343(6169): 408-411.

Heese, A., D. R. Hann, S. Gimenez-Ibanez, A. M. Jones, K. He, J. Li, J. I. Schroeder, S. C. Peck and J. P. Rathjen (2007). "The receptor-like kinase SERK3/BAK1 is a central regulator of innate immunity in plants." Proc Natl Acad Sci U S A 104(29): 12217-12222.

Hematy, K. and H. Hofte (2008). "Novel receptor kinases involved in growth regulation." Curr Opin Plant Biol 11(3): 321-328.

Hematy, K., P. E. Sado, A. Van Tuinen, S. Rochange, T. Desnos, S. Balzergue, S. Pelletier, J. P. Renou and H. Hofte (2007). "A receptor-like kinase mediates the response of Arabidopsis cells to the inhibition of cellulose synthesis." Curr Biol 17(11): 922-931.

Hunt, D. F., J. R. Yates, 3rd, J. Shabanowitz, S. Winston and C. R. Hauer (1986). "Protein sequencing by tandem mass spectrometry." Proc Natl Acad Sci U S A 83(17): 6233-6237.

Hwang, Y., H. Lee, Y. S. Lee and H. T. Cho (2016). "Cell wall-associated ROOT HAIR SPECIFIC 10, a proline-rich receptor-like kinase, is a negative modulator of Arabidopsis root hair growth." J Exp Bot 67(6): 2007-2022.

Johnson, L. N., M. E. Noble and D. J. Owen (1996). "Active and inactive protein kinases: structural basis for regulation." Cell 85(2): 149-158.

Jones, M. A., J. J. Shen, Y. Fu, H. Li, Z. Yang and C. S. Grierson (2002). "The Arabidopsis Rop2 GTPase is a positive regulator of both root hair initiation and tip growth." Plant Cell 14(4): 763-776.

Kadota, Y., J. Sklenar, P. Derbyshire, L. Stransfeld, S. Asai, V. Ntoukakis, J. D. Jones, K. Shirasu, F. Menke, A. Jones and C. Zipfel (2014). "Direct regulation of the NADPH oxidase RBOHD by the PRR-associated kinase BIK1 during plant immunity." Mol Cell 54(1): 43-55.

Kanaoka, M. M. and K. U. Torii (2010). "FERONIA as an upstream receptor kinase for polar cell growth in plants." Proc Natl Acad Sci U S A

107(41): 17461-17462.

Keinath, N. F., S. Kierszniowska, J. Lorek, G. Bourdais, S. A. Kessler, H. Shimosato-Asano, U. Grossniklaus, W. X. Schulze, S. Robatzek and R. Panstruga (2010). "PAMP (pathogen-associated molecular pattern)-induced changes in plasma membrane compartmentalization reveal novel components of plant immunity." J Biol Chem 285(50): 39140-39149.

Kessler, S. A., H. Shimosato-Asano, N. F. Keinath, S. E. Wuest, G. Ingram, R. Panstruga and U. Grossniklaus (2010). "Conserved molecular components for pollen tube reception and fungal invasion." Science 330(6006): 968-971.

Ketelaar, T., N. C. de Ruijter and A. M. Emons (2003). "Unstable F-actin specifies the area and microtubule direction of cell expansion in Arabidopsis root hairs." Plant Cell 15(1): 285-292.

Klepikova, A. V., A. S. Kasianov, E. S. Gerasimov, M. D. Logacheva and A. A. Penin (2016). "A high resolution map of the Arabidopsis thaliana developmental transcriptome based on RNA-seq profiling." Plant J 88(6): 1058-1070.

Kuppusamy, K. T., A. Y. Chen and J. L. Nemhauser (2009). "Steroids are required for epidermal cell fate establishment in Arabidopsis roots." Proc Natl Acad Sci U S A 106(19): 8073-8076.

Larsen, M. R., T. E. Thingholm, O. N. Jensen, P. Roepstorff and T. J. Jorgensen (2005). "Highly selective enrichment of phosphorylated peptides from peptide mixtures using titanium dioxide microcolumns." Mol Cell Proteomics 4(7): 873-886.

Lavy, M., D. Bloch, O. Hazak, I. Gutman, L. Poraty, N. Sorek, H. Sternberg and S. Yalovsky (2007). "A Novel ROP/RAC effector links cell polarity, root-meristem maintenance, and vesicle trafficking." Curr Biol 17(11): 947-

952.

Li, C., F. L. Yeh, A. Y. Cheung, Q. Duan, D. Kita, M. C. Liu, J. Maman, E. J. Luu, B. W. Wu, L. Gates, M. Jalal, A. Kwong, H. Carpenter and H. M. Wu (2015). "Glycosylphosphatidylinositol-anchored proteins as chaperones and co-receptors for FERONIA receptor kinase signaling in Arabidopsis." Elife 4.

Li, H., Y. Lin, R. M. Heath, M. X. Zhu and Z. Yang (1999). "Control of pollen tube tip growth by a Rop GTPase-dependent pathway that leads to tip-localized calcium influx." Plant Cell 11(9): 1731-1742.

Li, S., L. Lei, C. R. Somerville and Y. Gu (2012). "Cellulose synthase interactive protein 1 (CSI1) links microtubules and cellulose synthase complexes." Proc Natl Acad Sci U S A 109(1): 185-190.

Li, S. and Y. Zhang (2014). "To grow or not to grow: FERONIA has her say." Mol Plant 7(8): 1261-1263.

Li, Z., Y. Takahashi, A. Scavo, B. Brandt, D. Nguyen, P. Rieu and J. I. Schroeder (2018). "Abscisic acid-induced degradation of Arabidopsis guanine nucleotide exchange factor requires calcium-dependent protein kinases." Proc Natl Acad Sci U S A 115(19): E4522-E4531.

Lin, D., L. Cao, Z. Zhou, L. Zhu, D. Ehrhardt, Z. Yang and Y. Fu (2013). "Rho GTPase signaling activates microtubule severing to promote microtubule ordering in Arabidopsis." Curr Biol 23(4): 290-297.

Lin, D., S. Nagawa, J. Chen, L. Cao, X. Chen, T. Xu, H. Li, P. Dhonukshe, C. Yamamuro, J. Friml, B. Scheres, Y. Fu and Z. Yang (2012). "A ROP GTPase-dependent auxin signaling pathway regulates the subcellular distribution of PIN2 in Arabidopsis roots." Curr Biol 22(14): 1319-1325.

Lin, W., B. Li, D. Lu, S. Chen, N. Zhu, P. He and L. Shan (2014). "Tyrosine phosphorylation of protein kinase complex BAK1/BIK1 mediates Arabidop-

sis innate immunity." Proc Natl Acad Sci U S A 111(9): 3632-3637.

Lin, W., W. Tang, C. Anderson and Z. Yang (2018). "FERONIA's sensing of cell wall pectin activates ROP GTPase signaling in Arabidopsis." bioRxiv.

Liu, J., J. M. Elmore, A. T. Fuglsang, M. G. Palmgren, B. J. Staskawicz and G. Coaker (2009). "RIN4 functions with plasma membrane H+-ATPases to regulate stomatal apertures during pathogen attack." PLoS Biol 7(6): e1000139.

Liu, J., J. M. Elmore, Z. J. Lin and G. Coaker (2011). "A receptor-like cytoplasmic kinase phosphorylates the host target RIN4, leading to the activation of a plant innate immune receptor." Cell Host Microbe 9(2): 137-146.

Liu, J. X., R. Srivastava, P. Che and S. H. Howell (2007). "Salt stress responses in Arabidopsis utilize a signal transduction pathway related to endoplasmic reticulum stress signaling." Plant J 51(5): 897-909.

Makarov, A., E. Denisov, O. Lange and S. Horning (2006). "Dynamic range of mass accuracy in LTQ Orbitrap hybrid mass spectrometer." J Am Soc Mass Spectrom 17(7): 977-982.

Mao, D., F. Yu, J. Li, B. Van de Poel, D. Tan, J. Li, Y. Liu, X. Li, M. Dong, L. Chen, D. Li and S. Luan (2015). "FERONIA receptor kinase interacts with S-adenosylmethionine synthetase and suppresses S-adenosylmethionine production and ethylene biosynthesis in Arabidopsis." Plant Cell Environ 38(12): 2566-2574.

Masucci, J. D. and J. W. Schiefelbein (1996). "Hormones act downstream of TTG and GL2 to promote root hair outgrowth during epidermis development in the Arabidopsis root." Plant Cell 8(9): 1505-1517.

McCann, M. C. and N. C. Carpita (2008). "Designing the deconstruction of plant cell walls." Curr Opin Plant Biol 11(3): 314-320.

Mingossi, F. B., J. L. Matos, A. P. Rizzato, A. H. Medeiros, M. C. Falco,

M. C. Silva-Filho and D. S. Moura (2010). "SacRALF1, a peptide signal from the grass sugarcane (Saccharum spp.), is potentially involved in the regulation of tissue expansion." Plant Mol Biol 73(3): 271-281.

Miyawaki, K. N. and Z. Yang (2014). "Extracellular signals and receptor-like kinases regulating ROP GTPases in plants." Front Plant Sci 5: 449.

Molendijk, A. J., F. Bischoff, C. S. Rajendrakumar, J. Friml, M. Braun, S. Gilroy and K. Palme (2001). "Arabidopsis thaliana Rop GTPases are localized to tips of root hairs and control polar growth." EMBO J 20(11): 2779-2788.

Monaghan, J. and X. Li (2010). "The HEAT repeat protein ILITYHIA is required for plant immunity." Plant Cell Physiol 51(5): 742-753.

Monshausen, G. B., T. N. Bibikova, M. A. Messerli, C. Shi and S. Gilroy (2007). "Oscillations in extracellular pH and reactive oxygen species modulate tip growth of Arabidopsis root hairs." Proc Natl Acad Sci U S A 104(52): 20996-21001.

Moon, S. Y. and Y. Zheng (2003). "Rho GTPase-activating proteins in cell regulation." Trends Cell Biol 13(1): 13-22.

Morato do Canto, A., P. H. Ceciliato, B. Ribeiro, F. A. Ortiz Morea, A. A. Franco Garcia, M. C. Silva-Filho and D. S. Moura (2014). "Biological activity of nine recombinant AtRALF peptides: implications for their perception and function in Arabidopsis." Plant Physiol Biochem 75: 45-54.

Murphy, E. and I. De Smet (2014). "Understanding the RALF family: a tale of many species." Trends Plant Sci 19(10): 664-671.

Nan, Q., D. Qian, Y. Niu, Y. He, S. Tong, Z. Niu, J. Ma, Y. Yang, L. An, D. Wan and Y. Xiang (2017). "Plant Actin-Depolymerizing Factors Possess Opposing Biochemical Properties Arising from Key Amino Acid Changes throughout Evolution." Plant Cell 29(2): 395-408.

Nibau, C. and A. Y. Cheung (2011). "New insights into the functional roles of CrRLKs in the control of plant cell growth and development." Plant Signal Behav 6(5): 655-659.

Nuhse, T. S., A. R. Bottrill, A. M. Jones and S. C. Peck (2007). "Quantitative phosphoproteomic analysis of plasma membrane proteins reveals regulatory mechanisms of plant innate immune responses." Plant J 51(5): 931-940.

Nuhse, T. S., S. C. Peck, H. Hirt and T. Boller (2000). "Microbial elicitors induce activation and dual phosphorylation of the Arabidopsis thaliana MAPK 6." J Biol Chem 275(11): 7521-7526.

Nuhse, T. S., A. Stensballe, O. N. Jensen and S. C. Peck (2004). "Phosphoproteomics of the Arabidopsis plasma membrane and a new phosphorylation site database." Plant Cell 16(9): 2394-2405.

Olsen, J. V. and M. Mann (2004). "Improved peptide identification in proteomics by two consecutive stages of mass spectrometric fragmentation." Proc Natl Acad Sci U S A 101(37): 13417-13422.

Pearce, G., D. S. Moura, J. Stratmann and C. A. Ryan, Jr. (2001). "RALF, a 5-kDa ubiquitous polypeptide in plants, arrests root growth and development." Proc Natl Acad Sci U S A 98(22): 12843-12847.

Pearce, G., Y. Yamaguchi, G. Munske and C. A. Ryan (2010). "Structure-activity studies of RALF, Rapid Alkalinization Factor, reveal an essential--YISY--motif." Peptides 31(11): 1973-1977.

Perkins, D. N., D. J. Pappin, D. M. Creasy and J. S. Cottrell (1999). "Probability-based protein identification by searching sequence databases using mass spectrometry data." Electrophoresis 20(18): 3551-3567.

Pursiheimo, A., A. P. Vehmas, S. Afzal, T. Suomi, T. Chand, L. Strauss, M. Poutanen, A. Rokka, G. L. Corthals and L. L. Elo (2015). "Optimization of Statistical Methods Impact on Quantitative Proteomics Data." J Proteome

Res 14(10): 4118-4126.

Richmond, T. (2000). "Higher plant cellulose synthases." Genome Biol 1(4): REVIEWS3001.

Roux, M., B. Schwessinger, C. Albrecht, D. Chinchilla, A. Jones, N. Holton, F. G. Malinovsky, M. Tor, S. de Vries and C. Zipfel (2011). "The Arabidopsis leucine-rich repeat receptor-like kinases BAK1/SERK3 and BKK1/SERK4 are required for innate immunity to hemibiotrophic and biotrophic pathogens." Plant Cell 23(6): 2440-2455.

Schiefelbein, J. W. and C. Somerville (1990). "Genetic Control of Root Hair Development in Arabidopsis thaliana." Plant Cell 2(3): 235-243.

Schippers, J. H., H. M. Nguyen, D. Lu, R. Schmidt and B. Mueller-Roeber (2012). "ROS homeostasis during development: an evolutionary conserved strategy." Cell Mol Life Sci 69(19): 3245-3257.

Schoenaers, S., D. Balcerowicz, G. Breen, K. Hill, M. Zdanio, G. Mouille, T. J. Holman, J. Oh, M. H. Wilson, N. Nikonorova, L. D. Vu, I. De Smet, R. Swarup, W. H. De Vos, I. Pintelon, D. Adriaensen, C. Grierson, M. J. Bennett and K. Vissenberg (2018). "The Auxin-Regulated CrRLK1L Kinase ERULUS Controls Cell Wall Composition during Root Hair Tip Growth." Curr Biol 28(5): 722-732 e726.

Schulze-Muth, P., S. Irmler, G. Schroder and J. Schroder (1996). "Novel type of receptor-like protein kinase from a higher plant (Catharanthus roseus). cDNA, gene, intramolecular autophosphorylation, and identification of a threonine important for auto- and substrate phosphorylation." J Biol Chem 271(43): 26684-26689.

Shah, K., E. Russinova, T. W. Gadella, Jr., J. Willemse and S. C. De Vries (2002). "The Arabidopsis kinase-associated protein phosphatase controls internalization of the somatic embryogenesis receptor kinase 1." Genes Dev

16(13): 1707-1720.

Shih, H. W., N. D. Miller, C. Dai, E. P. Spalding and G. B. Monshausen (2014). "The receptor-like kinase FERONIA is required for mechanical signal transduction in Arabidopsis seedlings." Curr Biol 24(16): 1887-1892.

Shiu, S. H., W. M. Karlowski, R. Pan, Y. H. Tzeng, K. F. Mayer and W. H. Li (2004). "Comparative analysis of the receptor-like kinase family in Arabidopsis and rice." Plant Cell 16(5): 1220-1234.

Srivastava, R., J. X. Liu, H. Guo, Y. Yin and S. H. Howell (2009). "Regulation and processing of a plant peptide hormone, AtRALF23, in Arabidopsis." Plant J 59(6): 930-939.

Staskawicz, B. J., F. M. Ausubel, B. J. Baker, J. G. Ellis and J. D. Jones (1995). "Molecular genetics of plant disease resistance." Science 268(5211): 661-667.

Stegmann, M., J. Monaghan, E. Smakowska-Luzan, H. Rovenich, A. Lehner, N. Holton, Y. Belkhadir and C. Zipfel (2017). "The receptor kinase FER is a RALF-regulated scaffold controlling plant immune signaling." Science 355(6322): 287-289.

Takeda, S., C. Gapper, H. Kaya, E. Bell, K. Kuchitsu and L. Dolan (2008). "Local positive feedback regulation determines cell shape in root hair cells." Science 319(5867): 1241-1244.

Tao, L. Z., A. Y. Cheung and H. M. Wu (2002). "Plant Rac-like GTPases are activated by auxin and mediate auxin-responsive gene expression." Plant Cell 14(11): 2745-2760.

Thole, J. M., J. E. Vermeer, Y. Zhang, T. W. Gadella, Jr. and E. Nielsen (2008). "Root hair defective4 encodes a phosphatidylinositol-4-phosphate phosphatase required for proper root hair development in Arabidopsis thaliana." Plant Cell 20(2): 381-395.

Tyanova, S., T. Temu, P. Sinitcyn, A. Carlson, M. Y. Hein, T. Geiger, M. Mann and J. Cox (2016). "The Perseus computational platform for comprehensive analysis of (prote)omics data." Nat Methods 13(9): 731-740.

van Wijk, K. J., G. Friso, D. Walther and W. X. Schulze (2014). "Meta-Analysis of Arabidopsis thaliana Phospho-Proteomics Data Reveals Compartmentalization of Phosphorylation Motifs." Plant Cell 26(6): 2367-2389.

Verbelen, J. P., T. De Cnodder, J. Le, K. Vissenberg and F. Baluska (2006). "The Root Apex of Arabidopsis thaliana Consists of Four Distinct Zones of Growth Activities: Meristematic Zone, Transition Zone, Fast Elongation Zone and Growth Terminating Zone." Plant Signal Behav 1(6): 296-304.

Wolf, S., T. Rausch and S. Greiner (2009). "The N-terminal pro region mediates retention of unprocessed type-I PME in the Golgi apparatus." Plant J 58(3): 361-375.

Wu, G., Y. Gu, S. Li and Z. Yang (2001). "A genome-wide analysis of Arabidopsis Rop-interactive CRIB motif-containing proteins that act as Rop GTPase targets." Plant Cell 13(12): 2841-2856.

Wu, H. M., O. Hazak, A. Y. Cheung and S. Yalovsky (2011). "RAC/ROP GTPases and auxin signaling." Plant Cell 23(4): 1208-1218.

Xu, T. (2012). "Rho GTPase activity analysis in plant cells." Methods Mol Biol 876: 135-144.

Yang, Z. (2008). "Cell polarity signaling in Arabidopsis." Annu Rev Cell Dev Biol 24: 551-575.

Yeats, T. H., H. Sorek, D. E. Wemmer and C. R. Somerville (2016). "Cellulose Deficiency Is Enhanced on Hyper Accumulation of Sucrose by a H+-Coupled Sucrose Symporter." Plant Physiol 171(1): 110-124.

Yu, F., J. Li, Y. Huang, L. Liu, D. Li, L. Chen and S. Luan (2014). "FERONIA receptor kinase controls seed size in Arabidopsis thaliana." Mol Plant

7(5): 920-922.

Yu, F., L. Qian, C. Nibau, Q. Duan, D. Kita, K. Levasseur, X. Li, C. Lu, H. Li, C. Hou, L. Li, B. B. Buchanan, L. Chen, A. Y. Cheung, D. Li and S. Luan (2012). "FERONIA receptor kinase pathway suppresses abscisic acid signaling in Arabidopsis by activating ABI2 phosphatase." Proc Natl Acad Sci U S A 109(36): 14693-14698.

Zhang, M., Y. H. Chiang, T. Y. Toruno, D. Lee, M. Ma, X. Liang, N. K. Lal, M. Lemos, Y. J. Lu, S. Ma, J. Liu, B. Day, S. P. Dinesh-Kumar, K. Dehesh, D. Dou, J. M. Zhou and G. Coaker (2018). "The MAP4 Kinase SIK1 Ensures Robust Extracellular ROS Burst and Antibacterial Immunity in Plants." Cell Host Microbe 24(3): 379-391 e375.

Zhu, X., S. Li, S. Pan, X. Xin and Y. Gu (2018). "CSI1, PATROL1, and exocyst complex cooperate in delivery of cellulose synthase complexes to the plasma membrane." Proc Natl Acad Sci U S A 115(15): E3578-E3587.

Appendix

Supplementary Table S.1: FER-GFP CoIP significantly enriched proteins.

Accession	Name	Category	Sample
AT1G01800	NAD(NAD(P)-binding Rossmann-fold superfamily protein	Cell wall	Core
AT2G02560	CAND1	Cell wall	Core
AT4G20360	RabE1b	Cell wall	Core
AT5G19820	ARM repeat superfamily protein	Cell wall	Core
AT5G65270	RABA4a	Cell wall	Core
AT4G29350	PROFILIN 2	Cytoskeleton	Core
AT3G02260	BIG	Hormone	Core
AT1G64790	ILITYHIA	Immunity	Core
AT3G51550	FERONIA	Kinase	Core
AT1G70730	PHOSPHOGLUCOMUTASE 2	Metabolism	Core
AT2G40890	CYTOCHROME P450	Metabolism	Core
AT2G42790	CSY3	Metabolism	Core
AT3G16400	NSP1	Metabolism	Core
AT3G29410	TPS25	Metabolism	Core
AT3G53110	LOS4	Metabolism	Core
AT4G35830	ACONITASE 1	Metabolism	Core
AT5G43010	RPT4A	Proteasome	Core
AT3G02200	Proteasome component	Proteasome	Core

Accession	Name	Category	Sample
AT5G45620	26S proteasome non-ATPase regulatory subunit 13 homolog A	Proteasome	Core
AT5G23540	Mov34/MPN/PAD-1 family protein	Proteasome	Core
AT5G16070	TCP-1/cpn60 chaperonin family protein	Trafficking	Core
AT1G52760	CAFFEOYL SHIKIMATE ESTERASE	Trafficking	Core
AT2G46520	Exportin-2 (Exp2)	Trafficking	Core
AT3G56190	ALPHA-SNAP2	Trafficking	Core
AT4G04910	N-ETHYLMALEIMIDE SENSITIVE FACTOR	Trafficking	Core
AT5G63190	MRF1	Trafficking	Core
AT2G46280	TRIP1	Translation	Core
AT5G36230	ARM repeat superfamily protein	Translation	Core
AT1G66200	GLUTAMINE SYNTHETASE 1;2	Potential contaminant	Core
AT2G04030	HSP88.1	Potential contaminant	Core
AT3G07770	HSP89.1	Potential contaminant	Core
AT3G08943	ARM repeat superfamily protein	Potential contaminant	Core

Accession	Name	Category	Sample
AT3G10920	SUPEROXIDE DISMUTASE 1	Potential contaminant	Core
AT5G12470	RETICULATA-RELATED 4	Potential contaminant	Core
AT5G43780	APS4	Potential contaminant	Core
AT5G54810	TRYPTOPHAN SYNTHASE BETA-SUBUNIT 1	Potential contaminant	Core
ATMG00510	NADH DEHYDROGENASE SUBUNIT 7	Potential contaminant	Core
AT1G08360	60S ribosomal protein L10a-1	Potential contaminant	RALF1 Elicited
AT1G15500	ATNTT2	Potential contaminant	RALF1 Elicited
AT1G22840	CYTOCHROME C-1	Potential contaminant	RALF1 Elicited
AT1G24180	IAA-CONJUGATE-RESISTANT 4	Potential contaminant	RALF1 Elicited
AT1G53240	MITOCHONDRIAL MALATE DEHYDROGENASE 1	Potential contaminant	RALF1 Elicited
AT2G24200	AMINOPEPTIDASE 1	Potential contaminant	RALF1 Elicited

Accession	Name	Category	Sample
AT3G15660	GLUTAREDOXIN S15	Potential contaminant	RALF1 Elicited
AT3G22890	ATP SULFURYLASE 1	Potential contaminant	RALF1 Elicited
AT3G55440	TRIOSEPHOSPHATE ISOMERASE	Potential contaminant	RALF1 Elicited
AT4G09320	NUCLEOSIDE DIPHOSPHATE KINASE 1	Potential contaminant	RALF1 Elicited
AT4G23100	ROOT MERISTEMLESS 1	Potential contaminant	RALF1 Elicited
AT4G26300	EMBRYO DEFECTIVE 1027	Potential contaminant	RALF1 Elicited
AT4G29410	60S ribosomal protein L28-2	Potential contaminant	RALF1 Elicited
AT5G04590	SULFITE REDUCTASE	Potential contaminant	RALF1 Elicited
AT5G13420	TRANSALDOLASE 2	Potential contaminant	RALF1 Elicited
AT5G48110	TERPENE SYNTHASE 20	Potential contaminant	RALF1 Elicited
ATMG00480	ATP SYNTHASE 8	Potential contaminant	RALF1 Elicited
AT1G03220	Eukaryotic aspartyl protease family protein	Cell wall	RALF1 Elicited

Accession	Name	Category	Sample
AT1G21750	PDI-LIKE 1-1	Cell wall	RALF1 Elicited
AT4G16260	Probable glucan endo-1,3-beta-glucosidase	Cell wall	RALF1 Elicited
AT5G64100	Peroxidase 69	Cell wall	RALF1 Elicited
AT5G65430	GRF8	Cell wall	RALF1 Elicited
AT2G30870	GSTF10	Cell wall	RALF1 Elicited
AT3G51460	RHD4	Cell wall	RALF1 Elicited
AT1G20450	ERD10	Cytoskeleton	RALF1 Elicited
AT5G59880	ADF3	Cytoskeleton	RALF1 Elicited
AT1G16890	UBIQUITIN-CONJUGATING ENZYME 36	degradation	RALF1 Elicited
AT5G15970	KIN2	Hormone	RALF1 Elicited
AT1G70850	MLP-like protein 34	Immunity	RALF1 Elicited
AT1G78380	GSTU19	Immunity	RALF1 Elicited

Accession	Name	Category	Sample
AT2G01530	MLP-LIKE PROTEIN 329	Immunity	RALF1 Elicited
AT5G12140	CYS-1	Immunity	RALF1 Elicited
AT5G67500	VOLTAGE DEPENDENT ANION CHANNEL 2	Immunity	RALF1 Elicited
AT4G23650	CPK3	Kinase	RALF1 Elicited
AT5G63400	ADENYLATE KINASE 1	Kinase	RALF1 Elicited
AT5G63680	Pyruvate kinase	Kinase	RALF1 Elicited
AT2G29560	ENOLASE 3	Metabolism	RALF1 Elicited
AT3G12290	MTHFD1	Metabolism	RALF1 Elicited
AT3G16450	JACALIN-RELATED LECTIN 33	Metabolism	RALF1 Elicited
AT3G32980	Peroxidase (EC 1.11.1.7)	Metabolism	RALF1 Elicited
AT2G46140	LEA27	Metabolism	RALF1 Elicited
AT5G11670	NADP-ME2	Metabolism	RALF1 Elicited

Accession	Name	Category	Sample
AT1G17880	BASIC TRANSCRIPTION FACTOR 3	TF	RALF1 Elicited
AT2G16950	TRANSPORTIN-1	Trafficking	RALF1 Elicited
AT4G13770	REDUCED EPIDERMAL FLUORESCENCE 2	Trafficking	RALF1 Elicited
AT5G42890	STEROL CARRIER PROTEIN 2	Trafficking	RALF1 Elicited
AT3G57290	EUKARYOTIC TRANSLATION INITIATION FACTOR 3E	Translation	RALF1 Elicited
AT3G56150	eIF3c	Translation	RALF1 Elicited
AT2G39730	RUBISCO ACTIVASE	Potential contaminant	Unelicited
AT3G62530	ARM repeat superfamily protein	Potential contaminant	Unelicited
ATCG00120	ATP SYNTHASE SUBUNIT ALPHA	Potential contaminant	Unelicited
AT1G28290	ARABINOGALACTAN PROTEIN 31	Cell wall	Unelicited
AT1G48630	RACK1B	Kinase	Unelicited
AT4G09000	GRF1	Metabolism	Unelicited
AT4G15093	LIGB	Metabolism	Unelicited

Accession	Name	Category	Sample
AT1G29150	REGULATORY PARTICLE NON-ATPASE 6	Proteasome	Unelicited
AT3G42170	DAYSLEEPER	TF	Unelicited
AT3G63460	SEC31B	Trafficking	Unelicited
AT2G36290	Alpha/beta-Hydrolases superfamily protein	Trafficking	Unelicited
AT4G11420	eIF3a	Trafficking	Unelicited

Supplementary Table S.2: Phosphosites that are dependent on FERONIA and RALF1 treatment

Protein	Name	Phosphosites	Multiplicity	Function	Significant in
AT1G01050	pyrophosphorylase 1	24	1	Cell growth	Genotype and RALF1
AT1G01580	ferric reduction oxidase 2	639	2	Metabolism	Genotype and RALF1
AT1G01580	ferric reduction oxidase 2	641	1	Metabolism	Genotype and RALF1
AT1G04700	PB1 domain-containing protein tyrosine kinase	346	2	Kinase	Genotype and RALF1
AT1G04700	PB1 domain-containing protein tyrosine kinase	342	2	Kinase	Genotype and RALF1

Protein	Name	Phosphosites	Multiplicity	Function	Significant in
AT1G05500	Calcium-dependent lipid-binding (CaLB domain) family protein	424	2	Calcium	Genotype and RALF1
AT1G06210	ENTH/VHS/GAT family protein	377	2	Trafficking	Genotype and RALF1
AT1G06210	ENTH/VHS/GAT family protein	378	1	Trafficking	Genotype and RALF1
AT1G06410	trehalose-phosphatase/synthase 7	50	2	Metabolism	Genotype and RALF1
AT1G06840	Leucine-rich repeat protein kinase family protein	604	2	LRR	Genotype and RALF1
AT1G06840	Leucine-rich repeat protein kinase family protein	601	1	LRR	Genotype and RALF1
AT1G07110	fructose-2,6-bisphosphatase	276	1	Metabolism	Genotype and RALF1
AT1G07990	SIT4 phosphatase-associated family protein	515	1	Metabolism	Genotype and RALF1
AT1G08800	Unknown	834	1	Unknown	Genotype and RALF1

Protein	Name	Phosphosites	Multiplicity	Function	Significant in
AT1G08820	vamp/synaptobrevin-associated protein 27-2	128	1	Trafficking	Genotype and RALF1
AT1G09170	P-loop nucleoside triphosphate hydrolases superfamily protein with CH (Calponin Homology) domain	778	2	Cytoskeleton	Genotype and RALF1
AT1G10200	GATA type zinc finger transcription factor family protein	71	1	TF	Genotype and RALF1
AT1G11480	eukaryotic translation initiation factor-related	499	1	Metabolism	Genotype and RALF1
AT1G11700	Unknown	115	1	Unknown	Genotype and RALF1
AT1G13420	sulfotransferase 4B	291	1	Metabolism	Genotype and RALF1
AT1G13940	Plant protein of unknown function (DUF863)	716	1	Unknown	Genotype and RALF1
AT1G14380	IQ-domain 28	570	1	Trafficking	Genotype and RALF1

Protein	Name	Phosphosites	Multiplicity	Function	Significant in
AT1G16860	SHOU4L	105	2	Degradation	Genotype and RALF1
AT1G16860	SHOU4L		1	Degradation	Genotype and RALF1
AT1G16860	SHOU4L	76	2	Degradation	Genotype and RALF1
AT1G16860	SHOU4L	169	2	Degradation	Genotype and RALF1
AT1G16860	SHOU4L	174	1	Degradation	Genotype and RALF1
AT1G17500	ATPase E1-E2 type family protein / haloacid dehalogenase-like hydrolase family protein	1212	1	Trafficking	Genotype and RALF1
AT1G17840	white-brown complex homolog protein 11	688	1	Transport	Genotype and RALF1
AT1G18390	Protein kinase superfamily protein	295	1	Hormone	Genotype and RALF1
AT1G18420	Aluminium activated malate transporter family protein	474	1	Transport	Genotype and RALF1

Protein	Name	Phosphosites	Multiplicity	Function	Significant in
AT1G18700	DNAJ heat shock N-terminal domain-containing protein	692	1	Metabolism	Genotype and RALF1
AT1G19350	BRASSINAZOLE-RESISTANT 2	183	1	Hormone	Genotype and RALF1
AT1G19870	IQ-domain 32	65	1	Calcium	Genotype and RALF1
AT1G20440	cold-regulated 47	14	1	Defence	Genotype and RALF1
AT1G20450	Dehydrin family protein	14	1	Metabolism	Genotype and RALF1
AT1G21170	Exocyst complex component SEC5	35	2	Trafficking	Genotype and RALF1
AT1G22310	methyl-CPG-binding domain 8	103	2	Metabolism	Genotype and RALF1
AT1G25580	NAC (No Apical Meristem) domain transcriptional regulator superfamily protein	237	2	TF	Genotype and RALF1

Protein	Name	Phosphosites	Multiplicity	Function	Significant in
AT1G25580	NAC (No Apical Meristem) domain transcriptional regulator superfamily protein	244	1	TF	Genotype and RALF1
AT1G26630	eIF-5A 1	2	1	Defence	Genotype and RALF1
AT1G29370	Unknown	531	2	Kinase	Genotype and RALF1
AT1G31460	Unknown	84	2	Unknown	Genotype and RALF1
AT1G34220	Regulator of Vps4 activity in the MVB pathway protein	478	1	Trafficking	Genotype and RALF1
AT1G34260	FORMS APLOID AND BINUCLEATE CELLS 1A	59	1	Transport	Genotype and RALF1
AT1G43850	SEUSS transcriptional co-regulator	250	2	TF	Genotype and RALF1
AT1G45688	Unknown	20	1	Unknown	Genotype and RALF1

Protein	Name	Phosphosites	Multiplicity	Function	Significant in
AT1G50500	Membrane trafficking VPS53 family protein	380	1	Transport	Genotype and RALF1
AT1G51140	basic helix-loop-helix (bHLH) DNA-binding superfamily protein	213	1	Metabolism	Genotype and RALF1
AT1G51600	ZIM-LIKE 2; ZIM-LIKE 2	125	2	Cell growth	Genotype and RALF1
AT1G51830	Leucine-rich repeat protein kinase family protein	357	1	LRR	Genotype and RALF1
AT1G54920	Unknown	323	2	Unknown	Genotype and RALF1
AT1G60640	Unknown	208	1	Unknown	Genotype and RALF1
AT1G62390	Octicosapeptide/ Phox/ Bem1p (PB1) domain-containing protein / tetratricopeptide repeat (TPR)-containing protein	215	2	Metabolism	Genotype and RALF1

Protein	Name	Phosphosites	Multiplicity	Function	Significant in
AT1G68060	microtubule-associated proteins 70-1	435	1	Cytoskeleton	Genotype and RALF1
AT1G70460	RHS10	312	1	Kinase	Genotype and RALF1
AT1G71010	FORMS APLOID AND BINUCLEATE CELLS 1C	1184	1	Transport	Genotype and RALF1
AT1G72160	Sec14p-like phosphatidylinositol transfer family protein	108	2	Cytoskeleton	Genotype and RALF1
AT1G72410	COP1-interacting protein-related	624	2	Trafficking	Genotype and RALF1
AT1G74830	Unknown	226	1	Trafficking	Genotype and RALF1
AT1G76970	Target of Myb protein 1	291	2	Trafficking	Genotype and RALF1
AT1G79280	nuclear pore anchor	1911	1	Metabolism	Genotype and RALF1
AT1G79440	aldehyde dehydrogenase 5F1	459	1	Metabolism	Genotype and RALF1
AT1G80180	Unknown	98	1	Metabolism	Genotype and RALF1

Protein	Name	Phosphosites	Multiplicity	Function	Significant in
AT1G80180	Unknown	17	1	Metabolism	Genotype and RALF1
AT2G02010	glutamate decarboxylase 4	8	1	Metabolism	Genotype and RALF1
AT2G02080	indeterminate(ID)-domain 4	73	1	Cell growth	Genotype and RALF1
AT2G16405	Transducin/WD40 repeat-like superfamily protein	93	1	Metabolism	Genotype and RALF1
AT2G17420	NADPH-dependent thioredoxin reductase A	377	1	Metabolism	Genotype and RALF1
AT2G17550	Unknown	322	1	Unknown	Genotype and RALF1
AT2G18960	AHA1	904	1	Cell growth	Genotype and RALF1
AT2G19470	Casein kinase I-like 5	387	1	Metabolism	Genotype and RALF1
AT2G19710	IST1-LIKE 5	898	2	Trafficking	Genotype and RALF1
AT2G19710	IST1-LIKE 5	903	2	Trafficking	Genotype and RALF1

Protein	Name	Phosphosites	Multiplicity	Function	Significant in
AT2G19710	IST1-LIKE 5	680	2	Trafficking	Genotype and RALF1
AT2G19710	IST1-LIKE 5	682	2	Trafficking	Genotype and RALF1
AT2G20010	Unknown	61	2	Unknown	Genotype and RALF1
AT2G20010	Unknown	63	1	Unknown	Genotype and RALF1
AT2G20900	diacylglycerol kinase 5	445	1	Defence	Genotype and RALF1
AT2G20900	diacylglycerol kinase 5	446	2	Defence	Genotype and RALF1
AT2G21390	Coatomer, alpha subunit	824	1	Trafficking	Genotype and RALF1
AT2G22560	NETWORKED 2D	894	1	Kinase	Genotype and RALF1
AT2G22560	NETWORKED 2D	911	1	Kinase	Genotype and RALF1
AT2G22560	NETWORKED 2D	896	1	Kinase	Genotype and RALF1
AT2G25480	TPX2 (targeting protein for Xklp2) protein family	308	1	Cytoskeleton	Genotype and RALF1

Protein	Name	Phosphosites	Multiplicity	Function	Significant in
AT2G25520	Drug/metabolite transporter superfamily protein	325	2	Transport	Genotype and RALF1
AT2G26100	Galactosyltransferase family protein	18	2	Metabolism	Genotype and RALF1
AT2G26190	Calmodulin-binding family protein	509	2	Calcium	Genotype and RALF1
AT2G26190	Calmodulin-binding family protein	505	1	Calcium	Genotype and RALF1
AT2G26280	CTC-interacting domain 7	172	1	Metabolism	Genotype and RALF1
AT2G26410	IQ-domain 4	349	1	Trafficking	Genotype and RALF1
AT2G26570	Plant protein of unknown function (DUF827)	778	1	Unknown	Genotype and RALF1
AT2G27100	C2H2 zinc-finger protein SERRATE (SE)	299	1	Metabolism	Genotype and RALF1
AT2G28290	P-loop containing nucleoside triphosphate hydrolases superfamily protein	2070	2	Defence	Genotype and RALF1

Protein	Name	Phosphosites	Multiplicity	Function	Significant in
AT2G30930	Unknown	94	2	Unknown	Genotype and RALF1
AT2G31370	Basic-leucine zipper (bZIP) transcription factor family protein	160	1	TF	Genotype and RALF1
AT2G34680	Outer arm dynein light chain 1 protein	218	2	Cytoskeleton	Genotype and RALF1
AT2G34680	Outer arm dynein light chain 1 protein		1	Cytoskeleton	Genotype and RALF1
AT2G34680	Outer arm dynein light chain 1 protein	213	1	Cytoskeleton	Genotype and RALF1
AT2G34970	Trimeric LpxA-like enzyme	522	2	Metabolism	Genotype and RALF1
AT2G34970	Trimeric LpxA-like enzyme	526	2	Metabolism	Genotype and RALF1
AT2G35230	VQ motif-containing protein	65	1	Cell growth	Genotype and RALF1
AT2G38670	PECT1	217	1	Metabolism	Genotype and RALF1
AT2G39200	Seven transmembrane MLO family protein	501	2	Defence	Genotype and RALF1

Protein	Name	Phosphosites	Multiplicity	Function	Significant in
AT2G39200	Seven transmembrane MLO family protein	503	1	Defence	Genotype and RALF1
AT2G39805	Integral membrane Yip1 family protein	62	1	Transport	Genotype and RALF1
AT2G40270	Protein kinase family protein	169	1	LRR	Genotype and RALF1
AT2G41900	CCCH-type zinc finger protein with ARM repeat domain	479	1	Metabolism	Genotype and RALF1
AT2G43680	IQ-domain 15	196	2	Calcium	Genotype and RALF1
AT2G43680	IQ-domain 15	201	1	Calcium	Genotype and RALF1
AT2G44730	Alcohol dehydrogenase transcription factor Myb/SANT-like family protein	246	3	TF	Genotype and RALF1
AT2G45200	golgi snare 12	146	1	Trafficking	Genotype and RALF1
AT2G45200	golgi snare 12	184	1	Trafficking	Genotype and RALF1
AT2G45820	Remorin family protein	14	1	Metabolism	Genotype and RALF1

Protein	Name	Phosphosites	Multiplicity	Function	Significant in
AT2G45820	Remorin family protein	58	2	Metabolism	Genotype and RALF1
AT2G45890	ROPGEF4	27	1	RHO	Genotype and RALF1
AT2G46860	pyrophosphorylase 3	28	1	Metabolism	Genotype and RALF1
AT2G47970	Nuclear pore localisation protein NPL4	104	1	Degradation	Genotype and RALF1
AT3G03050	cellulose synthase-like D3	15	2	Cell growth	Genotype and RALF1
AT3G03050	cellulose synthase-like D3	18	1	Cell growth	Genotype and RALF1
AT3G04120	glyceraldehyde-3-phosphate dehydrogenase C2	236	1	Metabolism	Genotype and RALF1
AT3G07410	RAB GTPase homolog A5B	192	2	Trafficking	Genotype and RALF1
AT3G07810	RNA-binding (RRM/RBD/RNP motifs) family protein	283	1	Metabolism	Genotype and RALF1
AT3G09560	Lipin family protein	162	1	Cell growth	Genotype and RALF1

Protein	Name	Phosphosites	Multiplicity	Function	Significant in
AT3G09670	Tudor/PWWP/MBT superfamily protein	541	2	Metabolism	Genotype and RALF1
AT3G12020	P-loop containing nucleoside triphosphate hydrolases superfamily protein	577	1	Cytoskeleton	Genotype and RALF1
AT3G12590	Unknown		2	Unknown	Genotype and RALF1
AT3G12590	Unknown	231	1	Unknown	Genotype and RALF1
AT3G13530	MAP3K 7	503	1	MAPK	Genotype and RALF1
AT3G14840	Leucine-rich repeat transmembrane protein kinase	967	1	LRR	Genotype and RALF1
AT3G17440	novel plant snare 13	74	1	Trafficking	Genotype and RALF1
AT3G20250	pumilio 5	177	1	Defence	Genotype and RALF1
AT3G20250	pumilio 5	303	2	Defence	Genotype and RALF1
AT3G20250	pumilio 5	520	1	Defence	Genotype and RALF1

Protein	Name	Phosphosites	Multiplicity	Function	Significant in
AT3G20410	Calmodulin-domain protein kinase 9	23	2	Calcium	Genotype and RALF1
AT3G21175	ZIM-like 1	121	1	Cell growth	Genotype and RALF1
AT3G22850	Aluminium induced protein with YGL and LRDR motifs	216	1	Hormone	Genotype and RALF1
AT3G23090	TPX2 (targeting protein for Xklp2) protein family	120	1	Cytoskeleton	Genotype and RALF1
AT3G23490	cyanase	167	2	Metabolism	Genotype and RALF1
AT3G25070	RPM1 interacting protein 4	112	3	Defence	Genotype and RALF1
AT3G43300	HOPM interactor 7	1406	2	Defence	Genotype and RALF1
AT3G43300	HOPM interactor 7	1423	2	Defence	Genotype and RALF1
AT3G45780	phototropin 1	58	2	Transport	Genotype and RALF1
AT3G47210	Unknown	29	1	Unknown	Genotype and RALF1
AT3G48190	ataxia-telangiectasia mutated	1641	1	Metabolism	Genotype and RALF1

Protein	Name	Phosphosites	Multiplicity	Function	Significant in
AT3G49590	Autophagy-related protein 15	454	1	Degradation	Genotype and RALF1
AT3G50350	Unknown	72	2	Unknown	Genotype and RALF1
AT3G51950	zinc finger (CCCH-type) family protein / RNA recognition motif (RRM)-containing protein	352	2	Metabolism	Genotype and RALF1
AT3G51950	zinc finger (CCCH-type) family protein / RNA recognition motif (RRM)-containing protein	359	2	Metabolism	Genotype and RALF1
AT3G52290	IQ-domain 3	65	1	Calcium	Genotype and RALF1
AT3G52870	IQ Calmodulin-binding motif family protein	440	1	Calcium	Genotype and RALF1
AT3G53020	Ribosomal protein L24e family protein	28	1	Hormone	Genotype and RALF1

Protein	Name	Phosphosites	Multiplicity	Function	Significant in
AT3G53520	UDP-glucuronic acid deCarboxylase 1	26	1	Metabolism	Genotype and RALF1
AT3G54760	dentin sialophosphoprotein-related	464	1	Unknown	Genotype and RALF1
AT3G55970	jasmonate-regulated gene 21	16	2	Hormone	Genotype and RALF1
AT3G57340	Heat shock protein DnaJ, N-terminal with domain of unknown function	233	1	Metabolism	Genotype and RALF1
AT3G58730	vacuolar ATP synthase subunit D (VATD) / V-ATPase D subunit / vacuolar proton pump D subunit (VATPD)	241	2	Cell growth	Genotype and RALF1
AT3G59690	IQ-domain 13	107	2	Calcium	Genotype and RALF1
AT3G60240	eukaryotic translation initiation factor 4G	1365	1	Metabolism	Genotype and RALF1

Protein	Name	Phosphosites	Multiplicity	Function	Significant in
AT3G60240	eukaryotic translation initiation factor 4G	981	1	Metabolism	Genotype and RALF1
AT3G62270	HCO3- transporter family	669	1	Transport	Genotype and RALF1
AT4G00752	UBX domain-containing protein	224	2	Degradation	Genotype and RALF1
AT4G01670	Unknown	216	1	Unknown	Genotype and RALF1
AT4G01810	Sec23/Sec24 protein transport family protein	35	2	Trafficking	Genotype and RALF1
AT4G01810	Sec23/Sec24 protein transport family protein	41	1	Trafficking	Genotype and RALF1
AT4G01810	Sec23/Sec24 protein transport family protein	69	1	Trafficking	Genotype and RALF1
AT4G02050	sugar transporter protein 7	5	1	Transport	Genotype and RALF1
AT4G08500	MAPK/ERK kinase kinase 1	69	1	MAPK	Genotype and RALF1
AT4G10730	Protein kinase superfamily protein	579	2	Kinase	Genotype and RALF1

Protein	Name	Phosphosites	Multiplicity	Function	Significant in
AT4G11740	Ubiquitin-like superfamily protein	288	2	Trafficking	Genotype and RALF1
AT4G11740	Ubiquitin-like superfamily protein	289	2	Trafficking	Genotype and RALF1
AT4G11740	Ubiquitin-like superfamily protein	295	2	Trafficking	Genotype and RALF1
AT4G15900	pleiotropic regulatory locus 1	145	1	Defence	Genotype and RALF1
AT4G22130	STRUBBELIG-receptor family 8	188	1	Kinase	Genotype and RALF1
AT4G24100	Protein kinase superfamily protein	516	1	Kinase	Genotype and RALF1
AT4G24275	Identified as a screen for stress-responsive genes.	44	1	Metabolism	Genotype and RALF1
AT4G26650	RNA-binding (RRM/RBD/RNP motifs) family protein	294	1	Metabolism	Genotype and RALF1
AT4G28400	Protein phosphatase 2C family protein	120	2	Unknown	Genotype and RALF1
AT4G30160	villin 4	775	1	Cytoskeleton	Genotype and RALF1

Protein	Name	Phosphosites	Multiplicity	Function	Significant in
AT4G30190	AHA 2 ; AHA 8; AHA 6	904	1	Cell growth	Genotype and RALF1
AT4G30190	AHA 5; AHA2; AHA 3; AHA 8; AHA 6	913	1	Cell growth	Genotype and RALF1
AT4G31880	Unknown	836	1	Metabolism	Genotype and RALF1
AT4G31880	Unknown	658	1	Metabolism	Genotype and RALF1
AT4G32850	nuclear poly(a) polymerase;	669	2	Metabolism	Genotype and RALF1
AT4G33080	AGC (CAMP-dependent, cGMP-dependent and protein kinase C) kinase family protein	438	1	Kinase	Genotype and RALF1
AT4G33530	K+ uptake permease 5	714	1	Transport	Genotype and RALF1
AT4G33700	CBS domain-containing protein with a domain of unknown function (DUF21)	336	2	Unknown	Genotype and RALF1

Protein	Name	Phosphosites	Multiplicity	Function	Significant in
AT4G34860	Plant neutral invertase family protein	50	2	Metabolism	Genotype and RALF1
AT4G34860	Plant neutral invertase family protein	57	2	Metabolism	Genotype and RALF1
AT4G38470	SERINE/THREONINE/TYROSINE KINASE 46	105	2	Kinase	Genotype and RALF1
AT4G38470	SERINE/THREONINE/TYROSINE KINASE 46	108	1	Kinase	Genotype and RALF1
AT4G38550	Phospholipase-like protein (PEARLI 4) family protein	164	1	Metabolism	Genotype and RALF1
AT4G39680	SAP domain-containing protein	417	3	Metabolism	Genotype and RALF1
AT4G39680	SAP domain-containing protein	421	1	Metabolism	Genotype and RALF1
AT4G39860	Unknown	249	1	Unknown	Genotype and RALF1
AT5G02170	Transmembrane amino acid transporter family protein	41	1	Transport	Genotype and RALF1

Protein	Name	Phosphosites	Multiplicity	Function	Significant in
AT5G03630	Pyridine nucleotide-disulphide oxidoreductase family protein	401	1	Calcium	Genotype and RALF1
AT5G04870	Calcium dependent protein kinase 1	44	2	Calcium	Genotype and RALF1
AT5G05170	CESA3	216	2	Cell growth	Genotype and RALF1
AT5G05970	Transducin/WD40 repeat-like superfamily protein	415	1	Metabolism	Genotype and RALF1
AT5G07350	TUDOR-SN protein 1	975	1	Metabolism	Genotype and RALF1
AT5G09960	Unknown	95	2	Unknown	Genotype and RALF1
AT5G11040	TRS120	971	1	Metabolism	Genotype and RALF1
AT5G13220	jasmonate-zim-domain protein 10	85	2	Hormone	Genotype and RALF1
AT5G13260	Unknown	136	1	Unknown	Genotype and RALF1
AT5G16210	HEAT repeat-containing protein	1134	1	Metabolism	Genotype and RALF1

Protein	Name	Phosphosites	Multiplicity	Function	Significant in
AT5G16840	binding partner of acd11 1	155	1	Metabolism	Genotype and RALF1
AT5G18230	transcription regulator NOT2/ NOT3/ NOT5 family protein	431	2	TF	Genotype and RALF1
AT5G19520	mechanosensitive channel of small conductance-like 9	30	1	Transport	Genotype and RALF1
AT5G20350	Ankyrin repeat family protein with DHHC zinc finger domain	21	2	Cell growth	Genotype and RALF1
AT5G20490	Myosin family protein with Dil domain	1451	1	Cytoskeleton	Genotype and RALF1
AT5G20490	Myosin family protein with Dil domain	1168	2	Cytoskeleton	Genotype and RALF1
AT5G20900	JASMONATE-ZIM-DOMAIN PROTEIN 12	100	1	Hormone	Genotype and RALF1
AT5G21170	KINβ1	53	3	Metabolism	Genotype and RALF1

Protein	Name	Phosphosites	Multiplicity	Function	Significant in
AT5G21170	KINβ1	43	2	Metabolism	Genotype and RALF1
AT5G23080	SWAP (Suppressor-of-White-APricot)/surp domain-containing protein	695	1	Cell growth	Genotype and RALF1
AT5G24760	GroES-like zinc-binding dehydrogenase family protein	223	1	Metabolism	Genotype and RALF1
AT5G37190	COP1-interacting protein 4	165	1	Trafficking	Genotype and RALF1
AT5G39570	Unknown	146	2	Unknown	Genotype and RALF1
AT5G40200	DegP protease 9		1	Degradation	Genotype and RALF1
AT5G40200	DegP protease 9	39	1	Degradation	Genotype and RALF1
AT5G41800	Transmembrane amino acid transporter family protein	17	1	Transport	Genotype and RALF1

Protein	Name	Phosphosites	Multiplicity	Function	Significant in
AT5G41950	Tetratricopeptide repeat (TPR)-like superfamily protein	168	1	Trafficking	Genotype and RALF1
AT5G42870	phosphatidic acid phosphohydrolase 2	132	2	Cell growth	Genotype and RALF1
AT5G42870	phosphatidic acid phosphohydrolase 2	139	2	Cell growth	Genotype and RALF1
AT5G43310	COP1-interacting protein-related	755	1	Trafficking	Genotype and RALF1
AT5G43830	Aluminium induced protein with YGL and LRDR motifs	12	1	Unknown	Genotype and RALF1
AT5G44090	Calcium-binding EF-hand family protein	110	2	Calcium	Genotype and RALF1
AT5G44090	Calcium-binding EF-hand family protein		1	Calcium	Genotype and RALF1
AT5G44240	aminophospholipid ATPase 2	1071	1	Transport	Genotype and RALF1
AT5G44610	microtubule-associated protein 18	148	2	Cytoskeleton	Genotype and RALF1

Protein	Name	Phosphosites	Multiplicity	Function	Significant in
AT5G44610	microtubule-associated protein 18		1	Cytoskeleton	Genotype and RALF1
AT5G46780	VQ motif-containing protein; VQ motif-containing protein	147	1	Cell growth	Genotype and RALF1
AT5G47480	RGPR-related	1290	1	Trafficking	Genotype and RALF1
AT5G47690	Unknown	1297	1	Metabolism	Genotype and RALF1
AT5G49100	Unknown	250	2	Unknown	Genotype and RALF1
AT5G51060	NADPH/respiratory burst oxidase protein D	115	1	Metabolism	Genotype and RALF1
AT5G52882	P-loop containing nucleoside triphosphate hydrolases superfamily protein	161	2	Metabolism	Genotype and RALF1
AT5G54440	CLUB	519	1	Transport	Genotype and RALF1

Protein	Name	Phosphosites	Multiplicity	Function	Significant in
AT5G55530	Calcium-dependent lipid-binding (CaLB domain) family protein	372	2	Calcium	Genotype and RALF1
AT5G56180	actin-related protein 8	16	1	Cytoskeleton	Genotype and RALF1
AT5G56980	Unknown	113	2	Unknown	Genotype and RALF1
AT5G56980	Unknown	120	1	Unknown	Genotype and RALF1
AT5G57110	autoinhibited Calcium2+ -ATPase, isoform 8	57	1	Calcium	Genotype and RALF1
AT5G57610	Protein kinase superfamily protein with octicosapeptide/Phox/Bem1p domain	258	1	Kinase	Genotype and RALF1
AT5G58350	with no lysine (K) kinase 4	522	1	Kinase	Genotype and RALF1
AT5G59010	Protein kinase protein with tetratricopeptide repeat domain	329	1	Kinase	Genotype and RALF1

Protein	Name	Phosphosites	Multiplicity	Function	Significant in
AT5G59960	Unknown	6	1	Unknown	Genotype and RALF1
AT5G61730	ABC2 homolog 11	594	1	Metabolism	Genotype and RALF1
AT5G62865	Unknown	151	2	Unknown	Genotype and RALF1
AT5G62865	Unknown	159	2	Unknown	Genotype and RALF1
AT5G64090	Unknown	434	1	Unknown	Genotype and RALF1
AT5G64200	ortholog of human splicing factor SC35	263	2	Metabolism	Genotype and RALF1
AT5G64200	ortholog of human splicing factor SC35	269	2	Metabolism	Genotype and RALF1
AT5G65200	plant U-box 38	553	1	Degradation	Genotype and RALF1

Supplementary Table S.3: Phosphosites that are dependent on FERONIA but independent of RALF1 treatment

Protein	Name	Phosphosites	Multiplicity	Function	Significant in
AT1G01100	60S acidic ribosomal protein family	102	2	Metabolism	Genotype
AT1G01550	Unknown	337	1	Metabolism	Genotype

Protein	Name	Phosphosites	Multiplicity	Function	Significant in
AT1G02080	transcription regulators	1809	1	TF	Genotype
AT1G02880	thiamin pyrophosphokinase1	179	2	Metabolism	Genotype
AT1G03080	NETWORKED 1D	1564	1	Kinase	Genotype
AT1G04280	P-loop containing nucleoside triphosphate hydrolases superfamily protein	199	1	Metabolism	Genotype
AT1G05520	Sec23/Sec24 protein transport family protein	238	3	Trafficking	Genotype
AT1G05910	BRAT1	295	1	Metabolism	Genotype
AT1G06840	Leucine-rich repeat protein kinase family protein	783	2	LRR	Genotype
AT1G07990	SIT4 phosphatase-associated family protein	508	1	Metabolism	Genotype
AT1G08420	BRI1 suppressor 1 (BSU1)-like 2	147	1	Hormone	Genotype
AT1G08420	BRI1 suppressor 1 (BSU1)-like 2	136	2	Hormone	Genotype

Protein	Name	Phosphosites	Multiplicity	Function	Significant in
AT1G08680	ARF GAP-like zinc finger-containing protein ZIGA4	157	1	Metabolism	Genotype
AT1G08680	ARF GAP-like zinc finger-containing protein ZIGA4	413	1	Metabolism	Genotype
AT1G08800	Unknown		1	Unknown	Genotype
AT1G08800	Unknown	872	1	Unknown	Genotype
AT1G08800	Unknown	875	1	Unknown	Genotype
AT1G09170	P-loop nucleoside triphosphate hydrolases superfamily protein with CH (Calponin Homology) domain	784	2	Cytoskeleton	Genotype
AT1G09170	P-loop nucleoside triphosphate hydrolases superfamily protein with CH (Calponin Homology) domain	782	1	Cytoskeleton	Genotype
AT1G10900	Phosphatidylinositol-4-phosphate 5-kinase family protein	647	1	Kinase	Genotype
AT1G11260	sugar transporter 1	252	1	Transport	Genotype

Protein	Name	Phosphosites	Multiplicity	Function	Significant in
AT1G11310	Seven transmembrane MLO family protein	510	2	Defence	Genotype
AT1G11360	Adenine nucleotide alpha hydrolases-like superfamily protein	23	1	Metabolism	Genotype
AT1G11700	Unknown	85	1	Unknown	Genotype
AT1G11700	Unknown	167	1	Unknown	Genotype
AT1G11700	Unknown	114	2	Unknown	Genotype
AT1G12920	eukaryotic release factor 1-2	425	1	Metabolism	Genotype
AT1G14850	nucleoporin 155	765	1	Transport	Genotype
AT1G15940	PDS5E	281	2	Metabolism	Genotype
AT1G15940	PDS5E	290	1	Metabolism	Genotype
AT1G16170	Unknown	9	1	Unknown	Genotype
AT1G16860	SHOU4L	95	2	Degradation	Genotype
AT1G17210	IAP-LIKE PROTEIN 1	566	2	Metabolism	Genotype
AT1G17210	IAP-LIKE PROTEIN 1	762	2	Metabolism	Genotype
AT1G17210	IAP-LIKE PROTEIN 1	769	2	Metabolism	Genotype
AT1G17580	myosin 1	1510	1	Cytoskeleton	Genotype

Protein	Name	Phosphosites	Multiplicity	Function	Significant in
AT1G19350	BRASSINAZOLE-RESISTANT 2	175	2	Hormone	Genotype
AT1G19350	BRASSINAZOLE-RESISTANT 2		2	Hormone	Genotype
AT1G19350	BRASSINAZOLE-RESISTANT 2	171	3	Hormone	Genotype
AT1G19350	BRASSINAZOLE-RESISTANT 2		1	Hormone	Genotype
AT1G19350	BRASSINAZOLE-RESISTANT 2		1	Hormone	Genotype
AT1G19450	Major facilitator superfamily protein	33	1	Metabolism	Genotype
AT1G20440	cold-regulated 47	22	2	Defence	Genotype
AT1G20450	Dehydrin family protein	220	2	Metabolism	Genotype
AT1G20540	Transducin/WD40 repeat-like superfamily protein	6	3	Metabolism	Genotype

Protein	Name	Phosphosites	Multiplicity	Function	Significant in
AT1G20540	Transducin/WD40 repeat-like superfamily protein	14	3	Metabolism	Genotype
AT1G20540	Transducin/WD40 repeat-like superfamily protein	16	1	Metabolism	Genotype
AT1G20760	ATEH1	988	1	Calcium	Genotype
AT1G20760	ATEH1	1008	1	Calcium	Genotype
AT1G20840	TONOPLAST MONOSACCHARIDE TRANSPORTER1	278	1	Metabolism	Genotype
AT1G20840	TONOPLAST MONOSACCHARIDE TRANSPORTER1	277	2	Metabolism	Genotype
AT1G21630	ATEH2	1002	2	Calcium	Genotype
AT1G21770	Acyl-CoA N-acyltransferases (NAT) superfamily protein	110	2	Metabolism	Genotype
AT1G22060	sporulation-specific protein	261	2	Unknown	Genotype
AT1G22060	sporulation-specific protein	252	1	Unknown	Genotype

Protein	Name	Phosphosites	Multiplicity	Function	Significant in
AT1G22300	GENERAL REGULATORY FACTOR 10	234	1	Hormone	Genotype
AT1G22500	RING/U-box superfamily protein	325	1	Degradation	Genotype
AT1G22530	PATELLIN 2	403	1	Cytoskeleton	Genotype
AT1G27210	ARM repeat superfamily protein	314	1	Cytoskeleton	Genotype
AT1G27430	GYF domain-containing protein	1332	1	Defence	Genotype
AT1G30440	Phototropic-responsive NPH3 family protein	279	1	Degradation	Genotype
AT1G30440	Phototropic-responsive NPH3 family protein	532	1	Degradation	Genotype
AT1G31660	Unknown	24	1	Metabolism	Genotype
AT1G31970	STRESS RESPONSE SUPPRESSOR 1	533	2	Metabolism	Genotype
AT1G34120	MYO-INOSITOL POLYPHOSPHATE 5-PHOSPHATASE 1	183	1	Kinase	Genotype
AT1G43130	like COV 2	28	2	Metabolism	Genotype
AT1G43130	like COV 2	32	2	Metabolism	Genotype

Protein	Name	Phosphosites	Multiplicity	Function	Significant in
AT1G43710	Pyridoxal phosphate (PLP)-dependent transferases superfamily protein	7	1	Metabolism	Genotype
AT1G44900	MINICHROMOSOME MAINTENANCE 2	478	2	Cell growth	Genotype
AT1G45688	Unknown	16	2	Unknown	Genotype
AT1G45688	Unknown		2	Unknown	Genotype
AT1G47820	Unknown	82	2	Unknown	Genotype
AT1G47900	Unknown	515	2	Unknown	Genotype
AT1G47900	Unknown	518	1	Unknown	Genotype
AT1G48490	Protein kinase superfamily protein	694	1	Kinase	Genotype
AT1G48600	PHOSPHOETHANOLAMINE N-METHYLTRANSFERASE	462	1	Metabolism	Genotype
AT1G50120	Unknown	265	2	Unknown	Genotype
AT1G51800	Leucine-rich repeat protein kinase family protein	561	3	LRR	Genotype
AT1G53165	ATMAP4K	654	2	Kinase	Genotype
AT1G54060	6B-interacting protein 1-like 1	383	2	TF	Genotype

Protein	Name	Phosphosites	Multiplicity	Function	Significant in
AT1G58350	Putative serine esterase family protein	234	2	Cell growth	Genotype
AT1G58350	Putative serine esterase family protein	474	1	Cell growth	Genotype
AT1G61560	MLO6	449	1	Defence	Genotype
AT1G61560	MLO6	445	1	Defence	Genotype
AT1G63010	Major Facilitator Superfamily with SPX (SYG1/Pho81/XPR1) domain-containing protein	41	1	Transport	Genotype
AT1G63700	MAP KINASE KINASE KINASE 4	797	2	Kinase	Genotype
AT1G63980	D111/G-patch domain-containing protein	100	1	Metabolism	Genotype
AT1G64780	ammonium transporter 1	488	2	Transport	Genotype
AT1G65030	Transducin/WD40 repeat-like superfamily protein	344	3	Metabolism	Genotype
AT1G65110	Ubiquitin Caboxyl-terminal hydrolase-related protein	1029	2	Degradation	Genotype

Protein	Name	Phosphosites	Multiplicity	Function	Significant in
AT1G68060	microtubule-associated proteins 70-1	475	2	Cytoskeleton	Genotype
AT1G68790	little nuclei3	903	2	Metabolism	Genotype
AT1G69410	EUKARYOTIC ELONGATION FACTOR 5A-3	2	2	Metabolism	Genotype
AT1G72200	RING/U-box superfamily protein	389	1	Degradation	Genotype
AT1G72710	Casein kinase 1-like protein 2	355	1	Metabolism	Genotype
AT1G77020	DNAJ heat shock N-terminal domain-containing protein	246	1	Metabolism	Genotype
AT1G78815	Unknown	31	1	Metabolism	Genotype
AT1G78880	Ubiquitin-specific protease family C19-related protein	74	2	Degradation	Genotype
AT1G78880	Ubiquitin-specific protease family C19-related protein	78	1	Degradation	Genotype
AT1G79340	metacaspase 4	296	1	Defence	Genotype
AT1G79660	Unknown	9	2	Unknown	Genotype

Protein	Name	Phosphosites	Multiplicity	Function	Significant in
AT1G79950	RAD3-like DNA-binding helicase protein	879	1	Metabolism	Genotype
AT2G03390	uvrB/uvrC motif-containing protein	216	1	Unknown	Genotype
AT2G05120	Nucleoporin	28	1	Transport	Genotype
AT2G05755	Nucleotide/sugar transporter family protein	61	1	Metabolism	Genotype
AT2G07360	SH3 domain-containing protein	1125	1	Unknown	Genotype
AT2G16405	Transducin/WD40 repeat-like superfamily protein		2	Metabolism	Genotype
AT2G16920	ubiquitin-conjugating enzyme 23	747	1	Degradation	Genotype
AT2G18960	AHA1	899	1	Cell growth	Genotype
AT2G19490	recA DNA recombination family protein	392	1	Metabolism	Genotype
AT2G19710	IST1-LIKE 5	621	1	Trafficking	Genotype

Protein	Name	Phosphosites	Multiplicity	Function	Significant in
AT2G19710	IST1-LIKE 5	678	2	Trafficking	Genotype
AT2G20190	CLIP-associated protein	613	1	Cytoskeleton	Genotype
AT2G20280	Zinc finger C-x8-C-x5-C-x3-H type family protein	370	1	Metabolism	Genotype
AT2G21390	Coatomer, alpha subunit	361	2	Trafficking	Genotype
AT2G21470	SUMO-ACTIVATING ENZYME 2	603	1	Metabolism	Genotype
AT2G21520	Sec14p-like phosphatidylinositol transfer family protein	398	1	Trafficking	Genotype
AT2G22125	binding CSI1	33	2	Cell growth	Genotype
AT2G22125	binding CSI1	37	1	Cell growth	Genotype
AT2G22560	NETWORKED 2D	909	1	Kinase	Genotype
AT2G23140	PLANT U-BOX 4	443	1	Metabolism	Genotype
AT2G26110	Unknown	235	2	Unknown	Genotype
AT2G26190	Calmodulin-binding family protein	61	1	Calcium	Genotype
AT2G26190	Calmodulin-binding family protein	51	1	Calcium	Genotype

Protein	Name	Phosphosites	Multiplicity	Function	Significant in
AT2G27740	RAB6-interacting golgin	13	1	Unknown	Genotype
AT2G28250	Protein kinase superfamily protein	530	2	Cell growth	Genotype
AT2G29210	splicing factor PWI domain-containing protein	462	1	Metabolism	Genotype
AT2G29210	splicing factor PWI domain-containing protein	444	2	Metabolism	Genotype
AT2G29620	dentin sialophosphoprotein	641	2	Unknown	Genotype
AT2G30930	Unknown	103	1	Unknown	Genotype
AT2G30930	Unknown		1	Unknown	Genotype
AT2G30930	Unknown	125	2	Unknown	Genotype
AT2G32150	Haloacid dehalogenase-like hydrolase superfamily protein	250	2	Unknown	Genotype
AT2G32450	Calcium-binding tetratricopeptide family protein	562	2	Calcium	Genotype
AT2G34680	Outer arm dynein light chain 1 protein	212	1	Cytoskeleton	Genotype

Protein	Name	Phosphosites	Multiplicity	Function	Significant in
AT2G34680	Outer arm dynein light chain 1 protein	233	1	Cytoskeleton	Genotype
AT2G35880	TPX2 (targeting protein for Xklp2) protein family	183	1	Cytoskeleton	Genotype
AT2G35880	TPX2 (targeting protein for Xklp2) protein family	98	1	Cytoskeleton	Genotype
AT2G36380	PLEIOTROPIC DRUG RESISTANCE 6	13	1	Transport	Genotype
AT2G38410	ENTH/VHS/GAT family protein	340	2	Degradation	Genotype
AT2G38670	PECT1	212	2	Metabolism	Genotype
AT2G42280	ABA-RESPONSIVE KINASE SUBSTRATE 3	22	1	Metabolism	Genotype
AT2G43680	IQ-domain 14	629	1	Calcium	Genotype
AT2G44380	Cysteine/Histidine-rich C1 domain family protein	240	1	Unknown	Genotype
AT2G45710	Zinc-binding ribosomal protein family protein	29	1	Metabolism	Genotype

Protein	Name	Phosphosites	Multiplicity	Function	Significant in
AT2G46340	SUPPRESSOR OF PHYA-105 1	97	1	Metabolism	Genotype
AT2G47000	ATP binding Cassette subfamily B4	667	1	Hormone	Genotype
AT2G47000	ATP binding Cassette subfamily B4	668	2	Hormone	Genotype
AT2G47000	ATP binding Cassette subfamily B4	671	1	Hormone	Genotype
AT3G04480	endoribonucleases	257	1	Metabolism	Genotype
AT3G06170	Serinc-domain containing serine and sphingolipid biosynthesis protein	306	1	Metabolism	Genotype
AT3G07660	Kinase-related protein of unknown function (DUF1296)	549	1	Kinase	Genotype
AT3G07660	Kinase-related protein of unknown function (DUF1296)	113	1	Kinase	Genotype
AT3G07790	DGCR14-related	13	2	Unknown	Genotype
AT3G07790	DGCR14-related	14	1	Unknown	Genotype
AT3G07790	DGCR14-related	137	2	Unknown	Genotype
AT3G07790	DGCR14-related	140	2	Unknown	Genotype

Protein	Name	Phosphosites	Multiplicity	Function	Significant in
AT3G10260	Reticulon family protein	37	1	Cytoskeleton	Genotype
AT3G10980	PLAC8 family protein	489	1	Metabolism	Genotype
AT3G10980	PLAC8 family protein		2	Metabolism	Genotype
AT3G10980	PLAC8 family protein	494	1	Metabolism	Genotype
AT3G12140	EMSY-LIKE 1	90	1	Defence	Genotype
AT3G12280	retinoblastoma-related 1	665	1	Cell growth	Genotype
AT3G12590	Unknown	218	1	Unknown	Genotype
AT3G13100	multidrug resistance-associated protein 7	888	1	Transport	Genotype
AT3G13990	Kinase-related protein of unknown function (DUF1296)	145	1	Kinase	Genotype
AT3G14940	phosphoenolpyruvate Carboxylase 3	705	2	Metabolism	Genotype
AT3G15820	REDUCED OLEATE DESATURATION 1	18	1	Metabolism	Genotype
AT3G16857	RESPONSE REGULATOR 1	161	2	Metabolism	Genotype
AT3G17430	Nucleotide-sugar transporter family protein	331	1	Transport	Genotype

Protein	Name	Phosphosites	Multiplicity	Function	Significant in
AT3G17850	Protein kinase superfamily protein	744	1	Cell growth	Genotype
AT3G18450	PLAC8 family protein	20	1	Metabolism	Genotype
AT3G19370	Unknown	49	2	Unknown	Genotype
AT3G19370	Unknown		1	Unknown	Genotype
AT3G20250	pumilio 5	178	1	Defence	Genotype
AT3G20250	pumilio 5	618	1	Defence	Genotype
AT3G20940	CYP705A30	429	1	Metabolism	Genotype
AT3G23900	RNA recognition motif (RRM)-containing protein	837	2	Metabolism	Genotype
AT3G23900	RNA recognition motif (RRM)-containing protein	841	2	Metabolism	Genotype
AT3G23920	beta-amylase 1	55	1	Metabolism	Genotype
AT3G25780	allene oxide cyclase 3	100	1	Hormone	Genotype
AT3G26400	eukaryotic translation initiation factor 4B1	269	1	Metabolism	Genotype
AT3G29075	glycine-rich protein	179	2	Metabolism	Genotype
AT3G29160	SNF1 kinase homolog 10	175	1	Kinase	Genotype
AT3G43300	HOPM interactor 7	1427	1	Defence	Genotype
AT3G48430	REF6	1124	1	Metabolism	Genotype

Protein	Name	Phosphosites	Multiplicity	Function	Significant in
AT3G49590	Autophagy-related protein 13	337	1	Degradation	Genotype
AT3G49601	Unknown	450	1	Unknown	Genotype
AT3G49601	Unknown	300	1	Unknown	Genotype
AT3G49601	Unknown	292	1	Unknown	Genotype
AT3G50370	Unknown	187	2	Unknown	Genotype
AT3G52870	IQ Calmodulin-binding motif family protein	315	1	Calcium	Genotype
AT3G52880	monodehydroascorbate reductase 1	416	1	Metabolism	Genotype
AT3G53500	RNA-binding (RRM/RBD/RNP motifs) family protein with retrovirus zinc finger-like domain	189	1	Metabolism	Genotype
AT3G54770	ARP1	106	1	Metabolism	Genotype
AT3G55970	jasmonate-regulated gene 21	121	1	Hormone	Genotype
AT3G58640	Mitogen activated protein kinase kinase kinase-related	336	1	Kinase	Genotype
AT3G59690	IQ-domain 13	138	2	Calcium	Genotype
AT3G59690	IQ-domain 13	143	2	Calcium	Genotype

Protein	Name	Phosphosites	Multiplicity	Function	Significant in
AT3G61050	CALCIUM-DEPENDENT LIPID-BINDING PROTEIN	496	2	Calcium	Genotype
AT3G61260	Remorin family protein	13	1	Metabolism	Genotype
AT3G61310	AT hook motif DNA-binding family protein	122	2	Metabolism	Genotype
AT3G61310	AT hook motif DNA-binding family protein	129	2	Metabolism	Genotype
AT3G61370	Unknown	103	1	Unknown	Genotype
AT3G61410	U-box kinase family protein	187	2	Kinase	Genotype
AT3G62700	MULTIDRUG RESISTANCE-ASSOCIATED PROTEIN 10	897	2	Transport	Genotype
AT3G63400	Cyclophilin-like peptidyl-prolyl cis-trans isomerase family protein	199	1	Metabolism	Genotype

Protein	Name	Phosphosites	Multiplicity	Function	Significant in
AT3G63400	Cyclophilin-like peptidyl-prolyl cis-trans isomerase family protein	556	2	Metabolism	Genotype
AT4G00238	STKL1	53	2	TF	Genotype
AT4G00700	MULTIPLE C2 DOMAIN AND TRANSMEMBRANE REGION PROTEIN 9	146	1	Calcium	Genotype
AT4G00700	MULTIPLE C2 DOMAIN AND TRANSMEMBRANE REGION PROTEIN 9	153	1	Calcium	Genotype
AT4G00810	60S acidic ribosomal protein family	103	1	Metabolism	Genotype
AT4G03550	glucan synthase-like 5	1053	2	Defence	Genotype
AT4G04210	plant UBX domain containing protein 4	181	3	Transport	Genotype
AT4G08180	OSBP(oxysterol binding protein)-related protein 1C	51	1	Cell growth	Genotype
AT4G08350	GLOBAL TRANSCRIPTION FACTOR GROUP A2	683	1	TF	Genotype

Protein	Name	Phosphosites	Multiplicity	Function	Significant in
AT4G08350	GLOBAL TRANSCRIPTION FACTOR GROUP A2	684	1	TF	Genotype
AT4G10730	Protein kinase superfamily protein	531	1	Kinase	Genotype
AT4G11740	Ubiquitin-like superfamily protein	394	1	Trafficking	Genotype
AT4G12340	copper ion binding	143	1	Metabolism	Genotype
AT4G12400	stress-inducible protein	493	1	Metabolism	Genotype
AT4G12780	Chaperone DnaJ-domain superfamily protein	663	1	Trafficking	Genotype
AT4G16310	LSD1-like 3	480	2	Metabolism	Genotype
AT4G16310	LSD1-like 3	481	1	Metabolism	Genotype
AT4G16340	SPIKE1	1051	1	Hormone	Genotype
AT4G17060	FRIGIDA interacting protein 2	77	1	Metabolism	Genotype
AT4G17330	G2484-1 PROTEIN	191	2	Unknown	Genotype
AT4G18120	MEI2-like 3	356	1	Cell growth	Genotype
AT4G19040	ENHANCED DISEASE RESISTANCE 2	434	1	Hormone	Genotype

Protein	Name	Phosphosites	Multiplicity	Function	Significant in
AT4G22290	Ubiquitin-specific protease family C19-related protein	112	1	Degradation	Genotype
AT4G24275	Identified as a screen for stress-responsive genes.	54	3	Metabolism	Genotype
AT4G25970	PHOSPHATIDYLSERINE DECARBOXYLASE 3	35	1	Metabolism	Genotype
AT4G25970	PHOSPHATIDYLSERINE DECARBOXYLASE 3	37	1	Metabolism	Genotype
AT4G26110	nucleosome assembly protein1	48	1	Metabolism	Genotype
AT4G26450	Unknown	410	2	Unknown	Genotype
AT4G26450	Unknown	412	1	Unknown	Genotype
AT4G26480	RNA-binding KH domain-containing protein	110	1	Metabolism	Genotype
AT4G26760	microtubule-associated protein 65-2	566	1	Cytoskeleton	Genotype
AT4G27060	ARM repeat superfamily protein	579	1	Cell growth	Genotype
AT4G27060	ARM repeat superfamily protein	335	2	Cell growth	Genotype

Protein	Name	Phosphosites	Multiplicity	Function	Significant in
AT4G27320	Adenine nucleotide alpha hydrolases-like superfamily protein	30	1	Defence	Genotype
AT4G27500	PROTON PUMP INTERACTOR 1	540	1	Cell growth	Genotype
AT4G27585	STOMATIN-LIKE PROTEIN 1	362	2	Metabolism	Genotype
AT4G30160	villin 4		2	Cytoskeleton	Genotype
AT4G30160	villin 4	777	1	Cytoskeleton	Genotype
AT4G30560	cyclic nucleotide gated channel 9	38	2	Calcium	Genotype
AT4G30890	ubiquitin-specific protease 24	171	1	Degradation	Genotype
AT4G31200	SWAP (Suppressor-of-White-APricot)/surp RNA-binding domain-containing protein	568	1	Metabolism	Genotype
AT4G31540	EXO70G1	663	1	Trafficking	Genotype
AT4G31880	Unknown	559	1	Metabolism	Genotype
AT4G31880	Unknown		1	Metabolism	Genotype
AT4G31880	Unknown	748	1	Metabolism	Genotype
AT4G32140	EamA-like transporter family	87	3	Transport	Genotype

Protein	Name	Phosphosites	Multiplicity	Function	Significant in
AT4G35100	plasma membrane intrinsic protein 3	279	2	Transport	Genotype
AT4G35100	plasma membrane intrinsic protein 3	276	1	Transport	Genotype
AT4G35300	TONOPLAST MONOSACCHARIDE TRANSPORTER2	130	1	Metabolism	Genotype
AT4G35860	GTP-binding 2	21	1	Trafficking	Genotype
AT4G36520	Chaperone DnaJ-domain superfamily protein	1266	1	Trafficking	Genotype
AT4G37070	PHOSPHOLIPASE A IVA	410	1	Cell growth	Genotype
AT4G38410	dehydrin family protein	65	2	Metabolism	Genotype
AT4G38410	dehydrin family protein	66	1	Metabolism	Genotype
AT4G38410	dehydrin family protein	64	1	Hormone	Genotype
AT4G38410	dehydrin family protein	63	2	Hormone	Genotype
AT4G38470	SERINE/THREONINE/TYROSINE KINASE 46	251	2	Kinase	Genotype

Protein	Name	Phosphosites	Multiplicity	Function	Significant in
AT4G38470	SERINE/THREONINE/TYROSINE KINASE 46	269	2	Kinase	Genotype
AT4G38550	Phospholipase-like protein (PEARLI 4) family protein	162	1	Metabolism	Genotype
AT4G38600	UBIQUITIN-PROTEIN LIGASE 3	1012	1	Metabolism	Genotype
AT4G38630	REGULATORY PARTICLE NON-ATPASE 10	263	1	Metabolism	Genotype
AT4G38710	glycine-rich protein	387	1	Metabolism	Genotype
AT4G38810	Calcium-binding EF-hand family protein	250	2	Calcium	Genotype
AT4G38900	Basic-leucine zipper (bZIP) transcription factor family protein	196	2	TF	Genotype
AT4G39150	DNAJ heat shock N-terminal domain-containing protein	324	1	Metabolism	Genotype
AT4G39260	cold, circadian rhythm, and RNA binding 1	103	1	Metabolism	Genotype

Protein	Name	Phosphosites	Multiplicity	Function	Significant in
AT4G39680	SAP domain-containing protein	320	3	Metabolism	Genotype
AT4G39680	SAP domain-containing protein	319	3	Metabolism	Genotype
AT5G03280	ETHYLENE INSENSITIVE 2	757	1	Hormone	Genotype
AT5G03280	ETHYLENE INSENSITIVE 2	924	2	Hormone	Genotype
AT5G03630	Pyridine nucleotide-disulphide oxidoreductase family protein	417	1	Calcium	Genotype
AT5G04510	3'-phosphoinositide-dependent protein kinase 1; 3	385	2	Kinase	Genotype
AT5G04550	Protein of unknown function (DUF668)	240	1	Unknown	Genotype
AT5G04550	Protein of unknown function (DUF668)	306	2	Unknown	Genotype
AT5G05170	CESA3		1	Cell growth	Genotype
AT5G05170	CESA3	151	1	Cell growth	Genotype

Protein	Name	Phosphosites	Multiplicity	Function	Significant in
AT5G05170	CESA3	226	1	Cell growth	Genotype
AT5G05170	CESA3	211	1	Cell growth	Genotype
AT5G05190	Unknown	322	1	Defence	Genotype
AT5G05600	JASMONIC ACID OXIDASE 2,	29	2	Metabolism	Genotype
AT5G05600	JASMONIC ACID OXIDASE 2,	398	2	Metabolism	Genotype
AT5G09960	Unknown	86	2	Unknown	Genotype
AT5G10950	Tudor/PWWP/MBT superfamily protein	231	1	Metabolism	Genotype
AT5G10950	Tudor/PWWP/MBT superfamily protein	297	1	Metabolism	Genotype
AT5G12350	Regulator of chromosome condensation (RCC1) family with FYVE zinc finger domain	184	2	Metabolism	Genotype
AT5G12350	Regulator of chromosome condensation (RCC1) family with FYVE zinc finger domain	188	2	Metabolism	Genotype

Protein	Name	Phosphosites	Multiplicity	Function	Significant in
AT5G12850	CCCH-type zinc finger protein with ARM repeat domain	606	2	Metabolism	Genotype
AT5G13010	PSR1-INTERACTING PROTEIN 1	232	1	Defence	Genotype
AT5G13010	PSR1-INTERACTING PROTEIN 1	239	1	Defence	Genotype
AT5G14250	Proteasome component (PCI) domain protein	428	1	Metabolism	Genotype
AT5G14720	Protein kinase superfamily protein	549	2	Kinase	Genotype
AT5G14730	Unknown	188	1	Unknown	Genotype
AT5G14930	SENESCENCE-ASSOCIATED GENE 101	80	1	Cell growth	Genotype
AT5G15270	RNA-binding KH domain-containing protein	137	2	Metabolism	Genotype
AT5G16280	Tetratricopeptide repeat (TPR)-like superfamily protein	1055	2	Trafficking	Genotype

Protein	Name	Phosphosites	Multiplicity	Function	Significant in
AT5G16590	Leucine-rich repeat protein kinase family protein	624	1	LRR	Genotype
AT5G16680	RING/FYVE/PHD zinc finger superfamily protein	414	1	Metabolism	Genotype
AT5G16880	Target of Myb protein 1	35	1	Trafficking	Genotype
AT5G18280	APYRASE 2	83	1	Transport	Genotype
AT5G18280	APYRASE 2	92	1	Transport	Genotype
AT5G20190	Tetratricopeptide repeat (TPR)-like superfamily protein	23	2	Trafficking	Genotype
AT5G20190	Tetratricopeptide repeat (TPR)-like superfamily protein	5	2	Trafficking	Genotype
AT5G20900	JASMONATE-ZIM-DOMAIN PROTEIN 12	94	2	Hormone	Genotype
AT5G20900	JASMONATE-ZIM-DOMAIN PROTEIN 12	97	2	Hormone	Genotype
AT5G20900	JASMONATE-ZIM-DOMAIN PROTEIN 12	101	1	Hormone	Genotype

Protein	Name	Phosphosites	Multiplicity	Function	Significant in
AT5G21170	KINβ1	42	1	Metabolism	Genotype
AT5G21170	KINβ1	45	1	Metabolism	Genotype
AT5G22450	spectrin beta chain	415	1	Unknown	Genotype
AT5G23430	KATANIN P80 SUBUNIT 4	422	3	Cytoskeleton	Genotype
AT5G23450	long-chain base (LCB) kinase 1	22	1	Cell growth	Genotype
AT5G23680	Sterile alpha motif (SAM) domain-containing protein	68	1	Metabolism	Genotype
AT5G23750	Remorin family protein	120	1	Metabolism	Genotype
AT5G24880	Unknown	111	1	Calcium	Genotype
AT5G25060	RNA recognition motif (RRM)-containing protein	759	2	Metabolism	Genotype
AT5G28350	Quinoprotein amine dehydrogenase, beta chain-like	308	2	Trafficking	Genotype
AT5G28370	Pentatricopeptide repeat (PPR) superfamily protein	311	1	Metabolism	Genotype

Protein	Name	Phosphosites	Multiplicity	Function	Significant in
AT5G35450	Disease resistance protein (CC-NBS-LRR class) family	143	1	Defence	Genotype
AT5G39380	Plant Calmodulin-binding protein-related	172	1	Calcium	Genotype
AT5G39990	Core-2/I-branching beta-1,6-N-acetylglucosaminyltransferase family protein	9	1	Cell growth	Genotype
AT5G40740	Unknown	486	1	Metabolism	Genotype
AT5G42950	GYF domain-containing protein	716	1	Defence	Genotype
AT5G43310	COP1-interacting protein-related	824	1	Trafficking	Genotype
AT5G44090	Calcium-binding EF-hand family protein	115	1	Calcium	Genotype
AT5G44240	aminophospholipid ATPase 2	1069	2	Transport	Genotype
AT5G44240	aminophospholipid ATPase 2	1061	2	Transport	Genotype
AT5G44610	microtubule-associated protein 18	160	1	Cytoskeleton	Genotype

Protein	Name	Phosphosites	Multiplicity	Function	Significant in
AT5G45400	Replication factor-A protein 1-related	204	1	Metabolism	Genotype
AT5G46870	RNA-binding (RRM/RBD/RNP motifs) family protein	264	1	Metabolism	Genotype
AT5G46870	RNA-binding (RRM/RBD/RNP motifs) family protein	266	2	Metabolism	Genotype
AT5G47730	Sec14p-like phosphatidylinositol transfer family protein	235	1	Trafficking	Genotype
AT5G47910	respiratory burst oxidase homologue D	347	1	Metabolism	Genotype
AT5G48620	Disease resistance protein (CC-NBS-LRR class) family	142	1	Defence	Genotype
AT5G49400	zinc knuckle (CCHC-type) family protein	146	1	Metabolism	Genotype
AT5G49770	Leucine-rich repeat protein kinase family protein	919	2	LRR	Genotype
AT5G49830	exocyst complex component 84B	733	2	Metabolism	Genotype
AT5G50760	SAUR55	14	2	Hormone	Genotype

Protein	Name	Phosphosites	Multiplicity	Function	Significant in
AT5G52040	RNA-binding (RRM/RBD/RNP motifs) family protein	320	1	Metabolism	Genotype
AT5G52240	membrane steroid binding protein 1	57	1	Cell growth	Genotype
AT5G53310	myosin heavy chain-related	27	1	Cytoskeleton	Genotype
AT5G53620	RNA polymerase II degradation factor	35	1	Unknown	Genotype
AT5G55230	microtubule-associated proteins 65-1	586	2	Cytoskeleton	Genotype
AT5G55300	TOPOISOMERASE 1	170	1	Cell growth	Genotype
AT5G55310	TOPOISOMERASE 1	131	2	Metabolism	Genotype
AT5G55530	Calcium-dependent lipid-binding (CaLB domain) family protein	388	1	Calcium	Genotype
AT5G55860	Unknown	639	2	Unknown	Genotype
AT5G56950	nucleosome assembly protein 1; 3	48	1	Metabolism	Genotype
AT5G57070	hydroxyproline-rich glycoprotein family protein	570	3	Metabolism	Genotype
AT5G57160	DNA ligase IV	991	1	Metabolism	Genotype

Protein	Name	Phosphosites	Multiplicity	Function	Significant in
AT5G57870	MIF4G domain-containing protein / MA3 domain-containing protein	542	1	Metabolism	Genotype
AT5G59290	UDP-glucuronic acid decarboxylase 3	16	2	Metabolism	Genotype
AT5G60580	RING/U-box superfamily protein	91	1	Metabolism	Genotype
AT5G60660	PLASMA MEMBRANE INTRINSIC PROTEIN 2; 4	283	2	Transport	Genotype
AT5G61960	MEI2-like protein 1	430	1	Metabolism	Genotype
AT5G62190	DEAD box RNA helicase (PRH75)	40	1	Metabolism	Genotype
AT5G62310	INCOMPLETE ROOT HAIR ELONGATION	457	1	Cell growth	Genotype
AT5G62810	PEROXISOME DEFECTIVE 2	310	1	Metabolism	Genotype
AT5G62810	PEROXISOME DEFECTIVE 2	312	1	Metabolism	Genotype

Protein	Name	Phosphosites	Multiplicity	Function	Significant in
AT5G63260	Zinc finger C-x8-C-x5-C-x3-H type family protein	240	2	Metabolism	Genotype
AT5G63270	RPM1-interacting protein 4 (RIN4) family protein	52	1	Defence	Genotype
AT5G63550	DEK domain-containing chromatin associated protein	238	1	Metabolism	Genotype
AT5G63550	DEK domain-containing chromatin associated protein	15	2	Metabolism	Genotype
AT5G63550	DEK domain-containing chromatin associated protein	10	2	Metabolism	Genotype
AT5G66490	Unknown	43	2	Unknown	Genotype
AT5G66760	SUCCINATE DEHYDROGENASE 1-1	495	1	Metabolism	Genotype
AT5G67340	ARM repeat superfamily protein	390	1	Cytoskeleton	Genotype
AT5G67470	formin homolog 6	196	2	Cytoskeleton	Genotype

Supplementary Table S.4: Phosphosites that are independent of FERONIA but dependent on RALF1 treatment

Protein	Name	Phosphosites	Multiplicity	Function	Significant in
AT1G02900	RALF1	81	2	Cell growth	RALF1
AT1G08050	Zinc finger (C3HC4-type RING finger) family protein	629	1	Metabolism	RALF1
AT1G20450	Dehydrin family protein	218	1	Metabolism	RALF1
AT1G20770	Unknown	135	2	Unknown	RALF1
AT1G24100	UDP-glucosyl transferase 74B1	172	2	Defence	RALF1
AT1G24160	Unknown	58	1	Unknown	RALF1
AT1G32730	Unknown	286	3	Unknown	RALF1
AT1G34220	Regulator of Vps4 activity in the MVB pathway protein	469	2	Trafficking	RALF1
AT1G45545	Unknown	431	1	Unknown	RALF1
AT1G53300	tetratricopetide-repeat thioredoxin-like 1	39	2	Hormone	RALF1
AT1G53300	tetratricopetide-repeat thioredoxin-like 1	42	1	Hormone	RALF1

Protein	Name	Phosphosites	Multiplicity	Function	Significant in
AT1G62390	Octicosapeptide/ Phox/ Bem1p (PB1) domain-containing protein / tetratricopeptide repeat (TPR)-containing protein	216	1	Metabolism	RALF1
AT1G74690	IQ-domain 31	31	1	Calcium	RALF1
AT1G74830	Unknown	265	1	Trafficking	RALF1
AT1G78880	Ubiquitin-specific protease family C19-related protein	163	1	Degradation	RALF1
AT2G16405	Transducin/WD40 repeat-like superfamily protein	96	2	Metabolism	RALF1
AT2G16485	nucleic acid binding	1430	1	Metabolism	RALF1
AT2G21270	ubiquitin fusion degradation 1	222	1	Degradation	RALF1
AT2G24590	RNA recognition motif and CCHC-type zinc finger domains containing protein	136	1	Metabolism	RALF1
AT3G05420	acyl-CoA binding protein 4	509	1	Cell growth	RALF1

Protein	Name	Phosphosites	Multiplicity	Function	Significant in
AT3G12020	P-loop containing nucleoside triphosphate hydrolases superfamily protein	581	1	Cytoskeleton	RALF1
AT3G13920	eif4a-2	140	1	Calcium	RALF1
AT3G17850	Protein kinase superfamily protein	509	1	Cell growth	RALF1
AT3G19370	Unknown	59	1	Unknown	RALF1
AT3G19370	Unknown	355	1	Unknown	RALF1
AT3G19640	magnesium transporter 4	345	1	Transport	RALF1
AT3G20250	pumilio 5	527	1	Defence	RALF1
AT3G24080	KRR1 family protein	178	2	Metabolism	RALF1
AT3G27320	alpha/beta-Hydrolases superfamily protein	142	1	Metabolism	RALF1
AT3G49590	Autophagy-related protein 14	407	1	Degradation	RALF1
AT3G55270	mitogen-activated protein kinase phosphatase 1	572	2	MAPK	RALF1
AT3G57410	villin 3	809	1	Cytoskeleton	RALF1
AT3G60240	eukaryotic translation initiation factor 4G	1064	2	Metabolism	RALF1

Protein	Name	Phosphosites	Multiplicity	Function	Significant in
AT3G60240	eukaryotic translation initiation factor 4G	1067	1	Metabolism	RALF1
AT3G60860	SEC7-like guanine nucleotide exchange family protein	1309	2	Trafficking	RALF1
AT4G01810	Sec23/Sec24 protein transport family protein	66	2	Trafficking	RALF1
AT4G02510	translocon at the outer envelope membrane of chloroplasts 159	609	1	Metabolism	RALF1
AT4G10840	Tetratricopeptide repeat (TPR)-like superfamily protein	581	2	Trafficking	RALF1
AT4G16830	Hyaluronan / mRNA binding family	341	1	Hormone	RALF1
AT4G17770	trehalose phosphatase/synthase 5	21	1	Metabolism	RALF1
AT4G25500	arginine/serine-rich splicing factor 35	294	2	Metabolism	RALF1
AT4G31880	Unknown	838	2	Metabolism	RALF1
AT4G34860	Plant neutral invertase family protein	83	2	Metabolism	RALF1

Protein	Name	Phosphosites	Multiplicity	Function	Significant in
AT5G04420	Galactose oxidase/kelch repeat superfamily protein	82	2	Unknown	RALF1
AT5G06140	sorting nexin 1	11	1	Hormone	RALF1
AT5G16300	Vps51/Vps67 family (components of vesicular transport) protein	660	1	Trafficking	RALF1
AT5G24880	Unknown	85	1	Calcium	RALF1
AT5G38640	NagB/ RpiA/ CoA transferase-like superfamily protein	85	2	Metabolism	RALF1
AT5G43830	Aluminium induced protein with YGL and LRDR motifs	18	2	Unknown	RALF1
AT5G46070	Guanylate-binding family protein	20	1	Metabolism	RALF1
AT5G52530	dentin sialophosphoprotein-related	88	1	Unknown	RALF1
AT5G56140	RNA-binding KH domain-containing protein	155	1	Metabolism	RALF1

Protein	Name	Phosphosites	Multiplicity	Function	Significant in
AT5G58040	homolog of yeast FIP1 [V]	522	1	Metabolism	RALF1
AT5G58620	zinc finger (CCCH-type) family protein	435	1	Metabolism	RALF1
AT5G64740	cellulose synthase 6	136	2	Cell growth	RALF1
AT5G65910	BSD domain-containing protein	38	1	Unknown	RALF1

Supplementary Table S.5: Potential ROP2 and ROP6 interactors from seedling GFP CoIPs

Accession	Name	Category	Significant in
AT1G01610	Glycerol-3-phosphate 2-O-acyltransferase 4	Metabolism	ROP2 and ROP6
AT1G04270	Cytoskeletonsolic ribosomal protein S15	Potential contaminant	ROP2 and ROP6
AT1G10670	ATP-citrate lyase A-1	Metabolism	ROP2 and ROP6
AT1G12840	V-type proton ATPase subunit C	proton transport	ROP2 and ROP6
AT1G15500	ADP,ATP carrier protein	Potential contaminant	ROP2 and ROP6
AT1G20020	Unknown	Potential contaminant	ROP2 and ROP6

Accession	Name	Category	Significant in
AT1G20090	RAC-like GTP-binding protein ARAC4	ROP	ROP2 and ROP6
AT1G20200	26S Degradation non-ATPase regulatory subunit 3 homolog A	Degradation	ROP2 and ROP6
AT1G25490	Serine/threonine-protein phosphatase 2A	Hormone	ROP2 and ROP6
AT1G27450	Adenine phosphoribosyl transferase 1	Potential contaminant	ROP2 and ROP6
AT1G29920	Chlorophyll a-b binding protein 2	Potential contaminant	ROP2 and ROP6
AT1G30380	AT1G30380 protein	Potential contaminant	ROP2 and ROP6
AT1G30630	Coatomer subunit epsilon-1	Trafficking	ROP2 and ROP6
AT1G55020	Linoleate 9S-lipoxygenase 1	Root	ROP2 and ROP6
AT1G63660	GMP synthase (Glutamine-hydrolyzing)	Metabolism	ROP2 and ROP6
AT1G64090	Reticulon-like protein	Trafficking	ROP2 and ROP6
AT1G64790	ILITYHIA	Defence	ROP2 and ROP6

Accession	Name	Category	Significant in
AT1G69830	Alpha-amylase 3	Potential contaminant	ROP2 and ROP6
AT1G70320	E3 ubiquitin-protein ligase UPL2	Degradation	ROP2 and ROP6
AT1G71880	Sucrose transport protein SUC1	Metabolism	ROP2 and ROP6
AT1G72150	Putative Cytoskeletonsolic factor protein	Trafficking	ROP2 and ROP6
AT1G79340	Metacaspase-4	Defence	ROP2 and ROP6
AT1G80480	At1g80480 (Plastid transcriptionally active 17)	Potential contaminant	ROP2 and ROP6
AT2G02560	CAND1	Cell growth	ROP2 and ROP6
AT2G04030	Heat shock protein 90-5	Potential contaminant	ROP2 and ROP6
AT2G14720	Vacuolar-sorting receptor 4	Trafficking	ROP2 and ROP6
AT2G16950	Transportin-1	Trafficking	ROP2 and ROP6
AT2G17840	Protein EARLY-RESPONSIVE TO DEHYDRATION 7	Potential contaminant	ROP2 and ROP6
AT2G20760	Clathrin light chain 1	Trafficking	ROP2 and ROP6
AT2G21160	Translocon-associated protein	Trafficking	ROP2 and ROP6

Accession	Name	Category	Significant in
AT2G22125	CellULOSE SYNTHASE INTERACTIVE 1	Cell growth	ROP2 and ROP6
AT2G24820	Protein TIC 55	Potential contaminant	ROP2 and ROP6
AT2G31660	Importin beta-like SAD2	Trafficking	ROP2 and ROP6
AT2G31810	AT2G31810 protein	Potential contaminant	ROP2 and ROP6
AT2G33450	50S ribosomal protein L28	Potential contaminant	ROP2 and ROP6
AT2G38040	Carboxyltransferase alpha subunit	Potential contaminant	ROP2 and ROP6
AT2G38550	Protein FATTY ACID EXPORT 3	Potential contaminant	ROP2 and ROP6
AT2G45820	Remorin (DNA-binding protein)	Unknown	ROP2 and ROP6
AT2G46520	Putative Cellular apoptosis susceptibility protein	Trafficking	ROP2 and ROP6
AT2G46820	AT2G46820 protein	Potential contaminant	ROP2 and ROP6
AT2G47650	UDP-xylose synthase 4	Trafficking	ROP2 and ROP6
AT3G02260	BIG	Hormone	ROP2 and ROP6
AT3G02530	T-complex protein 1 subunit zeta 1	chaperone	ROP2 and ROP6

Accession	Name	Category	Significant in
AT3G07770	Heat shock protein 90-6	Potential contaminant	ROP2 and ROP6
AT3G07880	Rho GDP-dissociation inhibitor 1	ROP	ROP2 and ROP6
AT3G08943	ARM repeat superfamily protein	Potential contaminant	ROP2 and ROP6
AT3G10610	40S ribosomal protein S17-3	Potential contaminant	ROP2 and ROP6
AT3G15480	MJK13_14	Unknown	ROP2 and ROP6
AT3G17020	Adenine nucleotide alpha hydrolases-like superfamily protein	Metabolism	ROP2 and ROP6
AT3G18820	RABG3f	Trafficking	ROP2 and ROP6
AT3G20050	T-complex protein 1 subunit alpha	chaperone	ROP2 and ROP6
AT3G26740	Light-regulated protein 1	Potential contaminant	ROP2 and ROP6
AT3G27820	Monodehydroascorbate reductase 4	Potential contaminant	ROP2 and ROP6
AT3G28300	UPF0496 protein At3g28300	Unknown	ROP2 and ROP6
AT3G42050	AT3G42050 protein	proton transport	ROP2 and ROP6
AT3G43300	BIG5	Trafficking	ROP2 and ROP6
AT3G48140	B12D	Unknown	ROP2 and ROP6

Accession	Name	Category	Significant in
AT3G53990	Adenine nucleotide alpha hydrolases-like superfamily protein	Unknown	ROP2 and ROP6
AT3G54470	Unknown	Metabolism	ROP2 and ROP6
AT3G56190	Alpha-soluble NSF attachment protein 2	Trafficking	ROP2 and ROP6
AT3G57280	Protein FATTY ACID EXPORT 1	Potential contaminant	ROP2 and ROP6
AT3G58730	Vacuolar-type H+-ATPase (V-ATPase) subunit D	proton transport	ROP2 and ROP6
AT3G59020	ARM repeat superfamily protein	Trafficking	ROP2 and ROP6
AT3G61430	PIP1-1	TM	ROP2 and ROP6
AT3G61470	Photosystem I chlorophyll a/b-binding protein 2	Potential contaminant	ROP2 and ROP6
AT3G62530	Unknown	Potential contaminant	ROP2 and ROP6
AT3G63410	AT3G63410 protein	Potential contaminant	ROP2 and ROP6
AT3G63460	Transducin family protein / WD-40 repeat family protein	Trafficking	ROP2 and ROP6
AT4G01690	Protoporphyrinogen oxidase 1	Potential contaminant	ROP2 and ROP6

Accession	Name	Category	Significant in
AT4G03280	Cytoskeletonchrome b6-f complex iron-sulfur subunit	Potential contaminant	ROP2 and ROP6
AT4G11150	V-type proton ATPase subunit E1	Potential contaminant	ROP2 and ROP6
AT4G16370	OPT3	Metabolism	ROP2 and ROP6
AT4G17170	RABB1c	Trafficking	ROP2 and ROP6
AT4G17530	RABD2c	Trafficking	ROP2 and ROP6
AT4G23630	Reticulon-like protein	Unknown	ROP2 and ROP6
AT4G27640	AT4G27640 protein	Trafficking	ROP2 and ROP6
AT4G29480	Mitochondrial ATP synthase subunit G protein	Potential contaminant	ROP2 and ROP6
AT4G33250	Unknown	Translation	ROP2 and ROP6
AT4G33510	Phospho-2-dehydro-3-deoxyheptonate aldolase	Potential contaminant	ROP2 and ROP6
AT4G34450	Coatomer subunit gamma	Trafficking	ROP2 and ROP6
AT4G34620	30S ribosomal protein S16-1	Potential contaminant	ROP2 and ROP6
AT4G35000	L-ascorbate peroxidase 3	Potential contaminant	ROP2 and ROP6
AT4G35020	RAC-like 3	ROP	ROP2 and ROP6
AT4G35100	Unknown	TM	ROP2 and ROP6

Accession	Name	Category	Significant in
AT4G35260	Isocitrate dehydrogenase [NAD] regulatory subunit 1	Potential contaminant	ROP2 and ROP6
AT4G35790	Phospholipase D	Calcium	ROP2 and ROP6
AT4G36250	Aldehyde dehydrogenase family 3 member F1	Metabolism	ROP2 and ROP6
AT4G38510	ATPase, V1 complex, subunit B protein	Cytoskeleton	ROP2 and ROP6
AT4G38630	REGULATORY PARTICLE NON-ATPASE 10	Degradation	ROP2 and ROP6
AT4G39980	Phospho-2-dehydro-3-deoxyheptonate aldolase 1	Potential contaminant	ROP2 and ROP6
AT5G01220	SQD2	Potential contaminant	ROP2 and ROP6
AT5G03880	Thioredoxin family protein	Potential contaminant	ROP2 and ROP6
AT5G08540	Ribosomal RNA small subunit methyltransferase J	Potential contaminant	ROP2 and ROP6
AT5G10450	14-3-3-like protein GF14 lambda	Cell growth	ROP2 and ROP6
AT5G12250	Tubulin beta-6 chain	Cytoskeleton	ROP2 and ROP6
AT5G12370	AT5G12370 protein	Trafficking	ROP2 and ROP6

Accession	Name	Category	Significant in
AT5G12470	Unknown	Potential contaminant	ROP2 and ROP6
AT5G12860	Dicarboxylate transporter 1	Potential contaminant	ROP2 and ROP6
AT5G13510	50S ribosomal protein L10	Potential contaminant	ROP2 and ROP6
AT5G13630	Magnesium-chelatase subunit chlH	Potential contaminant	ROP2 and ROP6
AT5G14320	EMB3137	Potential contaminant	ROP2 and ROP6
AT5G16620	Protein TIC 40	Potential contaminant	ROP2 and ROP6
AT5G17190	B-Cell receptor-associated-like protein	TM	ROP2 and ROP6
AT5G18660	Divinyl chlorophyllide a 8-vinyl-reductase2	Potential contaminant	ROP2 and ROP6
AT5G19780	Tubulin alpha-5 chain	Cytoskeleton	ROP2 and ROP6
AT5G19820	ARM repeat superfamily protein	Cell growth	ROP2 and ROP6
AT5G26742	DEAD box RNA helicase (RH3)	Potential contaminant	ROP2 and ROP6
AT5G35160	Transmembrane 9 superfamily member	TM	ROP2 and ROP6
AT5G36230	ARM repeat superfamily protein	Translation	ROP2 and ROP6

Accession	Name	Category	Significant in
AT5G39410	Probable mitochondrial saccharopine dehydrogenase-like oxidoreductase	Potential contaminant	ROP2 and ROP6
AT5G40950	50S ribosomal protein L27	Potential contaminant	ROP2 and ROP6
AT5G42570	B-Cell receptor-associated 31-like protein	Trafficking	ROP2 and ROP6
AT5G42650	Allene oxide synthase	Potential contaminant	ROP2 and ROP6
AT5G44340	Tubulin beta-4 chain	Cytoskeleton	ROP2 and ROP6
AT5G46290	3-ketoacyl-acyl carrier protein synthase I	Potential contaminant	ROP2 and ROP6
AT5G46580	Pentatricopeptide repeat-containing protein	Potential contaminant	ROP2 and ROP6
AT5G48810	Cytoskeletonchrome B5 isoform D	Defence	ROP2 and ROP6
AT5G51110	Transcriptional coactivator/pterin dehydratase	Potential contaminant	ROP2 and ROP6
AT5G53480	Importin subunit beta-1	Potential contaminant	ROP2 and ROP6

Accession	Name	Category	Significant in
AT5G54270	Chlorophyll a-b binding protein 3	Potential contaminant	ROP2 and ROP6
AT5G56630	ATP-dependent 6-phosphofructoKinase 7	Kinase	ROP2 and ROP6
AT5G56710	Ribosomal protein L31e family protein	Potential contaminant	ROP2 and ROP6
AT5G64290	Dicarboxylate transporter 2.1	Potential contaminant	ROP2 and ROP6
ATCG00150	ATP synthase subunit a	Potential contaminant	ROP2 and ROP6
ATCG00500	Acetyl-coenzyme A carboxylase carboxyl transferase subunit beta	Potential contaminant	ROP2 and ROP6
ATCG00730	Cytoskeletonchrome b6-f complex subunit 4	Potential contaminant	ROP2 and ROP6
ATCG00770	30S ribosomal protein S8	Potential contaminant	ROP2 and ROP6
ATCG00780	50S ribosomal protein L14	Potential contaminant	ROP2 and ROP6
ATMG00480	ATP synthase protein YMF19	Potential contaminant	ROP2 and ROP6

Supplementary Table S.6: Potential ROP2 or ROP6 interactors from seedling GFP CoIPs

Acession	Name	Category	Significant in
AT1G01080	RNA-binding (RRM/RBD/RNP motifs) family protein	Potential contaminant	ROP2
AT1G01320	Tetratricopeptide repeat (TPR)-like superfamily protein	Metabolism	ROP2
AT1G02150	Pentatricopeptide repeat-containing protein At1g02150	Potential contaminant	ROP2
AT1G03860	Prohibitin-2	Potential contaminant	ROP2
AT1G04170	Eukaryotic Translation initiation factor 2 gamma subunit	Translation	ROP2
AT1G04430	PMT8	Trafficking	ROP2
AT1G04750	Vesicle-associated membrane protein 721	Trafficking	ROP2
AT1G06950	TIC110	Potential contaminant	ROP2
AT1G07670	Endomembrane Ca2+ ATPase 4	Calcium	ROP2
AT1G07890	Unknown	Metabolism	ROP2
AT1G08480	Succinate dehydrogenase subunit 6	Potential contaminant	ROP2
AT1G08520	Magnesium-chelatase subunit ChlD	Potential contaminant	ROP2

Acession	Name	Category	Significant in
AT1G08640	Unknown	Potential contaminant	ROP2
AT1G09310	Unknown	Unknown	ROP2
AT1G09330	Golgi apparatus membrane protein TVP23	Trafficking	ROP2
AT1G09620	Leucine--tRNA ligase	Metabolism	ROP2
AT1G09780	PHOSPHOGLYCERATE MUTASE 1	Metabolism	ROP2
AT1G10510	RNI-like superfamily protein	Potential contaminant	ROP2
AT1G10950	Transmembrane 9 superfamily member	Trafficking	ROP2
AT1G12000	Phosphofructokinase family protein	Metabolism	ROP2
AT1G12010	1-aminocyclopropane-1-carboxylate oxidase 3	Metabolism	ROP2
AT1G14670	Transmembrane 9 superfamily member 2	Trafficking	ROP2
AT1G15120	Ubiquinol-Cytoskeletonchrome C reductase hinge protein	Potential contaminant	ROP2
AT1G15140	FAD/NAD(P)-binding oxidoreductase	Potential contaminant	ROP2
AT1G15950	Cinnamoyl coa reductase 1	Metabolism	ROP2
AT1G16460	Rhodanese homologue 2	Metabolism	ROP2

Acession	Name	Category	Significant in
AT1G16880	Uridylyltransferase-like protein	Potential contaminant	ROP2
AT1G16890	Unknown	Root	ROP2
AT1G20330	24-methylenesterol C-methyltransferase 2	Trafficking	ROP2
AT1G21080	DNAJ heat shock N-terminal domain-containing protein	Trafficking	ROP2
AT1G22300	GENERAL REGULATORY FACTOR 10	chaperone	ROP2
AT1G22410	Phospho-2-dehydro-3-deoxyheptonate aldolase	Potential contaminant	ROP2
AT1G22450	Cytoskeletonchrome c oxidase subunit 6b-1	Potential contaminant	ROP2
AT1G22530	PATELLIN 2	Trafficking	ROP2
AT1G22700	Tetratricopeptide repeat domain-containing protein PYG7	Potential contaminant	ROP2
AT1G23190	Probable phosphoglucomutase	Metabolism	ROP2
AT1G24020	MLP-like protein 423	Defence	ROP2

Acession	Name	Category	Significant in
AT1G24360	3-oxoacyl-[acyl-carrier-protein] reductase	Potential contaminant	ROP2
AT1G24510	TCP-1/cpn60 chaperonin family protein	chaperone	ROP2
AT1G26850	PMT2	Trafficking	ROP2
AT1G26880	Ribosomal protein L34e superfamily protein	Potential contaminant	ROP2
AT1G29150	26S Degradation non-ATPase regulatory subunit 11 homolog	Degradation	ROP2
AT1G29470	Unknown	Trafficking	ROP2
AT1G30360	ERD4	Potential contaminant	ROP2
AT1G32400	Tobamovirus multiplication protein 2A	Defence	ROP2
AT1G32990	50S ribosomal protein L11	Potential contaminant	ROP2
AT1G34430	EMBRYO DEFECTIVE 3003	Potential contaminant	ROP2
AT1G35160	GF14 protein phi chain	Hormone	ROP2
AT1G42960	Unknown	Potential contaminant	ROP2
AT1G43710	Serine decarboxylase	Metabolism	ROP2
AT1G43890	RABC1	Trafficking	ROP2
AT1G44170	Aldehyde dehydrogenase family 3 member H1	Metabolism	ROP2

Acession	Name	Category	Significant in
AT1G44835	YbaK/aminoacyl-tRNA synthetase-associated domain-containing protein	Metabolism	ROP2
AT1G45000	AAA-type ATPase family protein	Degradation	ROP2
AT1G47128	Unknown	Defence	ROP2
AT1G47260	Gamma carbonic anhydrase 2	Potential contaminant	ROP2
AT1G48630	Receptor for activated C Kinase 1B	Kinase	ROP2
AT1G48830	40S ribosomal protein S7-1	Potential contaminant	ROP2
AT1G48900	Signal recognition particle 54 kDa protein	Trafficking	ROP2
AT1G48920	Putative nuM1 protein	Potential contaminant	ROP2
AT1G50200	Alanine--tRNA ligase	Potential contaminant	ROP2
AT1G51980	Insulinase	Potential contaminant	ROP2
AT1G52360	Coatomer subunit beta'	Trafficking	ROP2
AT1G52760	Caffeoylshikimate esterase	Trafficking	ROP2
AT1G53000	Nucleotide-diphospho-sugar transferases superfamily protein	Potential contaminant	ROP2
AT1G53210	Unknown	Calcium	ROP2
AT1G53500	RHM2	Metabolism	ROP2

Acession	Name	Category	Significant in
AT1G53750	26S Degradation regulatory subunit 7 homolog A	Degradation	ROP2
AT1G54270	Unknown	Translation	ROP2
AT1G54780	THYLAKOID LUMEN PROTEIN 18.3	Potential contaminant	ROP2
AT1G55450	S-adenosyl-L-methionine-dependent methyltransferases superfamily protein	Metabolism	ROP2
AT1G56190	Phosphoglycerate Kinase	Potential contaminant	ROP2
AT1G57720	Unknown	Translation	ROP2
AT1G57860	Unknown	Potential contaminant	ROP2
AT1G58290	Glutamyl-tRNA reductase 1	Potential contaminant	ROP2
AT1G59870	Putative ABC transporter	Metabolism	ROP2
AT1G60660	Cytoskeletonchrome B5-like protein	Metabolism	ROP2
AT1G61790	OLIGOSACCHARYL-TRANSFERASE SUBUNIT 3/6	TM	ROP2
AT1G62020	Unknown	Trafficking	ROP2
AT1G62290	Saposin-like aspartyl protease family protein	Metabolism	ROP2
AT1G62390	CLMP1	Metabolism	ROP2

Acession	Name	Category	Significant in
AT1G63000	Unknown	Cell growth	ROP2
AT1G63970	Isoprenoid F	Potential contaminant	ROP2
AT1G64520	26S Degradation non-ATPase regulatory subunit 8 homolog A	Potential contaminant	ROP2
AT1G64650	Major facilitator superfamily protein	Trafficking	ROP2
AT1G65270	ER membrane protein complex subunit-like protein	Trafficking	ROP2
AT1G65960	Glutamate decarboxylase 2	Metabolism	ROP2
AT1G66580	Unknown	Potential contaminant	ROP2
AT1G67350	NADH-ubiquinone oxidoreductase	Potential contaminant	ROP2
AT1G67700	HHL1	Potential contaminant	ROP2
AT1G67730	Very-long-chain 3-oxoacyl-CoA reductase 1	Metabolism	ROP2
AT1G68590	Ribosomal protein PSRP-3/Ycf65	Potential contaminant	ROP2
AT1G69460	Unknown	Trafficking	ROP2
AT1G70770	Unknown	Trafficking	ROP2
AT1G70940	Auxin efflux carrier component	Hormone	ROP2

Acession	Name	Category	Significant in
AT1G71500	Rieske (2Fe-2S) domain-containing protein	Potential contaminant	ROP2
AT1G74060	60S ribosomal protein L6-2	Potential contaminant	ROP2
AT1G75500	WALLS ARE THIN 1	Hormone	ROP2
AT1G75950	SKP1-like protein 1A	Hormone	ROP2
AT1G76200	NADH dehydrogenase [ubiquinone] 1 beta subcomplex subunit 2	Potential contaminant	ROP2
AT1G76400	OLIGOSACCHARYL-TRANSFERASE 1B	Trafficking	ROP2
AT1G77490	Thylakoidal ascorbate peroxidase	Potential contaminant	ROP2
AT1G77590	Long chain acyl-CoA synthetase 9	Potential contaminant	ROP2
AT1G77940	Similar to ribosomal protein L30	Potential contaminant	ROP2
AT1G78300	General regulatory factor 2	Hormone	ROP2
AT1G78630	50S ribosomal protein L13	Potential contaminant	ROP2
AT1G79010	NADH dehydrogenase [ubiquinone] iron-sulfur protein 8-A	Potential contaminant	ROP2
AT1G79040	Unknown	Potential contaminant	ROP2

Acession	Name	Category	Significant in
AT1G79850	30S ribosomal protein S17	Potential contaminant	ROP2
AT1G79920	Heat shock protein 70 (Hsp 70) family protein	chaperone	ROP2
AT1G79940	DnaJ / Sec63 Brl domains-containing protein	Trafficking	ROP2
AT1G80030	Molecular chaperone Hsp40/DnaJ family protein	Potential contaminant	ROP2
AT1G80300	ADP,ATP carrier protein	Potential contaminant	ROP2
AT1G80410	Tetratricopeptide repeat (TPR)-containing protein	Metabolism	ROP2
AT2G01250	Ribosomal protein L30/L7 family protein	Potential contaminant	ROP2
AT2G01350	Quinolinate phoshoribosyltransferase	Potential contaminant	ROP2
AT2G01470	SEC12-like protein 2	Trafficking	ROP2
AT2G01970	Transmembrane 9 superfamily member 3	Trafficking	ROP2
AT2G02050	NADH dehydrogenase [ubiquinone] 1 beta subcomplex subunit 7	Potential contaminant	ROP2
AT2G02510	NADH dehydrogenase [ubiquinone] 1 beta subcomplex subunit 3-A	Potential contaminant	ROP2

Acession	Name	Category	Significant in
AT2G04350	Long chain acyl-CoA synthetase 8	Metabolism	ROP2
AT2G04842	Threonine--tRNA ligase, chloroplastic/mitochondrial 2	Potential contaminant	ROP2
AT2G05310	Unknown	Unknown	ROP2
AT2G05830	NagB/ RpiA/ CoA transferase-like superfamily protein	Metabolism	ROP2
AT2G10940	Bifunctional inhibitor/lipid-transfer protein/ seed storage 2S albumin superfamily protein	Unknown	ROP2
AT2G14880	SWIB/MDM2 domain superfamily protein	Unknown	ROP2
AT2G16060	Non-symbiotic hemoglobin 1	Metabolism	ROP2
AT2G19680	Copia-like retroelement pol polyprotein	Potential contaminant	ROP2
AT2G19860	Phosphotransferase	Potential contaminant	ROP2
AT2G20260	Photosystem I reaction center subunit IV B	Potential contaminant	ROP2

Acession	Name	Category	Significant in
AT2G20360	NADH dehydrogenase [ubiquinone] 1 alpha subcomplex subunit 9	Potential contaminant	ROP2
AT2G21870	MALE GAMETOPHYTE DEFECTIVE 1	Metabolism	ROP2
AT2G22250	PREPHENATE AMINOTRANSFERASE	Potential contaminant	ROP2
AT2G22425	Probable signal peptidase complex subunit 1	Trafficking	ROP2
AT2G24020	Nucleoid-associated protein	Potential contaminant	ROP2
AT2G25310	ER membrane protein complex subunit-like protein	Metabolism	ROP2
AT2G25450	Probable 2-oxoacid dependent dioxygenase	Metabolism	ROP2
AT2G26250	3-ketoacyl-CoA synthase 10	Metabolism	ROP2
AT2G27530	60S ribosomal protein L10a-2	Potential contaminant	ROP2
AT2G27720	60S acidic ribosomal protein family	Potential contaminant	ROP2
AT2G28800	Unknown	Potential contaminant	ROP2
AT2G28900	Outer envelope pore protein 16-1	Potential contaminant	ROP2

Acession	Name	Category	Significant in
AT2G30490	Trans-cinnamate 4-monooxygenase	Metabolism	ROP2
AT2G30740	PTI1-like tyrosine-protein Kinase 2	Kinase	ROP2
AT2G30930	Unknown	Unknown	ROP2
AT2G30950	FtsH extraCellular protease family	Potential contaminant	ROP2
AT2G32060	40S ribosomal protein S12-2	Potential contaminant	ROP2
AT2G32240	Early endosome antigen	Unknown	ROP2
AT2G32720	Cytoskeletonchrome B5 isoform B	Metabolism	ROP2
AT2G32730	26S Degradation non-ATPase regulatory subunit 1 homolog A	Degradation	ROP2
AT2G33150	3-ketoacyl-CoA thiolase 2	Metabolism	ROP2
AT2G33210	Heat shock protein 60-2	Metabolism	ROP2
AT2G33220	GRIM-19 protein	Potential contaminant	ROP2
AT2G33800	Unknown	Potential contaminant	ROP2
AT2G34250	SecY protein transport family protein	Trafficking	ROP2
AT2G35840	Probable sucrose-phosphatase 2	Metabolism	ROP2
AT2G36250	Tubulin/FtsZ family protein	Cytoskeleton	ROP2

Acession	Name	Category	Significant in
AT2G36580	Pyruvate Kinase	Kinase	ROP2
AT2G38280	EMBRYONIC FACTOR 1	Potential contaminant	ROP2
AT2G38670	PECT1	Potential contaminant	ROP2
AT2G38750	Annexin 4	Calcium	ROP2
AT2G39990	eIF3f	Translation	ROP2
AT2G40660	Putative methionyl-tRNA synthetase	Translation	ROP2
AT2G40765	Ubiquinol-- Cytoskeletonchrome-c reductase	Unknown	ROP2
AT2G41560	Calcium-transporting ATPase	Calcium	ROP2
AT2G44610	RABH1b	Trafficking	ROP2
AT2G44640	TRIGALACTO-SYLDIACYLGLYCEROL-like protein	Potential contaminant	ROP2
AT2G44690	ROP8	rop	ROP2
AT2G45300	3-phosphoshikimate 1-carboxyvinyltransferase	Potential contaminant	ROP2
AT2G46650	Cytoskeletonchrome B5 isoform C	Metabolism	ROP2
AT2G47320	Peptidyl-prolyl cis-trans isomerase CYP21-3	Potential contaminant	ROP2
AT2G47510	Unknown	Potential contaminant	ROP2

Acession	Name	Category	Significant in
AT2G47840	Protein TIC 20-II	Potential contaminant	ROP2
AT3G01280	Mitochondrial outer membrane protein porin 1	Potential contaminant	ROP2
AT3G01340	SEC13-like protein A	Trafficking	ROP2
AT3G01390	V-type proton ATPase subunit G1	proton transport	ROP2
AT3G02090	Unknown	Potential contaminant	ROP2
AT3G02360	6-phosphogluconate dehydrogenase	Potential contaminant	ROP2
AT3G02420	Dihydroflavonol 4-reductase/flavanone protein	Unknown	ROP2
AT3G02520	General regulatory factor 7	Metabolism	ROP2
AT3G03100	NADH dehydrogenase [ubiquinone] 1 alpha subcomplex subunit 12	Potential contaminant	ROP2
AT3G03780	METHIONINE SYNTHASE 2	Metabolism	ROP2
AT3G03960	T-complex protein 1 subunit theta	chaperone	ROP2
AT3G04120	Glyceraldehyde-3-phosphate dehydrogenase GAPC1	Metabolism	ROP2

Acession	Name	Category	Significant in
AT3G05230	Signal peptidase complex subunit 3	Trafficking	ROP2
AT3G05900	Neurofilament protein-like protein	Unknown	ROP2
AT3G05970	Long chain acyl-CoA synthetase 6	Metabolism	ROP2
AT3G07680	Transmembrane emp24 domain-containing protein p24beta2	Trafficking	ROP2
AT3G08920	Rhodanese-like domain-containing protein 10	Potential contaminant	ROP2
AT3G10380	Subunit of exocyst complex 8	Trafficking	ROP2
AT3G11070	Outer membrane OMP85 family protein	Potential contaminant	ROP2
AT3G11820	Syntaxin-121	Trafficking	ROP2
AT3G11830	T-complex protein 1 subunit eta	chaperone	ROP2
AT3G11930	Adenine nucleotide alpha hydrolases-like superfamily protein	chaperone	ROP2
AT3G12050	Aha1 domain-containing protein	chaperone	ROP2

Acession	Name	Category	Significant in
AT3G12290	Bifunctional protein FolD 2	Metabolism	ROP2
AT3G12390	Nascent polypeptide-associated complex subunit alpha-like protein 1	Metabolism	ROP2
AT3G13772	Transmembrane 9 superfamily member 7	Metabolism	ROP2
AT3G13870	RHD3	Root	ROP2
AT3G14110	Tetratricopeptide repeat (TPR)-like superfamily protein	Potential contaminant	ROP2
AT3G14420	Aldolase-type TIM barrel family protein	Metabolism	ROP2
AT3G14840	LYSM RLK1-INTERACTING KINASE 1	Kinase	ROP2
AT3G16000	MAR-binding filament-like protein 1	Potential contaminant	ROP2
AT3G16480	Unknown	Potential contaminant	ROP2
AT3G16640	Translationally-controlled tumor protein 1	Hormone	ROP2
AT3G17970	Translocon at the outer membrane of chloroplasts 64-III	Potential contaminant	ROP2

Acession	Name	Category	Significant in
AT3G22200	Gamma-aminobutyrate transaminase POP2	Potential contaminant	ROP2
AT3G24430	Fe-S cluster assembly factor HCF101	Potential contaminant	ROP2
AT3G26070	Probable plastid-lipid-associated protein 4	Potential contaminant	ROP2
AT3G27080	Mitochondrial import receptor subunit TOM20-3	Potential contaminant	ROP2
AT3G27240	Cytoskeletonchrome c1	Potential contaminant	ROP2
AT3G27570	Unknown	Unknown	ROP2
AT3G29360	UDP-glucose 6-dehydrogenase 2	Metabolism	ROP2
AT3G32930	6,7-dimethyl-8-ribityllumazine synthase	Potential contaminant	ROP2
AT3G44110	DNAJ homologue 3	chaperone	ROP2
AT3G44330	Unknown	Trafficking	ROP2
AT3G46440	UDP-glucuronic acid decarboxylase 5	Metabolism	ROP2
AT3G46740	Chloroplast import-associated channel protein homolog	Potential contaminant	ROP2
AT3G47520	Unknown	Potential contaminant	ROP2

Acession	Name	Category	Significant in
AT3G47930	L-galactono-1,4-lactone dehydrogenase	Potential contaminant	ROP2
AT3G48680	Unknown	Potential contaminant	ROP2
AT3G48750	Cyclin-dependent Kinase A-1	Kinase	ROP2
AT3G48870	Clp ATPase	Potential contaminant	ROP2
AT3G48930	40S ribosomal protein S11-1	Potential contaminant	ROP2
AT3G49140	Unknown	Unknown	ROP2
AT3G49560	Chloroplastic import inner membrane translocase subunit HP30-1	Potential contaminant	ROP2
AT3G49720	Probable pectin methylesterase	Trafficking	ROP2
AT3G51140	DnaJ	Potential contaminant	ROP2
AT3G51160	GDP-mannose 4,6 dehydratase 2	Root	ROP2
AT3G51460	Phosphoinositide phosphatase SAC7	Root	ROP2
AT3G51820	Chlorophyll synthase	Potential contaminant	ROP2
AT3G52180	Dual specificity protein phosphatase (DsPTP1) family protein	Potential contaminant	ROP2

Acession	Name	Category	Significant in
AT3G52730	Ubiquinol-Cytoskeletonchrome C reductase UQCRX/QCR9-like family protein	Potential contaminant	ROP2
AT3G53110	DEAD-box ATP-dependent RNA helicase 38	Metabolism	ROP2
AT3G54110	Mitochondrial uncoupling protein 1	Potential contaminant	ROP2
AT3G54840	Ras-related small GTP-binding family protein	Trafficking	ROP2
AT3G55360	Very-long-chain enoyl-CoA reductase	Metabolism	ROP2
AT3G55750	60S ribosomal protein L35a-4	Potential contaminant	ROP2
AT3G56150	eIF3c	Translation	ROP2
AT3G56340	40S ribosomal protein S26-3	Potential contaminant	ROP2
AT3G56430	Import inner membrane translocase subunit	Potential contaminant	ROP2
AT3G57020	STRICTOSIDINE SYNTHASE-LIKE 9	Metabolism	ROP2

Acession	Name	Category	Significant in
AT3G57030	STRICTOSIDINE SYNTHASE-LIKE 10	Metabolism	ROP2
AT3G57290	eIF3e	Degradation	ROP2
AT3G57650	1-acyl-sn-glycerol-3-phosphate acyltransferase 2	Metabolism	ROP2
AT3G58140	Phenylalanine--tRNA ligase, chloroplastic/mitochondrial	Potential contaminant	ROP2
AT3G58500	Serine/threonine-protein phosphatase PP2A-4	Root	ROP2
AT3G58510	DEAD-box ATP-dependent RNA helicase 11	Metabolism	ROP2
AT3G59540	60S ribosomal protein L38	Potential contaminant	ROP2
AT3G59780	Rhodanese/Cell cycle control phosphatase superfamily protein	Potential contaminant	ROP2
AT3G61260	Unknown	Unknown	ROP2
AT3G61870	Unknown	Potential contaminant	ROP2
AT3G62120	Class II aaRS and biotin synthetases superfamily protein	Metabolism	ROP2
AT3G62360	Carbohydrate-binding-like fold	TM	ROP2

Acession	Name	Category	Significant in
AT3G63160	Unknown	Potential contaminant	ROP2
AT3G63490	Ribosomal protein	Potential contaminant	ROP2
AT4G00630	K+ efflux antiporter 2	Potential contaminant	ROP2
AT4G00860	AT0ZI1 protein	Defence	ROP2
AT4G02080	SAR1A	Trafficking	ROP2
AT4G02510	Translocase of chloroplast 159	Potential contaminant	ROP2
AT4G02580	Unknown	Potential contaminant	ROP2
AT4G04200	Microsomal signal peptidase 25 kDa subunit	Potential contaminant	ROP2
AT4G04910	Vesicle-fusing ATPase	Trafficking	ROP2
AT4G10480	Nascent polypeptide-associated complex (NAC)	Unknown	ROP2
AT4G10790	Plant UBX domain-containing protein 10	TM	ROP2
AT4G11420	eIF3a	Translation	ROP2
AT4G12800	Photosystem I subunit l	Potential contaminant	ROP2
AT4G13770	REDUCED EPIDERMAL FLUORESCENCE 2	Trafficking	ROP2
AT4G14320	Zinc-binding ribosomal protein family protein	Potential contaminant	ROP2
AT4G14360	PMT3	Trafficking	ROP2
AT4G14960	Tubulin alpha chain	Cytoskeleton	ROP2

Acession	Name	Category	Significant in
AT4G15000	Ribosomal L27e protein family	Potential contaminant	ROP2
AT4G15560	1-deoxy-D-xylulose-5-phosphate synthase	Potential contaminant	ROP2
AT4G16390	Pentatricopeptide repeat-containing protein	Potential contaminant	ROP2
AT4G16450	Unknown	TM	ROP2
AT4G16500	Cysteine proteinase inhibitor 4	Defence	ROP2
AT4G19006	Degradation component (PCI) domain protein	Degradation	ROP2
AT4G19210	ABC transporter E family member 2	Potential contaminant	ROP2
AT4G21150	Ribophorin II (RPN2) family protein	Metabolism	ROP2
AT4G22890	PGR5-LIKE A	Potential contaminant	ROP2
AT4G23650	Calcium-dependent protein Kinase 3	Kinase	ROP2
AT4G23850	Long chain acyl-CoA synthetase 4	Metabolism	ROP2
AT4G24750	Rhodanese-like domain-containing protein 11	Potential contaminant	ROP2

Acession	Name	Category	Significant in
AT4G24820	26S Degradation non-ATPase regulatory subunit 6 homolog	Degradation	ROP2
AT4G25080	Magnesium-protoporphyrin IX methyltransferase	Potential contaminant	ROP2
AT4G25140	Oleosin	TM	ROP2
AT4G25450	Non-intrinsic ABC protein 8	TM	ROP2
AT4G25650	Protochlorophyllide-dependent translocon component 52	Potential contaminant	ROP2
AT4G26300	Arginyl-tRNA synthetase, class Ic	Potential contaminant	ROP2
AT4G26500	SufE-like protein 1	Potential contaminant	ROP2
AT4G27585	STOMATIN-LIKE PROTEIN 1	Potential contaminant	ROP2
AT4G27700	Rhodanese-like domain-containing protein 14	Potential contaminant	ROP2
AT4G28080	TSS	Metabolism	ROP2
AT4G28750	Unknown	Potential contaminant	ROP2
AT4G29040	26S Degradation regulatory subunit 4 homolog A	Potential contaminant	ROP2

Acession	Name	Category	Significant in
AT4G29130	Phosphotransferase	Metabolism	ROP2
AT4G30010	Unknown	Potential contaminant	ROP2
AT4G30190	ATPase 2, plasma membrane-type	proton transport	ROP2
AT4G30950	Omega-6 fatty acid desaturase	Potential contaminant	ROP2
AT4G31340	Myosin heavy chain-like protein	Unknown	ROP2
AT4G31490	Coatomer subunit beta-2	Trafficking	ROP2
AT4G31500	Cytoskeletonchrome P450 83B1	Metabolism	ROP2
AT4G31700	Ribosomal protein S6	Potential contaminant	ROP2
AT4G31830	Unknown	TM	ROP2
AT4G32470	Cytoskeletonchrome b-c1 complex subunit 7	Potential contaminant	ROP2
AT4G33360	NAD(P)-binding Rossmann-fold superfamily protein	Metabolism	ROP2
AT4G33865	Ribosomal S29 subunit	Potential contaminant	ROP2
AT4G35250	NAD(P)-binding Rossmann-fold superfamily protein	Potential contaminant	ROP2
AT4G36130	60S ribosomal protein L8-3	Potential contaminant	ROP2

Acession	Name	Category	Significant in
AT4G36220	Cytoskeletonchrome P450 84A1	Metabolism	ROP2
AT4G38350	Patched family protein	TM	ROP2
AT4G39080	V-type proton ATPase subunit a3	Potential contaminant	ROP2
AT4G39150	DNAJ heat shock N-terminal domain-containing protein	Unknown	ROP2
AT4G39330	Probable cinnamyl alcohol dehydrogenase 9	Metabolism	ROP2
AT4G39460	S-adenosylmethionine carrier 1	Potential contaminant	ROP2
AT4G39960	Molecular chaperone Hsp40/DnaJ family protein	Potential contaminant	ROP2
AT4G39990	RABA4b	Cell growth	ROP2
AT5G01590	TIC 56	Potential contaminant	ROP2
AT5G02960	40S ribosomal protein S23-2	Potential contaminant	ROP2
AT5G03940	Signal recognition particle 54 kDa protein	Potential contaminant	ROP2
AT5G04740	ACT domain-containing protein	Potential contaminant	ROP2
AT5G05010	Coatomer subunit delta	Trafficking	ROP2
AT5G05170	CESA3	Cell growth	ROP2

Acession	Name	Category	Significant in
AT5G05780	RP non-ATPase subunit 8A	Degradation	ROP2
AT5G08060	Unknown	Potential contaminant	ROP2
AT5G08530	NADH dehydrogenase	Potential contaminant	ROP2
AT5G08570	Pyruvate Kinase	Kinase	ROP2
AT5G09870	Cellulose synthase A catalytic subunit 5	Cell growth	ROP2
AT5G09900	26S Degradation regulatory subunit	Degradation	ROP2
AT5G10780	ER membrane protein complex subunit-like protein	Trafficking	ROP2
AT5G10840	Transmembrane 9 superfamily member 8	TM	ROP2
AT5G10860	CBS domain-containing protein CBSX3	Potential contaminant	ROP2
AT5G11560	Catalytics	Trafficking	ROP2
AT5G11770	NADH dehydrogenase	Potential contaminant	ROP2
AT5G13110	Glucose-6-phosphate 1-dehydrogenase	Potential contaminant	ROP2
AT5G13430	Cytoskeletonchrome b-c1 complex subunit Rieske-1	Potential contaminant	ROP2
AT5G13450	Delta subunit of Mt ATP synthase	Potential contaminant	ROP2

Acession	Name	Category	Significant in
AT5G13650	Elongation factor family protein	Potential contaminant	ROP2
AT5G13710	Cycloartenol-C-24-methyltransferase	Metabolism	ROP2
AT5G14030	TRAPB	Trafficking	ROP2
AT5G15090	Mitochondrial outer membrane protein porin 3	Potential contaminant	ROP2
AT5G15450	Chaperone protein ClpB3	Potential contaminant	ROP2
AT5G16130	40S ribosomal protein S7-3	Potential contaminant	ROP2
AT5G16660	Low-density receptor-like protein	Trafficking	ROP2
AT5G17020	EXPORTIN 1A	Trafficking	ROP2
AT5G19370	Rhodanese-like/PpiC domain-containing protein 12	Potential contaminant	ROP2
AT5G19760	Oxoglutarate/malate translocator-like protein	Potential contaminant	ROP2
AT5G19940	Plastid-lipid associated protein PAP / fibrillin family protein	Potential contaminant	ROP2
AT5G20890	T-complex protein 1 subunit beta	Cytoskeleton	ROP2
AT5G20920	eIF2-beta	Translation	ROP2
AT5G23300	Dihydroorotate dehydrogenase (quinone)	Potential contaminant	ROP2

Acession	Name	Category	Significant in
AT5G23540	Mov34/MPN/PAD-1 family protein	Degradation	ROP2
AT5G23575	Unknown	TM	ROP2
AT5G23860	Tubulin beta-8 chain	Cytoskeleton	ROP2
AT5G24650	Chloroplastic import inner membrane translocase subunit HP30-2	Potential contaminant	ROP2
AT5G24690	Unknown	Potential contaminant	ROP2
AT5G25100	Transmembrane 9 superfamily member	TM	ROP2
AT5G25940	Early nodulin-like protein	TM	ROP2
AT5G26360	T-complex protein 1 subunit gamma	chaperone	ROP2
AT5G26710	Glutamate--tRNA ligase	Metabolism	ROP2
AT5G27540	Unknown	Potential contaminant	ROP2
AT5G27600	Long chain acyl-CoA synthetase 7	Metabolism	ROP2
AT5G27640	eIF3b	Translation	ROP2
AT5G28840	GDP-mannose 3',5'-epimerase	Metabolism	ROP2
AT5G30510	Unknown	Potential contaminant	ROP2
AT5G37510	Unknown	Potential contaminant	ROP2
AT5G38480	General regulatory factor 3	Cell growth	ROP2
AT5G38660	Unknown	Potential contaminant	ROP2

Acession	Name	Category	Significant in
AT5G40770	ENHANCED ETHYLENE RESPONSE 3	Root	ROP2
AT5G40810	Cytoskeletonchrome c1 2, heme protein	Potential contaminant	ROP2
AT5G41520	RNA binding Plectin/S10 domain-containing protein	Hormone	ROP2
AT5G41670	6-phosphogluconate dehydrogenase	Potential contaminant	ROP2
AT5G42960	Outer envelope pore protein 24B	Potential contaminant	ROP2
AT5G43060	Probable cysteine protease RD21B	Metabolism	ROP2
AT5G44650	Ycf3-interacting protein 1	Potential contaminant	ROP2
AT5G45750	RABA1c	Trafficking	ROP2
AT5G45970	ROP7	ROP	ROP2
AT5G46110	Glucose-6-phosphate/phosphate translocator-like protein	Potential contaminant	ROP2
AT5G46430	60S ribosomal protein L32-2	Potential contaminant	ROP2
AT5G46800	Mitochondrial carnitine/acylcarnitine carrier-like protein	Potential contaminant	ROP2

Acession	Name	Category	Significant in
AT5G47190	50S ribosomal protein L19-2	Potential contaminant	ROP2
AT5G47200	RABD2b	Trafficking	ROP2
AT5G51820	Phosphoglucomutase	Potential contaminant	ROP2
AT5G52470	Probable mediator of RNA polymerase II transcription subunit 36b	Potential contaminant	ROP2
AT5G52520	Proline--tRNA ligase, chloroplas- tic/mitochondrial	Potential contaminant	ROP2
AT5G52840	NADH-ubiquinone oxidoreductase-like protein	Potential contaminant	ROP2
AT5G53170	ATP-dependent zinc metalloprotease FTSH 11	Potential contaminant	ROP2
AT5G54500	Flavodoxin-like quinone reductase 1	TM	ROP2
AT5G55070	Dihydrolipoamide succinyltransferase	Potential contaminant	ROP2
AT5G55190	Ras-related nuclear protein 3	Trafficking	ROP2
AT5G55220	Trigger factor-like protein TIG	Potential contaminant	ROP2
AT5G55610	Isopentenyl-diphosphate delta-isomerase	Potential contaminant	ROP2

Acession	Name	Category	Significant in
AT5G57870	Eukaryotic Translation initiation factor isoform 4G-1	Translation	ROP2
AT5G58070	Temperature-induced lipocalin-1	Translation	ROP2
AT5G58290	26S Degradation regulatory subunit 6B homolog	Degradation	ROP2
AT5G60790	ABC transporter F family member 1	TM	ROP2
AT5G65010	Asparagine synthetase [glutamine-hydrolyzing] 2	Metabolism	ROP2
AT5G65020	Annexin	Calcium	ROP2
AT5G65110	Acyl-coenzyme A oxidase	Metabolism	ROP2
AT5G65430	GRF8	Cell growth	ROP2
AT5G66120	3-dehydroquinate synthase	Potential contaminant	ROP2
AT5G66190	Unknown	Potential contaminant	ROP2
AT5G66680	DEFECTIVE GLYCOSYLATION 1	TM	ROP2
AT5G66760	SUCCINATE DEHYDROGENASE 1-1	Potential contaminant	ROP2
AT5G67500	Voltage dependent anion channel 2	Defence	ROP2

Acession	Name	Category	Significant in
AT5G67590	NADH dehydrogenase [ubiquinone] iron-sulfur protein 4	Potential contaminant	ROP2
ATCG00160	30S ribosomal protein S2	Potential contaminant	ROP2
ATCG00380	30S ribosomal protein S4	Potential contaminant	ROP2
ATCG00660	50S ribosomal protein L20	Potential contaminant	ROP2
ATCG00670	Chloroplastic ATP-dependent Clp protease proteolytic subunit 1	Potential contaminant	ROP2
ATCG00750	30S ribosomal protein S11	Potential contaminant	ROP2
ATCG00810	50S ribosomal protein L22	Potential contaminant	ROP2
ATCG01120	30S ribosomal protein S15	Potential contaminant	ROP2
ATCG01130	TIC 214	Potential contaminant	ROP2
ATCG01240	30S ribosomal protein S7	Potential contaminant	ROP2
ATMG00070	NADH dehydrogenase [ubiquinone] iron-sulfur protein 3	Potential contaminant	ROP2
ATMG00160	Cytoskeletonchrome c oxidase subunit 2	Potential contaminant	ROP2
ATMG00220	Cytoskeletonchrome b	Potential contaminant	ROP2
ATMG00510	NADH dehydrogenase subunit 7	Potential contaminant	ROP2
ATMG00640	ATP synthase protein MI25	Potential contaminant	ROP2

Acession	Name	Category	Significant in
AT5G02050	Mitochondrial glycoprotein family protein	Potential contaminant	ROP6

Supplementary Table S.7: Fold change of proteins in root ROP-GFP CoIPs

Protein ID	Name	Fold change ROP2	Fold change ROP6
AT2G17720	2-oxoglutarate (2OG) and Fe(II)-dependent oxygenase superfamily protein	∞	∞
AT2G20580	26S proteasome regulatory subunit S2 1A	∞	∞
AT1G48830	40S ribosomal protein S7-1	∞	∞
AT4G36130	60S ribosomal protein L8-3	∞	∞
AT4G01100	adenine nucleotide transporter 1	∞	∞
AT1G27450	Adenine phosphoribosyl transferase 1	∞	∞
AT3G56190	Alpha-soluble NSF attachment protein 2	∞	∞
AT4G33090	aminopeptidase M1	∞	∞
AT5G19820	ARM repeat superfamily protein	∞	∞
AT5G36230	ARM repeat superfamily protein	∞	∞
AT3G44330	M28 Zn-peptidase nicastrin	∞	∞
AT1G51650	ATP synthase epsilon chain	∞	∞
ATCG00120	ATP synthase subunit alpha	∞	∞

Protein ID	Name	Fold change ROP2	Fold change ROP6
AT3G61050	Calcium-dependent lipid-binding (CaLB domain) family protein	∞	∞
AT4G35310	calmodulin-domain protein kinase 5	∞	∞
AT2G02560	CAND1	∞	∞
AT3G62360	Carbohydrate-binding-like fold	∞	∞
AT5G11560	Catalytics	∞	∞
AT4G09520	Cofactor-independent phosphoglycerate mutase	∞	∞
AT1G11680	CYTOCHROME P450 51G1	∞	∞
AT3G53110	DEAD-box ATP-dependent RNA helicase 38	∞	∞
AT3G55610	delta 1-pyrroline-5-carboxylate synthase 2	∞	∞
AT4G23690	Disease resistance-responsive (dirigent-like protein) family protein	∞	∞
AT4G12650	Endomembrane protein 70 protein family	∞	∞
AT5G27640	eIF3b	∞	∞
AT3G56150	eIF3c	∞	∞
AT3G57290	eIF3e	∞	∞
AT5G66510	gamma carbonic anhydrase 3	∞	∞
AT2G33470	glycolipid transfer protein 1	∞	∞
AT2G33220	GRIM-19 protein	∞	∞

Protein ID	Name	Fold change ROP2	Fold change ROP6
AT4G35860	GTP-binding 2	∞	∞
AT3G07770	Heat shock protein 90-6	∞	∞
AT1G52740	histone H2A protein 9	∞	0.00
AT1G64790	ILITYHIA	∞	∞
AT2G31660	Importin beta-like SAD2	∞	∞
AT5G53480	Karyopherin subunit beta-1	∞	∞
AT1G18270	ketose-bisphosphate aldolase class-II family protein	∞	∞
AT2G39960	Microsomal signal peptidase 25 kDa subunit (SPC25)	∞	∞
AT3G54110	PUMP1	∞	∞
AT5G23540	Mov34/MPN/PAD-1 family protein	∞	∞
AT4G13180	NAD(P)-binding Rossmann-fold superfamily protein	∞	0.00
AT5G15910	NAD(P)-binding Rossmann-fold superfamily protein	∞	∞
AT4G05020	NAD(P)H dehydrogenase B2	∞	∞
AT3G03100	NADH dehydrogenase [ubiquinone] 1 alpha subcomplex subunit 12	∞	∞
AT5G08530	NADH dehydrogenase [ubiquinone] flavoprotein 1	∞	∞
AT5G65720	nitrogen fixation S (NIFS)-like 1	∞	∞
AT3G08510	phospholipase C 2	∞	0.00

Protein ID	Name	Fold change ROP2	Fold change ROP6
AT4G35790	Phospholipase D	∞	∞
AT4G29130	Phosphotransferase	∞	∞
AT2G34420	photosystem II light harvesting complex gene B1B2	∞	∞
AT5G39410	Saccharopine dehydrogenase	∞	∞
AT1G03860	Prohibitin-2	∞	∞
AT4G19006	Proteasome component (PCI) domain protein	∞	∞
AT2G22125	CELLULOSE SYNTHASE INTERACTIVE 1	∞	∞
AT5G11420	Unknown	∞	∞
AT5G43780	Pseudouridine synthase/archaeosine transglycosylase-like family protein	∞	∞
AT1G59870	Putative ABC transporter	∞	∞
AT2G46520	Putative cellular apoptosis susceptibility protein	∞	∞
AT2G40660	Putative methionyl-tRNA synthetase	∞	∞
AT1G16920	RAB GTPase homolog A1B	∞	∞
AT5G65270	RABA4a	∞	∞
AT1G20090	ROP2	∞	∞
AT3G18820	RABG3f	∞	∞
AT2G44610	RABH1b	∞	∞

Protein ID	Name	Fold change ROP2	Fold change ROP6
AT5G64760	regulatory particle non-ATPase subunit 5B	∞	∞
AT3G07880	Rho GDP-dissociation inhibitor 1	∞	∞
AT4G21150	Ribophorin II (RPN2) family protein	∞	∞
AT2G44120	Ribosomal protein L30/L7 family protein	∞	∞
AT3G02080	Ribosomal protein S19e family protein	∞	∞
AT5G41520	RNA binding Plectin/S10 domain-containing protein	∞	∞
AT3G15640	Rubredoxin-like superfamily protein	∞	∞
AT1G14810	semialdehyde dehydrogenase family protein	∞	∞
AT1G76090	sterol methyltransferase 3	∞	∞
AT5G26360	T-complex protein 1 subunit gamma	∞	∞
AT2G46280	TGF-beta receptor interacting protein 1	∞	∞
AT5G14030	Translocon-associated protein beta (TRAPB) family protein	∞	∞
AT3G07680	p24beta2	∞	∞
AT2G16950	Transportin-1	∞	∞
AT4G14960	Tubulin alpha chain	∞	∞

Protein ID	Name	Fold change ROP2	Fold change ROP6
AT5G23860	Tubulin beta-8 chain	∞	∞
AT1G22360	UDP-glucosyl transferase 85A2	∞	∞
AT3G62530	ARM repeat superfamily protein	∞	∞
AT4G39080	V-type proton ATPase subunit a3	∞	∞
AT1G12840	V-type proton ATPase subunit C	∞	∞
AT2G14740	vaculolar sorting receptor 3	∞	∞
AT1G67730	Very-long-chain 3-oxoacyl-CoA reductase 1	∞	∞
AT2G45710	Zinc-binding ribosomal protein family protein	∞	∞
AT2G39730	rubisco activase	2.49	2.50
AT4G24820	26S proteasome non-ATPase regulatory subunit 6 homolog	2.36	2.41
AT2G04030	Heat shock protein 90-5	2.35	1.28
AT5G17020	EXPORTIN 1A	2.33	2.44
AT3G43300	Brefeldin A-inhibited guanine nucleotide-exchange protein 5 (BIG5)	2.32	2.42
AT1G52760	Caffeoylshikimate esterase	2.32	2.41
AT1G09620	Leucine--tRNA ligase	2.30	2.41
AT1G74020	strictosidine synthase 2	2.30	2.35
AT5G50920	CLPC homologue 1	2.28	2.34
AT3G57020	STRICTOSIDINE SYNTHASE-LIKE 9	2.27	2.39

Protein ID	Name	Fold change ROP2	Fold change ROP6
AT2G42210	Mitochondrial import inner membrane translocase subunit Tim17/Tim22/Tim23 family protein	2.27	2.30
AT3G02560	Ribosomal protein S7e family protein	2.26	2.42
AT3G18190	TCP-1/cpn60 chaperonin family protein	2.26	2.42
AT5G17770	NADH:cytochrome B5 reductase 1	2.25	2.37
AT4G20360	RabE1b	2.25	2.20
AT2G27730	copper ion binding	2.25	2.36
AT3G13920	eukaryotic translation initiation factor 4A1	2.23	2.34
AT1G64520	26S proteasome non-ATPase regulatory subunit 8 homolog A	2.22	2.31
AT5G59840	Ras-related small GTP-binding family protein	2.21	2.21
AT1G67330	glucuronoxylan 4-O-methyltransferase-like protein	2.20	2.45
AT1G70770	Unknown	2.20	2.30
AT3G08530	Clathrin, heavy chain	2.20	2.31
AT3G42050	vacuolar ATP synthase subunit H family protein	2.19	2.29
AT1G13320	protein phosphatase 2A subunit A3	2.19	2.27

Protein ID	Name	Fold change ROP2	Fold change ROP6
AT5G52840	NADH-ubiquinone oxidoreductase-like protein	2.18	2.26
AT3G48530	SNF1-related protein kinase regulatory subunit gamma 1	2.18	2.24
AT5G63510	gamma carbonic anhydrase like 1	2.18	2.27
AT5G25100	Transmembrane 9 superfamily member	2.18	2.33
AT4G33360	NAD(P)-binding Rossmann-fold superfamily protein	2.18	2.36
AT5G04740	ACT domain-containing protein	2.17	2.24
AT5G63680	Pyruvate kinase family protein	2.17	2.30
AT1G43890	RABC1	2.16	2.24
AT3G54470	Unknown	2.16	2.25
ATMG00510	NADH dehydrogenase subunit 7 (Nad7)	2.16	2.25
AT1G79930	heat shock protein 91	2.15	2.20
AT3G03780	5-methyltetrahydropteroyltriglutamate--homocysteine methyltransferase 2	2.15	2.22
AT2G33210	Heat shock protein 60-2	2.15	2.23
AT5G59850	Ribosomal protein S8 family protein	2.14	2.27
AT5G40770	Prohibitin-3	2.13	2.32
AT2G38040	Carboxyltransferase alpha subunit	2.13	2.22

Protein ID	Name	Fold change ROP2	Fold change ROP6
AT3G53750	actin 3	2.13	2.16
AT5G56710	Ribosomal protein L31e family protein	2.11	2.33
AT4G35260	Isocitrate dehydrogenase [NAD] regulatory subunit 1	2.11	2.31
AT4G37910	mitochondrial heat shock protein 70-1	2.11	2.24
AT2G45960	plasma membrane intrinsic protein 1B	2.11	2.20
AT3G02520	General regulatory factor 7	2.10	2.25
AT4G23650	Calcium-dependent protein kinase 3	2.10	2.23
AT2G45820	Remorin (DNA-binding protein)	2.09	2.16
AT4G25740	RNA binding Plectin/S10 domain-containing protein	2.09	2.23
AT4G11150	V-type proton ATPase subunit E1	2.08	2.20
AT3G53420	plasma membrane intrinsic protein 2A	2.08	2.07
AT1G15690	Inorganic H pyrophosphatase family protein	2.07	2.23
AT5G67400	RHS19	2.07	2.19
AT1G54000	GDSL-like Lipase/Acylhydrolase superfamily protein	2.06	2.15
AT5G07440	glutamate dehydrogenase 2	2.06	2.12
AT1G05250	Peroxidase superfamily protein	2.05	2.21

Protein ID	Name	Fold change ROP2	Fold change ROP6
AT1G65930	cytosolic NADP+-dependent isocitrate dehydrogenase	2.01	2.05
AT5G59970	Histone superfamily protein	1.93	2.15
AT2G31390	pfkB-like carbohydrate kinase family protein	1.93	1.02
AT4G14320	Zinc-binding ribosomal protein family protein	1.92	2.04
AT5G26280	TRAF-like family protein	1.89	2.12
AT1G66270	Glycosyl hydrolase superfamily protein	1.85	2.11
AT3G16460	Mannose-binding lectin superfamily protein	1.77	2.05
AT3G16450	Mannose-binding lectin superfamily protein	1.69	1.97
AT4G30190	ATPase 2	1.22	1.27
AT1G09740	Adenine nucleotide alpha hydrolases-like superfamily protein	1.22	2.41
AT3G62120	Class II aaRS and biotin synthetases superfamily protein	1.22	1.23
AT5G62700	tubulin beta chain 3	1.21	1.24
AT1G78570	rhamnose biosynthesis 1	1.18	1.21
AT3G62790	NADH-ubiquinone oxidoreductase-related	1.18	2.42

Protein ID	Name	Fold change ROP2	Fold change ROP6
AT5G13450	DELTA SUBUNIT OF MT ATP SYNTHASE	1.17	1.23
AT3G08580	ADP/ATP carrier 1	1.17	1.22
AT5G58070	TIL1	1.16	1.21
AT2G37970	SOUL heme-binding family protein	1.16	1.18
AT1G22410	Phospho-2-dehydro-3-deoxyheptonate aldolase	1.16	1.18
AT3G17020	Adenine nucleotide alpha hydrolases-like superfamily protein	1.16	1.20
AT4G00100	ribosomal protein S13A	1.16	1.24
AT5G14040	phosphate transporter 3	1.16	1.19
AT5G44340	Tubulin beta-4 chain	1.16	1.19
AT2G21160	Translocon-associated protein (TRAP)	1.16	1.23
AT2G29550	tubulin beta-7 chain	1.16	1.17
AT5G42790	proteasome alpha subunit F1	1.16	2.39
AT1G20010	tubulin beta-5 chain	1.16	1.19
AT5G19990	regulatory particle triple-A ATPase 6A	1.15	1.21
AT3G25530	glyoxylate reductase 1	1.15	2.42
AT3G01420	Peroxidase superfamily protein	1.15	1.18
AT3G44110	DNAJ homologue 3	1.15	1.20

Protein ID	Name	Fold change ROP2	Fold change ROP6
AT4G31490	Coatomer subunit beta-2	1.15	1.18
AT3G01280	Voltage-dependent anion-selective channel protein 1	1.15	1.23
AT1G30630	Coatomer subunit epsilon-1	1.15	1.23
AT2G32730	26S proteasome non-ATPase regulatory subunit 1 homolog A	1.15	1.21
AT5G66420	TIM-barrel signal transduction protein	1.15	1.17
AT2G20360	NADH dehydrogenase [ubiquinone] 1 alpha subcomplex subunit 9	1.15	1.22
AT1G62020	Coatomer, alpha subunit	1.15	1.23
AT4G39980	Phospho-2-dehydro-3-deoxyheptonate aldolase 1	1.15	1.18
AT2G21390	Coatomer, alpha subunit	1.15	1.22
AT4G24190	Chaperone protein htpG family protein	1.14	1.17
AT2G21870	MALE GAMETOPHYTE DEFECTIVE 1	1.14	1.20
AT5G43010	regulatory particle triple-A ATPase 4A	1.14	1.19
AT5G13710	STEROL METHYLTRANSFERASE 1	1.14	1.23
AT5G37510	EMBRYO DEFECTIVE 1467	1.14	1.22

Protein ID	Name	Fold change ROP2	Fold change ROP6
AT1G50010	tubulin alpha-2 chain	1.14	1.18
AT1G20200	26S proteasome non-ATPase regulatory subunit 3 homolog A	1.14	1.19
AT3G12260	LYR family of Fe/S cluster biogenesis protein	1.14	2.37
AT2G33040	gamma subunit of Mt ATP synthase	1.14	1.23
AT1G23190	PHOSPHOGLUCOMUTASE 3	1.14	1.17
AT1G80460	Actin-like ATPase superfamily protein	1.14	1.16
AT5G13110	Glucose-6-phosphate 1-dehydrogenase 2	1.14	1.17
AT5G61790	calnexin 1	1.14	1.20
AT5G35360	acetyl Co-enzyme a carboxylase biotin carboxylase subunit	1.14	1.15
AT3G05560	Ribosomal L22e protein family	1.14	1.21
AT3G11130	Clathrin, heavy chain	1.14	1.21
AT5G58290	26S proteasome regulatory subunit 6B homolog	1.14	1.17
AT1G47260	Gamma carbonic anhydrase 2	1.14	1.21
AT4G29040	26S proteasome regulatory subunit 4 homolog A	1.14	1.18
AT1G14670	Transmembrane 9 superfamily member 2	1.13	1.20
AT5G48810	Cytochrome B5 isoform D	1.13	1.22

Protein ID	Name	Fold change ROP2	Fold change ROP6
AT5G19780	Tubulin alpha-5 chain	1.13	1.18
AT1G56330	secretion-associated RAS 1B	1.13	1.20
AT1G72160	Sec14p-like phosphatidylinositol transfer family protein	1.13	1.18
AT4G34450	Coatomer subunit gamma	1.13	1.19
AT3G02090	MPPBETA	1.13	1.23
AT5G46290	3-ketoacyl-acyl carrier protein synthase I	1.13	1.15
AT3G52300	ATP synthase D chain	1.13	1.20
AT5G56030	heat shock protein 81-2	1.13	1.17
AT1G63000	NUCLEOTIDE-RHAMNOSE SYNTHASE/EPIMERASE-REDUCTASE	1.13	1.18
AT4G23850	Long chain acyl-CoA synthetase 4	1.13	1.17
AT1G33140	Ribosomal protein L6 family	1.13	1.20
AT4G20890	tubulin beta-9 chain	1.13	1.18
AT1G52360	Coatomer subunit beta'	1.13	1.17
AT3G27240	Cytochrome c1 1, heme protein	1.13	1.19
AT1G51980	Peptidase family M16	1.13	1.21
ATMG00480	ATP synthase protein YMF19	1.13	1.23
AT1G20950	Phosphofructokinase family protein	1.13	1.17
AT3G29250	NAD(P)-binding Rossmann-fold superfamily protein	1.13	1.13

Protein ID	Name	Fold change ROP2	Fold change ROP6
AT3G05530	regulatory particle triple-A ATPase 5A	1.12	1.14
AT2G30490	Trans-cinnamate 4-monooxygenase	1.12	1.22
AT5G20830	sucrose synthase 1	1.12	1.15
AT3G59540	60S ribosomal protein L38	1.12	1.23
AT3G60750	Transketolase	1.12	0.00
AT5G10860	CBS domain-containing protein CBSX3	1.12	1.18
AT5G43370	phosphate transporter 2	1.12	1.21
ATMG01190	ATP synthase subunit 1	1.12	1.15
AT3G03960	T-complex protein 1 subunit theta	1.12	1.16
AT5G52240	membrane steroid binding protein 1	1.12	1.19
AT3G01390	V-type proton ATPase subunit G1	1.12	1.15
AT4G20260	plasma-membrane associated cation-binding protein 1	1.12	1.19
AT5G15090	HYPERSENSITIVE RESPONSE 2	1.12	1.17
AT1G64190	6-phosphogluconate dehydrogenase family protein	1.12	1.14
AT1G76030	ATPase, V1 complex, subunit B protein	1.12	1.19
AT5G47930	Zinc-binding ribosomal protein family protein	1.12	1.16

Protein ID	Name	Fold change ROP2	Fold change ROP6
AT5G33320	Glucose-6-phosphate/phosphate translocator-related	1.12	2.32
AT1G70490	Ras-related small GTP-binding family protein	1.12	1.17
AT1G78900	vacuolar ATP synthase subunit A	1.12	1.15
AT1G09780	BPG-independent PGAM 1	1.12	1.14
AT2G44060	Late embryogenesis abundant protein, group 2	1.12	1.17
AT5G47200	RABD2b	1.12	1.16
AT5G19760	Oxoglutarate/malate translocator-like protein (Fragment)	1.12	1.15
AT3G18780	actin 2	1.12	1.14
AT5G09810	actin 7	1.12	1.15
AT5G16130	40S ribosomal protein S7-3	1.12	1.20
AT4G19210	ABC transporter E family member 2	1.12	1.15
AT3G14990	Class I glutamine amidotransferase-like superfamily protein	1.12	1.15
AT1G24510	TCP-1/cpn60 chaperonin family protein	1.12	1.15
AT2G39770	Glucose-1-phosphate adenylyltransferase family protein	1.12	2.29
AT5G20890	T-complex protein 1 subunit beta	1.12	1.17

Protein ID	Name	Fold change ROP2	Fold change ROP6
AT1G79340	Metacaspase-4	1.12	1.17
AT5G05010	Coatomer subunit delta	1.12	1.16
AT4G02930	GTP binding Elongation factor Tu family protein	1.12	1.12
AT4G27450	Aluminium induced protein with YGL and LRDR motifs	1.11	1.16
AT5G43060	RD21B	1.11	1.17
AT1G53750	26S proteasome regulatory subunit 7 homolog A	1.11	1.16
AT4G39200	Ribosomal protein S25 family protein	1.11	1.22
AT2G47470	thioredoxin family protein	1.11	1.15
AT3G53990	Adenine nucleotide alpha hydrolases-like superfamily protein	1.11	1.13
AT4G01850	S-adenosylmethionine synthetase 2	1.11	1.13
AT1G54270	EIF4A-2	1.11	1.13
AT5G10450	14-3-3LAMBDA	1.11	1.17
AT1G27400	Ribosomal protein L22p/L17e family protein	1.11	1.18
AT3G62830	NAD(P)-binding Rossmann-fold superfamily protein	1.11	1.19
AT3G17390	S-adenosylmethionine synthetase family protein	1.11	1.13

Protein ID	Name	Fold change ROP2	Fold change ROP6
AT5G65430	General regulatory factor 8	1.11	1.17
AT5G19550	aspartate aminotransferase 2	1.11	1.11
AT5G66680	DEFECTIVE GLYCOSYLATION 1	1.11	1.15
AT2G33150	3-ketoacyl-CoA thiolase 2	1.11	1.14
AT3G04400	Ribosomal protein L14p/L23e family protein	1.11	1.17
AT3G04840	Ribosomal protein S3Ae	1.11	1.17
AT3G12110	actin-11	1.11	1.14
AT5G17820	Peroxidase superfamily protein	1.11	2.19
AT1G47128	RESPONSIVE TO DEHYDRATION 21A	1.11	1.14
AT3G63460	Transducin family protein / WD-40 repeat family protein	1.11	1.18
AT5G53560	cytochrome B5 isoform E	1.11	1.19
AT1G78300	General regulatory factor 2	1.11	1.16
AT2G19730	Ribosomal L28e protein family	1.11	1.17
AT2G36880	methionine adenosyltransferase 3	1.11	1.13
AT3G19820	DWARF1	1.10	1.16
AT3G08947	ARM repeat superfamily protein	1.10	2.36
AT4G27090	Ribosomal protein L14	1.10	1.20
AT1G79530	glyceraldehyde-3-phosphate dehydrogenase of plastid 1	1.10	1.18
AT5G17920	Cobalamin-independent synthase family protein	1.10	1.13

Protein ID	Name	Fold change ROP2	Fold change ROP6
AT1G72150	Putative cytosolic factor protein	1.10	1.18
AT3G02780	dimethylallyl pyrophosphate isomerase 2	1.10	1.15
AT1G12000	Pyrophosphate--fructose 6-phosphate 1-phosphotransferase subunit beta 1	1.10	1.14
AT1G22530	PATELLIN 2	1.10	1.16
AT3G09200	Ribosomal protein L10 family protein	1.10	1.15
AT3G46830	RAB GTPase homolog A2C	1.10	2.29
AT2G36160	Ribosomal protein S11 family protein	1.10	1.14
AT5G60390	GTP binding Elongation factor Tu family protein	1.10	1.14
AT3G43190	sucrose synthase 4	1.10	1.15
AT4G09800	S18 ribosomal protein	1.10	1.17
AT1G18540	Ribosomal protein L6 family protein	1.10	1.17
AT5G18380	Ribosomal protein S5 domain 2-like superfamily protein	1.10	1.14
AT3G53020	Ribosomal protein L24e family protein	1.10	1.18
AT2G30930	Expressed protein	1.10	1.16
AT3G62250	ubiquitin 5	1.10	1.16

Protein ID	Name	Fold change ROP2	Fold change ROP6
AT2G37170	plasma membrane intrinsic protein 2	1.10	1.12
AT3G49010	breast basic conserved 1	1.09	1.14
AT5G02960	40S ribosomal protein S23-2	1.09	1.16
AT1G28290	arabinogalactan protein 31	1.09	2.10
AT5G38480	1General regulatory factor 3	1.09	1.15
AT5G08690	ATP synthase alpha/beta family protein	1.09	1.15
AT3G07110	Ribosomal protein L13 family protein	1.09	1.14
AT2G31610	Ribosomal protein S3 family protein	1.09	1.16
AT5G54160	O-methyltransferase 1	1.09	1.14
AT4G31700	Ribosomal protein S6	1.09	1.13
AT5G66760	SUCCINATE DEHYDROGENASE 1-1	1.09	1.12
AT3G09840	cell division cycle 48	1.09	1.11
AT3G55280	ribosomal protein L23AB	1.09	0.59
AT5G27850	Ribosomal protein L18e/L15 superfamily protein	1.09	1.15
AT1G43170	ribosomal protein 1	1.09	1.16
AT5G15650	reversibly glycosylated polypeptide 2	1.09	1.14
AT1G72370	40s ribosomal protein SA	1.09	1.14

Protein ID	Name	Fold change ROP2	Fold change ROP6
AT5G62300	Ribosomal protein S10p/S20e family protein	1.09	1.12
AT3G25520	ribosomal protein L5	1.09	1.12
AT3G62870	Ribosomal protein L7Ae/L30e/S12e/Gadd45 family protein	1.09	1.16
AT1G70600	Ribosomal protein L18e/L15 superfamily protein	1.09	1.15
AT5G15200	Ribosomal protein S4	1.09	1.16
AT5G25757	RNA polymerase I-associated factor PAF67	1.09	2.24
AT3G20050	T-complex protein 1 subunit alpha	1.09	1.16
AT2G05220	Ribosomal S17 family protein	1.09	1.15
AT2G37270	ribosomal protein 5B	1.09	1.17
AT3G56340	40S ribosomal protein S26-3	1.09	1.14
AT5G17330	glutamate decarboxylase 4	1.09	1.14
AT5G54640	Histone superfamily protein	1.09	2.25
AT1G02500	S-adenosylmethionine synthetase 1	1.09	1.10
AT4G18100	Ribosomal protein L32e	1.09	1.15
AT2G18020	Ribosomal protein L2 family	1.09	1.14
AT5G54500	Flavodoxin-like quinone reductase 1	1.09	1.12

Protein ID	Name	Fold change ROP2	Fold change ROP6
AT2G27710	60S acidic ribosomal protein family	1.09	1.12
AT4G17390	Ribosomal protein L23/L15e family protein	1.09	1.14
AT3G02530	T-complex protein 1 subunit zeta 1	1.09	1.15
AT1G22300	GENERAL REGULATORY FACTOR 10	1.09	1.12
AT5G12140	cystatin-1	1.09	0.00
AT3G02360	6-phosphogluconate dehydrogenase	1.09	1.13
AT3G05730	Encodes a defensin-like (DEFL) family protein.	1.09	2.34
AT4G09000	general regulatory factor 1	1.08	1.12
AT1G35160	GF14 protein phi chain	1.08	1.13
AT1G63940	monodehydroascorbate reductase 6	1.08	1.12
AT5G67500	Voltage dependent anion channel 2	1.08	1.15
AT1G59359	Ribosomal protein S5 family protein	1.08	1.15
AT2G16060	Non-symbiotic hemoglobin 1	1.08	1.15
AT3G53430	Ribosomal protein L11 family protein	1.08	1.11

Protein ID	Name	Fold change ROP2	Fold change ROP6
AT1G03220	Eukaryotic aspartyl protease family protein	1.08	1.11
AT3G16640	Translationally-controlled tumor protein 1	1.08	1.13
AT5G20290	Ribosomal protein S8e family protein	1.08	1.15
AT5G45775	Ribosomal L5P family protein	1.08	1.15
AT2G47730	glutathione S-transferase phi 8	1.08	1.10
AT5G28060	Ribosomal protein S24e family protein	1.08	1.13
AT5G41670	6-phosphogluconate dehydrogenase	1.08	1.12
AT1G14320	Ribosomal protein L16p/L10e family protein	1.08	1.15
AT5G02450	Ribosomal protein L36e family protein	1.08	1.15
AT3G10920	manganese superoxide dismutase 1	1.08	2.25
AT1G04270	Cytosolic ribosomal protein S15	1.08	1.17
AT3G51160	GDP-mannose 4,6 dehydratase 2	1.08	2.21
AT3G47520	PLASTIDIC NAD-DEPENDENT MALATE DEHYDROGENASE	1.08	1.12
AT5G56630	ATP-dependent 6-phosphofructokinase 7	1.08	2.19
AT4G13930	serine hydroxymethyltransferase 4	1.08	1.12

Protein ID	Name	Fold change ROP2	Fold change ROP6
AT2G47510	FUMARASE 1	1.08	1.12
AT1G55020	Linoleate 9S-lipoxygenase 1	1.08	1.22
AT1G02780	Ribosomal protein L19e family protein	1.08	1.13
AT1G77120	alcohol dehydrogenase 1	1.08	1.13
AT3G48930	40S ribosomal protein S11-1	1.07	1.14
AT3G09630	Ribosomal protein L4/L1 family	1.07	1.13
AT3G15950	DNA topoisomerase-related	1.07	1.08
AT2G01250	Ribosomal protein L30/L7 family protein	1.07	1.12
AT2G32240	Early endosome antigen	1.07	1.14
AT5G07090	Ribosomal protein S4 (RPS4A) family protein	1.07	1.13
AT5G42980	thioredoxin 3	1.07	1.13
AT5G55190	Ras-related nuclear protein 3	1.07	1.13
AT3G03270	Adenine nucleotide alpha hydrolases-like superfamily protein	1.07	1.16
AT1G57720	Translation elongation factor EF1B	1.07	1.10
AT3G14940	phosphoenolpyruvate carboxylase 3	1.07	1.11
AT3G04120	Glyceraldehyde-3-phosphate dehydrogenase GAPC1	1.07	1.16

Protein ID	Name	Fold change ROP2	Fold change ROP6
AT2G34480	Ribosomal protein L18ae/LX family protein	1.06	1.13
AT4G14710	acireductone dioxygenase 1	1.06	1.11
AT5G02870	Ribosomal protein L4/L1 family	1.06	2.23
AT5G19510	Translation elongation factor EF1B/ribosomal protein S6 family protein	1.06	1.08
AT2G41840	Ribosomal protein S5 family protein	1.06	1.10
AT4G39260	cold, circadian rhythm, and RNA binding 1	1.06	1.07
AT1G79550	phosphoglycerate kinase	1.06	1.07
AT1G56070	Ribosomal protein S5/Elongation factor G/III/V family protein	1.06	1.09
AT5G40370	Glutaredoxin family protein	1.06	1.14
AT1G62660	Glycosyl hydrolases family 32 protein	1.05	1.08
AT5G64100	Peroxidase superfamily protein	1.05	1.12
AT1G13440	glyceraldehyde-3-phosphate dehydrogenase C2	1.05	1.17
AT3G09260	Glycosyl hydrolase superfamily protein	1.05	1.12
AT5G47210	Hyaluronan / mRNA binding family	1.05	1.00
AT4G15000	Ribosomal L27e protein family	1.05	2.21

Protein ID	Name	Fold change ROP2	Fold change ROP6
AT4G34200	D-3-phosphoglycerate dehydrogenase	1.05	1.10
AT1G20440	cold-regulated 47	1.05	1.07
AT2G02130	low-molecular-weight cysteine-rich 68	1.05	2.27
AT1G26630	eIF-5A 1	1.05	1.12
AT5G10360	Ribosomal protein S6e	1.05	1.10
AT5G22880	histone B2	1.05	2.15
AT5G37780	calmodulin 1	1.05	1.11
AT2G21045	Rhodanese/Cell cycle control phosphatase superfamily protein	1.05	1.10
AT1G04410	Lactate/malate dehydrogenase family protein	1.04	1.07
AT2G01520	MLP-like protein 328	1.04	0.00
AT1G07890	ASCORBATE PEROXIDASE 1	1.04	1.10
AT2G43610	Chitinase family protein	1.04	2.23
AT1G76180	Dehydrin family protein	1.04	1.04
AT3G14067	Subtilase family protein	1.03	0.55
AT1G31812	acyl-CoA-binding protein 6	1.03	1.05
AT2G36530	Enolase	1.03	1.06
AT3G20370	TRAF-like family protein	1.03	2.09
AT1G20450	Dehydrin family protein	1.03	2.12
AT3G52930	Aldolase superfamily protein	1.03	1.05
AT1G35720	annexin 1	1.03	1.08

Protein ID	Name	Fold change ROP2	Fold change ROP6
AT4G13940	S-adenosyl-L-homocysteine hydrolase	1.03	1.05
AT1G11000	Seven transmembrane MLO family protein	1.03	0.00
AT3G55440	triosephosphate isomerase	1.03	1.06
AT2G25980	Mannose-binding lectin superfamily protein	1.02	2.08
AT3G09440	Heat shock protein 70 (Hsp 70) family protein	1.02	1.07
AT3G16420	PYK10-binding protein 1	1.01	1.12
AT5G02500	heat shock cognate protein 70-1	1.01	1.06
AT4G35090	catalase 2	1.00	2.06
AT5G13850	nascent polypeptide-associated complex subunit alpha-like protein 3	1.00	2.09
GFP__Q9U6	GFP	1.00	1.00
AT4G38740	rotamase CYP 1	1.00	1.03
AT1G66200	glutamine synthase clone F11	0.99	1.01
AT1G54410	dehydrin family protein	0.98	2.03
AT4G34870	rotamase cyclophilin 5	0.98	0.97
AT5G28540	heat shock protein 70 (Hsp 70) family protein	0.95	1.01
AT4G11600	glutathione peroxidase 6	0.59	1.12
AT1G66280	Glycosyl hydrolase superfamily protein	0.57	1.17

Protein ID	Name	Fold change ROP2	Fold change ROP6
AT4G34670	Ribosomal protein S3Ae	0.56	1.18
AT3G49910	Translation protein SH3-like family protein	0.55	0.00
AT1G11910	aspartic proteinase A1	0.55	1.18
AT2G43910	HARMLESS TO OZONE LAYER 1	0.55	0.00
AT5G13490	ADP/ATP carrier 2	0.55	0.00
AT3G16400	nitrile specifier protein 1	0.54	0.58
AT4G33070	Thiamine pyrophosphate dependent pyruvate decarboxylase family protein	0.54	1.11
AT3G15730	phospholipase D alpha 1	0.54	1.11
AT3G22850	Aluminium induced protein with YGL and LRDR motifs	0.54	1.08
AT5G13420	Aldolase-type TIM barrel family protein	0.54	1.09
AT5G11670	NADP-malic enzyme 2	0.53	1.10
AT5G03630	Pyridine nucleotide-disulphide oxidoreductase family protein	0.53	0.00
AT2G16600	rotamase CYP 3	0.53	1.11
AT1G70850	MLP-like protein 34	0.53	0.00
AT1G21750	PDI-like 1-1	0.53	0.00
AT3G03250	UDP-GLUCOSE PYROPHOSPHORYLASE 1	0.53	0.00
AT3G56240	copper chaperone	0.53	0.00

Protein ID	Name	Fold change ROP2	Fold change ROP6
AT2G30860	glutathione S-transferase PHI 9	0.53	1.11
AT3G09820	adenosine kinase 1	0.53	0.00
AT2G38380	Peroxidase superfamily protein	0.51	1.10
AT4G24280	chloroplast heat shock protein 70-1	0.45	1.00
AT3G55410	2-oxoglutarate dehydrogenase	0.00	0.00
ATCG00500	Acetyl-coenzyme A carboxylase carboxyl transferase subunit beta	0.00	∞
AT1G68300	Adenine nucleotide alpha hydrolases-like superfamily protein	0.00	∞
AT1G50200	Alanine--tRNA ligase	0.00	2.24
AT3G59020	ARM repeat superfamily protein	0.00	∞
AT1G70320	E3 ubiquitin-protein ligase UPL2	0.00	∞
AT1G07810	ER-type Ca2+-ATPase 1	0.00	∞
AT4G11420	eIF3a	0.00	∞
AT2G30870	glutathione S-transferase PHI 10	0.00	0.57
AT1G66240	homolog of anti-oxidant 1	0.00	0.00
AT5G35950	Mannose-binding lectin superfamily protein	0.00	∞
AT4G04830	methionine sulfoxide reductase B5	0.00	2.24
AT1G12110	nitrate transporter 1.1	0.00	∞
AT1G05260	Peroxidase superfamily protein	0.00	∞
AT2G25450	Probable 2-oxoacid dependent dioxygenase	0.00	∞

Protein ID	Name	Fold change ROP2	Fold change ROP6
AT2G30740	PTI1-like tyrosine-protein kinase 2	0.00	∞
AT4G35020	ROP6	0.00	∞
AT3G09500	Ribosomal L29 family protein	0.00	∞
AT5G02610	Ribosomal L29 family protein	0.00	∞
AT3G11940	ribosomal protein 5A	0.00	2.28
AT5G05780	RP non-ATPase subunit 8A	0.00	∞

Supplementary Table S.8: Significantly enriched proteins in RIC affinity purification

Accession	Name	Enriched in
AT3G14067	Subtilase family protein	FER4 RIC4
AT5G59613	ATP synthase	FER4 RIC4
AT3G62730	desiccation-like protein	FER4 RIC4
AT1G30900	VACUOLAR SORTING RECEPTOR 6	FER4 RIC4
AT2G33460	RIC1	FER4 RIC4
AT2G41475	Embryo-specific protein 3	FER4 RIC4
AT5G16490	RIC4	FER4 RIC4
AT4G17170	RAB GTPase homolog B1C	FER4 RIC4
AT1G62750	Translation elongation factor EFG/EF2 protein	FER4 RIC4
AT3G23175	HR-like lesion-inducing protein-related	FER4 RIC4
AT4G17170	RAB GTPase homolog B1C	Col-0 RIC4

Accession	Name	Enriched in
AT1G62750	Translation elongation factor EFG/EF2 protein	Col-0 RIC4
AT3G57020	Calcium-dependent phosphotriesterase superfamily protein	Col-0 RIC4
AT5G42150	Glutathione S-transferase family protein	Col-0 RIC4
AT1G30900	VACUOLAR SORTING RECEPTOR 6	Col-0 RIC4
AT2G33460	RIC1	Col-0 RIC4
AT2G41475	Embryo-specific protein 3	Col-0 RIC4
AT3G14067	Subtilase family protein	Col-0 RIC4
AT1G20090	ROP2	Col-0 RIC4
AT5G59613	ATP synthase	Col-0 RIC4
AT3G62730	desiccation-like protein	Col-0 RIC4
AT5G39900	Small GTP-binding protein	Col-0 RIC4
AT5G16490	RIC4	Col-0 RIC4
AT5G39900	Small GTP-binding protein	FER4 RIC1
AT1G07320	ribosomal protein L4;ribosomal protein L4	FER4 RIC1
AT1G32990	plastid ribosomal protein l11	FER4 RIC1
AT1G48050	Ku80 family protein	FER4 RIC1
AT4G35950	ROP5	FER4 RIC1

Accession	Name	Enriched in
AT5G55920	S-adenosyl-L-methionine-dependent methyltransferases superfamily protein	FER4 RIC1
AT2G33460	RIC1	FER4 RIC1
AT2G41475	Embryo-specific protein 3	FER4 RIC1
AT3G62730	desiccation-like protein	FER4 RIC1
AT4G17170	RAB GTPase homolog B1C	FER4 RIC1
AT5G42150	Glutathione S-transferase family protein	FER4 RIC1
AT1G78630	Ribosomal protein L13 family protein	FER4 RIC1
AT2G33800	Ribosomal protein S5 family protein	FER4 RIC1
AT4G23430	NAD(P)-binding Rossmann-fold superfamily protein	FER4 RIC1
AT4G25340	FK506 BINDING PROTEIN 53	FER4 RIC1
AT1G10290	dynamin-like protein 6	FER4 RIC1
AT2G42710	Ribosomal protein L1p/L10e family	FER4 RIC1
AT4G22010	SKU5 similar 4	FER4 RIC1
AT5G10730	NAD(P)-binding Rossmann-fold superfamily protein	FER4 RIC1
AT5G54640	Histone superfamily protein	FER4 RIC1
AT1G76010	Alba DNA/RNA-binding protein	FER4 RIC1
AT3G07030	Alba DNA/RNA-binding protein	FER4 RIC1
AT3G55220	SPLICEOSOME-ASSOCIATED PROTEIN 130 B	FER4 RIC1
AT3G57150	homologue of NAP57	FER4 RIC1

Accession	Name	Enriched in
AT4G13010	Oxidoreductase, zinc-binding dehydrogenase family protein	FER4 RIC1
AT5G12940	Leucine-rich repeat (LRR) family protein	FER4 RIC1
AT1G11390	Protein kinase superfamily protein	FER4 RIC1
AT1G35680	Ribosomal protein L21	FER4 RIC1
AT1G66260	RNA-binding (RRM/RBD/RNP motifs) family protein	FER4 RIC1
AT1G75350	Ribosomal protein L31	FER4 RIC1
AT2G30930	Unknown	FER4 RIC1
AT2G36290	alpha/beta-Hydrolases superfamily protein	FER4 RIC1
AT2G40410	Staphylococcal nuclease homologue	FER4 RIC1
AT2G43030	Ribosomal protein L3 family protein	FER4 RIC1
AT3G06810	acyl-CoA dehydrogenase-related	FER4 RIC1
AT3G25920	ribosomal protein L15	FER4 RIC1
AT3G55460	SC35-like splicing factor 30	FER4 RIC1
AT3G56170	Ca-2+ dependent nuclease	FER4 RIC1
AT3G61820	Eukaryotic aspartyl protease family protein	FER4 RIC1
AT3G63490	Ribosomal protein L1p/L10e family	FER4 RIC1
AT4G01310	Ribosomal L5P family protein	FER4 RIC1
AT4G35020	ROP6	FER4 RIC1
AT5G30510	ribosomal protein S1	FER4 RIC1
AT5G37720	ALWAYS EARLY 4	FER4 RIC1

Accession	Name	Enriched in
AT5G49930	zinc knuckle (CCHC-type) family protein	FER4 RIC1
AT5G65250	Unknown	FER4 RIC1
ATCG01310	ribosomal protein L2	FER4 RIC1
AT1G20090	ROP2	Col-0 RIC1
AT5G16490	RIC4	Col-0 RIC1
AT5G39900	Small GTP-binding protein	Col-0 RIC1
AT3G62730	desiccation-like protein	Col-0 RIC1
AT5G42150	Glutathione S-transferase family protein	Col-0 RIC1
AT5G54640	Histone superfamily protein	Col-0 RIC1
AT2G40410	Staphylococcal nuclease homologue	Col-0 RIC1
AT3G55460	SC35-like splicing factor 30	Col-0 RIC1
AT4G01310	Ribosomal L5P family protein	Col-0 RIC1
AT5G49930	zinc knuckle (CCHC-type) family protein	Col-0 RIC1
AT3G57020	Calcium-dependent phosphotriesterase superfamily protein	Col-0 RIC1
AT2G45220	Plant invertase/pectin methylesterase inhibitor superfamily	Col-0 RIC1
AT3G10710	RHS12	Col-0 RIC1
AT4G01700	Chitinase family protein	Col-0 RIC1
AT1G07830	ribosomal protein L29 family protein	Col-0 RIC1
ATCG00380	chloroplast ribosomal protein S4	Col-0 RIC1

Accession	Name	Enriched in
ATCG00780	ribosomal protein L14	Col-0 RIC1
AT1G07320	ribosomal protein L4	Col-0 RIC1
AT1G32990	plastid ribosomal protein l11	Col-0 RIC1
AT1G48050	Ku80 family protein	Col-0 RIC1
AT4G35950	ROP5	Col-0 RIC1
AT5G55920	ROP5	Col-0 RIC1
AT2G33460	RIC1	Col-0 RIC1
AT2G41475	Embryo-specific protein 3	Col-0 RIC1
AT1G78630	Ribosomal protein L13 family protein	Col-0 RIC1
AT2G33800	Ribosomal protein S5 family protein	Col-0 RIC1
AT4G23430	NAD(P)-binding Rossmann-fold superfamily protein	Col-0 RIC1
AT4G25340	FK506 BINDING PROTEIN 53	Col-0 RIC1
AT1G10290	dynamin-like protein 6	Col-0 RIC1
AT2G42710	Ribosomal protein L1p/L10e family	Col-0 RIC1
AT4G22010	SKU5 similar 4	Col-0 RIC1
AT3G07030	Alba DNA/RNA-binding protein	Col-0 RIC1
AT3G57150	homologue of NAP57	Col-0 RIC1
AT4G13010	Oxidoreductase, zinc-binding dehydrogenase family protein	Col-0 RIC1
AT5G12940	Leucine-rich repeat (LRR) family protein	Col-0 RIC1
AT1G11390	Protein kinase superfamily protein	Col-0 RIC1
AT1G35680	Ribosomal protein L21	Col-0 RIC1

Accession	Name	Enriched in
AT1G66260	RNA-binding (RRM/RBD/RNP motifs) family protein	Col-0 RIC1
AT1G75350	Ribosomal protein L31	Col-0 RIC1
AT2G30930	Unknown	Col-0 RIC1
AT2G36290	alpha/beta-Hydrolases superfamily protein	Col-0 RIC1
AT3G06810	acyl-CoA dehydrogenase-related	Col-0 RIC1
AT3G25920	ribosomal protein L15	Col-0 RIC1
AT3G56170	Ca-2+ dependent nuclease	Col-0 RIC1
AT3G61820	Eukaryotic aspartyl protease family protein	Col-0 RIC1
AT3G63490	Ribosomal protein L1p/L10e family	Col-0 RIC1
AT4G35020	ROP6	Col-0 RIC1
AT5G30510	ribosomal protein S1	Col-0 RIC1
AT5G37720	ALWAYS EARLY 4	Col-0 RIC1
AT5G65250	Unknown	Col-0 RIC1
ATCG01310	ribosomal protein L2	Col-0 RIC1